Disaster & Development

Volume 13 • Issue 02 • July to December 2024 ISSN : 0973-6700

- Landslide Susceptibility Mapping In Darjeeling Hills
- Assessing Causes and Impacts of Landslides in the Sikkim Himalaya, India
- Assessing Forest Fire Severity Using Remote Sensing: A Case Study in Western Rajaji National Park, Uttarakhand, India
- Measuring Adaptive Capacity of Indian Agriculture to Climate Change: An Application of Indicator Approach
- Impact on the Pune city's food accessibility during a rare, disastrous event: A case of the COVID-19 lockdown in India
- Multi-Hazard Susceptibility Assessment in the Mountainous Regions Using Machine Learning Techniques: A Review
- Soil Erosion Assessment Using the RUSLE Model and Geospatial Analysis: A Case Study of Majuli Island of Assam, India
- Identification of flood ulnerable village clusters in the southwestern fringe of Guwahati City using GIS-based spatial autocorrelation technique and real-time SAR imagery

nidm
Resilient India - Disaster free India

Journal of the National Institute of Disaster Management, Delhi

Disaster & Development

Journal of the National Institute of Disaster Management, Delhi

Editorial Advisory Board

Dr. M. Ravichandran
Secretary, MoES,
Govt. of India

Dr. Anil Kumar Sinha, IAS
Former Vice Chairman,
Bihar SDMA

Dr. M. Mohapatra
Director General,
India Meteorological Department (IMD)

Prof. Rama Baru
Professor
Centre of Social Medicine and
Community Health
Jawaharlal Nehru University
New Delhi

Dr. R.K. Bhandari
Distinguished Visiting Professor,
Centre of Excellence in Disaster Mitigation and
Management (CoEDMM),
Indian Institutes of Technology (IIT), Roorkee

Dr. Dhar Chakraborty, IAS (Retd.)
Former Executive Director,
National Institute of Disaster
Management (NIDM)

Chief Editor

Shri Rajendra Ratnoo, IAS
Executive Director
National Institute of Disaster Management (NIDM), Delhi
ed.nidm@nic.in

Editor

Prof. Surya Parkash
Head, GMR Division, NIDM
surya.nidm@nic.in

nidm
Resilient India - Disaster free India

Mailing Address

The Editor
Journal 'Disaster & Development'
National Institute of Disaster Management
Ministry of Home Affairs
Government of India
Plot No. 15, Pocket 3, Block B, Sector 29, Rohini, Delhi 110042

Disaster & Development

Journal of the National Institute of Disaster Management

Volume 13, Issue 02, July to December 2024

© National Institute of Disaster Management (NIDM), Delhi.

All rights reserved. No part of this publication may be reproduced or transmitted in any form or by any means, electronic or mechanical, including photocopying, recording or by any information storage and retrieval system without permission from National Institute of Disaster Management (NIDM), Delhi.

ISSN: 0973-6700

Disaster & Development Journal is published biannually

Printed and Published by National Institute of Disaster Management (NIDM), Ministry of Home Affairs, Govt. of India, Plot No. 15, Block B, Pocket 3, Sector 29, Rohini, Delhi 110042

Contents

Volume 13, Issue 02,
July to December, 2024

Editor-in-Chief *v*

Editorial Note *vii*

1. Landslide Susceptibility Mapping In Darjeeling Hills 1
   Passang Sherpa, Uttam Lal and Rajesh Kumar

2. Assessing Causes and Impacts of Landslides in the Sikkim Himalaya, India 29
   Dilli Ram Dahal, Vimal Khawas, Prabuddh Kumar Mishra and Aster Pradhan

3. Assessing Forest Fire Severity Using Remote Sensing: A Case Study in Western Rajaji National Park, Uttarakhand, India 55
   Suraj Dev, V. S. Negi, B.W. Pandey, Chatter Singh and Ravi Kesharwani

4. Measuring Adaptive Capacity of Indian Agriculture to Climate Change: An Application of Indicator Approach 69
   Surendra Singh Jatav

5. Impact on the Pune City's Food Accessibility During a Rare, Disastrous Event: A Case of the Covid-19 Lockdown in India 95
   Amruta Garud and Bakul Rao

6. Multi-Hazard Susceptibility Assessment in the Mountainous Regions Using Machine Learning Techniques: A Review 117
Hemwati Nandan Bahuguna, Sushma Bahuguna, Syed Hameedur Rahman Zaini and Sudipta Sen Gupta

7. Soil Erosion Assessment Using the RUSLE Model and Geospatial Analysis: A Case Study of Majuli Island of Assam, India 151
Pragyashree Mahanta and Nitashree Mili

8. Identification of Flood Vulnerable Village Clusters in the South-Western Fringe of Guwahati City Using GIS Based Spatial Auto-correlation Technique and Real Time SAR Imagery 169
Rakesh Kumar Sarmah and Santanu Sarma

Editor-in-Chief

It is with great sense of responsibility and a pride that I present to you this issue of the Disaster and Development Journal. The period from July to December 2024 has been particularly challenging for India, marked by a series of devastating disasters that have profoundly impacted lives, livelihoods, and ecosystems. These events underscore the critical importance of advancing disaster risk reduction strategies and enhancing resilience across all sectors.

The monsoon season of the year 2024 brought catastrophic floods across India, with significant damage and losses in terms of human lives, public and private assets as also loss of natural resources including bio-diversity loss. The tragic *Surat building collapse on 6th July 2024* serve as stark reminders of the vulnerabilities inherent in densely populated and urbanizing regions. The Western Ghats and other hilly terrains witnessed a series of landslides, including the *Ankola landslide on 16th July 2024, Vilangad landslide on 30th July 2024*, and *Wayanad landslides on 31th July 2024*, highlighting the interplay between heavy rainfall and anthropogenic pressures in exacerbating geological hazards.

The industrial explosion in *Atchutapuram on 21st August 2024 and the Vijayawada floods on 1st September 202*4 further demonstrated the need for stringent industrial safety protocols and urban flood management systems. The *Jivitputrika tragedy* in Bihar on 26th September 2024 where atleast 46 people were reported to have drowned, emphasizing the importance of crowd management and safety planning during religious and public gatherings. The month of November and December brought additional sorrow with the *Almora bus accident on 4th November 2024* and *the Mumbai boat accident on 18th December 2024*, both of which highlighted transportation safety challenges in both remote as well as urban areas.

Amid these adversities, this issue of the journal presents a diverse collection of research aimed at enhancing our understanding of disaster risks and developing actionable solutions. As these articles demonstrate, interdisciplinary approaches, technological advancements, and community engagement are vital to addressing the challenges posed by disasters.

This journal remains committed to fostering dialogue and collaboration among researchers, practitioners, and policymakers to build a safer and more resilient future.

I extend my heartfelt gratitude to the authors, reviewers, and editorial team for their dedication to advancing disaster science and resilience. Let us remain steadfast in our efforts to mitigate risks and protect lives and livelihoods.

Warm regards,



Rajendra Ratnoo, IAS

Editorial Note

The second half of 2024 witnessed a series of impactful disasters worldwide, emphasizing the urgent need for enhanced resilience, adaptive governance, and the integration of disaster risk reduction (DRR) into development strategies. In India, the monsoon season brought widespread floods, flash floods, and landslides, particularly in the Himalayan regions of India. These disasters, exacerbated by climate change and poor land-use planning, highlighted the vulnerability of communities in high-risk zones and underscored the critical need for robust early warning systems and preparedness measures.

The period also saw intensified cyclonic activity in the Bay of Bengal, severely affecting coastal states such as Odisha, Andhra Pradesh, Tamil Nadu and West Bengal. These storms caused significant destruction to infrastructure, displaced thousands, and disrupted livelihoods. While disaster recovery efforts showcased resilience, they also highlighted ongoing challenges in rebuilding sustainably and ensuring long-term support for affected populations. Globally, other disasters such as earthquakes, wildfires, and extreme heat waves underscored the interconnected nature of disaster risks and the need for international collaboration and comprehensive management frameworks.

This issue of the journal provides valuable insights through articles, case studies, and policy discussions, drawing lessons from recent disasters and exploring innovative solutions. By fostering collaboration among stakeholders and integrating DRR into development policies, we aim to pave the way for a more disaster-resilient and sustainable future.

The studies include in journal gives insights into landslide-prone regions through Landslide Susceptibility Mapping in Darjeeling Hills and Assessing Causes and Impacts of Landslides in the Sikkim Himalaya, strategies for fire management using geospatial tools in Assessing Forest Fire Severity in Western Rajaji National Park, Uttarakhand, and an

evaluation of India's agricultural resilience to climate variability in Measuring Adaptive Capacity of Indian Agriculture to Climate Change. Urban vulnerabilities during emergencies are highlighted in Impact on Pune City's Food Accessibility During a Rare, Disastrous Event: A Case of the COVID-19 Lockdown in India, while the potential of AI in hazard mapping is explored in Multi-Hazard Susceptibility Assessment in Mountainous Regions Using Machine Learning Techniques. Lastly, sustainable land management practices are emphasized in Soil Erosion Assessment Using the RUSLE Model and Geospatial Analysis: A Case Study of Majuli Island of Assam Together, these contributions underscore the importance of interdisciplinary research and innovative approaches to disaster risk reduction. Let us harness knowledge, technology, and collaboration to create a more resilient future in the face of disasters.

Finally, the editor would like to thank and convey gratitude and congratulation to all the authors, reviewers, publication team (especially Dr. Ravinder Singh, Shri S. K. Tiwari, Shri Shubham Badola and Ms Karanpreet Kaur Sodhi), and readers for keeping their faith on the journal and associating with at over the years to make this periodical a successful blind peer-reviewed open access UGC CARE listed journal. The editorial team expects continuous support and cooperation in the coming years as well.



Surya Parkash, Ph.D.

Landslide Susceptibility Mapping in Darjeeling Hills

Passang Sherpa[1], Uttam Lal[1], Rajesh Kumar[1]

Abstract

Landslides are recurrent natural events that pose significant risks to human settlements and infrastructure, particularly in craggy Himalayan terrains like the Darjeeling Hills. This study aims to examine landslide events in the region, analyze their occurrence, underlying factors, and implications for the local community. Various datasets, including landslide point data, geology maps, road networks, rainfall data, slope maps, and physiography maps, were utilized for spatial analysis of landslides. The findings reveal that landslide occurrences are concentrated in the high and middle altitudinal hills, particularly in areas with extremely steep slopes. The high precipitation and weak geology of the region contribute to the vulnerability of these areas to landslides. Rainfall, road density, slope, and geology were utilized for landslide susceptibility mapping using weighted overlay method in GIS environment. The landslide susceptibility zones were divided into four classes i.e., highly unstable, moderately unstable, moderately stable and stable that cover 1%, 45%, 46% and 7% of the total study area (1265.1 km^2). The findings of the study can be used for mitigation of landslides and land use planning.

Keywords: *Landslides, Darjeeling Hills, Landslide Susceptibility Zonation, GIS*

1. Introduction

Landslides are - widespread and devastating calamity, particularly in the Himalayas, due to the physical makeup of the terrain and the presence of loose rock and debris materials. They are sporadic and simultaneous natural hazards in mountainous regions, leading to altered landscapes and significant losses (De, 2017; Dikshit et al., 2020). One of the primary factors behind landslides is the gravitational force, causing slopes to shift from stable to unstable condition (Chawla et al., 2018). Landslides

[1] Department of Geography, School of Human Sciences, Sikkim University, Gangtok 737102, Sikkim, India

pose significant hydrogeological and man-made elements, posing risks to human settlements, transportation networks, civil infrastructures, and natural resources such as agricultural land and forests (Nad, 2015).

In the Darjeeling Himalayas, landslides are notably prevalent along overflowing water sources that intersect with roads like the 'Hill Cart Road' and other hill-lowland connections (De, 2017). One particularly vulnerable area is near the Upper and Lower 'Pagal Jhoras', where the road has experienced subsidence up to a depth of approximately 7-9 meters since 1979 (Basu, 2001). The region has a history of significant landslides, with documented occurrences in 1899, 1950 (resulting in 127 fatalities), and 1968 (with 667 fatalities) (Pal et al., 2016). The Darjeeling hills are frequently affected by landslides that cause loss of human lives and damage to public and private properties (District Disaster Management Plan Darjeeling, 2022-23). The present study aims to comprehensively identify the multifaceted factors associated with occurrence of landslides in the Darjeeling Hills and to prepare a landslide susceptibility map.

2. Study Area

Darjeeling Hill comprises the northern part of the Indian state of West Bengal. It is situated in the Eastern Himalayan region which is located at a height of 300 to 12000 feet from mean sea level (DCHB, 2011). Darjeeling Hill includes three hilly subdivisions of Darjeeling Sadar, Kalimpong, and Kurseong, comprising an area of 2476 km^2 and hosting a population of 7,90,591 in 2011. Geographically, the Darjeeling district is divided into two large sub-areas i.e., the hill region and the plains region (Nad, 2015).

Kalimpong is a separate district were carved out from the Darjeeling district in 2017 and has not been considered in the present study. Presently, the Darjeeling Hill region consists of two subdivisions named Darjeeling Sadar and Kurseong, comprising an area of 1265.1 km^2. while the Plain region consist of Siliguri Subdivision, comprising an area of 802.01 km^2.

The Darjeeling Hills are bordered by the state of Sikkim to the north, while in the east, they adjoin the captivating district of Kalimpong. To the south, the boundaries of the Darjeeling Hills extend towards the bustling subdivision of Siliguri, and in the west, they share an international border with Nepal (Figure 1).

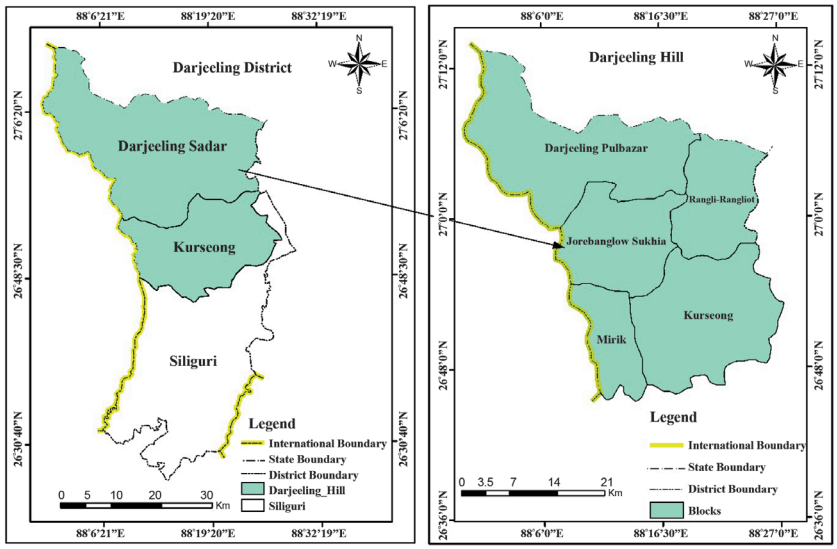


Figure 1: Location Map of the Study Area

Source: District Census Handbook, Darjeeling, 2011.

3. Materials and Methods

The present study focuses on investigating landslides in the Darjeeling Hills, utilizing diverse datasets and information sources. The key datasets employed in the research include landslide point (1991-2017) and geology data were collected from the Geological Survey of India (GSI) Bhukosh platform. Additionally, Road Network Data extracted from Open Street Map is utilized to understand the road infrastructure, including national highways and state highways, connecting the hills to the lowlands. Rainfall Data obtained from the India Water Resource Information System (WRIS) offers annual rainfall expressed in millimeters and records of the normal rainfall over the region. Forest And Buildings removed Copernicus (FAB) digital elevation model (DEM) version 1-0 was obtained from Hawker and Neal (2021). Spatial resolution of DEM is 30m. The Physiography of Darjeeling Hills is collected from Cajee (2018). All the spatial data sets were assimilated at 30 m spatial resolution using UTM 45 N projection system and WGS 84 datum in GIS environment.

Geospatial analysis techniques are then employed to identify the factors associated with landslides. Slope was computed using FAB DEM in GIS environment.

Road density was computed using 1km x 1km mesh size in GIS environment. Datasets related to geology, physiography, slope, road density, and rainfall are integrated and analyzed to assess their influence on landslide occurrences. Subsequently, Landslide susceptibility zonation maps are generated through weighted overlay analysis in GIS environment, considering factors such as slope, rainfall density, road density, and geology. These maps classify areas into highly unstable, moderately unstable, and stable zones, providing valuable insights into the distribution of landslide-prone areas. The study results are visually presented using ArcGIS 10.2, allowing for clear visualization of landslide occurrences, susceptibility zones, and the spatial relationship between influencing factors (Figure 2).

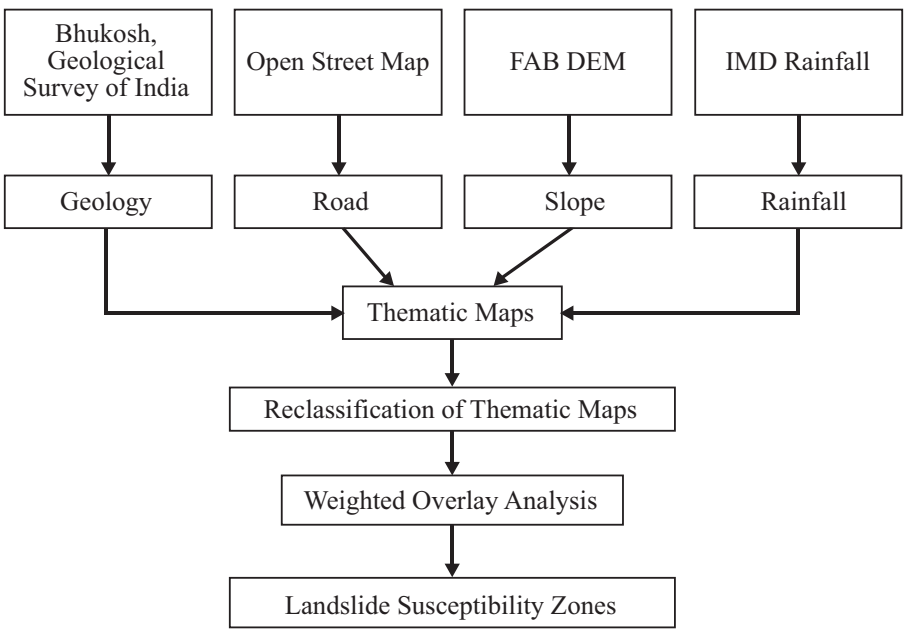


Figure 2: Flow diagram showing Methodology used for Landslide Susceptibility Zonation

4. Results and Discussion

Spatial Analysis of Landslides in Darjeeling Hills

In Darjeeling, a landslide is the more frequently occurring natural disaster and is

caused by several factors such as the geological makeup of the area, slope, rainfall, soil, physiography, and by human interventions. To know the past landslide occurrence in Darjeeling a landslide inventory map is prepared, which is a geospatial representation that identifies and documents the location, extent, and characteristics of past landslides in a given area. It serves as a valuable tool for understanding the distribution and frequency of landslides, which can aid in assessing landslide susceptibility zonation and informing land-use planning, disaster management, and mitigation strategies (Martha et al., 2021).

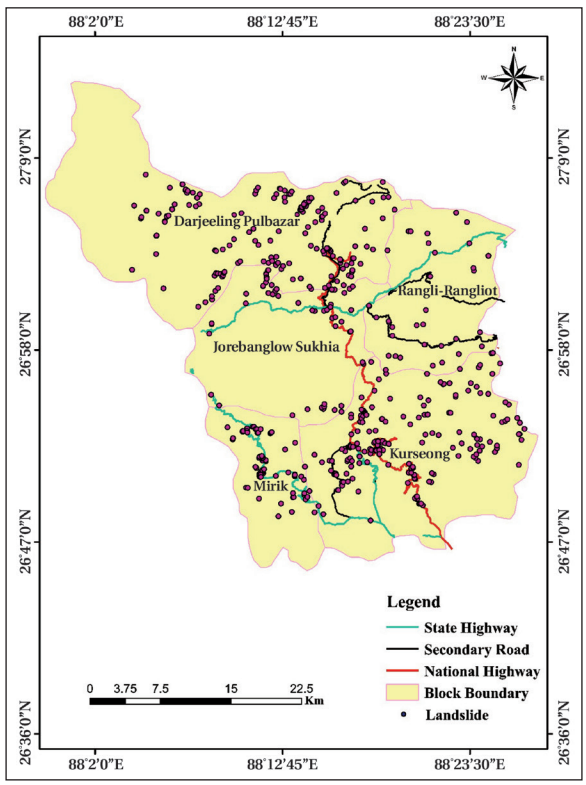


Figure 3: Landslide Inventory Map of Darjeeling Hills (1991-2017)

Source: Bhukosh, Geological Survey of India, extracted on 14/11/2022.

Figure 3 displays landslide occurrences in different blocks of Darjeeling hills from 1991 to 2017, with Kurseong and Darjeeling-Pulbazar areas experiencing a

higher frequency of landslides. These occurrences can be attributed to various factors, including geology, slope, rainfall, physiography, soil, and human activities such as road construction and urban development. The high and middle hills are particularly susceptible to landslides, while the lower hills have fewer incidents.

Darjeeling, Kurseong, and Mirik are prominent towns in the region and are composed of soft schists, phyllite, and gneiss, making them prone to landslides due to their complex physical characteristics, high precipitation, and weak geology (Cajee, 2018).

The slope analysis reveals that these areas mainly fall under extremely steep slopes (34°-66°) to steep slopes (24°-33°), contributing to landslide formation. Combined with the high annual rainfall, the presence of such steep slopes enhances the risk of landslides in the region.

The soil in Darjeeling primarily consists of red and clayey soil, which covers most parts of the area. These soil types are highly susceptible to landslides as they are easily eroded during heavy rainfall (Mitra et al., 2018).

Furthermore, the figure demonstrates that landslides have occurred predominantly along or near the presence of roads, including national highways, state highways, and secondary roads. This indicates that the development of road infrastructure in the Darjeeling hills is contributing to the growing number of landslides in the region. The high amount of average rainfall in Darjeeling, which surpasses normal levels, also plays a significant role in the increasing number of landslides on the hill.

In conclusion, the analysis highlights the key factors influencing landslide occurrences in Darjeeling hills, emphasizing the importance of implementing appropriate measures to manage and mitigate landslide risks. Sustainable land-use practices, slope stabilization measures, early warning systems, and close monitoring of vulnerable areas are essential for safeguarding human lives and infrastructure from the devastating impact of landslides (Cajee, 2018; Mitra et al., 2018).

Factors Affecting Landslide

A landslip is a natural event caused by gravity that results in the falling of elements such as rock, soil, mud, and so on (Fayaz et al., 2022). Various underlying environmental

and human factors influence the occurrence of landslides in any given location. Natural factors include the area's geological makeup, physiographic layout, soil composition, and rainfall patterns. Human qualities or elements include interventions by humans in the form of huge projects such as infrastructure development in the shape of highways, tunnels, and hydropower constructions. Some of the factors which affect landslides are discussed below:

Geology

The core Himalayan structure consists of massive thrusts formed by the rising Indian continent's basement. The Siwalik rocks are folded sedimentary rocks from the Pliocene-Pleistocene era. The Middle Hills are thrust sheets comprising prehistoric limestone and gneiss from the Indian shield. The Greater Himalayas consist of Precambrian gneisses intruded by Tertiary granites. The Darjeeling Himalaya shares the same geology, with prominent formations like Tertiary and Metamorphized Darjeeling Gneiss, Daling Series, and Damuda Series (Gerrard, 1994; Goscombe, 2000) (Figure 4).

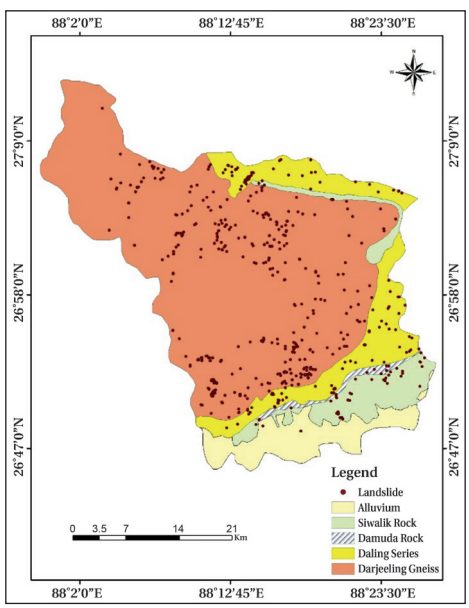


Figure 4: Occurrence of Landslide in different Geology of Darjeeling Hills, (1991-2017).

Source: Bhukosh, Geological Survey of India, Extracted on 17/02/2023

Table 1: Area and number of landslides occurrence in different geological structure (1991-2017)

Geological Structure	Area in Sq. km.	No. of Landslide	Percentage
Darjeeling Gneiss	879.9	410	73.2
Daling Series	177.4	103	18.4
Damuda Rock	13.3	9	1.6
Siwalik Rock	98.1	35	6.3
Alluvium	96.4	3	0.5
Total	**1265.1**	**560**	**100**

Source: Bhukosh, Geological Survey of India, Extracted on 17/02/2023.

The table highlights the dominant geological structure, "Darjeeling Gneiss," covering 879.9 sq. km, with the highest landslide frequency of 410 incidents (around 73.2%). The "Daling Series" and "Siwalik Rock" also have significant landslides (103 and 35 incidents) despite their smaller areas. On the other hand, "Damuda Rock" and "Alluvium" are the least prone to landslides, with 9 and 3 incidents, respectively from 1991-2017 (Table 1).

The occurrence of landslides is high in Darjeeling Gneiss due to its composition of weak metamorphic rocks like quartzites, biotite-kyanite, garnetiferous mica-schists, and sillimanite gneiss (Cajee, 2018). These types of rocks are susceptible to landslides, especially when combined with factors such as high precipitation and steep slopes. In contrast, Damuda rocks are less prone to landslides due to their low porosity, sedimentary formation, and weathering resistance. Their stable and well-layered composition reduces water infiltration and maintains strength over time. However, landslides can still occur under certain conditions, influenced by slope angle, geological structure, and external forces like rainfall or earthquakes (Gerrard, 1994).

Physiography

The Darjeeling Hills exhibit a diverse and intricate physical landscape, ranging from plains to the lofty Sandakphu, featuring steep valleys, Jhoras (streams), and springs. The region is characterized by ridges, valleys, spurs, and various micro-topographical units. It can be categorized into lower hills (200-800m altitude) in the central portion,

middle hills (800m-1400m) with tea plantations in the western and north-eastern parts, and upper hills (above 1400m) hosting peaks like Sandakphu, Phalut, and Singalila. Eroded tracts, tea estates, and majestic peaks shape the distinct geography of the Darjeeling Hills (Cajee, 2018) (Figure 5).

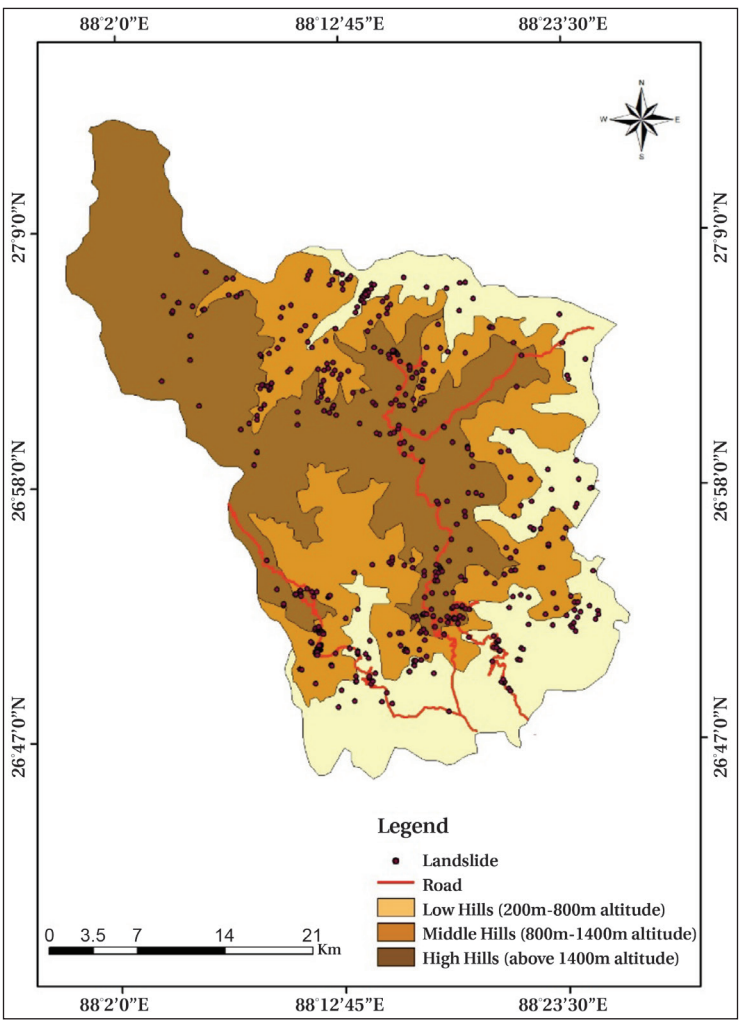


Figure 5: Landslides occurred along different Physiography of Darjeeling Hills (1991-2017)

Source: Adopted & Modified after Cajee, 2018.

Table 2: Area and number of landslides occurrence in different physiography (1991-2017)

Physiography	Area in Sq.km.	No. of Landslide	Percentage
High Hills	528.8	194	34.6
Middle Hills	389.4	233	41.6
Lower Hills	346.9	133	23.8
Total	**1265.1**	**560**	**100**

Source: Bhukosh, Geological Survey of India, Extracted on 17/02/2023.

The table highlights three physiographic zones: "High Hills," "Middle Hills," and "Lower Hills." The "Middle Hills" have the highest landslide frequency (233 incidents) and the highest percentage of landslides (41.6%), indicating greater vulnerability. On the other hand, the "Lower Hills" have the lowest landslide percentage, suggesting they are relatively less prone to landslides during the study period (Table 2).

Areas like Darjeeling, Kurseong, and Mirik, characterized by soft schists, phyllite, and gneiss, are highly susceptible to landslides due to weak geology, high precipitation, and hilly terrain. These factors lead to frequent and significant landslides, causing substantial damage to infrastructure and endangering lives (Dikshit et al., 2020; Sumantra & Ragunathan, 2016).

Rainfall

The landslide has a direct relationship with the structure of the rock formation in the area, the slope of the area, lithology, etc. Darjeeling is composed of relatively new geological formations that are prone to landslides. Though the cause of a landslip varies by location, heavy monsoon rains are frequently to blame in Darjeeling. Precipitation constitutes one of the primary causes of a "geological disaster." The scale of geological disasters and the intensity of rainfall are inversely associated; rain penetration decreases soil strength and friction resistance between soil and bedrock, as well as increasing soil gravity, which causes the geological disaster (Zhang, 2020).

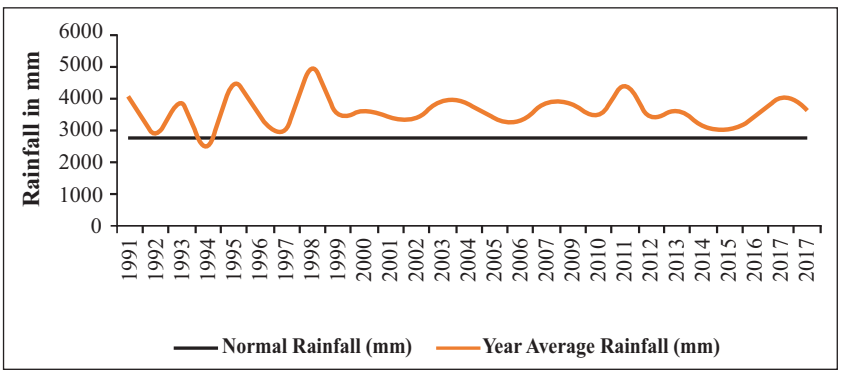


Figure 6: Patterns of rainfall in Darjeeling Hills (1991-2017).

Source: India, Water Resource Information System extracted on 17/04/2023.

Figure 6 indicates a significant deviation of average rainfall in Darjeeling from normal conditions. High rainfall is a critical factor contributing to landslides on steep slopes. In subtropical and tropical climates, such slopes may remain stable until intense rainstorms trigger failures (Tsaparas et al., 2002). Throughout the study period, Darjeeling experienced above-normal rainfall, leading to increased soil moisture and elevated pore pressures, resulting in slope failure and devastating landslides (Dai & Lee, 2001).

Slope

The slope is crucial for researching the formation, progress, and vulnerability of landslides. The horizontal distance across two points is expressed by this topographic feature. The slope is an aspect of the digital elevation model that is studied in the topographical parameter classification. In landslide susceptibility investigations, slopes with the highest landslip frequency are determined by classifying slopes (Cellek, 2020).

Slope, along with other variables such as physiography, geology, and drainage, determines the formation of landslides in any place. Darjeeling is a steep terrain with a slope ranging from 0° to 66°. The Fabdem is used to categorise the slope, based on the natural break (Jenks), the slope has been categorised into four distinct categories: Gentle slopes range from 0° to 11°, moderate slopes range from 12° to 23°, steep slopes range from 24° to 33°, and extremely steep slopes range from 34° to 66° (Figure 7).

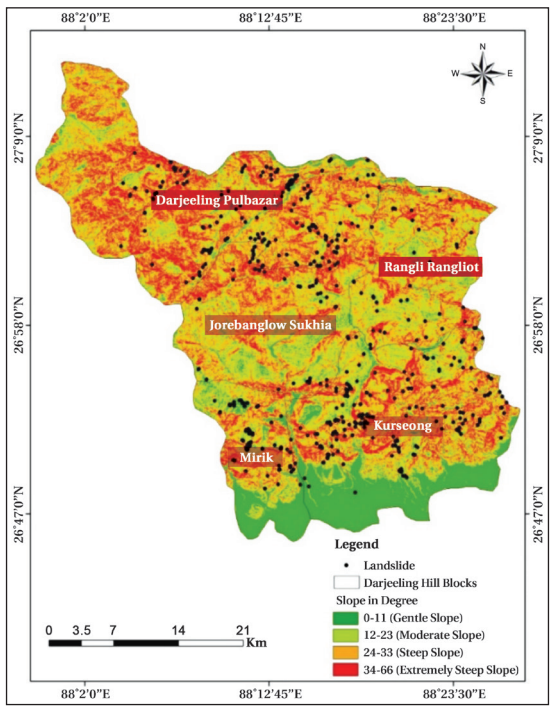


Figure 7: Landslides occurred along different Slopes of Darjeeling Hills, (1991-2017).

Source: Forest and Building removed Copernicus DEM, Extracted on 04/05/2023.

Table 3: Area and number of landslides occurrence along different slope (1991-2017)

Slope	Area in Sq.km.	No. of Landslides	Percentage
Gentle Slope	172	11	3.9
Moderate Slope	371.5	112	20
Steep Slope	454.3	224	40
Extremely Steep Slope	267.3	202	36.1
Total	**1265.1**	**560**	**100**

Source: Bhukosh, Geological Survey of India, Extracted on 17/02/2023.

The data reveals a clear relationship between slope steepness and landslide occurrences. Gentle slopes, covering 172 sq. km, experienced 11 landslides (3.9% of the total), indicating lower vulnerability. Moderate slopes, spanning 371.5 sq. km, had 112 landslides (20% of the total), showing a higher percentage of landslides. Steep

slopes, covering 454.3 sq. km, had 224 landslides (40% of the total), indicating significant vulnerability. Extremely steep slopes, covering 267.3 sq. km, had 202 landslides (36.1% of the total), suggesting the highest vulnerability during 1991-2017 (Table 3). Notably, Darjeeling-Pulbazar and Kurseong blocks, classified as having steep to extremely steep slopes, experienced high landslide occurrences, while Jorebunglow-Sukhia and Rangli-Rangliot blocks, with moderate to gentle slopes, had fewer landslide cases. The occurrence of landslides in Darjeeling is directly related to the slope of the area. Slope characteristics play a critical role in landslide initiation when forces exceed material resilience, leading to collapse and downhill slipping. In addition to slope parameters, natural conditions, weathering, soil moisture, vegetation, and human activity also contribute to landslides (Dong et al., 2021). Understanding these factors is crucial for effective landslide mitigation and disaster management strategies, particularly in areas with steeper terrain.

Soil

Darjeeling hills soils have been formed by both river activity and lithological deterioration. The soils that have formed in the Kalimpong region are primarily reddish due to the abundance presence of phyllites and schist, black soils are encountered rarely. Soils in the district's highlands, which span from west to east along most of the interfluvial zones, are primarily mixed sandy loam and loamy, but those on the southern slopes of Mirik and Kurseong are primarily clayey loam and reddish. Sandy soils are mostly found to the east of the Tista River (Mitra et al., 2018).

Darjeeling has soil types such as sandy and sandy clay (which are generally prone to erosion and instability), and due to the presence of slopes along with the high amount of rainfall in the area, the occurrence of landslides is a continuous phenomenon. In the Darjeeling hills, there has been a high amount of deforestation due to the rapid increase in population leading to build-up area increase due to loss of vegetation and exposure of grounds leading to erosion and subsequent landslides.

Human Intervention in Landslide Events

Human activities have been identified as a significant initiating cause for numerous landslides. Human-caused landslides typically occur on excavated slopes, causing several deaths and extensive damage. Numerous investigations have discovered that

breakdowns on cut slopes are connected with stress release caused by excavation (Zhang, 2012).

Human-induced landslides refer to landslides that are directly caused or significantly influenced by human activities. These activities can directly alter the stability of slopes and trigger landslide events. Here are some examples of human-induced factors that can lead to landslides:

Construction of Road Network

Engineering structures connected with road networks possess a significant influence in generating landslides (Wang et al., 2014). In Darjeeling Hills, during the study period if focused it shows that the landslide is more frequent in the areas where there is a high and medium density of road networks. It explains how in Darjeeling hills landslides are influenced by the road network. In the building of roads, large slopes or tracts were cleared which can lead to greater exposure to rain and leading to slope failure due to the presence of a high amount of infiltration and saturation with the presence of high slopes.

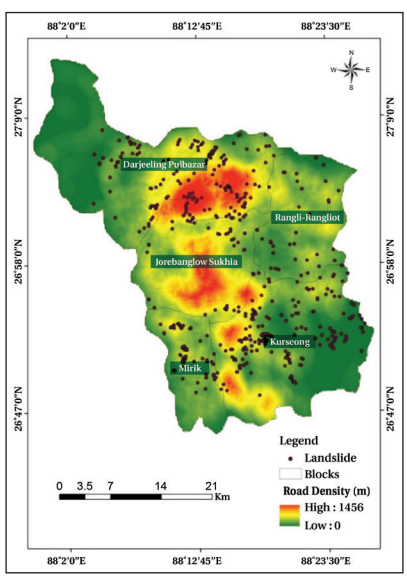


Figure 8: Relationship between Road Networks and Landslides (1991-2017).
Source: Open Street Map, extracted on 06/04/2023.

Table 4: Area and number of landslides occurrence along different road density (1991-2017)

Road Density (m/km)	No. of Landslides	Percentage
0-142	88	15.7
142-331	185	33
331-576	195	34.8
576-879	47	8.4
879-1455	45	8
Total	**560**	**100**

Source: Bhukosh, Geological Survey of India, Extracted on 17/02/2023.

Landslide occurrence is more prevalent in areas with medium and high road network areas compared to low road networks. The occurrence of landslide is frequent in high road density areas (879-1455m) with 45 cases within 63.6 km^2, whereas the occurrence of landslide is less in low road network areas (0-142m) with 88 cases within 413.5 km^2 (Figure 8 and Table 4). This suggests that landslides are commonly observed in hills near road networks, and road construction plays a significant role in their incidence in Darjeeling hills. The construction of roads is widely recognized for its potential to exacerbate landslip activity through the creation of steep and rapidly weathering roadcut cliffs, removal of basal support from hill slopes, increased burden on unstable surfaces, concentration of seepage and runoff, use of blasting during construction causing disturbances, and subsequent vibrations from heavy traffic (Haigh et al., 1995).

Population Growth

Darjeeling Hills' population has grown since the British took it from the Raja (King) of Sikkim and promoted it as a hill resort. When the East India Company initially acquired the area in 1835, it was said to have a population of barely 100 individuals. The Company's decision to develop Darjeeling as a hill resort created an opportunity for people to move and participate in the development process. The indigenous population, predominantly Lepchas, was quickly outnumbered by settlers from Nepal and Sikkim. The population of the Darjeeling Hills has fluctuated over time. However, the Darjeeling Hills have supported a growth rate of more than 20% every

decade on average. Since 1970, the Darjeeling Hills' growth rate has greatly surpassed the district's growth rate (Chhetri & Tamang, 2013).

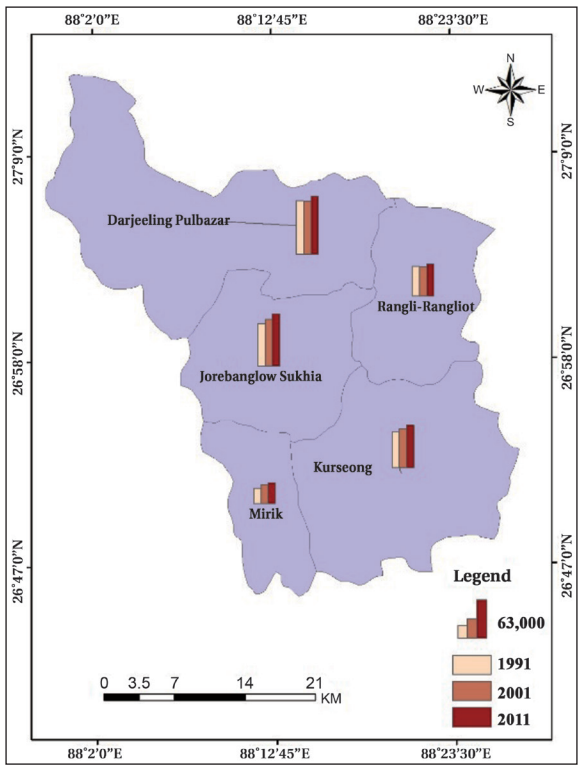


Figure 9: Block-wise Population Growth in Darjeeling Hills (1991, 2001 & 2011)
Source: District Census Handbook, 1991, 2001 & 2011.

Figure 9 shows the block-wise population growth of the Darjeeling Hills. The population in each of the blocks of the Darjeeling Hills is increasing from 1991-2011. Population growth can have an impact on the occurrence of landslides, particularly in areas with steep slopes or unstable terrain. Population growth increases housing and infrastructure demand, causing construction on slopes or landslide-prone areas. Excavation, deforestation, and natural drainage patterns weaken land stability, increasing landslide risk (Crozier et al., 2005). Population growth necessitates land use changes, converting agricultural areas into residential zones, and improper planning can lead to hazardous construction (Carrara et al., 1999).

Categories of landslides

A landslide is the most prevalent natural disaster. Landslides comprise all sorts of mass wasting, funneling, and descending made up of debris, rocks, dirt, and material from the earth sometimes mixed or alone. Landslides are categorized into five types based on the volume of water present: "falling", "toppling", "sliding", "spreading", and "flowing" (Alimohammadlou et al., 2013) (Table 5).

According to Cruden and Varnes, 1996, the following five types of landslides are depicted and described:

a. **Falls**: Falls are sudden movements of geologic masses such as boulders and stones that get separated from upward slopes or mountains. Separation happens at discontinuities like breaks, ligaments, and deposited surfaces, while movement happens via free fall, jumping, and tumbling. The force of gravity, weathering by mechanical means, and the presence of interstitial water all have a major impact on falls.

b. **Topples**: Toppling failures can be defined by the forward motion of the components about some essential point, either below or down along the unit, caused by the forces of gravitation and surrounding units or fluids in cracks.

c. **Slides**: 'Mass wasting' that involves the movement of the materials downward of a 'cohesive block' of soil or rock is referred to as a slide. The factors which trigger the Slide landslide are 'saturation' of the soils with water in the slope and loss of 'shearing strength'. It is often been referred to as 'Slumping'. Rotational slides and longitudinal slides are the two major kinds of slides.

d. **Spread**: The different slides include lateral/horizontal movement over the fairly mild ground. Rapid ground motion, such as an earthquake, induces instability of the damages, cohesionless sediments below a harder, stronger lithological layer.

e. **Flow**: Flow is the landslide that moves the materials downslope in the form of liquid materials.

Table 5: Types of landslides based on 'Varnes' classification of slope movements (Varnes, 1978)

Types of Movement		Types of Material		
		Bedrock	Engineering Soils	
			Predominantly coarse	Predominantly Fine
Falls		Rock Fall	Debris Fall	Earth Fall
Topples		Rock Topple	Debris Topple	Earth Topple
Slides	Rotational	Rock Slide	Debris Slide	Earth Slide
	Translational			
Lateral Spreads		Rock Spread	Debris Spread	Earth Spread
Flows		Rock Flow	Debris Flow	Earth Flow
Complex		Combination of two or more principal types of movement		

Table 6: Landslides based on different attributes in Darjeeling Hills (1991-2017)

Landslide Occurred from 1991-2017 Based on different attributes							
Movement	No. of Land-slide	Material	No. of Land-slide	Activity	No. of Land-slide	Distribution	No. of Land-slide
Fall	4	Debris	386	Active	329	Widening	58
Flow	18	Rockfall	145	Dormant	68	Retrogressive	93
Slide	477	Rock cum Debris	29	Reactivated	77	Enlarging	43
Subsid-ence	61			Stabilised	8	Diminishing	20
				Suspended	76	Confined	315
				Relict	2	Advancing	31

Source: Bhukosh, Geological Survey of India, extracted on 14/11/2022.

Table 6 represents the categories of landslide based on the different attributes in Darjeeling Hills as given by Bhukosh, Geological Survey of India.

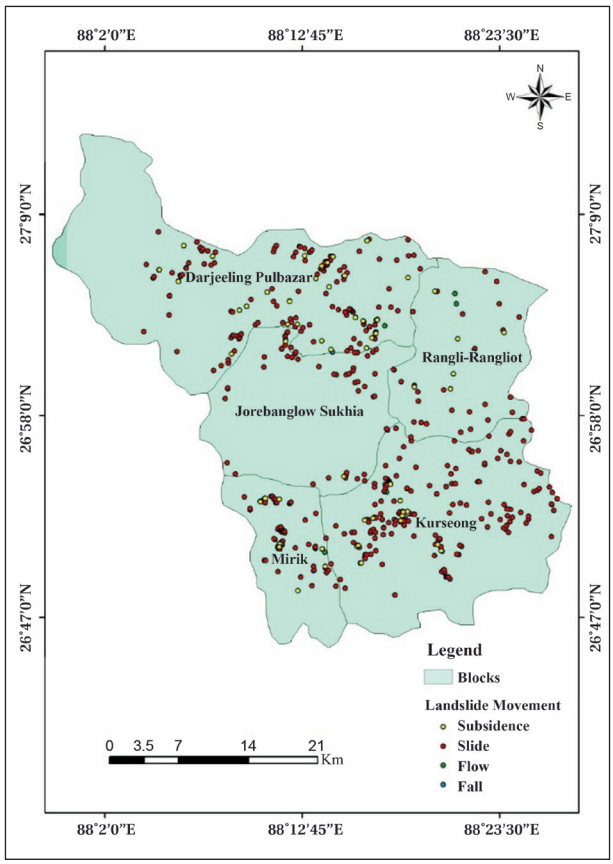


Figure 10: Movement of Landslide occurred in Darjeeling Hills (1991-2017)

Source: Bhukosh, Geological Survey of India, extracted on 14/11/2022.

Figure 10 shows the landslide categories based on movement in Darjeeling hills from 1991-2017. Based on the category of movement, falls in Darjeeling hills have very less occurrence with 4 cases. Whereas slide is the highest occurring landslide type in the Darjeeling hills with 477 cases followed by the subsidence landslide with 61 cases. The maximum of the landslides has occurred due to slide failure and subsidence, which occurs when the soil gets saturated with water and losses its strength to hold.

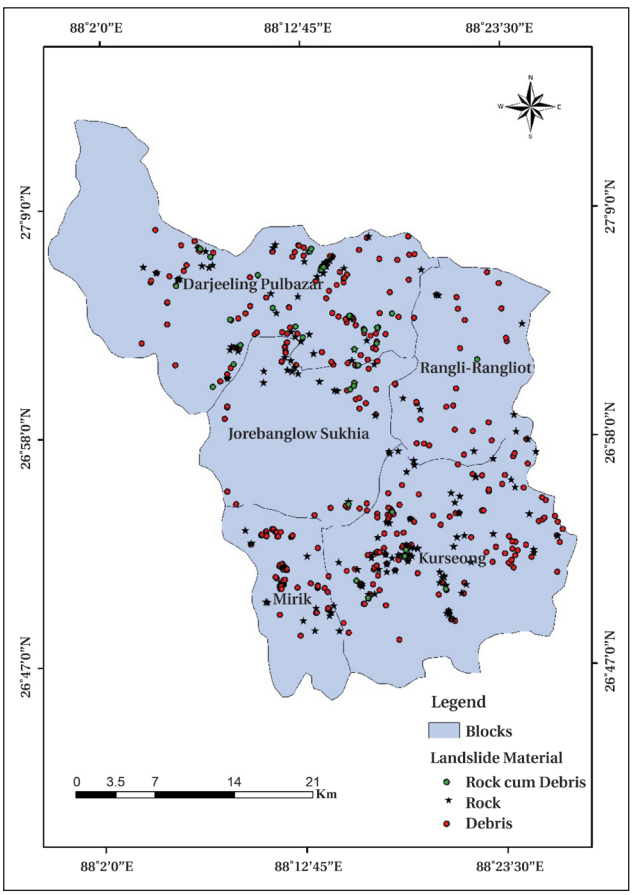


Figure 11: Material of Landslide occurred in Darjeeling Hill (1991-2017)

Source: Bhukosh, Geological Survey of India, extracted on 14/11/2022.

If the material-wise occurrence of the landslide was examined it shows that the Debris slide with 386 cases is the highest occurring landslide in the classification based on material, followed by rockfall with 145 cases and fewer cases of rock cum debris. Most of the debris fall cases can be found in Darjeeling-Pulbazar, Kurseong, and Mirik as these areas fall under extremely steep to moderate slopes which along with the mixture of other factors like rain and geology of the area. Based on Varnes' classification of landslide, it shows that slope failure causes the debris slide, which is mainly induced by rainfall occurrence (Figure 11).

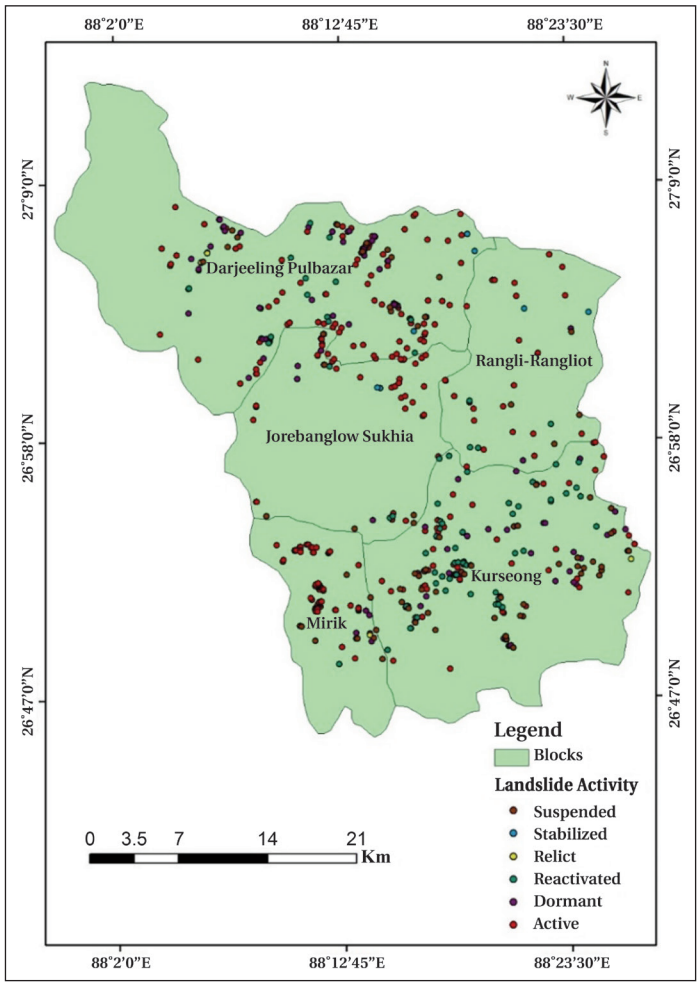


Figure 12: Activity of Landslide occurred in Darjeeling Hills (1991-2017)

Source: Bhukosh, Geological Survey of India, extracted on 14/11/2022.

Figure 12 shows the activity of landslides in the Darjeeling hills from 1991 to 2017. The different categories of landslides and their respective counts are as follows:

Active Landslides (329 cases): These are landslides that are currently occurring or showing signs of movement and pose an ongoing hazard to the area. The reason for the high number of active landslides could be attributed to various factors, such as

heavy and prolonged rainfall, geological conditions, steep slopes, and human activities like deforestation and construction.

Reactivated Landslides (77 cases): Reactivated landslides are those that have experienced movement again after being dormant or stable for some time. The reasons for landslides reactivating could be additional rainfall or seismic activity that destabilizes the slope, leading to movement.

Suspended Landslides (76 cases): Suspended landslides are those where movement has ceased for the time being, but there is a possibility of reactivation in the future. The reasons for the suspension could be reduced rainfall or a temporary change in slope stability conditions.

Stabilised Landslides (8 cases): Stabilized landslides are those where some measures or natural processes have helped to prevent further movement or reduce the landslide's activity. The reason for stabilization could be the implementation of engineering measures like retaining walls or drainage systems.

Relict Cases (2 cases): Relict landslides are old landslide deposits that are no longer active. The reason for their inactivity could be the natural process of erosion and weathering, which has led to the stabilization of the slope over time.

If the landslide classification based on distribution is examined it shows that the cases of confined landslides are maximum in numbers with 315 cases, followed by retrogressive landslides with 93 cases and widening with 58 cases. Once a landslide occurs in a specific area, it often alters the landscape and slope conditions. Confined cases are high in numbers due to the different physical and human factors like slope failure, road cutting, and high intensity of rainfall.

Landslide Susceptibility Zones: Landslide susceptibility zonation (LSZ) maps are extremely useful to policymakers and field engineers when deciding where to execute development plans in hilly terrain, as well as when implementing suitable mitigation strategies in unstable hazard-prone geographic areas (Anbalagan, 1992). Landslide susceptibility mapping/zonation is the classification of terrain into zones based on the time and space likelihood of landslide incident, which includes an overview of the setting, volume, and forecast of future landslip incidence in a region (Shano et al., 2020).

Table 7: Rank and Weightages of Parameters for Landslide Susceptibility Zonation

Sl. No.	Parameters	Classes	Rank	Weightage (%)
1.	Rainfall (in mm)	455-563	1	30
		563-625	2	
		625-687	3	
		687-740	4	
		740-846	5	
2.	Road density (m/km)	0-142	1	20
		142-331	2	
		331-576	3	
		576-879	4	
		879-1455	5	
3.	Slope (in degree)	<11°	1	20
		12°-23°	2	
		24°-33°	3	
		33°-66°	4	
4.	Geology	Alluvial	1	30
		Siwalikh	2	
		Lower Gondwana	3	
		Daling Series	4	
		Darjeeling Gneiss	5	

This study used the four major factors which mainly affect the landslide in the Darjeeling hills. Rainfall, Road density, Slope, and Geology are used to analyze the Landslide Susceptibility Zonation (LSZ) of Darjeeling Hills (Table 7). The main triggering factor of landslides found in Darjeeling is Rain as the mean average rainfall during the study period is 3480 mm along with the presence of extremely steep slopes ranging from 33°-66°. Rainfall serves as one of the strongest and most prominent causative factors that cause slope failure in various parts of the world (Zhang et al., 2011).

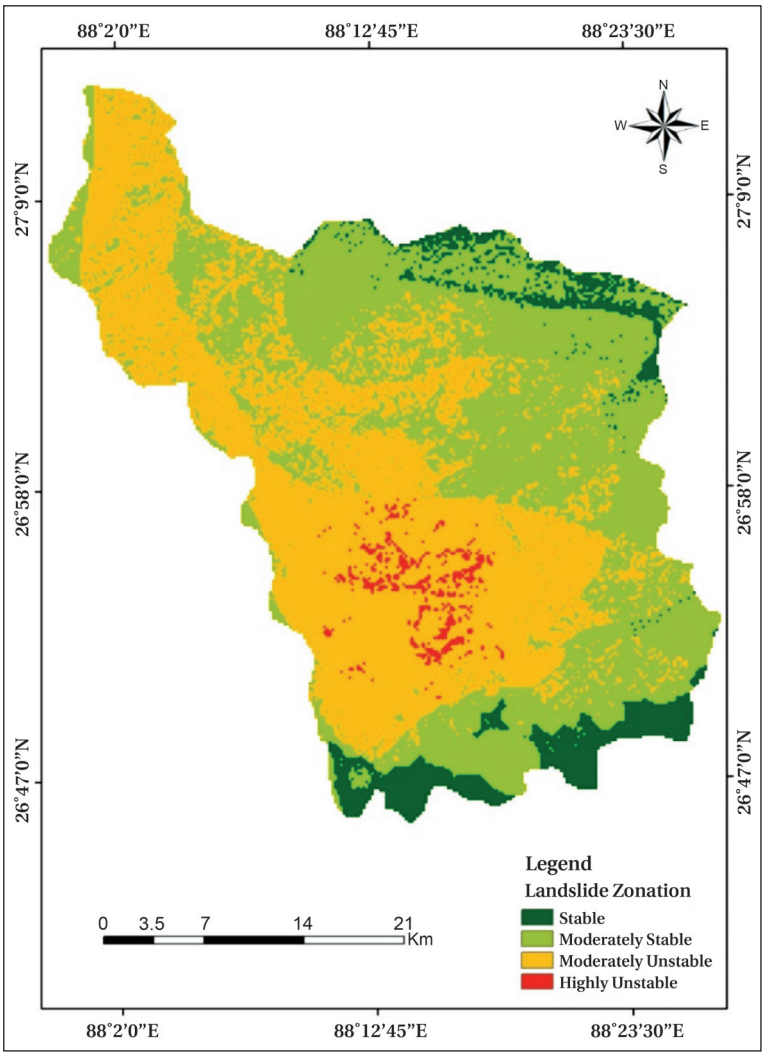


Figure 13: Landslide Susceptibility Zonation Map of Darjeeling Hills

Source: Prepared after data extracted from Bhukosh, Geological Survey of India (GSI)

Landslide susceptibility zonation map of Darjeeling hills was created using four major landslide triggering factors which include rainfall, slope, road density, and geology of the study area (Figure 13).

From the analysis, it is found that about 15.39 km^2 of land is highly unstable. This highly unstable zone lies mostly in the north-western part of the Kurseong block, as this part falls under the extremely steep slope category. Approximately 573.26 km^2 of the area falls under a moderately unstable zone, as these areas are dominated by built-up areas along with high road density. Around 582.88 km^2 falls under a moderately stable zone, covering most of the remaining areas, as this region has low road density, as shown in Figure 8, indicating low human settlement. The remaining 93.57 km^2 area falls under the stable zone, as it encompasses the foothills of the Darjeeling hills.

From the above Landslide Susceptibility Zonation map, it can be observed that landslides are more prone to steeper slopes that receive a high amount of average rainfall. The southern frontier of the Darjeeling-Bhutan Himalaya receives among the highest yearly precipitation (3000-6000 mm) and frequently experiences severe rains (up to 800 mm per day) throughout the entire southern Himalayan edge due to multi-scale interaction between monsoonal airflow and regional terrain (Prokop, 2017).

5. Findings and Conclusions

This study reveals that landslide occurrence is most frequent in the Darjeeling Gneiss geological formation with 410 cases, followed by the Daling series with 103 cases, Siwalik rocks with 35 cases, Damuda rocks with 9 cases, and alluvium with only 3 cases during the study period from 1991-2017 Darjeeling hills.

The "Middle Hills" have the highest landslide frequency with 233 incidents. The "High Hills" rank second with 194 landslides, and the "Lower Hills" have the lowest landslide count, 133 incidents. "Middle Hills" are the most vulnerable to landslides, while the "Lower Hills" are relatively less prone during the study period. These findings are crucial for effective disaster management and mitigation in the region.

Landslide occurrences were most frequent on steep slopes (24° - 33°) with 224 cases, followed by extremely steep slopes (34°- 66°) with 202 cases, moderate slopes (12° - 23°) with 112 cases, and gentle slopes (0° - 11°) with only 22 cases during the study period from 1991-2017 in Darjeeling hills.

Landslide occurrence is more prevalent in areas with medium and high road network areas compared to low road networks. The occurrence of landslide is frequent in high road density areas (879-1455m) with 45 cases within 63.6 km^2, whereas the

occurrence of landslide is less in low road network areas (0-142m) with 88 cases within 413.5 km^2.

The research highlights the crucial role of rainfall in triggering landslides in Darjeeling Hills. Higher-than-normal rainfall during the study period increased the moisture content in the soil, exceeding the threshold for slope stability, and leading to devastating landslides.

The study provides valuable insights into the occurrence, frequency, and patterns of landslides in the Darjeeling Hills. Landslides pose significant risks to human settlements and infrastructure in this hilly terrain. Understanding the underlying factors, such as slope characteristics and rainfall, is essential for effective disaster preparedness and infrastructure planning. To enhance community resilience and reduce the impact of landslides, policymakers and disaster management authorities must prioritize the implementation of early warning systems and comprehensive disaster management plans. Institutional arrangements, such as the District Disaster Management Authority, play a crucial role in coordinating response and relief efforts during landslide events. By incorporating findings of the study into decision-making processes, the region can be better equipped to mitigate the impact of landslides on lives and livelihoods. Proactive measures and investments in disaster management strategies are vital to safeguarding the local community and infrastructure from the recurrent and devastating effects of landslides in the Darjeeling Hills.

References

1. Alimohammadlou, Y., Najafi, A., & Yalcin, A. (2013). Landslide process and impacts: A proposed classification method. *Catena*, 104, 219-232.
2. Anbalagan, R. (1992). Landslide hazard evaluation and zonation mapping in mountainous terrain. *Engineering geology*, 32(4), 269-277.
3. Basu, S. R. (2001, December). A systematic study of landslides along the arterial routes to Darjeeling and their control. In *Geotechnical Engineering–Meeting Society's Needs, Proceedings of the 14th Southeast Asian Geotechnical Conference* (pp. 10-14).
4. Cajee, L. (2018). Physical aspects of the Darjeeling Himalaya: understanding from a geographical perspective. *IOSR Journal of Humanities and Social Science*, 2(3), 66-79.
5. Carrara, A., Cardinali, M., Guzzetti, F., & Reichenbach, P. (1999). Use of GIS technology in the prediction and monitoring of landslide hazards. *Natural Hazards*, 20(2-3), 117-135.
6. Cellek, S. (2020). Effect of the slope angle and its classification on a landslide. *Natural Hazards and Earth System Sciences Discussions*, 1-23.
7. Chawla, A., Chawla, S., Pasupaleti, S., Rao, A. C. S., Sarkar, K., & Dwivedi, R. (2018). Landslide Susceptibility Mapping in Darjeeling Himalayas, India. *Advances in Civil Engineering, 2018*, 1-17.
8. Chhetri, B., & Tamang, L. (2013). Population growth and associated problems: a case study of Darjeeling Town. *International Journal of Humanities and Social Science Invention*, 2(5), 63-67.

9. Crozier, M. J., & Glade, T. (2005). Landslide hazard and risk: issues, concepts, and approach. *Landslide hazard and risk*, 1-40.
10. Dai, F. C., & Lee, C. F. (2001). Frequency–volume relation and prediction of rainfall-induced landslides. *Engineering geology*, 59(3-4), 253-266.
11. De, S.K. (2017). Landslides and human interference in Darjiling Himalayas, India. *Revista de Geomorfologie*, 19, 44-57.
12. Dikshit, A., Sarkar, R., Pradhan, B., Segoni, S., & Alamri, A. M. (2020). Rainfall induced landslide studies in Indian Himalayan region: a critical review. *Applied Sciences*, 10(7), 2466.
13. District Disaster Management Plan Darjeeling (2022-2023). District disaster management plan Darjeeling. Govt. of West Bengal, 1-229.
14. Dong, J., Wang, C., Huang, Z., Yang, J., & Xue, L. (2021). Dynamic response characteristics and instability criteria of a slope with a middle-locked segment. *Soil Dynamics and Earthquake Engineering*, 150, 106899.
15. Fayaz, M., Khader, S. A., & Rafiq, M. (2022). Landslides in the Himalayas: Causes, Evolution, and Mitigation—A Case Study of National Highway 44, India. In Disaster Management in the Complex Himalayan Terrains: Natural Hazard Management, Methodologies and Policy Implications (pp. 43-58). *Cham: Springer International Publishing*.
16. Gerrard, J. (1994). The landslide hazard in the Himalayas: geological control and human action. In *Geomorphology and natural hazards* (pp. 221-230). Elsevier.
17. Goscombe, B. E. N., & HAND, M. (2000). Contrasting P–T paths in the Eastern Himalaya, Nepal: inverted isograds in a paired metamorphic mountain belt. *Journal of Petrology*, 41(12), 1673-1719.
18. Government of West Bengal Office of District Magistrate, District Disaster Management Plan, Darjeeling (2022). Retrieved on 30.06.2023 from https://darjeeling.gov.in/notice/district-disaster-management-plan-darjeeling-2023-24/
19. Government of West Bengal Office of District Magistrate, District Disaster Management Plan, Darjeeling (2023). Retrieved on 30.06.2023 from https://darjeeling.gov.in/notice/district-disaster-management-plan-darjeeling-2023-24/
20. Haigh, M. J., Rawat, J. S., Rawat, M. S., Bartarya, S. K., & Rai, S. P. (1995). Interactions between forest and landslide activity along new highways in the Kumaun Himalaya. *Forest Ecology and Management*, 78(1-3), 173-189.
21. Martha, T. R., Roy, P., Jain, N., Khanna, K., Mrinalini, K., Kumar, K. V., & Rao, P. V. N. (2021). Geospatial landslide inventory of India—an insight into occurrence and exposure on a national scale. *Engineering geology*, 18(6), 2125-2141.
22. Mitra, D., Bhandery, C., Mukhopadhyay, A., Chanda, A., & Hazra, S. (2018). Landslide risk assessment in Darjeeling hills using multi-criteria decision support system: a Bayesian network approach. *Disaster risk governance in India and cross cutting issues*, 361-386.
23. Nad, C. (2015). Landslide Hazard Management of Darjeeling Hill-A Critical Need for Inhabited. *International Journal of Humanities and Social Science Invention, 4(3)*, 48-60.
24. Pal, R., Biswas, S.S., Modal, B., & Pramanik, M.K. (2016). Landslides and Floods in the Tista Basin (Darjeeling and Jalpaiguri Districts): Historical Evidence, Causes and Consequences. The Journal of Indian Geophysical Union, 20(2), 209-215.
25. Prokop, P., & Walanus, A. (2017). Impact of the Darjeeling–Bhutan Himalayan front on rainfall hazard pattern. *Natural Hazards, 89*, 387-404.
26. Shano, L., Raghuvanshi, T. K., & Meten, M. (2020). Landslide susceptibility evaluation and hazard zonation techniques–a review. *Geo-environmental Disasters*, 7(1), 1-19.
27. Sumantra, S. B., & Raghunath, P. (2016). Causes of Landslides in Darjeeling Himalayas during June-July, 2015. Journal of Geography and Natural Disasters, 6(173), 2167-0587.
28. Tsaparas, I., Rahardjo, H., Toll, D. G., & Leong, E. C. (2002). Controlling parameters for rainfall-induced landslides. *Computers and geotechnics*, 29(1), 1-27.
29. Wang, X., Zhang, L., Wang, S., & Lari, S. (2014). Regional landslide susceptibility zoning with considering the aggregation of landslide points and the weights of factors. *Landslides*, 11, 399-409.
30. Zhang, F., Liu, G., Chen, W., Liang, S., Chen, R., & Han, W. (2012). Human-induced landslide on a high cut slope: a case of repeated failures due to multi-excavation. *Journal of Rock Mechanics and Geotechnical Engineering*, 4(4), 367-374.
31. Zhang, L. L., Zhang, J., Zhang, L. M., & Tang, W. H. (2011). Stability analysis of rainfall-induced slope failure: a review. *Proceedings of the Institution of Civil Engineers-Geotechnical Engineering*, 164(5), 299-316.
32. Zhang, Y. (2020). Research on the relationship between precipitation and landslide. *In E3S Web of Conferences* (Vol. 198, p. 04027).
33. Hawker, L. & Neal, J. (2021). FABDEM V1-0. https://doi.org/10.5523/bris.25wfy0f9ukoge2gs7a5mqpq2j7

Assessing Causes and Impacts of Landslides in the Sikkim Himalaya, India

Dilli Ram Dahal[1], Vimal Khawas[2], Prabuddh Kumar Mishra[3], Aster Pradhan[1]

Abstract

Landslide has been common phenomenon in Sikkim after earthquakes. The occurrence of landslides is ascribed to adverse geology, high rainfall, earthquakes, toe erosion, slope instability, vibrations, stone chips quarrying, poor drainage and lack of timely rim treatment at reservoirs sites at Dikchu, Rongli, Chungthang, Ranipul, Legship and Saagbari. The mean area (m^2) and failed volume (m^3) of the classified landslides is around 227176m^2 (cumulative area=10904044m^2) and 14884033m^3 (cumulative volume=714433604m^3), respectively. Among the four districts, East district has witnessed the highest number of landslides, followed by North, South and West districts of Sikkim because the state average annual rainfall has never gone down below 2,000mm in the last 10 years (2522.92mm) (2012-2022). The participants during PRA consultation ascribed the causes of the landslides to developmental activities (25%), catchment degradation/deforestation (21.43%), rainfall and drainage (17.86%), land use transformation (14.29%), cloudburst events (10.71%), adverse geology (7.14%), water impoundment (3.57%) and seismic events/earthquakes, respectively. The landslide events disrupt tourist movements, blockage of national and state highways, water supply pipeline causing shortage of drinking water in the municipal bodies of Sikkim.

Keywords: *Landslide, Rainfall, SSDMA, Earthquakes, Sikkim Himalaya*

[1] PG Extension Centre of Geography, Sikkim University, Department of Geography, Sikkim Government College, Namchi, Sikkim 737126, India
[2] Special Centre for the Study of North East India, Jawaharlal Nehru University- New Delhi -110067
[3] Department of Geography, Shivaji College, University of Delhi, New Delhi - 110027, India

1. Introduction

Landslide has been a most common phenomenon in Sikkim after earthquakes. Owing to its location in the seismically active zone, this young state has been severally hit by landslides and earthquakes of varying magnitudes during 2006-2023. Further, its geographical location exposes it to geological, meteorological and hydrological disasters. In the contemporary era, landslides caught attention due to their considerable impact on the national highways/state highways, tourists movement, rural roads and riverine mega- infra structures (dams and barrages) etc. The earthquake-induced and rainfall-triggered landslides are common in Sikkim (Bhasin et al.2023). Recently, Uttarakhand High Court while addressing a PIL over the lack of compliance to the Doon Valley notification said that 'disasters in the Himalayan states are completely man-made'[1] .

According to IPCC's special report on "*Managing the Risks of Extreme Events and Disasters to Advance Climate Change Adaptation*" there is a high likelihood that the frequency of shallow landslides would increase owing to rise in temperature and rainfall extremes (Sultana & Tan, 2021).In the contemporary era, mostly satellite-based interferometric synthetic aperture radar (InSAR) has been utilised for detecting and monitoring hill slope movements (Crosetto *et al.*, 2016; Lacroix *et al.*, 2020; Aslan et al., 2021).The review of literature and governments records showed that landslide in Sikkim is mostly caused by incessant rainfall, high magnitude earthquakes, fragile geology, and catchment degradation. Majority of the landslide in Sikkim is triggered by the average monsoon rainfall of 350mm/day which can reach upto 500 mm during cloudburst events (Gurung & Dar, 2023). Alternatively, the state has also experienced smaller Rock Slope Failures (RSF) after the major earthquake of 2011 (Bhasin *et al.* 2023). States rapid increase in population since 1991 census, higher rate of urbanisation (25.26%) (Census, 2011) and a rapid increase in the number of developmental projects and pharmaceuticals has led to greater stress on the fragile landscape of Sikkim. The study primarily focuses upon the classification and characterisation of the landslides with regard to area, depth and failed volume of the landslides individually. Besides, probable cause of the landslides and its impacts (damage) and *ex-gratia* provided to the landslide victims by the authority in 2020-2022 has been reported. Through this

[1] The Times of India, New Delhi, Thursday, September 7 2023

work, the researchers mainly address the following Research Questions (RQs) (i) What are the causes of increasing incidences of landslides in Sikkim? (ii) What is the extent of the failed volume and mean area of the landslides individually? (iii) Does the ex-gratia amount provided to the landslide victims economically sufficient during the occurrence of the landslides? The study can provide useful information to the citizens, especially to the line departments to frame specific strategies to cope up with increasing incidences of landslides in the era of contemporary climate change.

1.1. Description of Study Area

Sikkim, a small and unique land with diverse topography, climate, and vegetation is a NE state of the Indian union, its 7096 km^2 of the geographical area entirely lies in Eastern Himalaya between 27° 04'46" and 28° 07'45" North latitude and 88°00'56" and 88° 55'25'East longitude (Census, 2011). The topography is rugged as most of its land area is occupied by greater and lesser Himalaya. It is a landlocked Indian state surrounded by Tibet in the North and NE, the Himalayan Kingdom of Bhutan in the SE, Nepal in the West, and the Darjeeling district of West Bengal in the South (GSI, 2012). The state is characterized by mountainous terrain. Almost, the entire state is hilly, with an elevation ranging from 284m at the confluence of Teesta and Rangit near Chitrey, Kalimpong district, West Bengal to 8,598m at the summit of Mt. Kanchenjunga (8,598m). For the administrative purpose, Sikkim has been reorganized into six districts (Mangan, Gangtok, Geyzing, Namchi, Pakyong, and Soreng) and 18 sub-sub-districts by the authority. The states geology is too young, as it is surrounded by young fold mountains. The formation is still ongoing with strongly folded and faulted strata in various locations. The entire state of Sikkim lies in zone IV of the seismic zonation map of India, the seismic zone IV is broadly associated with seismic intensity VIII on the Modified Mercalli Intensity[2]. The average annual normal rainfall of the state is 2544.40 mm (CISM&HE, 2005). Throughout the year, precipitation in Sikkim Himalaya varies greatly. Periods of heavy rain in Sikkim contributes to rapid erosion and weathering of the rock mass, and raise groundwater levels, reducing the stability of natural slopes (Bhasin et al. 2002) (Figure 1). Sikkim is the least populated state in India, with a population of around 610577 persons with a population density of only 86/km^2 (Census, 2011).

[2] Disaster Mitigation and Management Centre Report Uttarakhand Secretariat, 2011

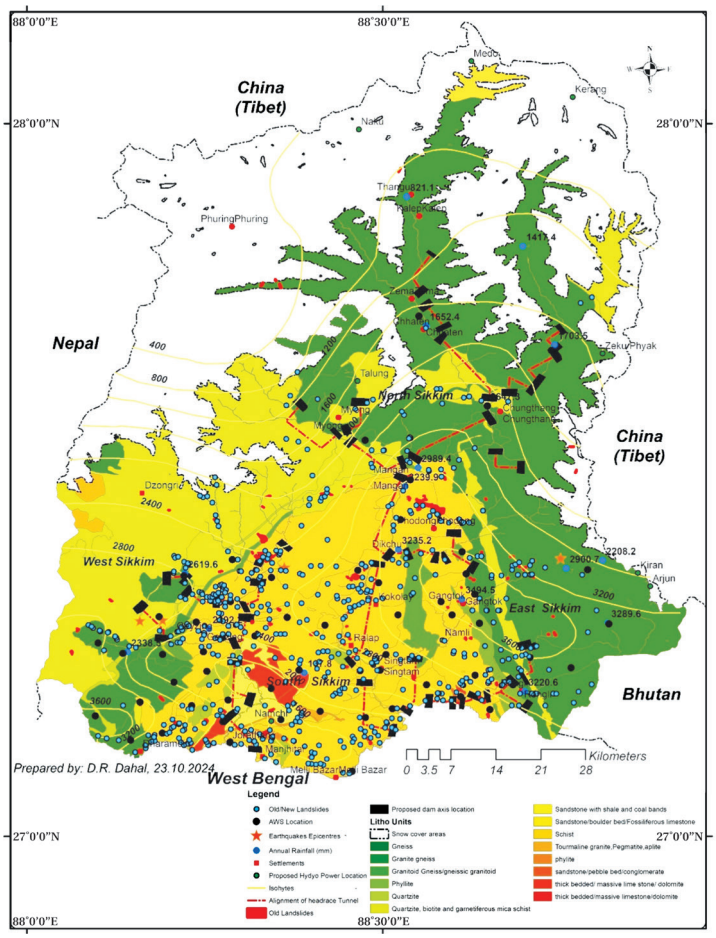


Figure 1: Relative location of landslides points/polygons, past earthquakes epicentres, and a concise overview of the proposed dam axis location and tunnel alignment on the geological map of Sikkim, India

2. Database and Methodology

This study is based on primary and secondary sets. The study is based on transect/ field work carried out in the landslide affected areas in North, East and West districts of Sikkim. Tabulated data on the major landslides of Sikkim (old and new) were analysed to find out the area, failed volume, causes and impacts of the landslides. Before going

to the field, a list of geological/ non-geological factors causing landslides has been prepared and the list were shared with the respondents (about 40 participants) for pair wise ranking on a scale 1-8. Secondary datasets were mainly derived from the SSDMA web portal, Government of Sikkim, local newspapers (Sikkim Express, Summit Times and Face Book etc). LULC retrieved from Copernicus web portal and Isohyet map of Tejwani (1981) has been used to superimpose landslide points/polygons over the rainfall zones receiving high, medium and low rainfall and the geological map of the state. Structural framework of the study has been divided into pre-field stage, field stage and *post-field* stage and the steps followed are described below in a flow chart (Figure 2) and the list of datasets/tools utilised in the present study is mentioned below (Table 1).

Pre-Field Stage

- Initial thought for the preparation of concept note on the landslides and causative factors and map-based inquiry though Swiss maps, Google Earth, Landsat imagery and government reports
- Selection and delineation of the reported landslides, desk work on the reported/seasonal landslides (newspaper/ media) of Sikkim ad causative factors through google scholar (Scopus / UGC Care/ peer-review journals, government reports, newspaper and media etc.)

Field Stage

- Field work regarding spatial attributes of the landslides
- Setting of the research objectives and research questions
- Compilation of the secondary data sets and primary data from the field
- Spatial layer of landslide/past earthquakes epicentres (points and polygons). roads using QGIS/ArcGIS software and attributes generation (type of landslide, area and failed volumes etc.)
- PRA consultation regarding causative factors of the landslide
- Ranking of the causative factors as per PRA consultation.

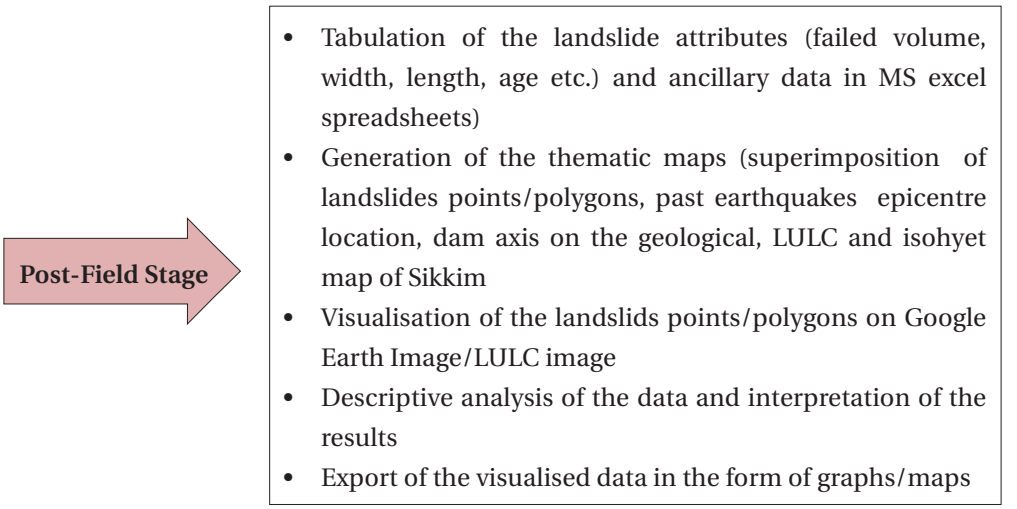


Figure 2: Flow chart showing the structural framework of the study

Table 1: Datasets/tools used for the study

Thematic maps/data/reports/ software	Sources
Swiss map of Sikkim	Department of Geography, Visva Bharati Santiniketan-731235
Google Earth Pro *Ver.* 7.3.4.8642	http://www.googleearth.com;accessed on 17.05.2022
QGIS Desktop *Ver*. 3.22/ArcGIS	http://www.qgis.com;installed on 12.04.2020
Global Positioning System	Garmin Etrex
Past Earthquakes epicentre location	Gazetteer of Sikkim (2013), Indian Meteorological Department, Government of India
Average annual rainfall (mm) at district /state level 2011-2022	Hydrome Division, India Meteorological Department, New Delhi
Old landslides points (1962-63)	Survey of India topographical maps at 1:50K
New landslides points	Landsat satellite imageries and google earth
Geological map of Sikkim	GSI, 2012
Isohyte map of Sikkim	Tejwani, 1981

Global Land cover, 2019 Landcover classification (*discrete classification*)	*https://land.copernicus.eu/global/products/lc, accessed on 03/03/ 2022*
List of the factors causing landslide were identified during PRA consultation by landslide affected people	Respondents from East, West and North districts of Sikkim

3. Results and Discussion

(i) District Wise Classification and Characterisation of Landslides

In this study, attempt has been made by the researchers to locate and map the occurrence of major and reported landslides in Sikkim along with their area (m^2) and the failed volume (m^3) individually. The Sikkim Himalaya is characterised by a mountainous topography and it is susceptible to various kinds of hazard which often turn into disaster. About 1,569 landslide occurrences in the state has been reported (NRSC, 2023). Conversely, 141 landslides have been reported in the NE states including Sikkim in 2020 based on newspapers, online media, SDMA reports, GSI reports and field visits (NESAC, 2020). The forms of landslide vary from literature to literature. The incidence of the landslides in the districts/state has increased because the state average annual rainfall has never gone down below 2,000 mm in the last 10 years (2522.92 mm (2012-2022) (Figure 3).

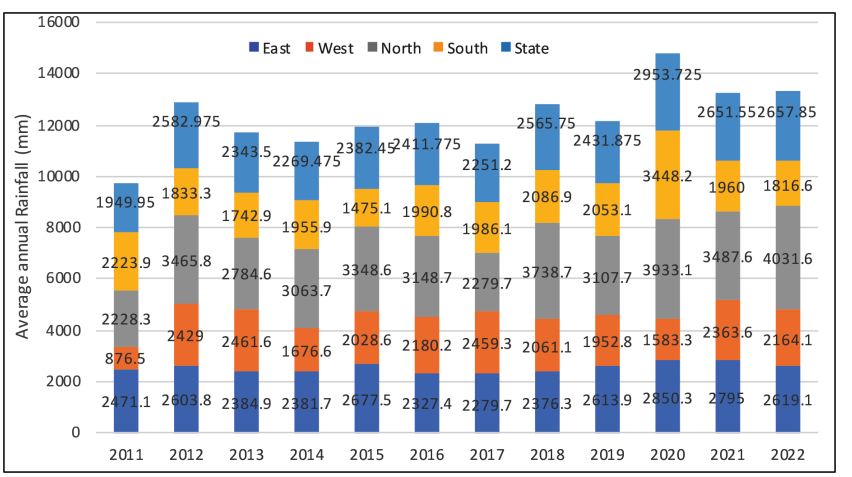


Figure 3: State vs. districts average annual rainfall (2011-2022)

During monsoon season, heavy rainfall increases the possibility of landslides and flashfloods (SSDMA, 2012). The study by Singh (2014) reported occurrence of 552 landslides in Sikkim with an average occurrence of 138 landslides per districts. Database of the landslides occurred between 1999-2014 and some of the major landslides occurred during 2014-2022 reported by newspaper and media such as Sikkim Express, Sikkim Chronicle, Summit Times and landslide victims in the social media platforms has been discussed (Figure 4A, 4B & 4C) (Table 2). The district wise characterisation of the landslides is in (Table 3A, 3B & 3C).

Table 2: District wise distribution of landslides in Sikkim vis a'- vis rainfall

District	No. of Landslides (SSDMA, 2012)	No. of Landslides (Singh, 1999- 2014)	Only seasonal landslides reported by newspaper and Media (2014-2020)	District average rainfall (mm) of 11 years * (2011-2022)	Annual average rainfall(mm) of 11 years* (2011-2022)
West	32	91	17	2019.72	2454.34mm
South	23	77	16	2047.73	
East	36	227	42	2531.72	
North	17	157	11	3218.17	
Total	108	552	89	2454.34	

Source: Compiled by the researcher through literature review and filed work[3]

* computed by the author based on the rainfall database retrieved from http://hydro.imd.gov.in/hydrometweb/(S(uw4ptqehyw3huc452eqfpi55))/DistrictRaifall.aspx

[3] Sources include SSDMA (2012), Singh (2014), field work, Sikkim Now, Sikkim Express, Sikkim Chronicle, Summit Times and landslide victims in the social media platforms

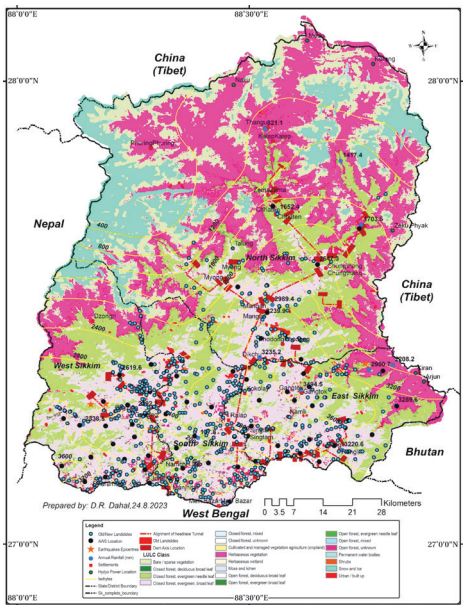


Figure 4A: Landslides points superimposed over different land use and land cover class along with isohyets

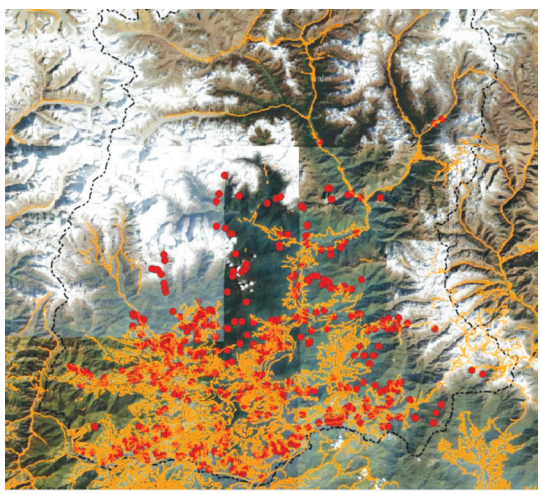


Figure 4B: Point cloud of the landslides superimposed on the road network of Sikkim
Image: *Yandex satellite image*

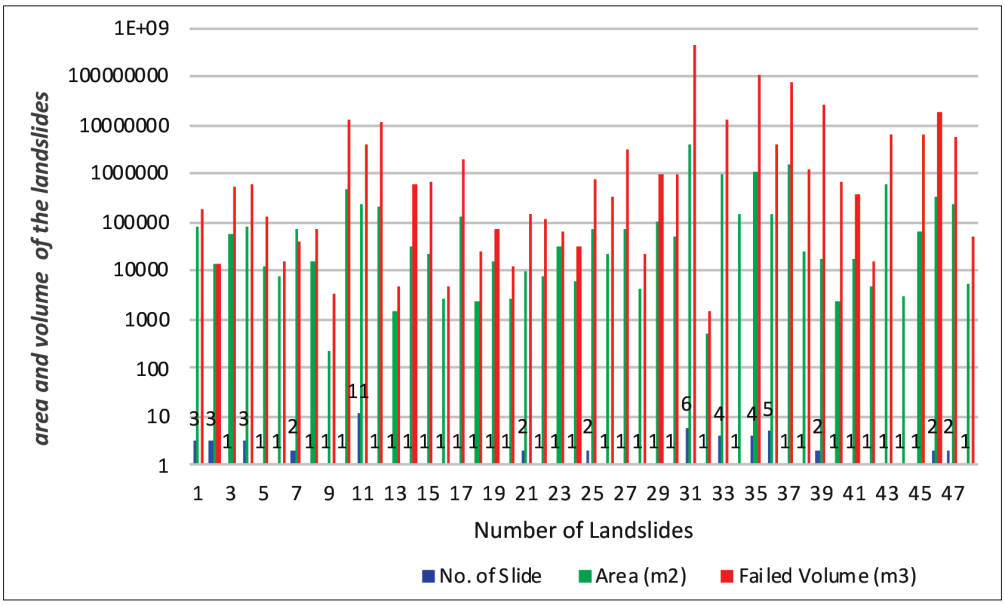


Figure 4C: Number of landslides vs. area and the vozlume of the landslides

(ii) Scenario of Landslides in East Sikkim (Gangtok & Pakyong District)

In East Sikkim mostly complex, planner, debris, translational, massive subsidence and rotational, subsidence, rotational, active subsidence, wedge type failure, rotational controlled by wedge failure, rock topple and complex: translational type mainly rock fall, debris fall wedge type dominates, complex-translational type dominating, mainly wedge type, block and wedge failure type of landslides are pre-dominant. They are classified and their failed volume, area, damage and causative factors has been presented in a tabular form.

Mostly complex type of slide occurred in East district due to failure start suddenly in a small area and spread rapidly. Often the initial failure is a slump, but in some material, movement occurs for no clear reason. The causes of this type of landslide are due to adverse geology, rainfall, toe erosion, steep slope, surface runoff, sheared rock, toe cutting and high-water regime. Secondly, rotational types of slides are dominant due to sheared rocks, ground water, toe erosion, rock floor, adverse geology, wet agriculture proactive, vibrations due to developmental activities, stone chips quarrying,

steep slope and poor drainage. Thirdly, occurrence of subsidence type of slide is ascribed to steep slope, weak geology, excessive water runoff, slope, vibrations due to developmental activities, unstable slope with deposits of boulders, untimely treatment of landslides in the periphery of the water pondage created by public and private hydro-power developers at Dikchu (area of pondage:43.1ha), Rongli, Chungthang (area of pondage:1.31ha), Ranipul (near Namli), Rangti near Saagbari and Legship (area of pondage: 20.4 ha) etc. As medium to large sized water pondage (water impoundment) exists in the mid and lower stretch of Tista and Rangit river and its tributaries in Sikkim, Kalimpong and Darjeeling district, West Bengal.

Table 3A: Classification and characterisation of landslide: East Sikkim

Types of Slide	No. of slide	Area (m^2)	Failed Volume (m^3)	Damaged Done	Causes
Complex	6	3899000	418350000	Road, agriculture, Forest, Habitation, NH 31A, Trees, Road cut off since 1997	Toe erosion, adverse geology, steep slope, Surface runoff, Sheared rock, Toe cutting, high water regime
Planner-debris slide	1	500	1500	forest/ agricultural land	Surface water, adverse geology-toe cutting
Translational	4	974000	12030000	Road, forest, Pachak village, Pache-Samsing road, Agricultural land	Steep slope, toe erosion, ground water, sheared slope farming materials, Down slope dipping foliation, toe cutting, Down slope dipping Daling group of rocks, Water, adverse geology

Types of Slide	No. of slide	Area (m^2)	Failed Volume (m^3)	Damaged Done	Causes
massive subsidence and rotational	1	150000	0	Pache-Samsing road, Agricultural land	Excessive Ground water thick slope material
Subsidence	4	1088000	102415000	Road, Agriculture, Trees, Forest,	Steep slope, weak geology, Excessive water runoff, Slope, Vibration, Unstable slope with deposit of boulders and debris ground water, lack of rim treatment at reservoir of Dikchu Dam
Rotational	5	139250	4000000	Road, agricultural land, forest, habitation, Damage to Houses and Housing site, Road between Rongli and Rorathang/ Rhenock forest	Sheared rocks ground water, Toe erosion, rock floor, adverse geology, wet agriculture proactive, vibrations, quarrying, steep slope, poor drainage, high ground water,
Complex, wedge type dominating	1	1500000	75000000	Thekabong road, houses, fields, Forest, Cardamom	Jointed, blocky nature of bedrock

Types of Slide	No. of slide	Area (m^2)	Failed Volume (m^3)	Damaged Done	Causes
Rotational, active subsidence	1	24000	1200000	Road	Ground water seepage, adverse geology (wedge failure in brittle country rock)
Wedge type failure	2	17250	25225000	Road, agriculture land, health quarters, Pakyong-Linkey Road, forest	Adverse geology, ground water, Joint failures, water (underground) Steep slope,
Rotational controlled by wedge failure	1	2250	675000	Road, agriculture land	Wedge failure, toe cutting by Diking khola
Rock topple and complex failure	1	18000	360000	Roads, Trees, Agriculture	Water, Adverse geology, Steep slope
Debris avalanche	1	5000	15000	Road, house, (9 houses) buried, Agriculture land	Weak geology, excusive rainfall (unmanaged drain) upside is wet farming paddy field
Complex: Translational type mainly	1	630000	6300000	Agriculture land, houses, forest, road	Bedrock dipping down slope, high ground water, Steep sloppy
Rock fall	1	3000	0	Forest	Weak geology, Steep slope, Rainfall
Debris fall wedge type dominates	1	60000	6300000	Road	Steep slope, sheared rocks, water

Types of Slide	No. of slide	Area (m^2)	Failed Volume (m^3)	Damaged Done	Causes
Complex, translational type dominating	2	350000	17500000	Rongli-Dalapchand Road, Forest, Cardamom, J.N. Road	Steep slope, down slope dipping rock foliation freeze and thaw, rain water, high ground water
Mainly wedge type	2	233000	5330000	J.N. Road, Rongli-Rhenock road	Steep slope, jointed nature of rock, vibration, fractured nature of rocks
Block and wedge failure type	1	5200	52000	JN Road	Steep slope, jointed / sheared rock vibrations

Source: Cf. SSDMA, 2012

East district of Sikkim is a part of lesser Himalaya; altitude naturally range from 350m to 4630m; terrain is heavily dissected, with steep gorges, large valleys and ridges. Since the landslide is meticulously associated with the rain precipitation and East district receives considerably high rainfall during monsoon (district 11 years (2011-2022) annual average rainfall = 2531.72 mm). Thus, weak geology and the presence of sedimentary rocks such as phyllites, quartzite, gneiss, sandstone and high surface runoff have triggered some of the large landslides in East district of Sikkim (SSDMA, 2012). Other anthropogenic factor includes developmental activities including road construction, hydro-power development, road widening and high rate of urbanization (25.15%) led to higher construction activities which have resulted into different forms of mass wasting in the district.

iii. Landslides Scenario in West Sikkim (Geyzing and Soreng)

West district is dominated by Daling group of rocks, which is fully within the Lesser Himalaya and has undergone multiple periods of loading, unloading and uplift during the time of orogeny (SSDMA, 2012). Triggering factors of these slides are attributed to adverse geology, steep slope, highly jointed rock, high rainfall (district 11 years

(2011-2022) annual average rainfall =2019.72mm), vibration, road construction, seasonal surface runoff, fault zone and toe cutting by Rangit river and vibrations caused due to high magnitude earthquakes in the past (e.g. earthquake of 18th sept. 2011) and on-going developmental activities such as construction, hydro power development and widening of the roads etc.

Table 3B: Classification of landslide and its characterisation: West Sikkim

Types of slides	No. of slides	Area (m^2)	Failed Volume(m^3)	Damaged Done	Causes
Rotational	11	219210	3964000	Agricultural land, Cardamom field, Forest, Road, Road disruption, cultivated land, Frequent blocking of road traffic, Forest trees etc., Simithang under impact, Cardamom field	Strike slip faulting, Weak geology, Ground water/ rain water, vibration, Water movement, highly jointed rocks, soil cover, toe cutting, disturbed rocksequence, steep slope, Water seepage, Toe cutting by Bhutey *Khola*, poor drainage, Weathered nature of slope material, foliation down dip, ground water, Adverse geology, water, road construction, Loose crushed materials, surface/subsurface water runoff, Thrusting, toe cutting, vehicular vibration, sheared nature of slope material, poor drainage.

Types of slides	No. of slides	Area (m^2)	Failed Volume(m^3)	Damaged Done	Causes
Mainly planner	1	216000	10800000	Road, forest	Adverse geology, slope parallel to foliation plane, steep slope poor drainage, vibration
Wedge failure-Planner	1	1500	4500	Road	Sheared rock with immature soil cover/ surface run off
Rotational (creep)	1	30000	600000	Sinking of road, Tilted trees	Degraded slope materials, seasonal water runoff, Toe cutting
Wedge failure controlled by an active fault	1	22500	675000	Agricultural land	Strike slip faulting, Weak geology, Ground water/ rain water, vibration
Planner, rock toppling	1	2500	5000	Road traffic period disruption for long period during monsoon	High degree slope, toe cutting by Rangit river
Complex with displaced rock f ormations in the slide body	1	132000	1980000	Road, Forest	Adverse geology, steep slope, high rainfall, vibration
Planner due to ailure of joint plane	1	2400	24000	Agricultural land, Forest	Steep slope, brittle rocks

Types of slides	No. of slides	Area (m^2)	Failed Volume(m^3)	Damaged Done	Causes
Rock slide failure along joint	1	15000	75000	Forest, Road	Highly jointed rocks, steep slope
A unique case of rock toppling or fall	1	2500	12500	Road disruption, trees	Highly jointed rock
Planner	2	10000	137500	Agriculture land, Trees, Road (Bermoik - Legship Road	Toe cutting, Seasonal surface run off, Soil collapse above the rock bed during rainfall
Complex	1	7500	112500	Road destabilization, forest cover	Weak geological highly jointed rocks
Translational	1	30000	60000	Road destabilization	Water seepage/runoff, rock slip along foliation
Fault controlled complex	1	6000	30000	Road, Cardamom	Soil collapse above the rock bed during rainfall
Rotational and Complex	2	75000	750000	Road disruption, Agriculture land, trees, Road sinking	Adverse geo setting, toe cutting by Rangit river, road construction, Geological formation, water runoff,
Rotational as well as wedge failure	1	21000	315000	Forest	Surface/ sub-surface water movement, slide materials, Brittle rock, Toe cutting, vibration

Types of slides	No. of slides	Area (m^2)	Failed Volume(m^3)	Damaged Done	Causes
Complex and rotational rock toppling	1	75000	3000000	Road disruption, Forest cover and agriculture land	Weak geology, surface/ subsurface runoff, Toe cutting
Rock failure and planner	1	4375	21875	Vehicles and traffic disruption	Highly jointed rock, steep slope, surface runoff
Planner as well as Rotational	1	100000	1000000	Habitation, cultivation, road	Adverse geology, high ground, road construction, Toe cutting
Rotational S65E- 15SE	1	50000	1000000	Road, Forest, agriculture	Fault Zone, Surface/ subsurface water movement, steep slope

Sou†rce: Cf. SSDMA, 2012

In West Sikkim planner, rotational and complex types of slides are pre-dominant. It is known for wedge failure-planner, rotational (creep), wedge failure controlled by an active fault, planner, rock toppling, complex with displaced rock formations in slide body, planner due to failure of joint plane, rock slide failure along joint, planner, complex, translational, fault controlled complex, rotational and complex rotational as well as wedge failure, complex and rotational rock toppling, rock failure and planner form of slides had occurred in the past.

(iii) Landslides Scenario in North Sikkim (Mangan district)

North Sikkim is the least populous district (population density 10/km^2) of the state and largest in terms of geographical area (4,226 km^2). The landscape is mountainous with lush vegetation that reaches alpine altitude before thinning out to the cold desert scrub as it approaches the northern tundra. Landslides are frequently seen as a result of steepness of the valleys reworked by fluvio-glacial action in the past. The region

consists of rock from the inner, axial, and trans-axial belts in the super-positional flow order. Sandstones, limestone, and fossil bearing shales formed the Tsho-Lahmu series. Latchi series are made by slates, pebble beds, carbonate shells, and sandstone. Chhubakha series formed by granite with fine grains that has granet tourmaline, and pegmatite, lime silicates, hornblende inclusion, etc. (SSDMA, 2012).

Table 3C: Classification of landslide and its characterisation: North Sikkim

Type of slide	No. of slide	Area (m^2)	Failed Volumye (m^3)	Damaged Done	Causes
Subsidence	3	80000	192500	Forest, Agricultural field, Settlement, Agricultural land, Road highways	Adverse Geology, high ground/rain water, Bad geology, High water regime, ground water and vehicular vibration
Debris slide	3	13000	13000	Agricultural land, Forest, houses, road	Bad geology, high ground/ rain water, steep slope, water, Adverse geology, slope, rainfall
Debris Fall	1	55380	553800	Forest	Adverse geology, slope, rainfall
Debris Flow	3	82000	595000	Forest, Road, forest cover	Adverse geology, steep slope, rainfall, ground water activities, rain water, scouring by nala, vehicular traffic vibration
Complex	1	12500	125000	Road	Highly jointed rocks, debris overburden of rock and soil on both abutment and scouring by active water

Type of slide	No. of slide	Area (m^2)	Failed Volumye (m^3)	Damaged Done	Causes
Wedge Failure	1	7500	15000	Road distance	Steep slope, highly jointed and fractured rocks, excess water, vibration
Complex, Fault controlled	2	67500	40500	Road, forest, agricultural land	Weak geology, excess water, Weak geology (Jointed rock/sheared), steep slope, vibration
Complex, Debris Flow or Fall dominating	1	15000	75000	casualties at GREF Camp 10/11 September, 1983	Weak geology (Jointed rock/sheared) excess water, steep slope, vibration
Rotational	1	228.6	3429	Road strike, Overburden material, boulders	Hydrology, weak geology, slope failure
Planner on the catchment of Nalas main tributary	1	450000	13500000	Forest	Hydrology, weak geology, forest load

Source: *Cf. SSDMA, 2012*

In North district, subsidence, debris slide, debris fall, debris flow, complex, wedge failure, complex fault controlled, complex debris flow or fall dominating, rotational and planner on the catchment of nalas are very common. Frequently occurring slides includes subsidence, debris slide, debris flow and complex fault controlled. The frequent occurrence of these slides has been ascribed to adverse geology, high ground or rain water, high water regime, vehicular vibration, high rainfall (district 11 years

annual average rainfall = 3218.17 mm), developmental activities, steep slope, catchment degradation and dam construction (hydrology). All these triggers affected settlement, tourism movement, agricultural land, forest retaining walls and road ways which has created inconvenience in road transportation throughout the year. Similarly, to get insights regarding the factors causing landslides in Sikkim, fourty (40) experienced participants from the villages who have been affected by large and medium sized landslides in the last 5-15 years have been prepared through PRA consultation. The views of the participants (respondents) regarding triggering factors of the landslides have been analysed and tabulated. On the basis of the pairwise ranking, factors triggering landslides during monsoon and non-monsoon months in Sikkim have been categorized into high, medium and low on a scale of 1-8. (Table 4).

Table 4: Major factors causing landslides in Sikkim (Respondents) PRA consultation

Factors triggering Landslides in Sikkim	1. Rainfall, drainage	2. Adverse geology	3. Seismic events	4. Developmental Activities	5. Cloud Burst	6. Catchment Degradation/ deforestation	7. Water pondage	8. Land Use Transformation	Total points	Rank	Percentage
1. Rainfall, drainage		1	1	4	1	6	1	1	5	3	17.86
2. Adverse geology	1		2	4	5	6	2	8	2	6	7.14
3. Seismic events/ Earthquakes	1	2		4	5	6	7	8	0	8	0
4. Developmental Activities (Road construction Tunnelling/ blasting/	4	4	4		4	4	4	4	7	1	25

vibration, toe erosion)											
5. Cloud Burst	1	5	5	4		6	5	8	3	5	10.71
6. Catchment Degradation/ deforestation	6	6	6	4	6		6	6	6	2	21.43
7. Water Impound-ment by hydro projects	1	2	7	4	5	6		8	1	7	3.57
8. Land Use Transforma-tion	1	8	8	4	8	6	8		4	4	14.29

The respondents argued that developmental activities (road construction tunnelling/blasting/vibration, toe erosion) (25%) and catchment degradation/ deforestation (21.43%) are the most important factor triggering landslides in Sikkim followed by rainfall and drainage (17.86%), land use transformation (14.29%), cloud burst (10.71%), adverse geology (7.14%). The respondents had given less importance to the seismic events/earthquakes as they firmly believed that they mostly cause rock blocks/boulders to slide from the steep slopes, collapse of the buildings and triggers landslides only in case of their high intensity/magnitude. They further alleged that huge water impoundments (pondage) of about 81.23 ha by the hydro projects in the mid-stream of the river Tista and Rangit has triggered landslides and subsidence in and around the rim of the reservoirs in the recent past. As the past landslides in Sikkim have caused enormous damage to the community and individual assets. Thus, to sustain the loss, District Disaster Management Offices (DDMO) provides ex- gratia to the landslides victims. The ex- gratia relief according to degree of damage for the landslides victims during 2020-2022 is highlighted below:

Table 5: Ex-gratia to the landslide victims of South Sikkim (2020-2022)

Nature of damage	No. of damage/ area (hectare)	Amount (Rs.)
Land damage with crops	1 hectare	37500/
Barren land	1 hectare	65500/
Kutcha House damage	190	3200/
Pucca House partially damage	-	5200/
Pucca house severely damaged	317	101900/
Lives	-	400000/
Death of milching cow	1	30000/
Cowshed/Goat shed/Pig shed	1	2100/
Chickens	1	50/
Protection wall	-	Approx. 5000 – 200000/
Toilet with septic tank damaged	-	7000/

Source: DDMO, Namchi, South Sikkim, 2020-2022

The authority has provided ex-gratia according to the nature of damage, area and number of damages caused by the landslides. Loss of life during the landslide events have been compensated with the amount of Rs.4 lakhs individually. For the damage of the land (about1 hectare) with crops are compensated with the amount of Rs. 37,500/ and for the damage of barren land (about1 hectare) compensation amount was around Rs.65,500/. For damage of kutcha house compensation amount was Rs. 3,200/ and for pucca house partially damaged by landslides had been given Rs. 5,200/ and severely damaged pucca house had been given Rs. 10,1900. For damage of toilet with septic tank ex-gratia amount was Rs.7,000; similarly, compensation amount for the protection wall was approximately Rs. 5,000-2,00000.

4. Conclusion

State of Sikkim is extremely susceptible to natural hazards like landslides (1,569 incidences), earthquakes, snow avalanche, GLOFs, forest fires (1,050 incidences),

and cloudburst events. The mean depth (m) and failed volume (m^3) of the major landslides in Sikkim is around 57m (cumulative depth=4,718m) and 8518488.94m^3 (cumulative volume = 689997604m^3). The incidence of the landslides in the state has increased mainly because the state average annual rainfall has never gone down below 2,000 mm in the last 10 years (2454.34mm) (2012-2022). Respondents ascribed the causes of the landslides to developmental activities (25%), catchment degradation/ deforestation (21.43%), rainfall and drainage (17.86%), land use transformation (14.29%), cloudburst events (10.71%), adverse geology (7.14%), water impoundment (3.57%) and seismic events/earthquakes during PRA consultation.

As a hilly area, it lies in seismic zone IV of the seismic map of India. Natural hazards affect a staggering number of people annually, with landslides being the most common phenomenon in the state. In Sikkim, long-term rainfall and other anthropogenic influences, such as construction of buildings in the prone areas, rapid road widening, and vibration caused by developmental projects are the most common landslide triggers in Sikkim. Additionally, it affects the denizens who reside very close to the major national (NH-10) and state highways (NH-10, NH -710, NH- 510, NH -710A) of the state. Sikkim is extremely affected by landslides as they led to the loss of lives and property, tourists movements due to blockage of national and state highways. The landslides often swept away water supply pipelines or pollute and destroy water sources, urban dwellers occasionally have to deal with water shortages during monsoon seasons. In order to prevent the loss of life and property in the event of a natural disaster, an intervention from the authority is required. The Sikkim State Disaster Management Authority, NDMA, NIDM and UNDP have all initiated several research projects, trainings, workshops/seminars and mock drills in this regard for the communities, students and institutions etc. Ex-gratia is provided by the district authority as per the extent of damage by the landslides. The study is delimited to the major and the seasonal landslides of East, North and West districts of Sikkim as the legacy data of the landslides are very limited and due to unavailability of the rainfall datasets at the GPU level, precipitation threshold could be calculated even for the major landslides. Though, this study has identified, characterized and mapped the landslides, still a comprehensive inventory of the landslides using Sentinel datasets (Sentinel-B/Landsast/Google hybrid/ Yandex) can be done. The present study will assist the concerned authority in making further assessments of landslides and the damages arising out of them.

Further, the findings can help policymakers and authority to formulate effective strategies and policies in reducing disaster risks and mitigating plans to minimize the threat of landslides in the state. Besides, disaster management frameworks such as Sendai, Hyogo/GSI guidelines and national/state disaster management frameworks can be followed for such studies. The following recommendations are suggested to the authorities concerned:

1. Regularly training programme, workshops/seminars and mock drill should be organised for the capacity building of the youths and senior citizens and women in specific.
2. Involvement of the grassroot level community including old age/differently abled people in participatory planning and disaster management plans.
3. Inclusion of landslides and its mitigation techniques in the Sikkim State Disaster Management Plans and Climate Change Action Plan and such other policy documents of the state incorporating five major pillars viz; NDM Act 2005, NPDM 2009, participating proactively in realizing the global goals focusing upon Sendai Framework for DRR, Sustainable Development Goals (SDGs) and Hon'ble Prime Minister Ten Point Agenda for DRR, Social inclusion and mainstreaming DRR.
4. Appropriate database development of landslides at Village Administrate Centre (VAC) as their catchment area is large as compared to ward panchayats.
5. Vulnerability assessment at GPU level based on physical and bio-physical methods using tier-III approach.
6. Landslide hazard zonation at GPU level.
7. Geo-hydrological assessment/geo-technical assessment should be made compulsory for the construction's sites.
8. Use of UAVs and SAR technology in landslide monitoring and prediction/ deformation studies.
9. Use of advanced Early Warning System for the prediction of the landslides.
10. Geotagging of the landslides by the authority concerned.

5. Acknowledgments

The authors would like to thank Dinesh Dhakal, Assistant Town Planner, SSDMA for sharing landslides database of Sikkim and Durga Pd. Sharma of Lingee, South Sikkim for PRA consultation. We also thank respondents who have participated in PRA consultation for eagerly sharing their experiences and response with regard to the triggering factors of landslide in Sikkim. The use of Copernicus LULC and GSI geological map is appreciatively acknowledged.

6. Conflict of Interest

The authors declare no potential conflict of interest.

7. Funding for Research

Nil

References

1. Aslan, G., De Michele, M.; Raucoules, D., Bernardie, S., Cakir, Z (2021). Transient motion of the largest landslide on Earth, modulated by hydrological forces. *Sci. Rep. 11, 10407*.
2. Bhasin, R., Aslan, G., Dehls, J. (2023). Ground Investigations and Detection and Monitoring of Landslides Using SAR Interferometry in Gangtok, Sikkim Himalaya. GeoHazards 2023, 4(1), 25-39; *doi.org/10.3390/geohazards4010003*.
3. Bhasin, R., Grimstad, E., Larsen, J.O., Dhawan, A.K.; Singh, R., Verma, S.K.,Venkatachalam, K. (2002). Landslide hazards and mitigation measures at Gangtok, Sikkim Himalaya. *Eng. Geol.* 64, 351–368.
4. Census of India. (2011). *District Census Handbook, Part A & B. North, West, South & East Districts. Directorate of Census Operations Sikkim*. Author.
5. Centre for Inter-disciplinary Studies of Mountain and Hill Environment (CISM&HE). (2005). In Carrying Capacity Study of Teesta Basin in Sikkim, Ministry of Environment and Forests, Government of India, (1). 1–263.
6. Crosetto, M., Monserrat, O., Cuevas-González, M., Devanthéry, N., Crippa, B. (2016). Persistent scatterer interferometry: A review. ISPRS *J. Photogramm. Remote Sens.,* 115, 78–89.
7. GSI (2012). *Miscellaneous Publications, Government of India, (Sikkim) 30 (19). Author*.
8. Gurung, B., & Dar, S.N. Landslide Vulnerability Assessment in Sikkim Himalayas in India (2023). *Eur. Chem. Bull. 2023, 12(Special Issue 5), 2071 – 2078*.
9. Lacroix, P., Handwerger, A.L., Bièvre, G (2020). Life and death of slow-moving landslides. Nat. Rev. *Earth Environ. 1, 404–419*.
10. Nadim, F., Kalsnes, B., Solheim, A. (2014). Landslide Risk in Europe. In: Sassa, K., Canuti, P., Yin, Y. (eds) Landslide Science for a Safer Geoenvironment. *Springer, Cham, 3–20, https://doi.org/10.1007/978-3-319-04999-1_1*.
11. NESAC, GoI. (2020). Seasonal landslide inventory for NER -2020. Retrieved from *https://www.nerdrr.gov.in/ accessed on 24.10.2024*. Document Control No. *NESAC-SR-261-2021, 1-72*.
12. Nirmala Jain, Priyom Roy, Tapas Ranjan Martha, Punit Jalan and Aishwarya Nanda (2023). Landslide Atlas of India (Mapping, Monitoring and R&D studies using Remote Sensing data). NRSC special publication. *NRSC/ISRO. Document number: NRSC-RSA-GSG-GMED-FEB 2023-TR-0002167-V1.0*.
13. Singh, A. (2014). Spatial Variability, Social Vulnerability and Adaptability to Landslide in Sikkim. *M.Phil dissertation submitted to Sikkim University in partial fulfilment of the requirement for the award of the degree of Master of Philosophy,1-133*.
14. SSDMA (2012). Multi-Hazard Risk and vulnerability Assessment of North, East, West and South Sikkim. *Sikkim State Disaster Management Authority, Land Revenue and Disaster Management Department, Government of Sikkim. 1-258*.

Assessing Forest Fire Severity Using Remote Sensing: A Case Study in Western Rajaji National Park, Uttarakhand, India

Suraj Dev[1], V. S. Negi[2], B. W. Pandey[3]
Chatter Singh[4], Ravi Kesharwani[5]

Abstract

Forest fires produces notable global threat and it can damage various ecosystems, human lives and infrastructure. This article take a look at the uses of remote sensing satellite data and techniques. In this paper the Normalized Burn Ratio (NBR) and Differenced Normalized Burn Ratio (dNBR) indices is used to estimate and visualise the burn intensity of forest fires. The Western Rajaji National Park (RNP) in Uttarakhand, India is selected as study area for this paper. Landsat satellie imagery and SNPP-VIIRS data used in this method to calculate NBR and dNBR. The research highlights the significance of appropriate satellite imagery collection and precisely prepare pre-and post-fire images. The obtained pre- and post-fire are used to create burn severity (intensity) images, produce significant observations into the impact of the forest fire ecosystems. The findings shows the efficiency of NBR and dNBR in mapping and visualizing the severity of the fire incident, helping in forest fire prevention, monitoring and evaluation. The paper contributes to the comprehensive understanding of geospatial applications for assessing various impacts and aiding decision-making actions for controlling and reduce the effects of forest fires.

Keywords: *Remote Sensing, Forest Fires, Normalized Burn Ratio (NBR), Severity and Delta Normalized Burn Ratio (NBR)*

[1] Research Scholar, Department of Geography, University of Delhi
[2] Professor, Department of Geography, Shaheed Bhagat Singh Evening College, University of Delhi
[3] Professor, Department of Geography, University of Delhi
[4] Research Assistant, Department of Geography, Shaheed Bhagat Singh Evening College, University of Delhi
[5] Research Scholar, Department of Geography, University of Delhi

1. Introduction

Over the past 2 decades, there has been an annual growth in forest fires of 5.4 percent, with over 120 lakh hectares destroyed in year 2023 (MacCarthy et al., 2024). Thus, it is important to develop useful methods for estimating and monitoring the burn intensity of forest fires.

Remote sensing and satellite imagery are now un-avoidable techniques and dataset to proceed in this type of work. Remote-sensed satellite data provide a valuable resource for mapping burned area and estimating burn intensity (Prabowo et al., 2022).

To support forest fire prevention, monitoring and evaluation, and at the global to local levels, optical remote sensing methods have shown to be effective in developing models for precisely estimating fire-affected areas and burn intensity (Novo et al.,2022). Three recognizable temporal fire-related stages have been addressed by these methods: pre-fire situation, burn intensity, and post-fire vegetation growth. NBR and dNBR are are widely used indices in forest fire assessment. These quantitative indices prepared from satellite imageries that provide significant information on the intensity of burn patches (De Santis & Chuvieco, 2007).

These indices are based on the spectral reflectance values of satellite imagery's Near-Infrared and Shortwave Infrared bands. NBR and dNBR are commonly used remote sensing indices to estimate and monitor the intensity of wildfires or post-fire vegetation conditions. NBR and dNBR fomulas are as following:

$$NBR=(NIR-SWIR)/(NIR+SWIR)$$

Where,

NIR= Near Infrared image and SWIR= Shortwave Infrared image

$$dNBR=NBR\ post\text{-}fire-NBR\ pre\text{-}fire$$

Where,

NBR pre-fire is Normalized Burn Ratio of pre-fire event and NBR post-fire is vice versa.

They are derived by using of satellite images, usually from Landsat or Sentinel programs. NBR is quantify by dividing the result by the sum of the satellite's near-infrared and mid-infrared images, then multiplying the result by 1000. Subtracting

post-fire NBR data from pre-fire NBR values yields continuous values between -2 and 2, which are then used to construct differenced NBR (dNBR) products. Increases in soil exposure and vegetation degradation are correlated with higher dNBR values (Key & Benson, 2006).

2. Study Area

Rajaji National Park (RNP) is a renowned national park located in the northern state of Uttarakhand, India. Established in 1983, it covers an extensive area and is named after C. Rajagopalachari, a prominent freedom fighter and the last Governor-General of India. The Park is situated in the Shivalik range of the Himalayas and is known for its rich biodiversity, stunning landscapes, and varied wildlife. Rajaji National Park covers an area of approximately 820 square kilometers. It extends across three districts of Uttarakhand: Haridwar, Dehradun, and Pauri Garhwal.

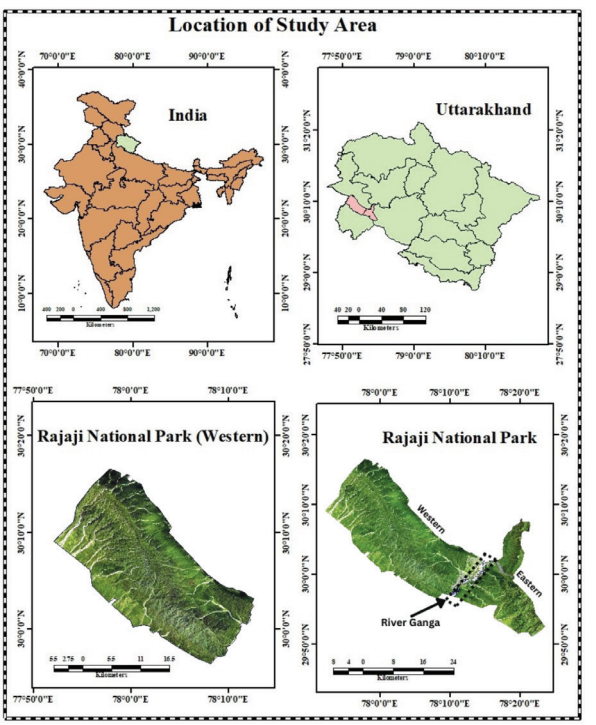


Figure 1: Map of Study Area in Rajaji National Park

The Shivalik hills, river valleys, and dense forests characterize the Park. Rajaji National Park [29º15' North to 30º 31' North Latitude, 77º 52' East to 78º 22' East Longitude] is spread over an area of 820.42 Km^2. As shown in the study area map River Ganga flows between RNP near Haridwar. The forest fire event happened between the 13th to 16th of May on the western side of RNP. Thus, I choose Western Rajaji National Park as the study area for better analysis. Western RNP is spread over 564.32 km^2 or 56432 hectares.

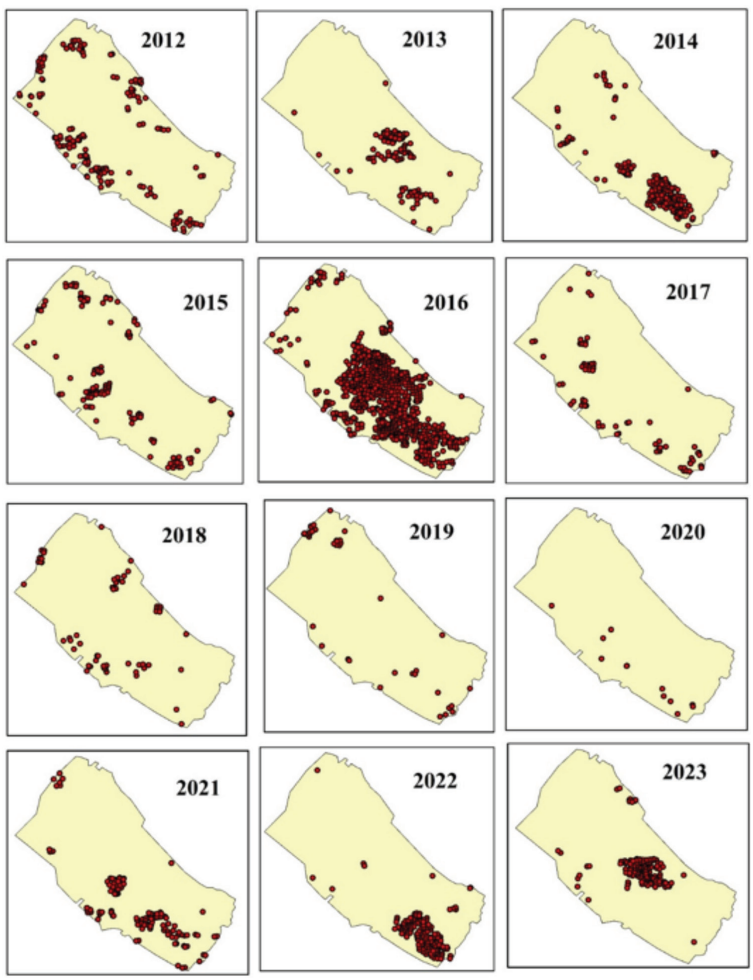


Figure 2: Historic locations of forest fires from 2012 to 2023 in Western Rajaji National Park

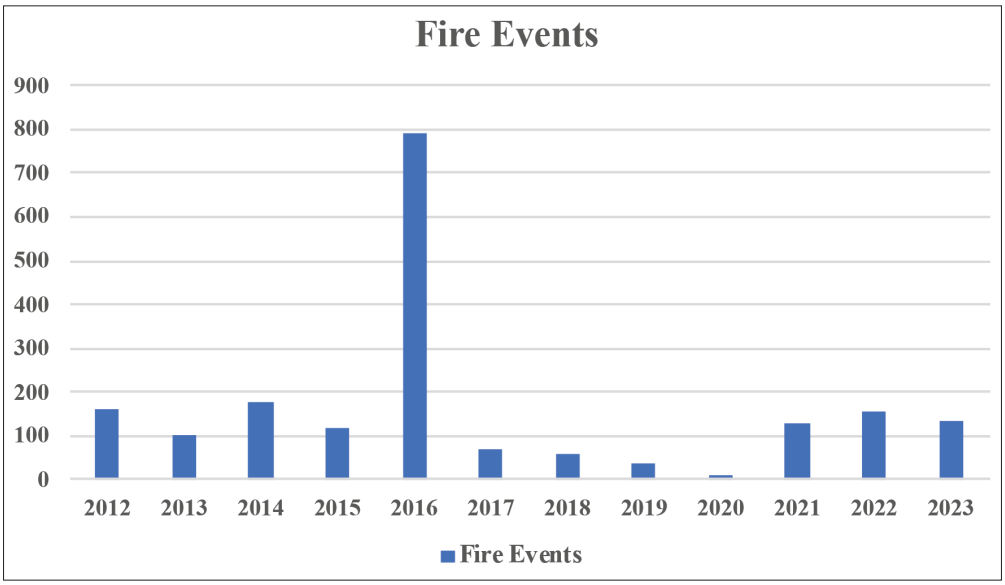


Figure 3: Historic pattern of forest fires from 2012 to 2023 in Western Rajaji National Park

The above figure 2 and 3 shows the historic pattern of forest fires from 2012 to 2023 in Western Rajaji Nation Park. One thing is important that forest fire event occurs in different places in successive years due to lack of fuel wood after forest fire event. In 2016 a massive fire erupted in this region and the number of forest fires declined in subsequent years. In 2020 number of forest fire events is lowest due to lockdown, where human activities were restricted, temperature declines and rainfall is equally distributed in the season.

3. Materials and Methodology for Calculating NBR and dNBR

The information on fire events is collected from the forest fire alert system of Forest survey of India. The bunch of polygon shown fire regions in following figure 4 are collected by SNPP-VIIRS (Visible Infrared Imaging Radiometer Suite) sensor which hast resolution of 375m. India Landsat imagery is commonly used due to its availability and spectral bands. Landsat imagery is collected from USGS Earth Explorer. Infrared (NIR) and Short-Wave Infrared (SWIR) bands were collected from the above data

source. Atmospheric correction and Geometric correction of the spectral band were carried out on QGIS software. NBR is collected by using raster calculator in QGIS. To attain severity of forest fire delta NBR is calculated by measuring of difference between Pre-NBR and Post-NBR.

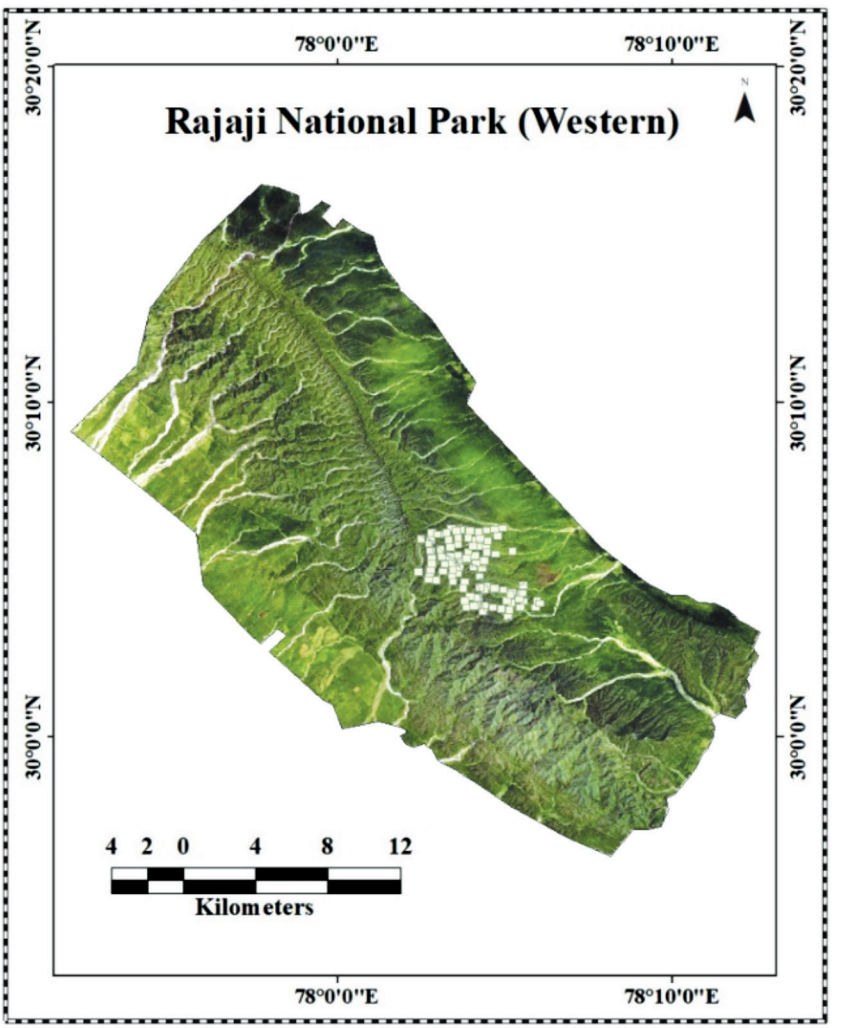


Figure 4: Showing fire region in Rajaji National Park

Data Processing: For calculating NBR satellite data of pre-fire event and post fire events are important. Condition of just before fire and just after fire is crucial for to assess severity of the fire event. If satellite data is taken much before fire event the actual condition of vegetation of the respective area is uncertain. Vegetation condition or health may be increase or decrease at the time of fire and after the fire. After some time vegetation regrowth may be start on the surface. All above condition affects the result of calculation of NBR. So satellite image collected as possible as close to the pre-fire event and post-fire event. Table 1 shows fire event date and satellite imagery acquisition date. Here satellite image of before fire event is four day older whereas satellite image is collected next day of Post-fire event.

NBR is calculated using the formula: NBR = (NIR - SWIR2) / (NIR + SWIR2)

NIR = Reflectance in the Near Infrared band

SWIR2 = Reflectance in the Short-Wave Infrared 2 band

Table 1: Pre-fire and post-fire events satellite imageries

Satellite Imagery (Acquisition Date)	Fire Event Date
09/05/2023 (Pre-Fire)	13/05/2023
17/05/2023 (Post-Fire)	16/05/2023

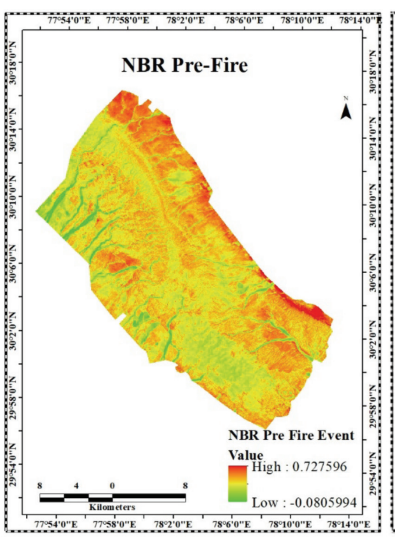


Figure 5: NBR pre-fire event

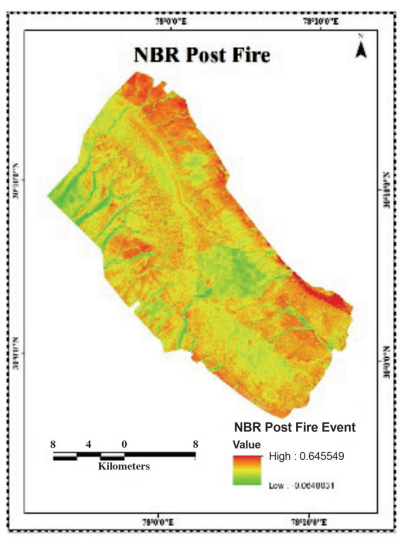


Figure 6: NBR post-fire event

Calculation of dNBR or ΔNBR: A fire's magnitude is determined by how much of an immediate impact it has on soils and vegetation due to the loss or degradation of organic matter (Keeley, 2009). The difference between the NBR composites before and after the fire is then used to calculate the Delta NBR (dNBR). The difference between the pre-fire and post-fire NBRs is known as the dNBR:

$$dNBR = NBRpost - NBRpre$$

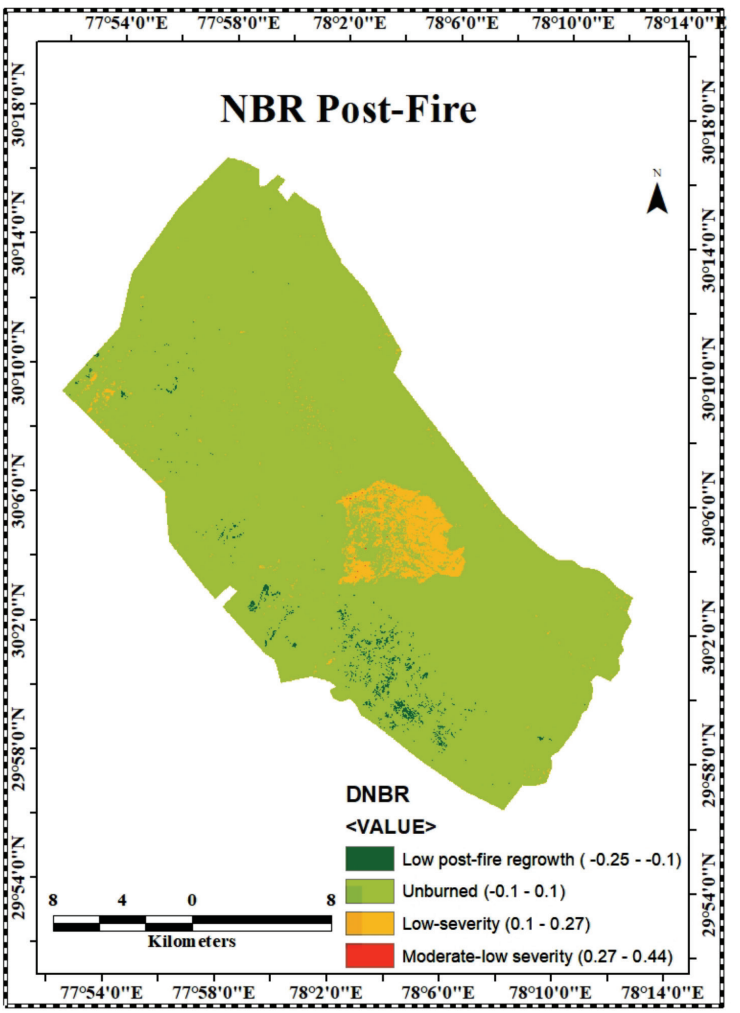


Figure 7: Showing dNBR value of post-fire

4. Results

Using formulas, NBR is calculated for the study area by using respective bands. In Figure 4 some polygons which represent fire spot by the SNPP-VIIRS sensor are shown. When we compare pre-fire and post-fire NBR data, a change recognizable change in both images are spotted in the same place as the fire spot pixel given by FSI. In post-fire events that specific place reflects less radiance as compared to other areas in both images.

The NBR indices work on reflectance values of vegetation in near-infrared and short-wave infrared. As shown in the above figure reflectance of healthy vegetation is highest in near infrared and lowest in short-wave infrared. Thus, the computation of differences between these highlight burned areas and estimate fire scar.

Table 2: Fire severity with range of dNBR

Fire Severity	Range of dNBR	Area in km²	Area in percent
Very low Burn or post-fire regrowth	-0.25 - -0.1	4.8402	0.858
Un-burned	-0.1 - 0.1	534.2949	94.679
Low-burn	0.1 - 0.27	25.1433	4.456
Moderate-Burn	(0.27 - 0.44)	0.045	0.008

dNBR is a measure of the change in vegetation and surface conditions caused by a fire. The above table shows four classes of dNBR that exist in the study area. Based on dNBR data, the fire severity study shows that 534.29 km² (94.68%) of the area is still unburned, indicating little to no fire impact in this substantial area of the region. Smaller but no less significant, 25.14 km² (4.46%) of the area is classified as having low-burn severity, meaning that the fire only slightly damaged or destroyed some vegetation. 4.84 km² (0.86%) of the land is categorized as having very low burn severity or exhibiting post-fire regrowth, meaning that it was either hardly affected by the fire or is now regenerating. A small portion of 0.45 Km² areas lies under moderate burn.

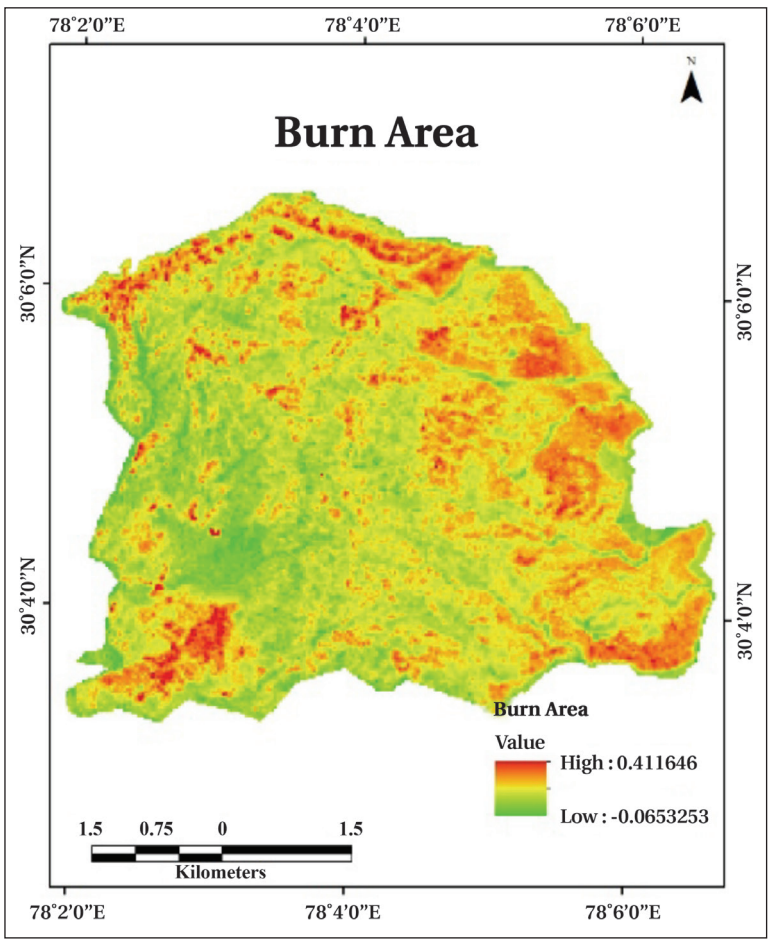


Figure 8: Showing burnt area

The above table shows the area which was impacted by fire from 13/05/2023 to16/05/2023. This area is extracted with the help of polygons downloaded from fsi.nic.in and dNBR map. During the respective period around 34 km^2 area is effected by forest fire in which some area faces moderate fire where some are facing very low or entered in the stage of plant regrowth. One the basis above image we can say polygons cannot show the exact figures of fire but they are important to locate the area where the event was happened.

5. Discussion

The study evaluated the intensity of a forest fire in the Western Rajaji National Park (RNP), Haridwar district, Uttarakhand, India, using the Normalized Burn Ratio (NBR) and differentiated NBR (dNBR). The findings show that 94.68% of the region was left unburned, indicating that the fire had little effect. Just 0.008% of the terrain was classed as having moderate burn severity, 4.46% as having low burn severity, and 0.86% as having extremely low burn or post-fire regrowth.

The capacity of dNBR to distinguish between these different levels of burn intensity was demonstrated by its successful use in remote sensing applications for assessing forest fires. But the study also raises questions about how accurate these indices are, particularly in heavily vegetated areas where it may be difficult for satellite images to properly catch surface fires because of thick canopies. Pre-fire imagery was acquired four days prior to the fire, and post-fire imagery was obtained the day following the fire's conclusion. The satellite imagery utilized in this study was meticulously selected to guarantee closeness to the fire event. To delineate the burn areas and accurately determine the intensity of the burns, earliest data collection was important.

Very low area of moderate burn intensity suggests that the fire's intensity was relatively low, and much of the area either escaped the fire or is now recovering. The ability of dNBR to detect post-fire regrowth is particularly useful in assessing vegetation recovery, providing views of how fast the forest is healing to its pre-fire state.

Beside the application of NBR and dNBR in mapping fire intensity, this paper highlights the requirement for further validation through ground-based observation or survey will improve accuracy, especially in regions with dense forest canopy. The combination of high-resolution satellite image could also improve the estimation of fire intensity assessments. Overall, this paper illustrates the application of remote sensing techniques in monitoring forest fire patches and recovery in RNP, providing significant information for forest management and conservation efforts.

When evaluating ecosystem recovery, the capacity of dNBR to identify post-fire regrowth is very helpful since it offers information on how quickly the forest is reverting to its pre-fire state.

This study emphasizes the necessity for additional validation through ground-based assessments to increase accuracy, especially in places with dense forest cover, not withstanding the usefulness of NBR and dNBR in mapping fire intensity. The accuracy of fire severity evaluations may potentially be improved by integrating igher-resolution satellite data. Several scholarly articles explore the complexities of NBR and dNBR, enhancing our comprehension of its advantages and disadvantages. Here are a few examples:

- "Explaining Sentinel 2-based dNBR and RdNBR variability with reference data from the bird's eye (UAS) perspective" examines how dNBR relates to actual burn severity on the ground, using high-resolution drone imagery for validation.
- **"Fire and burn severity assessment**: Calibration of Relative Differenced Normalized Burn Ratio (RdNBR) with field data" explores the use of RdNBR, anormalized version of dNBR, for more accurate mapping of burn severity indifferent vegetation types.
- **"Normalized Burn Ratio Plus (NBR+)**: A New Index for Sentinel-2 Imagery" proposes an NBR variation specifically tailored for Sentinel-2 satellite data, improving its sensitivity to burn scars in diverse landscapes.

The NBR and dNBR raises several interesting questions:

- **Accuracy and limitations**: What elements, such as the kind of vegetation and the severity of the fire, can influence their accuracy? Updates and improvements: How might these indices be modified and enhanced to suit other satellite data sets and particular use cases?
- **Beyond mapping**: Can the behavior of fires be predicted, the effects of fires on ecosystems modeled, or even fire management activities supported by NBR and dNBR??

5. Conclusion

NBR and dNBR are just the tip of the fiery iceberg in remote sensing of fire. By delving into their nuances and the rich tapestry of research surrounding them, we can better understand the dance of fire in our landscapes and use this knowledge to

inform fire management and ecology, and perhaps even predict future flames. Let the discussion continue, fueled by research and data, as we unravel the secrets of fire from the dizzying heights of satellite imagery.

References

1. Alcaras, E., Costantino, D., Guastaferro, F., Parente, C., & Pepe, M. (2022). Normalized Burn Ratio Plus (NBR+): a new index for Sentinel-2 imagery. *Remote Sensing, 14(7)*, 1727.
2. Batistella, M., Ribeiro, P. V., de Carvalho, L. A., Batista, G. T., & Soares, J. V. (2013). Mapping fire probability and severity in the Atlantic forest hotspot using the tri-temporal differenced Normalized Burn Ratio (dNBR). *International Journal of Applied Earth Observation and Geoinformation*, 24, 182-193.
3. Cardil, A., Mola-Yudego, B., Blázquez-Casado, Á., & González-Olabarria, J. R. (2019). Fire and burn severity assessment: Calibration of relative differenced normalized burn ratio (rdnbr) with Field Data. *Journal of Environmental Management*, 235, 342–349. https://doi.org/10.1016/j.jenvman.2019.01.077
4. Chuvieco, E., Aguado, I., & Yebra, M. (2010). Detection of global burn scars from satellite data: algorithms, challenges, and trends. *International Journal of Wildland Fire*, 19(4), 225-237.
5. ClimateEngine.org. (n.d.-a). *Normalized burn ratio (NBR)*. ClimateEngine.org Support. https://support.climateengine.org/article/123-normalized-burn-ratio#:~:text=The%20differenced%20(or%20delta)%20Normalized%20Burn%20Ratio,the%20vegetation%20community%20present%20before%20the%20fire.
6. De Santis, A., & Chuvieco, E. (2007). Burn severity estimation from remotely sensed data: Performance of simulation versus Empirical Models. *Remote Sensing of Environment*, 108(4), 422–435. https://doi.org/10.1016/j.rse.2006.11.022
7. Eidenshink, J., Schwind, B., Brewer, K., Zhu, Z. L., Quayle, B., & Howard, S. (2007). A project for monitoring trends in burn severity. *Fire Ecology*, 3(1), 1-21.
8. Fassnacht, F. E., Schmidt-Riese, E., Kattenborn, T., & Hernández, J. (2021). Explaining sentinel 2-based DNBR and RDNBR variability with reference data from the bird's eye (UAS) perspective. *International Journal of Applied Earth Observation and Geoinformation*, 95, 102262. https://doi.org/10.1016/j.jag.2020.102262
9. Fernández-Carrillo, J. L., de la Riva, J., & Riaño, D. (2018). Remote sensing analysis of fire severity in Mediterranean ecosystems: the case of the 2012 fire in Sierra Nevada (Spain). *International Journal of Remote Sensing*, 39(15-16), 4864-4883.
10. Keeley, J. E. (2009). Fire intensity, fire severity and burn severity: a brief review and suggested usage. *International Journal of Wildland Fire*, 18(1), 116-126.
11. Key, C. H., & Benson, N. C. (2006). Landscape assessment: Remote sensing of severity, the Normalized Burn Ratio and ground measure of severity. *International Journal of Wildland Fire*, 15(4), 167-179.
12. Lentile, L. B., Holden, Z. A., Smith, A. M. S., Falkowski, M. J., Hudak, A. T., Morgan, P., ... & Keane, R. E. (2006). Remote sensing techniques to assess post fire effects. *International Journal of Wildland Fire*, 15(4), 319-345.
13. Mac Carthy, J., Richter, J., Tyukavina, S., Weisse, M., & Harris, N. (2024, August 13). The latest data confirms: Forest fires are getting worse. World Resources Institute. https://www.wri.org/insights/global-trends-forest-fires
14. Miller, J. D., & Thode, A. E. (2007). Quantifying burn severity in a heterogeneous landscape: Integrating dNBR and geospatial data in a large wildfire. *Remote Sensing of Environment*, 109(3), 411-421.
15. Pant, M., & Purohit, V. (2019). Forest fire-a case study on the four national park of Uttarakhand. Int J Eng Res Technol (IJERT), 24(12), 347-354.
16. Parks, S. A., Dillon, G. K., & Miller, C. (2014). A new metric for quantifying burn severity: the relative differenced Normalized Burn Ratio (RdNBR). Remote Sensing of Environment, 143, 1-14.
17. Parks, S. A., Miller, C., & Nelson, R. F. (2016). Post-fire recovery of a semi-arid shrubland ecosystem assessed by remotely sensed vegetation indices and field measurements. *International Journal of Remote Sensing*, 37(11), 2326-2342.
18. Pérez-Cabello, F., & Castaño, S. (2010). Burn severity assessment using the differenced Normalized Burn Ratio (dNBR) index in the 2004 Chiva (Valencia, Spain) forest fire. *Journal of Environmental Management*, 91(12), 2515-2525.

19. Pérez-Cabello, F., Rogan, J., & López-Granados, F. (2014). Mapping fire severity from the dNBR index: a comparison of Landsat data and advanced multispectral sensors. *International Journal of Remote Sensing*, 35(17), 6120-6135.
20. Roy, D. P., Boschetti, L., & Justice, C. O. (2009). The use of MODIS fire products to estimate burned area in South America. *International Journal of Remote Sensing*, 30(17), 4615-4632.
21. Roy, D. P., Huang, H., Boschetti, L., Justice, C. O., & Li, J. (2019). The MODIS MCD64A1 Burned Area Mapping Algorithm: User's Guide. University of Maryland.
22. Verma, A. K., & Kumar, S. (2015) Mapping Fire Hazard In Rajaji National Park, Future Perspective of Wildlife Habitat Conservation by Using Remote Sensing And GIS.

Measuring Adaptive Capacity of Indian Agriculture to Climate Change: An Application of Indicator Approach

Surendra Singh Jatav

Abstract

The present study is an attempt to examine the adaptive capacity of mainstream agro-climatic regions in India to climate change. The study uses unit-level data from the 77th round of NSSO and district-level data from the Population Census 2011, and Agricultural Census 2015-16. This study first normalized the differential data using an indicator approach, and then calculated an adaptive capacity index for different mainstream agro-climatic regions of India, excluding the Island region. A total of 31 indicators, covering three dimensions - environmental, social, and economic, to capture the regional extent and dimensions of climate change adaptations in Indian agriculture were used to construct an adaptive capacity index. The result shows Eastern Himalayan Region (EHR) had the highest environmental resource capacity (i.e., 0.702 index value), making it the best agro-climatic region to deal with changing climate. On the other hand, the East Coast Plains and Hills Region (ECPHR) had the lowest adaptive capacity (i.e., 0.438 index value), due to its relatively low environmental resource capacity. This indicates that environmental factors are essential to maintain higher resource capacity in dealing with climate change. Despite having higher economic and social resource capacities, the Western Dry Region (WDR) and the Trans-Gangetic Plain Region (TGPR) have lower environmental resource capacities. However, these agro-climatic regions rank 7 and 4, respectively, in the adaptive capacity index. The results provide the grass-roots status of Indian farmers' adaptive capacity across regional dimensions. The study emphasized the need for more research into the prospects for successful involvement in local and regional risk assessment and the improvement of adaptive capability.

Assistant Professor, Department of Economics, Babasaheb Bhimrao Ambedkar University, Lucknow, India

Keywords: *Agro climatic zone, Agriculture, Adaptation, Adaptive Capacity Index, Climate Change, Regional Analysis, Temperature, India*

1. Introduction

The main cause of the observed increase in temperature during the mid-20th century is attributed to the influence of human activities on climate change. During the period from 1880 to 2012, the global average surface temperature increased by 0.80°C (Intergovernmental Panel on Climate Change, 2013b). According to the IPCC (2013b), several locations worldwide have already seen significant warming at a regional level. Approximately 20-40% of the global population has experienced a temperature increase of above 1.50°C. The current increase in temperature has already caused significant changes to both human and ecological systems, such as an increase in droughts, floods, and other forms of severe weather. It led to rising sea levels and a loss of biodiversity. The alterations are giving rise to unparalleled hazards for susceptible groups, such as farmers (Mysiak et al., 2016). Most vulnerable individuals residing in low- and middle-income nations, such as India, depend on agriculture and face periodic food insecurity, which is partially associated with increasing migration and poverty (IPCC, 2012b). Globally, a multitude of ecosystems face the threat of significant consequences (IPCC, 2014a). The expansion of the global economy has led to longer life expectancy and higher income levels in many parts of the world. However, despite these positive developments, there are still regions that suffer from widespread poverty and extreme inequality in terms of income distribution and access to resources. These conditions further exacerbate the vulnerability of these regions to the impacts of climate change, in addition to the existing problems of environmental degradation and pollution (Dryzek, 2016).

About 22% of India's GDP comes from agriculture, making it a major economic sector. Because it employs 58% of the population, it also has a significant impact on employment. Furthermore, agriculture fulfils the nation's food and nutritional requirements, supplies raw materials for industries, and contributes to about 14% of total exports (Swain, 2014).

According to the predicted climatic changes, India is predicted to suffer from significant agricultural losses, ranking among the highest in the world (Guntukula 2020). According to Aggarwal (2008), even after taking into account the impact of carbon fertilisation, India is still projected to see a crop output decline of 10 to 40% by 2100 owing to rising temperatures and unpredictable rainfall patterns. Hence, given the swiftly shifting climatic conditions and the diminishing water supplies, it is imperative for farmers to implement suitable adaptation strategies in order to mitigate the negative consequences (Jatav, 2020). Nevertheless, the implementation of adaptation strategies incurs economic expenses and limits farmers' ability to adapt enough (Jatav, 2023). Indeed, this is particularly true in the Indian context, where a significant majority (i.e., 80%) of Indian farmers are smallholders and typically possess little financial resources (Jatav and Sanatan, 2022; Jatav, 2024).

Adaptation to climate change will be highly crucial in the 1.5° C warmer world as major consequences would be seen in every area (IPCC, 2014a). Climate adaptation choices include several types of responses, including structural, physical, institutional, and social measures. The efficacy of these alternatives primarily relies on factors such as governance, political determination, adaptable capabilities, and financial resources (Sovacool et al., 2015). According to the simulation findings, if warming is limited to 1.50° C, there will be a decrease in the number of individuals who are affected by hunger, water stress, and sickness (Clements, 2009). The findings also suggest that implementing measures to adapt to climate change might reduce the vulnerability of impoverished populations to the risks of flooding and drought, particularly in African and Asian nations (Winsemius et al., 2018). As far as regional advantages to climate change adaptations are concerned, obstacles for impoverished communities pertaining to food and water security, clean energy availability, and environmental well-being are expected to be fewer at 1.5° C as opposed to 2° C (Byers et al., 2016).

Moreover, previous studies have either measured the adaptation ability of farmers in a village or made comparisons between two districts or regions (Gupta and Bandyopadhyay, 2014; Datta and Bhagirath, 2022; Dasgupta et al., 2022). Furthermore, field survey-based studies primarily focus on identifying the determinants of adaptive capacity, which may limit the generalizability of results to countries such as India, given their diverse socioeconomic and geographical characteristics. This research

gap is bridged by this study. The main aim of this study is to measure the adaptive capacity of Indian farmers to changing climates.

2. Materials and Methods

2.1 Study Area and Data Sources

The present study covers 14 mainstream agro-climatic zones, excluding the Island zone. As far as spatial characteristics are concerns, the Himalayan region is distributed into two agro-climatic regions, viz., Western Himalayan Region and Eastern Himalayan Region, and covers about 18.44% of geographical area. Gangetic Plain Region has distributed into four agro-climatic zones, viz., Lower Gangetic Plain, Middle Gangetic Plain, Upper Gangetic Plain & Trans Gangetic Plain, and covers about 15.89% of geographical area. Plateau and Hills region has distributed into four agro-climatic regions, viz., Eastern Plateau & Hills, Central Plateau & Hills, Western Plateau & Hills and Southern Plateau & Hills, and covers 44.19% of geographical area. Coastal Plains and Hill region has distributed into two regions, viz., East Coast Plains & Hills and West Coast Plains & Ghats, and covers 9.69% of geographical area. While Gujarat Plains & Hills and Western Dry regions jointly cover about 11.53% of geographical area (Singh et al., 2020).

As far as climatic conditions of all agro-climatic zones are concerns, it varies from cold arid to humid in the Himalayan region, and humid to dry in Gangetic Plains. Plateau regions remain semi-arid to dry, while coastal regions having semi-arid to dry sub-humid climate conditions. Gujarat plains climatic conditions vary from arid to dry sub-humid, while Western Dry region climate varies from arid to extremely arid (Jatav and Kalu, 2023).

The present study has used NSSO's 77th round (2019-20), agriculture census (2015-16), Census (2011) Indian Meteorological department, Government of India, and Ministry of Agriculture and Farmers Welfare, Government of India data to develop adaptive capacity index for different agro-climatic regions of India.

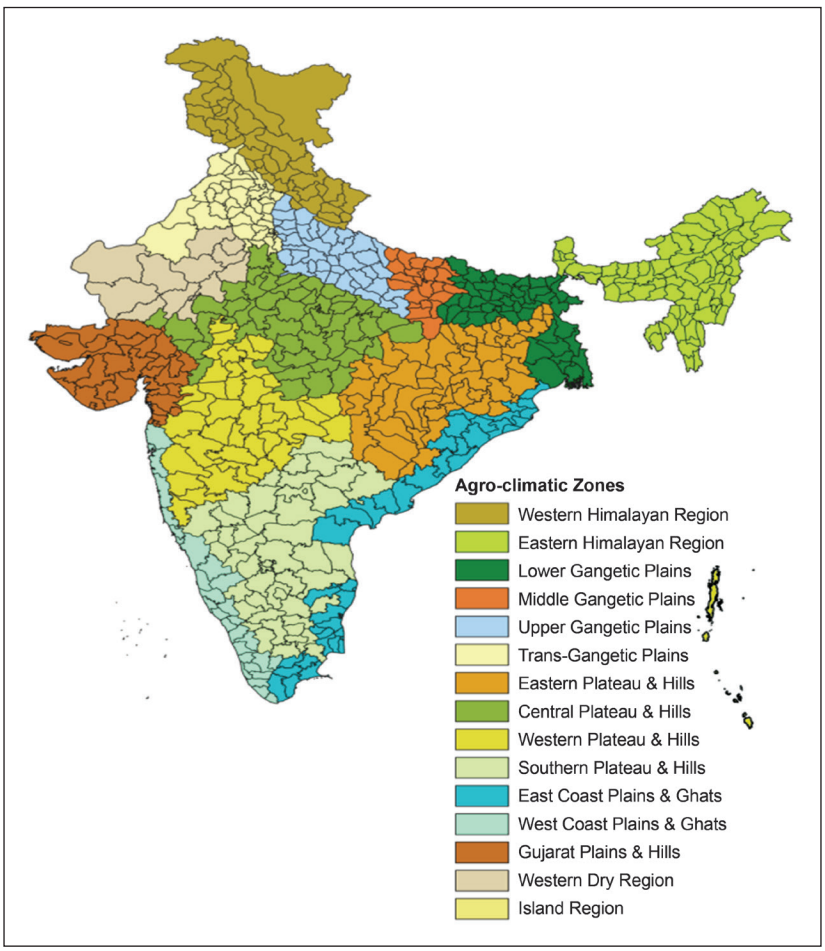


Figure 1: Mainstream Agro-climatic Regions of India

Source: Author's preparation, 2024. Note: Map has been drawn using GIS, not to be scaled.

2.2 Rationalisation of Adaptive Capacity Indicators

Researchers are now making a concerted effort to understand why some individuals are more adept at adjusting to shifting climate circumstances. This topic has been explored by several scholars, including Hassan and Nhemachena (2008), Pelling et al. (2008), Deressa et al. (2008, 2009), Paavola (2008), Asian Development Bank

(2014), and Newton et al. (2016). The discrepancy in the availability of resources is extensively recorded. When confronted with change, some people and organisations possess the ability to promptly and comprehensively innovate and adjust in order to minimise damage and capitalise on potential advantages. Variations in adaptive capacity may account for the disparity between the theoretically achievable amount of adaptation and the actual level of adaptation (Fussel and Klein, 2006). Gaining insight into these distinctions is anticipated to be valuable for both theoretical and practical application in the realm of adaptation research.

Adaptive capacity refers to a human system's ability to adjust to climate change, including fluctuations and extreme occurrences, to mitigate potential damage, capitalize on opportunities, and manage the ensuing consequences. (Adger et al., 2003). The adaptive capacity of a system depends on the availability of financial resources, human resources, and adaptation alternatives. This capacity varies depending on the specific risks and sectors involved. For example, an area that is well equipped to manage floods may consider a heat wave to be unforeseen (Fussel and Klein, 2006). Considering the information provided, this part examines the process of choosing reasonable and practically feasible indicators for adaptive ability. The indicators are categorised into three major groups, namely environment resources capacity, social resources capacity, and economic resources capacity (Fig. 2).

2.2.1 Environmental Resources Capacity Indicators

Scholars working on environmental issues, including climate change, generally agree that recent decades have seen a drastic change in climate parameters. We are witnessing a sudden shift in climate patterns, leading to sudden floods, droughts, and cyclonic activity worldwide, with the intensity of these events being comparatively higher in Asian and African countries than in European ones. This further intensifies the degree of vulnerability and lowers adaptive capacity against climate change.

Further, available climate change literature indicates that anthropogenic causes are key drivers of rapid temperature increases (i.e., 0.85°C mean surface temperature has increased in the past 100 years). The IPCC (2014a) predicts a further increase of at least 1.50°C by the end of the 21st century. Many regions and systems anticipate greater risks from global warming at 1.50°C compared to today, necessitating adaptation

both now and up to 1.50°C. Given that India is a climate-vulnerable and resource-scarce country in terms of ecological diversity and forest cover, it is imperative to examine the environmental capacity of the Indian farming system in general, and of its farmers in particular. Therefore, a thorough review of the literature led to the selection of ten indicators. Table 1 provides a detailed explanation for each indicator.

2.2.2 Social Resources Capacity Indicators

Social resources play a crucial role in helping societies cope with climate change, especially in India, where there are multiple livelihood vulnerabilities and complicated hierarchies (Singh, 2019a & b). Social vulnerability to a changing climate is also restricting farmers from coping with it. So, this study used six indicators to show how well Indian farmers' social resources were adapting to the changing climate. These were the literacy rate, the average age of farmers, the number of female-headed households, the number of joint families, the number of progressive farmers, and the number of farmers who left the country. All these indicators are assumed to be positively associated with the social resources capacity except female-headed households. The Indian society is male-dominant, and in the majority of cases, decisions in the family solely have to be made by the male counterpart. Hence, it is assumed the female-headed households have lower adaptive capacity compared with male-headed households. This assumption is also validated by Singh (2020a). He reported that in the majority, males owned property rights and had access to information and power to make decisions, while females, in the majority, were restricted to playing the role of housewife. Though females support in numerous ways, their role is limited within the family. Table 1 provides a detailed explanation for each indicator.

2.2.3 Economic Resources Capacity Indicators

The accessibility of economic resources helps in dealing with a changing climate. The economic resources index includes 15 indicators: average land size, area under marginal farms, transportation, livestock, membership in agricultural credit societies, crop insurance, remittance, institutional credit, tractors, agricultural training, working population, farmers working in MGNREGA, crop diversification, income from farm produce, and awareness of the minimum support price. For instance, there is clear evidence that average land size has declined from 1970-71 to 2015-16 (GoI, 2017).

This resulted in a sharp increase in marginal land holdings. The number of marginal farmers increased from 36,200 in 1970-71 to 100,251 in 2021-22 (GoI, 2017). Further, in 2021–22, it was observed that only 11.84% of farmers belonging to the scheduled caste and 8.65% of farmers belonging to the scheduled tribe owned land, while the rest of the 79.33% of land was owned by other social groups. This also highlights the susceptibility of Indian farmers to changing climate (Singh and Sanatan, 2018). In other words, we expect the adaptive capacity to cope with changing climate to decrease as the number of marginal farmer increases. Among the 15 considered indicators, this indicator is considered a negative impact on economic resources capacity, while the rest of the indicators are considered to have a positive relationship with the economic resources capacity indicators. For instance, better transportation connectivity helps in the mobility of farm produce, while ownership of livestock ensures regular income even in the off-cropping season. Further, access to credit from institutional sources at marginal interest rates also helps in dealing with rural distress, which leads to suicides. Access to credit motivates farmers to diversify their cropping patterns. All these efforts have started a series of actions and created a safety net against climate change. Table 1 provides a detailed explanation for each indicator.

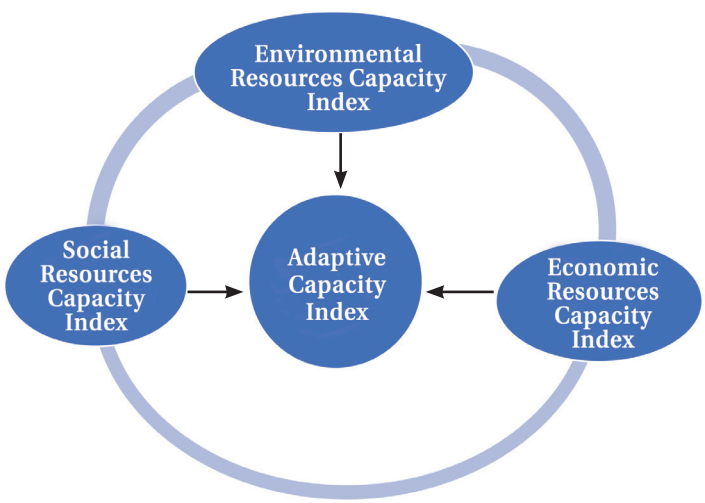


Figure 2: Conceptual framework for assessing the adaptive capacity to Climate Change

Source: Authors Conceptualization, 2024.

Table 1: Selected Rational Adaptive Capacity Indicators

Sub-components	Indicators	Description	Data Source	Literature Source
Environmental Resources Capacity Indicators (ECI)	Irrigation Intensity (%) (+)	Irrigation improves agricultural resilience and influences farmers' adaptive ability.	MoAFW, 2019	Birthal and Ali, 2005
	Forest Area (%) (+)	The expanse of forested land significantly contributes to improving farmers' adaptive ability.	MoAFW, 2019	World Bank, 2005
	Farmers' perception on natural calamities (%) (+)	The understanding of agricultural loss caused by natural catastrophes is positively associated with farmers' ability to adjust to climate change.	NSSO, 2019	Hahn et al., 2009
	Cropping Intensity (%) (+)	Higher cropping intensity significantly improves adaptive ability.	MoAFW, 2019	Birthal and Ali, 2005
	Rainfall variability (CV) (-)	Variability in rainfall adversely impacts adaptive capability.	IMD, 2019	Jatav and Kalu, 2023
	Minimum temperature variability (CV) (-)	The fluctuation of minimum temperatures negatively impacts adaptive capability.	IMD, 2019	Jatav and Kalu, 2023
	Agricultural chemical use intensity (kg/hm^2) (-)	The widespread use of agrochemicals negatively impacts the ecosystem and reduces farmers' adaptive potential.	MoAFW, 2019	Jatav and Kalu, 2023
	Agricultural land use intensity (+)	Land expansion negatively impacts ecological stability and reduces adaptive capacity.	MoAFW, 2019	Jatav and Kalu, 2023
	Ground Water Depletion (%) (-)	The depletion of groundwater impacts the hydrological cycle and therefore the adaptive ability of farmers.	CGWB, 2019	Jatav and Kalu, 2023
	Maximum temperature variability (CV) (-)	Extreme temperature fluctuations negatively impact farmers' adaptation capabilities.	IMD, 2019	Jatav and Kalu, 2023

Sub-components	Indicators	Description	Data Source	Literature Source
Social Resources Capacity Indicators (SCI)	Literacy Rate (%) (+)	The literacy rate is positively correlated with the adaptive ability of farmers.	Census, 2011	Deressa et al., 2009
	Average Age (Years) (+)	Younger farmers are anticipated to possess a greater ability to adapt to climate change.	Census, 2011	Hassan and Nhemachena, 2008
	Female-headed Households (%) (-)	Female-headed families are anticipated to possess a diminished adaptation potential in comparison to male-headed households.	NSSO, 2019	Deressa et al., 2008
	Joint family (%) (+)	Farmers living in joint families have increased resilience in coping with adversity and substantially boost adaptive ability.	NSSO, 2019	Deressa et al., 2009
	Progressive Farmers (%) (+)	Collaboration among farmers is anticipated to enhance adaptive capability.	NSSO, 2019	Deressa et al., 2008
	Out-migration (%) (+)	Out-migration is often used by farmers as a last mitigation option to cope with changes. When one or two family members relocate periodically for job, they not only remit funds to their relatives but also provide a consistent household income.	NSSO, 2019	Deressa et al., 2009
Economic Resources Capacity Indicators	Land Size (Hac.) (+)	Larger land size enhances adaptive ability to address climate change.	Agricultural Census, 2015-16	Chand et al., 2011
	Marginal Farmers Area (%) (-)	It is anticipated that marginal farmers possess less adaptation potential to climate change.	Agricultural Census, 2015-16	Chand et al., 2011
	Transportation (%) (+)	Road mobility substantially influences agricultural productivity and has a favourable correlation with adaptive capability.	Census, 2011	Sklenicka et al., 2014
	Livestock (%) (+)	Integrated crop-livestock systems improve nutrient cycling, maximize biomass consumption, and facilitate soil carbon buildup.	NSSO, 2019	World Bank, 2005
	Agri. Credit Societies (%) (+)	Affiliation with agricultural credit organizations enhances farmers' access to financial resources.	Census, 2011	Birthal and Ali, 2005

Sub-components	Indicators	Description	Data Source	Literature Source
	Crop Insurance (%) (+)	Crop insurance serves as a proactive strategy for mitigating the impacts of climate change. Consequently, increased insurance coverage enhances farmers' adaptation ability to climate change.	NSSO, 2019	Newton et al, 2016
	Remittance (%) (+)	Migrant workers provide remittances to their family, who then invest in agriculture, so improving adaptive capacity.	NSSO, 2019	Newton et al, 2016
	Institutional credit (%) (+)	Institutional agricultural loan is relatively more affordable and includes crop insurance coverage.	NSSO, 2019	Newton et al, 2016
	Tractors (%) (+)	Enhanced access to machinery, including tractors, improves the adaptive capacity of farmers.	NSSO, 2019	Huang and Wang, 2014
	Agri. Training (%) (+)	Agricultural training is essential for the efficient and sustainable use of agricultural resources.	NSSO, 2019	Newton et al, 2016
	Working population (%) (+)	Farmers between the ages of 15 and 45 who adopt compact modern technology demonstrate a higher likelihood of utilizing agricultural resources in an efficient and sustainable manner.	NSSO, 2019	Ellis, 2000
	MGNREGA (%) (+)	MGNREGA is essential for providing employment assurance to unskilled rural populations.	NSSO, 2019	Hassan and Nhemachena, 2008
	Crop diversification (+)	A higher SDI results in a lower level of economic risk.	NSSO, 2019	Paavola, 2008
	NSSO, 2019	A higher SDI results in a lower level of economic risk.	NSSO, 2019	Ziervogel et al., 2008 and Adger et al., 2003
	Farm income (%) (+)	A greater proportion of farm income signifies enhanced livelihood security for farmers, which in turn fosters increased adaptive capacity to climate change.	NSSO, 2019	Adger et al., 2003
	MSP (%) (+)	Understanding the minimum support price sets a suitable price for agricultural products and motivates farmers to grow market-oriented crops, thus improving their adaptive capacity.	NSSO, 2019	Hahn et al., 2009

Source: Author's Calculation, 2024. Note: (-) sign indicates negative relationship of indicator with targeted index, while (+) sign indicates positive relationship.

2.4 Estimation Method

Two ontological approaches exist for measuring adaptive capacity (IPCC, 2007; Smit and Wandel, 2006; Below et al., 2012). These represent inductive (data-driven) and deductive (theory-driven) approaches. The inductive approach utilized in this study emphasizes the identification of determinants, indicators, and a composite capacity index score derived from expert opinion or correlation with previous climate change-induced disasters. The approach employs proxy variables as a benchmark for assessing adaptive capacity.

This study employs the indicator method to evaluate the adaptive capacity of mainstream agro-climatic regions in India. The selected indicators effectively represent the focal development policy objective, employing a systematic approach to address climate change impacts, development linkages, and the economic, social, and environmental dimensions associated with the adaptive capacity of Indian agriculture (Halsnas and Trarup, 2009). The indicator approach for quantifying adaptive capacity utilized selected key indicators from a comprehensive set to systematically integrate these indicators, thereby reflecting the levels of adaptive capacity. Key indicators were chosen based on literature that outlines the extent and dimensions of adaptive capacity in various agro-ecological environments.

The indicators were standardized to employ a uniform scale reflecting their functional correlation with adaptive capacity; equation (1) was applied for a positive correlation, while equation (2) was utilized for a negative correlation with adaptive capacity (Pandey and Jha, 2012; Jatav and Kalu, 2023):

$$Index_{sv} = \frac{S_v - S_{min}}{S_{max} - S_{min}} \ldots\ldots\ldots\ldots\ldots\ldots\ldots\ldots (1)$$

$$Index_{sv} = \frac{S_{max} - S_v}{S_{max} - S_{min}} \ldots\ldots\ldots\ldots\ldots\ldots\ldots\ldots (2)$$

Where, S_v is the actual value of the indicator at agro-climatic region level, and S_{min} and S_{max} are the minimum and maximum values of the indicator agro-climatic region (Hahn et al., 2009; Jatav, 2024). In this way, the indicators were normalized on a scale of 0 to 1.

2.5 Assigning Weight

The assignment of appropriate weights to various components is crucial in index construction; therefore, this study utilized the statistical weight method proposed by Iyengar and Sudarshan (1982).

$$W_i = \frac{1}{\sum_{i=1}^{n} \frac{1}{\sqrt{var(Index_{sv})}} * \sqrt{Var(Index_{sv})}} \text{.....(3)}$$

Where, *Wi* is the weight of ith indicator; and $Var(Index_{sv})$ is variance of standardized value of ith indicator in the jth agro-climatic region. The calculated weights were used to construct the component index P_i for the jth agro-climatic region using equation (4).

$$P_i = \frac{\sum_{i=1}^{n} Index_{sv} * W_i}{\sum_{i=1}^{n} W_i} \left(0 < W_i < 1, \sum_{i=1}^{n} W_i = 1 \right) \text{..... (4)}$$

The adaptive capacity index for each agro-climatic region is determined by calculating the average of the size components, which include the environmental resources capacity index, social resources capacity index, and economic resources capacity index. The agro-climatic regions were ranked in descending order according to the index score derived from this study. A higher index score in an agro-climatic region indicates an increased adaptive capacity.

3. Results

3.1 Socioeconomic Status of Indian Farmers

The socioeconomic characteristics indicate that families are composed of young individuals who possess a high level of education and live in nuclear family arrangements (Table 2). Most farmers own marginal and tiny plots of land, often less than 2 hectares in size. Regarding technical proficiency, a mere 1.12% of farmers have received formal agricultural training. In contrast, around 18.98% and 16.53% of farmers have sought guidance from other farmers and self-help organisations (SHGs), respectively. MGNREGA served as the only source of hope during the off-cropping season, with around 45.07% of farmers engaging in MGNREGA to guarantee their

livelihood stability. As a result of connections in the institutional credit system, around 60% of farmers have obtained loan from institutions, whereas farmers have a 52% rate of indebtedness. The situation extends beyond loans and include a lack of information about the Minimum Support Price (MSP). Furthermore, a mere 19.72% of farmers possess knowledge about the Minimum Support Price (MSP). Consequently, due to limited access to advanced technology and market trends, approximately 12.87% of farmers have not diversified their cropping pattern as an adaptation strategy to mitigate the negative effects of climate change and cope with market disruptions. There was just one encouraging aspect: farmers had a reasonable level of awareness about natural disasters. Approximately 63.89% of farmers acknowledged that natural disasters were the primary cause of crop losses.

Table 2: Socioeconomic Characteristics of Indian Farmers

Indicators	India
Average Family Size (Nos.)	5.27
Literacy Rate (%)	74.04
Average Age (Years)	29.89
Farmers taken Professional Training (%)	1.12
Seasonal Migration for Employment (%)	1.47
Average Annual Farm Income (Rs.)	52, 272
Average Land Size (Hac.)	1.15
Indebtedness Rate (%)	52.00
Farmers have taken Credit from Institutional Source (%)	60.00
Irrigation Intensity (%)	123.10
Cropping Intensity (%)	142.13
Area not available for Cultivation (%)	16.11
Farmers are Member of SHG (%)	16.53
Farmers having Livestock (%)	74.34
Farmers working under MGNREGA (%)	45.07

Indicators	India
Female-headed household (%)	12.97
Farmers aware of Minimum Support Price (%)	19.72
Farmers sharing Knowledge to Fellow Farmers (%)	18.98
Farmers receiving Remittances (%)	10.17
Farmers living in Joint Family (%)	40.45
Farmers growing more than one Crop in a Season (%)	12.87
Farmers perceived that Natural Calamities was main reason for Crop Loss (%)	63.89

Source: Estimated from NSSO, 77th round unit level data, 2019, Census, 2011, MoAFW, 2019.

3.2 Environmental Resources Capacity Index (ERCI)

Tackling climate change as a unified effort is a major current obstacle to maintaining the long-term viability of socio-ecological systems. Few et al. (2007) emphasised that the main obstacle is in establishing a significant connection between comprehending worldwide processes, local susceptibilities, and the ability to react. Communities that have more access to resources are likely to have a higher ability to respond sustainably to the actual or predicted effects of climate change. Access to both material and intangible resources not only enables practical actions, such as sustaining one's livelihood, but also fosters the development of purposeful lives and disrupts established social systems (Smit and Wandel, 2006).

Among the 14 agro-climatic regions of India, the Eastern Himalayan Region (EHR) demonstrates greater ecological sustainability, while the South Plateau & Hills Region (SPHR) exhibits significantly lower environmental sustainability (Table 2). The cross-indicator analysis identifies that the primary factors contributing to lower environmental sustainability in the SPHR, as opposed to the EHR, include reduced forest coverage, decreased livestock ownership, and lower cropping intensity. The EHR constitutes 24.13% of the total forest area, while the SPHR represents only 16.60%. Additionally, approximately 86.63% of farmers in EHR owned livestock, whereas the figure for SPHR is only 70.00%. Irrigation intensity measured 125.25% in EHR, compared to 116.73% in SPHR. Farmers in the SPHR employ a greater quantity of chemical fertilizers compared to those in the EHR.

3.3 Social Resources Capacity Index (SRCI)

The connection between community change agents and the individuals they want to influence implies the existence of extensive networks that may facilitate social learning in response to the intricate problems presented by climate change. Pelling et al. (2008) argue that the impact of informal networks on adaptive capacity is determined by the quality, quantity, and goals of individuals who are linked within communities of practice, as well as the persons who bridge the boundaries between these communities and the objects they interact with.

This study has selected nine indicators to create a social resources capacity index for various agro-climatic regions of India. Among the agro-climatic regions, the Trans Gangetic Plain region (TGPR) has the highest social resource capacity (i.e., 0.529), while the East Coast Plains and Hills region (ECPHR) has the lowest social resource capacity to deal with changing climates (Table 3). The cross-indicator analysis shows that the population in the TGPR is relatively younger and literate compared with the ECPHR. In other words, about 76.29% of farmers in TGPR are literate, while only 68.73% of farmers in ECPHR are literate. This study assumes that households headed by women are less able to adapt, and the fact that only 8.77% of households in TGPR were headed by women was confirmed by the results. In ECPHR, that number rose to 18.15 %. On the contrary, joint family structure is assumed to be positively associated with the adaptive capacity. It is reported that about 42.24% of farmers lived in a joint family system in the TGPR, while only 21.98% of farmers lived in ECPHR.

3.4 Economic Resources Capacity Index (ERCI)

This study selected 15 indicators to create an economic resource capacity index for various agro-climatic regions of India. According to the data mentioned in Table 4, the western dry region, which includes parts of Rajasthan and Punjab, has the highest economic resource capacity, while the eastern Himalayan region, which includes north-eastern states such as Mizoram, Assam, Manipur, Tripura, Nagaland, and so on, has the lowest economic resource capacity among the agro-climatic regions.

The cross-indicator analysis shows that WDR has higher economic security than EHR because it has fewer marginal farmers, better access to all seasonal roads, more livestock ownership, higher membership in agriculture credit societies, larger insured

cropped areas, higher remittances, better access to institutional credit, a higher working population, a diversified cropping pattern, and more awareness of the minimum support price. These are some of the main factors that make WDR more economically secure compared to EHR.

In other words, the mean land size in WDR was 0.51 hectare, while it was only 0.41 hectare in EHR. Further, only 29.62% of marginal farmers were reported in WDR, while 66.33% of marginal farmers were reported in EHR. Likewise, about 17.35% of farmers have taken credit from agricultural credit societies at a marginal interest rate in WDR, while only 10.30% of farmers have taken credit in EHR. Similarly, 89.28% of farmers owned livestock in WDR, while only 86.88% of farmers owned livestock in EHR. Furthermore, 84.64% of farmers have diversified their employment portfolio and worked in MGNEGA in WDR, while only 44.60% of farmers worked in MGNREGA in EHR. These statistics in totality revealed that farmers in the western dry region are relatively more economically secure than those in the eastern Himalayan region.

3.5 Adaptive Capacity Index (ACI)

The emphasis of a rapidly expanding field of study is the significance of adaptive ability in long-term adaptation to climate change. According to Adger (2003), adaptive capacity is triggered by a mix of factors including a shift in perceived risk or effect, attitudes, regulations, or market circumstances, together with a supporting institutional framework for networking. Household-scale evaluations of adaptive capacity, which prioritise vulnerability reduction, have their origins in the domains of hazard management, global environmental change, and sustainable lifestyles. Their goal is to acquire information that may improve the ability to minimise exposure and respond effectively to dangers.

The Eastern Himalayan Region (EHR) ranked top among agro-climatic regions due to its higher environmental resource capacity (environmental resource capacity index value, i.e., 0.702), while ECPHR's relatively limited environmental resource capacity resulted in a lower adaptive capacity (i.e., 0.438). This indicates that environmental factors are very important to maintain higher resource capacity in dealing with climate change (Table 5). Despite having higher economic and social resource capacities, the western dry region (WDR) and the trans-Gangetic plain region (TGPR) have lower

environmental resource capacities. However, these agro-climatic regions rank 7 and 4 respectively in the adaptive capacity index.

Table 2: Rank of the 14 agro-climatic regions in environmental dimension of Adaptive Capacity to Changing Climate

Indicators	Agro- Climatic Regions													
	EHR	WHR	EPHR	CPHR	LGPR	WDR	ECPHR	WCPGR	GPHR	UGPR	MGPR	TGPR	WPHR	SPHR
Area under forests	0.923	0.739	1.000	0.516	0.405	0.289	0.785	0.625	0.411	0.041	0.081	0.000	0.582	0.468
Agricultural land use intensity	0.814	0.943	1.000	0.522	0.295	0.456	0.800	0.729	0.464	0.113	0.351	0.000	0.381	0.623
Agricultural chemical use intensity	1.000	0.899	0.795	0.604	0.031	0.853	0.546	0.865	0.364	0.254	0.652	0.119	0.000	0.246
Groundwater depletion	0.813	0.710	0.517	0.134	1.000	0.024	0.536	0.303	0.000	0.088	0.199	0.163	0.218	0.269
Rainfall variability	0.521	1.000	0.492	0.649	0.229	0.640	0.000	0.077	0.513	0.614	0.663	0.763	0.387	0.030
Minimum temperature variability	1.000	0.962	0.259	0.467	0.345	0.650	0.037	0.182	0.000	0.654	0.497	0.745	0.056	0.044
Maximum temperature variability	0.213	0.437	0.059	0.596	0.002	0.879	0.524	0.097	1.000	0.597	0.356	0.764	0.512	0.624
Cropping intensity	0.404	0.194	0.198	0.473	1.000	0.305	0.160	0.150	0.000	0.684	0.531	0.967	0.338	0.074
Farmers' perception on natural calamities	0.632	0.399	0.703	0.894	0.815	0.000	0.552	0.728	1.000	0.684	0.391	0.146	0.697	0.644

Indicators	Agro- Climatic Regions													
	EHR	WHR	EPHR	CPHR	LGPR	WDR	ECPHR	WCPGR	GPHR	UGPR	MGPR	TGPR	WPHR	SPHR
Rank	1	2	3	4	5	6	7	8	9	10	11	12	13	14

Source: Author's estimation, 2024. **Note:** WHR, Western Himalayan Region; EHR, Eastern Himalayan Region; CPHR, Central Plateau and Hills Region; WDR, Western Dry Region; EPHR, Eastern Plateau and Hills Region; ; TGPR, Trans-Gangetic Plain Region; LGPR, Lower Gangetic Plain Region; UGPR, Upper Gangetic Plains Region; GPHR, Gujarat Plains and Hills Region; MGPR, Middle Gangetic Plains Region; ECPHR, East Coast Plains and Hills Region; WCPHR, West Coast Plains and Ghats Region; WPHR, Western Plateau and Hills Region; SPHR, Southern Plateau and Hills Region

Table 3: Rank of the 14 agro-climatic regions in social dimension of Adaptive Capacity to Changing Climate

Indicators/ ACZ	TGPR	MGPR	GPHR	CPHR	LGPR	WPHR	EHR	WCPGR	UGPR	WDR	EPHR	SPHR	WHR	ECPHR
Literacy Rate	0.713	0.623	0.730	0.641	0.722	0.716	0.721	0.821	0.660	0.596	0.658	0.672	0.711	0.687
Average Age	0.910	0.499	0.250	0.500	0.556	0.503	0.513	0.479	0.275	0.426	0.295	0.413	0.307	0.414
Female-headed house-holds	0.912	0.909	0.895	0.910	0.866	0.883	0.876	0.789	0.876	0.871	0.868	0.820	0.861	0.181
Joint Family	0.464	0.550	0.415	0.465	0.318	0.337	0.430	0.252	0.543	0.449	0.353	0.275	0.400	0.220
Pro-gressive Farmers	0.171	0.217	0.474	0.204	0.260	0.220	0.083	0.181	0.130	0.089	0.281	0.247	0.105	0.261
Out-migration	0.003	0.014	0.019	0.033	0.023	0.027	0.019	0.012	0.009	0.035	0.008	0.008	0.010	0.011
Social Resources Capacity Index	0.529	0.468	0.464	0.459	0.458	0.447	0.440	0.422	0.415	0.411	0.411	0.406	0.399	0.296
Rank	1	2	3	4	5	6	7	8	9	10	11	12	13	14

Source: Author's estimation, 2024.

Table 4: Rank of the 14 agro-climatic regions in Economic dimension of Adaptive Capacity to Changing Climate

Indicators/ ACZ	WDR	GPHR	WPHR	CPHR	SPHR	TGPR	MGPR	ECPHR	WCPGR	EPHR	WHR	LGPR	UGPR	EHR
Land size	0.507	0.499	0.561	0.523	0.628	0.473	0.559	0.449	0.424	0.327	0.380	0.642	0.004	0.515
marginal farmers Area	0.704	0.674	0.579	0.599	0.461	0.324	0.843	0.343	0.257	0.506	0.337	0.205	0.260	0.553
Transportation	0.490	0.943	0.671	0.386	0.855	0.882	0.374	0.650	0.911	0.437	0.567	0.356	0.406	0.362
Livestock	0.893	0.822	0.732	0.876	0.710	0.936	0.790	0.639	0.586	0.608	0.865	0.725	0.819	0.574
Agri. Credit Societies	0.174	0.356	0.379	0.115	0.210	0.284	0.159	0.152	0.409	0.103	0.103	0.103	0.070	0.029
Crop Insurance	0.226	0.166	0.078	0.147	0.060	0.004	0.013	0.090	0.050	0.096	0.008	0.051	0.044	0.004
Remittances	0.105	0.028	0.061	0.081	0.086	0.084	0.090	0.263	0.180	0.067	0.140	0.152	0.196	0.020
Institutional Credit	0.470	0.606	0.614	0.543	0.666	0.559	0.435	0.536	0.653	0.405	0.494	0.306	0.584	0.357
Tractors	0.039	0.026	0.017	0.034	0.008	0.041	0.022	0.004	0.008	0.014	0.014	0.002	0.020	0.002
Agri. Training	0.002	0.007	0.012	0.007	0.035	0.011	0.009	0.016	0.021	0.011	0.009	0.015	0.003	0.008
Working Population	0.442	0.370	0.354	0.434	0.295	0.334	0.456	0.322	0.280	0.355	0.339	0.310	0.435	0.368
MGNREGA	0.846	0.221	0.452	0.635	0.455	0.058	0.162	0.618	0.307	0.677	0.446	0.589	0.261	0.674
Crop diversification	0.149	0.101	0.287	0.177	0.195	0.100	0.192	0.145	0.144	0.045	0.146	0.003	0.200	0.031
Farm Income	0.287	0.243	0.264	0.321	0.169	0.372	0.383	0.187	0.129	0.325	0.298	0.244	0.326	0.310
MSP	0.102	0.167	0.110	0.135	0.156	0.387	0.294	0.152	0.150	0.382	0.130	0.265	0.251	0.051

Indicators/ ACZ	WDR	GPHR	WPHR	CPHR	SPHR	TGPR	MGPR	ECPHR	WCPGR	EPHR	WHR	LGPR	UGPR	EHR
Economic Resources Capacity Index	0.362	0.349	0.345	0.334	0.333	0.323	0.319	0.304	0.301	0.290	0.285	0.264	0.259	0.257
Rank	1	2	3	4	5	6	7	8	9	10	11	12	13	14

Source: Author's estimation, 2024.

Table 5: Rank of the 14 agro-climatic regions in Adaptive Capacity Index

ACZ	Environment Resource Capacity Index	Social Resources Capacity Index	Economic Resources Capacity Index	Adaptive Capacity Index	Rank
EHR	0.702	0.440	0.257	0.467	1
WHR	0.698	0.399	0.285	0.461	2
CPHR	0.539	0.459	0.334	0.444	3
TGPR	0.407	0.529	0.323	0.420	4
EPHR	0.558	0.411	0.290	0.420	5
GPHR	0.417	0.464	0.349	0.410	6
WDR	0.455	0.411	0.362	0.409	7
MGPR	0.413	0.468	0.319	0.400	8
LGPR	0.458	0.458	0.264	0.393	9
WPHR	0.352	0.447	0.345	0.381	10
WCPGR	0.417	0.422	0.301	0.380	11
UGPR	0.414	0.415	0.259	0.363	12

ACZ	Environment Resource Capacity Index	Social Resources Capacity Index	Economic Resources Capacity Index	Adaptive Capacity Index	Rank
SPHR	0.336	0.406	0.333	0.358	13
ECPHR	0.438	0.296	0.304	0.346	14

Source: Author/s estimation, 2024

4. Discussion

Policies regarding climate change adaptation need meticulous formulation due to their intricate context among impoverished and susceptible cultures exposed to a diverse array of hazards. They should be an essential component of a development process that ensures the incorporation of climate adaptation into all relevant sectors of society, while also considering other significant factors such as social, economic, and environmental concerns. Mertz et al. (2009) proposed that national-level strategies should include targeted investments in physical and institutional assets. These investments should aim to decrease susceptibility to climate change and enhance the capacity to adapt while avoiding any unintended negative consequences. The present study results also align with the Mertz et al. (2009). This study also observed that investment in environmental protection resources may offset the negative impact of climate change and enhance the adaptive capacity of Indian farmers living in diverse agro-climatic conditions. Further, Aggarwal (2008) projected that a rise in temperature would lead to more frequent hot extremes, floods, droughts, cyclones, and gradual glacier recession, which in turn would result in greater instability in food production and adaptive capacity for Indian farmers. These results also align with the present study. Due to higher variability in rainfall and temperature, it resulted in lower environmental resource capacity (Table 2) and increased the degree of vulnerability. Furthermore, Hassan and Nhemachena's (2008) study highlights the critical role of improved market access, extension and credit services, technology, and farm assets such as labour, land, and capital in assisting farmers in adapting to climate change. These findings also coincide with the results of the current study. This study also reported that access to extension services like consultation with agricultural experts, insurance, credit, and

awareness of remunerative prices are key drivers responsible for adapting to a changing climate. Datta and Bhagirath's (2022) study highlights variations in natural, physical, and financial capital primarily account for the varying adaptive capacities among farming households. These results also align with our study on a broader spectrum. Our findings confirmed that lower social and economic resource capacity leads to lower adaptive capacity to deal with a changing climate.

5. Conclusion and Policy Recommendations

This research first inquired about the mechanisms of adaptation and the entities involved in the agricultural sector that undergo adaptation to address the challenges posed by climate change. This research utilises data collected at the household level and employs an indicator-based method to assess the adaptation potential of Indian farmers in the primary agro-climatic regions, with the exception of the island zone. The empirical findings emphasise that the scarcity of forest land in the Upper Gangetic Plains is constraining the farmers' ability. In the Eastern Himalayan region and the Eastern Plateau & Hills region, inexperienced farmers who lack training are depending on non-institutional sources and neglecting to protect their crops from natural disasters. Additionally, the Eastern Coast Plains & Hills region has the highest number of households headed by females, which further increases the vulnerability of the agriculture sector in this area. The limited availability of non-farm work, namely under the Mahatma Gandhi National Rural Employment Guarantee Act (MGNREGA), and the lack of crop diversification have reduced the capabilities of farmers in the Trans Gangetic Plains area. Similarly, farmers in the Western Dry region have faced restrictions in accessing climatic information. The overall analysis of the relative adaptation capacity index scores indicates that the Eastern Himalayan Region (EHR) exhibits the strongest adaptable ability, whilst the East Coast Plains and Hills Region (ECPHR) has the lowest adaptive capacity in addressing climate change.

This paper emphasised the need for more investigation into the possibilities for successful involvement in local and regional methods of vulnerability assessment and the improvement of adaptive capacity. This study's empirical findings indicate that female-headed households should be prioritized in both ongoing and new intervention projects concerning climate change and agriculture. Providing financial

resources enables engagement in supplementary income-generating activities. This will contribute to diversifying their livelihood sources and improving their resilience to the impacts of climate change and variability. Possible adaptation options for the most vulnerable region include diversifying agricultural systems by cultivating crops that require less water, adopting advanced farming technology such as using different crop varieties, harvesters, and irrigation pumps, constructing dams and roads, and improving the plantation mangrove forest programme in the coastal area.

This study encompasses over 95% of India's geographical area. There are a few limitations of this study that may motivate researchers to do future research. First, tracking temperature and rainfall trends in different agro-climatic zones helps in robust climate policy for regional climate-resilient planning. Second, this study only gives a spatial picture of the adaptive capacity of farmers, while spatial-temporal analysis is better to track the progress of climate policies initiated by the Indian government and farmers. Third, this study's results only rely on secondary data, while success case studies give signals about how suggested policy enhances the adaptive capacity of farmers. Lastly, determinants of adaptive capacity are also important to effect climate adaptation policy; this study ignores this aspect. By using grassroots data, future researchers may identify the determinant.

References

1. Adger, W. N., S. Huq, K. Brown, D. Conway & M. Hulme (2003). Adaptation to Climate Change in the Developing World. Progress in Development Studies, 3(3), 20-35.
2. Aggarwal, P.K. (2008). Global climate change and Indian agriculture: impacts, adaptation and mitigation. *Indian Journal of Agricultural Sciences*, 78 (10), 911-919.
3. Asian Development Bank (2014). "Technologies to support climate change adaptation". Asian Development Bank, Mandaluyong City 1550 Metro Manila, Philippines.
4. Below, T.B., Khamaldin, D.M., Dieter, K., Christian, F., Stefan, S., Rosemarie, S. & Karen T. (2012). Can farmers' adaptation to climate change be explained by socio-economic household-level variables?. Global Environmental Change, 22(1), 223-235.
5. Birthal, P. S. & Ali, J. (2005). Potential of livestock sector in rural transformation, In: Rural Transformation in India: The Role of Non-farm Sector (Rohini Nayyar and A N Sharma editors) Institute for Human Development and Manohar Publishers and Distributors, New Delhi.
6. Byers, E.A., J.W. Hall, J.M. Amezaga, G.M. O'Donnell & A. Leathard (2016). Water and climate risks to power generation with carbon capture and storage. Environmental Research Letters, 11(2), 11-24.
7. Chand, R., P.A. Lakshmi Prasanna & Aruna, S. (2011). Farm size and productivity: understanding the strengths of smallholders and improving their livelihoods. Economic & Political Weekly, 48, (26&27), 5-11.
8. Clements, R. (2009). The Economic Cost of Climate Change in Africa. Pan African Climate Justice Alliance (PACJA), 1-52.
9. Dasgupta, S., Ruchi, B., S.K. Zeeshan Ali, J.S. Jiju, & Prashant, T. (2022). Adaptive Capacity and Vulnerability of the Socio-ecological system of Indian Himalayan Villages under Present and Predicted Future Scenarios. *Journal of*

Environmental Management. 302 (A), 113946.
10. Datta, P. & Bhagirath, B. (2022). Assessment of Adaptive Capacity and Adaption to Climate Change in the Farming Households of Eastern Himalayan Foothills of West Bengal, India. Environmental Challenges, 7, 100462.
11. Dryzek, J.S. (2016). Institutions for the Anthropocene: Governance in a Changing Earth System. *British Journal of Political Science*, 46(4), 937-956.
12. Deressa T, Hassan RM, Alemu T, Yesuf M & Ringler C. (2008). "Analysing the determinants of farmers' choice of adaptation methods and perceptions of climate change in the Nile Basin of Ethiopia". Washington DC: International Food Policy Research Institute.
13. Deressa, T.T., Hassan, R.M., Ringler, C., Alemu, T. & Yesuf, M. (2009). Determinants of farmers' choice of adaptation methods to climate change in the Nile Basin of Ethiopia. Global Environmental Change 19 (2), 248-255.
14. Ellis, F. (2000). "Rural Livelihoods and Diversity in Developing Countries". Oxford University Press, New York.
15. Few, R., Brown, K. & Tompkins, E.L. (2007). Climate change and coastal management decisions: insights from Christchurch Bay, UK. Coastal Management, 35 (2& 3), 255–270.
16. Fussel, H.M. & Richard, J.T. Klein (2006). Climate Change Vulnerability Assessments: An Evaluation of Conceptual Thinking. Climate Change, 75(1), 20-35.
17. Feder, G. (1988). Land policies and farm productivity in Thailand. Baltimore, Maryland: Johns Hopkins University Press.
18. Gupta, H.S. & S.K. Bandyopadhyay (2014). "Strategies to enhance adaptive capacity to climate change in Vulnerable Regions". Centre for Environment Science and Climate Resilient Agriculture, Indian Agricultural Research Institute, New Delhi, 1-129.
19. Guntukula, R. (2020). Assessing the impact of climate change on Indian agriculture: Evidence from major crop yields. *Journal of Public Affairs*, 20(1), 20- 40.
20. Huang, J.K. & Wang Y.J. (2014). Financing sustainable agriculture under climate change. *Journal of Integrative Agriculture*, 13(4): 698-712.
21. Hassan, R. & Nhemachena, C. (2008). Determinants of African farmers' strategies for adapting to climate change: multinomial choice analysis. *African Journal of Agricultural Resources Economics*, 2 (1), 83-104.
22. Halsnas K. & Trarup S. (2009). Development and climate change: A mainstreaming approach for assessing economic, social, and environmental impacts of adaptation measures. Environmental Management. 43(5): 765-778.
23. Hahn, M.B., Riederer, A. M. & S.O. Foster (2009). The Livelihood Vulnerability Index:
24. A Pragmatic Approach to Assessing Risks from Climate Variability and Change- A Case
25. Study in Mozambique. Global Environmental Change, 19(2), 1-19.
26. IPCC (2007). "Climate Change 2007: Impacts, Adaptation and Vulnerability". Contribution of Working Group II to the Fourth Assessment Report of the Intergovernmental Panel on Climate Change, M.L. Parry, O.F. Canziani, J.P. Palutikof, P.J. van der Linden and C.E. Hanson, Eds., Cambridge University Press, Cambridge, UK.
27. IPCC (2012b). "Meeting Report of the Intergovernmental Panel on Climate Change Expert Meeting on Geoengineering". Edenhofer, O., R. Pichs-Madruga, Y. Sokona, C. Field, V. Barros, T.F. Stocker, Q. Dahe, J. Minx, K. Mach, G.-K. Plattner, S. Schlomer, G. Hansen, and M. Mastrandrea (eds). IPCC Working Group III Technical Support Unit, Potsdam Institute for Climate Impact Research, Potsdam, Germany.
28. IPCC (2013b). "Summary for Policymakers. In: Climate Change 2013: The Physical Science Basis". Contribution of Working Group I to the Fifth Assessment Report of the Intergovernmental Panel on Climate Change. Stocker, T.F., D. Qin, G.K. Plattner, M. Tignor, S.K. Allen, J. Boschung, A. Nauels, Y. Xia, V. Bex, and P.M. Midgley (eds.). Cambridge University Press, Cambridge, United Kingdom and New York, NY, USA, pp. 3-29.
29. IPCC (2014a). "Summary for Policymakers. In: Climate Change 2014: Impacts, Adaptation, and Vulnerability". Part A: Global and Sectoral Aspects. Contribution of Working Group II to the Fifth Assessment Report of the Intergovernmental Panel on Climate Change. Field, C.B., V.R. Barros, D.J. Dokken, K.J. Mach, M.D. Mastrandrea, T.E. Bilir, M. Chatterjee, K.L. Ebi, Y.O. Estrada, R.C. Genova, B. Girma, E.S. Kissel, A.N. Levy, S. MacCracken, P.R. Mastrandrea, and L.L. White (eds.)]. Cambridge University Press, Cambridge, United Kingdom and New York, NY, USA, pp. 1-32.
30. Iyengar, N.S. & Sudarshan, P. (1982). A method of classifying regions from multivariate data. Economic and Political Weekly. 17, 2047–2052.
31. Jatav, S.S. (2020). Bridging the gap between biological and social vulnerability in rural India: A community livelihood vulnerability approach. Area Development and Policy, 5(4): 390-411.
32. Jatav, S.S. (2023). Factors affecting household food security in Bundelkhand region of India. Indian Journal of Traditional Knowledge, 59(4), 1-9.
33. Jatav, S.S. & Sanatan, N. (2022). Access and determinants of formal agriculture credit in Uttar Pradesh, India. *Journal of Rural Development*, 42(2), 185-197.

34. Jatav, S.S. & Kalu, N. (2023). Measuring the agricultural sustainability of India: An application of pressure-state-response (PSR) model. Regional Sustainability, 4(3): 218-234.
35. Jatav, S.S. (2024). Farmers' perception of climate change and livelihood vulnerability: A comparative study of Bundelkhand and Central regions of Uttar Pradesh, India. Discover Sustainability, 5(11), 1-16.
36. Mysiak, J., S. Surminski, A. Thieken, R. Mechler, & J. Aerts (2016). Brief communication: Sendai framework for disaster risk reduction – Success or warning sign for Paris? Natural Hazards and Earth System Sciences, 16(10), 2189-2193.
37. Mertz, O., Kirsten, H., Jorgen, E. O. & Kjeld, R. (2009). Adaptation to climate change in Developing Countries. Environmental Management, 43, 743-752.
38. Newton, P., Gomez, A.E.A., Jung, S., Kelly, T., de Araújo Mendes, T., Vang Rasmussen, L., dos Reise, J.C., de Aragão Ribeiro Rodrigues, R., Tipper, R., van der Horst, D. & Watkins, C. (2016). Overcoming barriers to low carbon agriculture and forest restoration in Brazil: the Rural Sustentável project. World Development Perspective 4, 5-7.
39. Pelling, M., High, C., Dearing, J. & Smith, D. (2008). Shadow spaces for social learning: a relational understanding of adaptive capacity to climate change within organisations. Environmental Planning A: Economy and Space, 40(4), 867-884.
40. Paavola, J. (2008). Livelihoods, vulnerability and adaptation to climate change in Morogoro, Tanzania. Environmental Science and Policy, 11, 642-654.
41. Pandey, R., & Shashidhar, K. Jha. (2012). Climate vulnerability index - measure of climate change vulnerability to communities: a case of rural Lower Himalaya, India. Mitigation and Adaption Strategies to Global Change, 17, 487-506.
42. Singh, S.S. & Sanatan, N. (2018). Land inequality and agricultural sustainability in Uttar Pradesh, India: A Regional Analysis. Asian Journal of Science and Technology, 9(11), 923-932.
43. Singh, S. (2020a). Bridging the gap between biophysical and social vulnerability in rural India: the community livelihood vulnerability approach. Area and development policy, 5(2), 1-23.
44. Singh, S. (2020b). Farmers' perception of climate change and adaptation decisions: A micro-level analysis of farmers in the Bundelkhand region, India. Ecological Indicators, 116, 1-15.
45. Singh, N.P., Bhawna, A. & Surendra, S. (2020). Impact of climate change on agriculture in India: Assessment for Agro-climatic Zones. Policy Paper No. 35, ICAR- National Institute of Agricultural Economics and Policy Research (NIAP), New Delhi, 7-83.
46. Smit, B. & Wandel, J. (2006). Adaptation, adaptive capacity and vulnerability. Global Environmental Change, 16 (3), 282–292.
47. Sklenicka P, Janovska V, Salek M, Vlasak J. & Molnarova, K. (2014). The farmland rental paradox: extreme land ownership fragmentation as a new form of land degradation. Land Use Policy 38, 587-593.
48. Sovacool, B.K., B.-O. Linnér, & M.E. Goodsite (2015). The political economy of climate adaptation. Nature Climate Change, 5(7), 616-618.
49. Swain, M. (2014). Crop insurance for adaptation to climate change in India. Asia research centre working paper. London School of Economics & Political Science Houghton Street London, United Kingdom.
50. World Bank (2005). "Land Consolidation Issues in Northern Vietnam- Institutions, Implementation, Impacts". Working Paper, The World Bank.
51. Winsemius, H., Jongman, B., Veldkamp, T., Hallegatte, S., Bangalore, M. & Ward, P. (2018). Disaster risk, climate change, and poverty: assessing the global exposure of poor people to floods and droughts. Environment and Development Economics, 23(3), 328-348.
52. Ziervogel, G., A. Cartwright, A. Tas, J. Adejuwon, F Zermoglio, M. Shale & B. Smith. (2008). "Climate change and adaptation in African agriculture". Stockholm environment institute, 17-19.

Impact on the Pune City's Food Accessibility During a Rare, Disastrous Event: A Case of the COVID-19 Lockdown in India

Amruta Garud[1], Bakul Rao[2]

Abstract

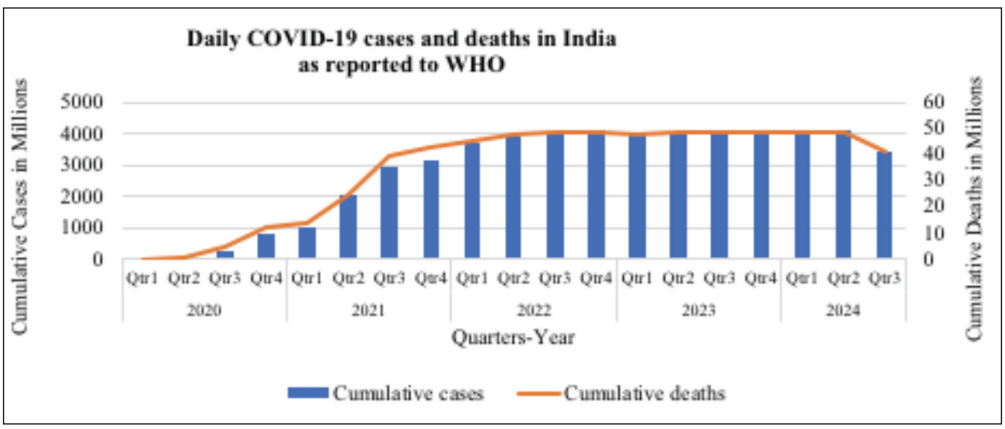
Undoubtedly, the COVID-19 outbreak caught the world off guard, exposing the unpreparedness to mitigate such biological disastrous event and its's impact on the socio-economic life. Amidst the pandemic the management of healthcare infrastructure was the prime focus across the globe, many countries had to extend social assistance programs to mitigate the impact on food security caused by unavailability due to mobility restrictions, and inaccessibility due to loss of income to buy food. This research provides empirical evidence of the implications of the COVID-19 national lockdown on Pune city's food supply chain, daily food inflows and prices; derived from the local market level data and field insights. The implications are quantified by comparing three scenarios which are predominantly considered while addressing any disaster namely before, during, and after the national lockdown. There is sufficient evidence to affirm that not only the restricted food miles resulted in a sudden-sharp dip in the food inflows and higher fluctuations in the prices, but also resulted in evolution of a parallel resilient supply chain making the local markets redundant. This calls for an inclusion of mitigation and response plan for such mobility restriction led disaster in the District Disaster Management Plan in consultation with policy makers, regional planners and business owners to strategically harness the food self-sufficiency opportunities.

Keywords: *COVID-19-Lockdown, Disaster Mitigation, Food Security, Food Supply Chain, Self-sufficiency*

[1] Assistant Professor, BNCA, Pune, India
[2] Professor, Sustainable Development Group, CTARA, IIT Bombay, Mumbai, India

1. Introduction

The COVID-19 outbreak has caught the world off guard and continued to have an unprecedented impact on the health, economic, and social sectors threatening the lives and livelihoods (Nundy et al., 2021; Ranjbari et al., 2021; UN, 2020), which has made the achievement of Sustainable Development Goals even more challenging. Moreover, for developing countries like India, the agony in achieving SDGs, predominantly, the second SDG focusing on zero hunger, continues to decline further as the pandemic has become an additional threat to food security, especially for poor households (Fan et al., 2020; Food Security Information Network, 2020; Reardon et al., 2020). The mobility restrictions and the sudden non-availability of migrant labor disrupted the harvesting activities during the nationwide lockdown (Dev, 2020; Gray, 2020), leading to a reduction in purchasing power, supply shortage, and price fluctuation in the market thus the food security (Siche, 2020). While most of the literature highlighted the disruptions in the food supply chain in mainly the distribution phase, there were very few studies highlighting the food inadequacy and nutrition deficiency due to quarantine period (Elsahoryi et al., 2020; Madzorera et al., 2021)



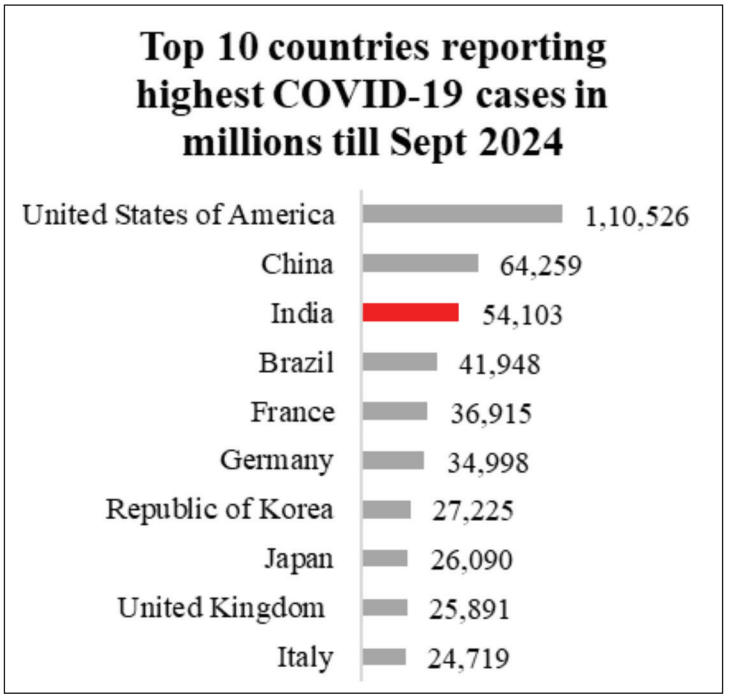


Figure 1 (a): The COVID-19 cumulative cases and deaths in India; and (b) comparison of top 10 countries in daily cases as of 28th September 2024

Source: (WHO, 2024)

India recorded its first COVID-19 case on 30th January 2020 and on 24th March 2020 the national lockdown was announced which lasted till 8th June 2020 followed by the unlock phase 1. The research focuses on the food inaccessibility during the first wave of the pandemic in India (30th January 2020 to 31st August 2020) when mobility restrictions were maximum. The trajectory of India and the Pune city selected for the research has been presented in Figure 1. In response, the Government of India constituted 11 empowered groups[4] on 29th March 2020 for taking informed decisions, in which one

[4] Eleven empowered groups constituted by the Government of India are: (i) medical emergency planning, (ii) availability of hospitals, isolation and quarantine facility, disease surveillance and testing, (iii) ensuring availability of essential medical equipment, (iv) augmenting human resource and capacity building, (v) supply chain and logistics management, (vi) coordination with private sector, (vii) economic and welfare measures, (viii) information, communications and public awareness, (ix) technology and data management, (x) public grievance and (xi) strategic issues related to lockdown

of the group was focusing on the on supply chain and logistics management specific to mobility of food and pharma industry during the nationwide lockdown (PIB, 2021). Mohamed Shaluf, (2007) suggests three broad categories of disaster namely natural, man-made, and hybrid disasters covering all the possible types of disasters. Unlike other disasters such as flood management, drought management (Tirivangasi, 2018) where strategies for prevention and mitigation are already in place through various policies and agencies on national, state and local level; however the first wave of the COVID-19 lockdown allowed response and recovery strategies only. Although after the first wave, the pandemic lockdown did give some time to the government to prepare action plan for the 1st line of response but unpreparedness and lack of mitigation strategy towards such events initially did amplify impact. Thus, this research categorises lockdown kind of situation where mobility restrictions are imposed as an aftermath of biological disaster and aims at assessing in-accessibility of food in such situations.

2. Data and Method

The presented research provides empirical evidence of the impact of the COVID-19 lockdown on the food security of one of the worst-pandemic-hit cities in India, that is Pune city, which is highly dependent on the longer food miles to cater its humongous urban food demand. The research uses three scenarios namely before, during, and after the national lockdown to build the empirical evidences for (1) alteration in the food supply chain due to the mobility restrictions amidst the COVID-19 lockdown using the insights from field and literature by comparing the before and during COVID-19 lockdown food supply chains; and (2) sudden inaccessibility of bare essential food items due to the altered food supply chains amidst the COVID-19 lockdown, using the daily food inflow data for bare essential food groups concerning the optimum food security, by comparing fluctuations in the average monthly inflows and prices for the three scenarios namely, pre-COVID-19, during-COVID-19-lockdown, and during-COVID-19-unlock. The period before the 23rd March 2020 is considered as the pre-lockdown phase, hereafter mentioned as pre-COVID-19; from 23rd March 2020 to 8th June 2020 is the lockdown phase, hereafter mentioned as during-COVID-19-lockdown, and post 8th June 2020 to 31st August 2020 is the unlock phase, hereafter mentioned as during-COVID-19-unlock.The research also maps the food miles for the Pune city to highlight the dependency on the food travel from longer distances to cater its daily

food demands, followed by the impact on food supply chains and daily food inflows for which the summary of the data and method is given in Figure 2.

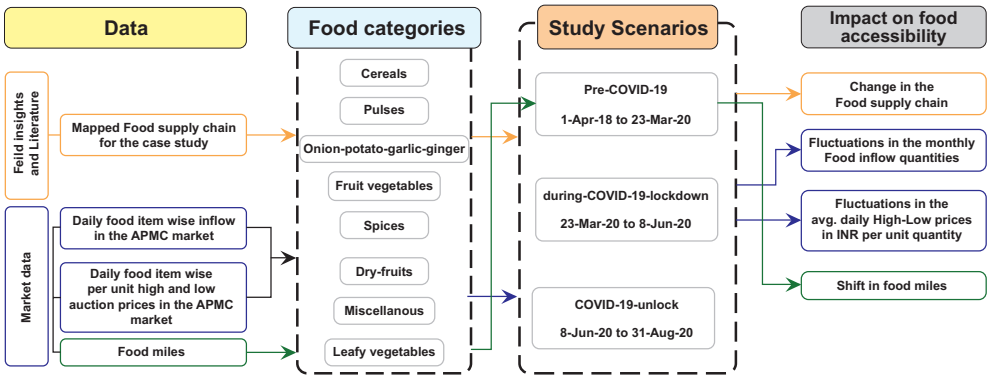


Figure 2: Summary of data and methodology

The lockdown and unlock terms used in this research are as per the timely guidelines (Ministry of Home Affairs, 2020) issued by the Ministry of Home Affairs during the pandemic period. The food supply chain for the Pune city was acquired from (Garud & Rao, 2018a) for the pre-COVID-19 scenario and for the during-COVID-19-lockdown scenario insights on the food supply alterations were collected through field observations and newspaper articles. The daily food inflow data from April 2018 to August 2020 was acquired daily from the Pune APMC's bulletin website (APMC, n.d.) and was documented systematically with reference to the food groups. The data ranging from 1st April 2018 to 31st August 2020 is analysed totalling to 884 days, of which the daily food inflow data for 703 days (79.5%) was available, and the auction prices for 519 days (58.71%) were available as shown in Table 1.

Table 1: Month and year wise summary of the APMC daily inflow data used for the research

Year	*Jan*	*Feb*	*Mar*	*Apr*	*May*	*Jun*	*Jul*	*Aug*	*Sep*	*Oct*	*Nov*	*Dec*
2018	----------➡			Y	Y	Y	Y	Y	YY	YY	YY	YY
2019	YY					YY	YY	YY			YY	YY
												🔴

Year	Jan	Feb	Mar	Apr	May	Jun	Jul	Aug	Sep	Oct	Nov	Dec
2020	YY	YY	YY	YY	YY	YY	YY	YY				
	🟡	🔵	during COVID-19 lockdown			COVID-19-unlock			⬅			

Y: only daily inflow data available; YY: both inflow and high and low rate data available

🔴 *World's first COVID-19 patient;* 🟡 *India's first COVID-19 patient;* 🔵 *Pune's first COVID-19 patient;*

***Lockdown**: 25th March – 8th Jun; **Unlock**: 8th Jun – 31st Aug*

Number of total days in the period considered from 1st April 2018 to 31st Aug 2020	884
Number of days for which daily inflow data is available	703 (79.5% of the total days)
Number of days for which both daily inflow and high and low prices data is available	519 (58.71% of the total days)

Note: The data comprised of the quantity coming into the market with its maximum and minimum per-unit price offered for that day by the producers to the local vendors. The ultimate price, inclusive of the supply chain costs, where the vendors sell the food items to the consumers, varies according to the variety, quality and location and has not been considered in this research. The food items considered for the research are grouped under eight categories, namely, cereals, pulses, onion-potato-garlic-ginger, fruit-vegetables, leafy-vegetables, spices, dry fruits, and miscellaneous.

3. Results and Discussion

A) Impact on Food Miles

The accessibility of food is essentially about the functioning food flows in the food supply chain and therefore, 'food miles' can be considered as a measure to assess accessibility. 'Food miles' as a concept advocating the local foodshed concept has been discussed widely in the literature by the developed countries. However, actual mapping of the food miles with respect to food groups and food items for an Indian city is a novel contribution of this research. For the calculation of food miles, the place at which

food was produced was considered as an origin, while the Pune APMC which receives food was considered as a destination, and by estimating the origin-destination distance in kilometres (travel distance by road estimated using google maps), the average food miles for overall food groups (presented in Figure 3) were derived. In Figure 3, the y-axis is the distance in kilometres while the x-axis the food groups are given. The whisk plot shows the longest food mile for dry fruits and miscellaneous items. It can be seen that the spices, which are mainly place specific specialities, have longer food miles. The food miles for dry-fruits show an outlier, which is especially because of the dates imported from Iraq. Interestingly, in the case of fruits, the food miles vary as per the variety due to the consumer's preference for a particular geographic variety of the produce. Overall, the food groups which cater to the bare essential dietary preference like cereals, vegetables, and pulses show comparatively lesser food miles than the other food groups, leafy-vegetables with the least food miles of all. The food miles for the date dry fruit is the highest (food mile of 3053km), and the only food item procured from out of the country; followed by the tea from Aasam and West Bangal (food miles of 1893km); rice from Haryana, Uttar Pradesh, Rajasthan, Andhra Pradhesh, Karnataka,

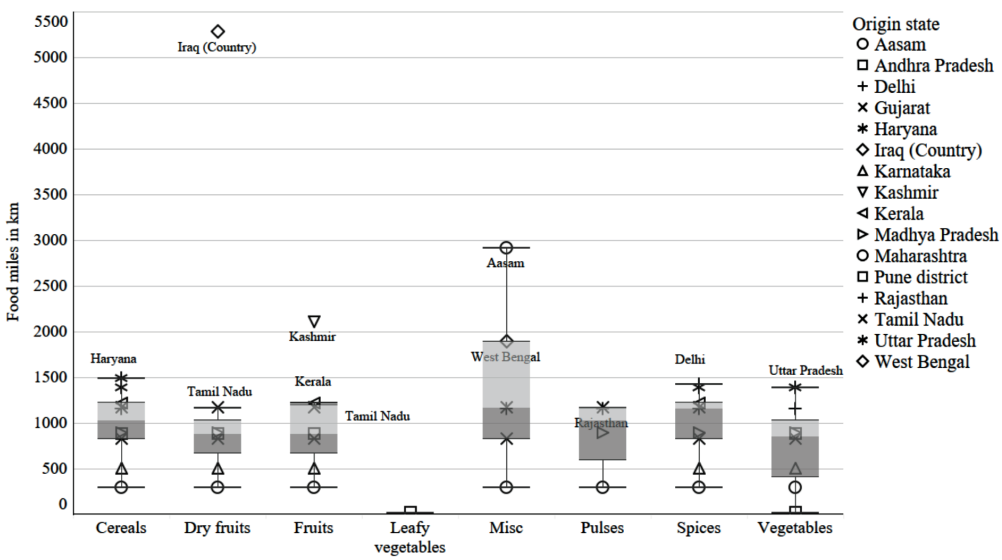


Figure 3: Food miles for Pune city as on 26th November 2019

and Maharashtra (food mile of 1021km); and for wheat from Uttar Pradhesh, Rajasthan, Andhra Pradesh, Gujarat, Karnataka, and Maharashtra (food mile of 880km). Thus, it can be understood that lesser the food miles, lesser time will be required to mitigate the impact on food security and having longer food miles increases vulnerability in the disaster kind of situation.

Note: For every incoming food produce, the origin of food produce, the quantity of the produce and vehicle details are recorded at the entrance of the APMC market. The data inventory for daily food inflow with respect to its origin for the considered time frame was huge and the authority did not agree to give access for the same. Hence, the food miles mapped here are only for 26th November 2019.

B) Impact on food supply chain

The food supply chain for Pune was derived from the food supply chain mapped for the Pune Metropolitan Region (Garud & Rao, 2018b). The food supply chain essentially consists of the production links, supply links and market links, which vary with the food category. The food categories were broadly classified into perishable and non-perishable items. The perishable items consist of vegetables, fruits, milk, meat, and poultry, whereas the non-perishable include cereals, pulses, and oilseeds. The food supply chain prior to the COVID-19 for cereals, pulses, spices, vegetables, fruits, and dairy for Pune has been given in Figure 4 (a). The local, regional and wholesale markets in the PMR region play an important role in ensuring the functioning of the regional food supply chains. The city's daily dairy supply chain was predominantly catered by regional cooperative societies from Gujarat to southern Maharashtra. The Mumbai-Bangalore (NH4) highway has made the dairy supply chain least interrupted during the lockdown period. However, one of the changes observed in the dairy supply chain was that the sanitization of the packaged milk became a standard practice during the COVID-19 outbreak. In the Pune Metropolitan Region, from the field insights, it is seen that all the census towns have a local market that serves the nearby villages. In the case of vegetables, farmers from nearby villages around the city prefer to go directly to the urban areas and sell their produce. This concept can be seen as a direct farm to the fridge; though, the number of such farmers is low. All the large farmers approach the regional APMC's with their produce in order to get a better price with optimum transport. The markets at the APMC level usually serves as a platform for daily auction

for the local vendors. However, during the COVID-19 lockdown, the large farmers or mediators or vendors (food providers) seem to have taken an advantage and skipped the usual supply chain by approaching the consumers through electronic medium and served at their doorstep or at the entrance gate in case of the gated communities.

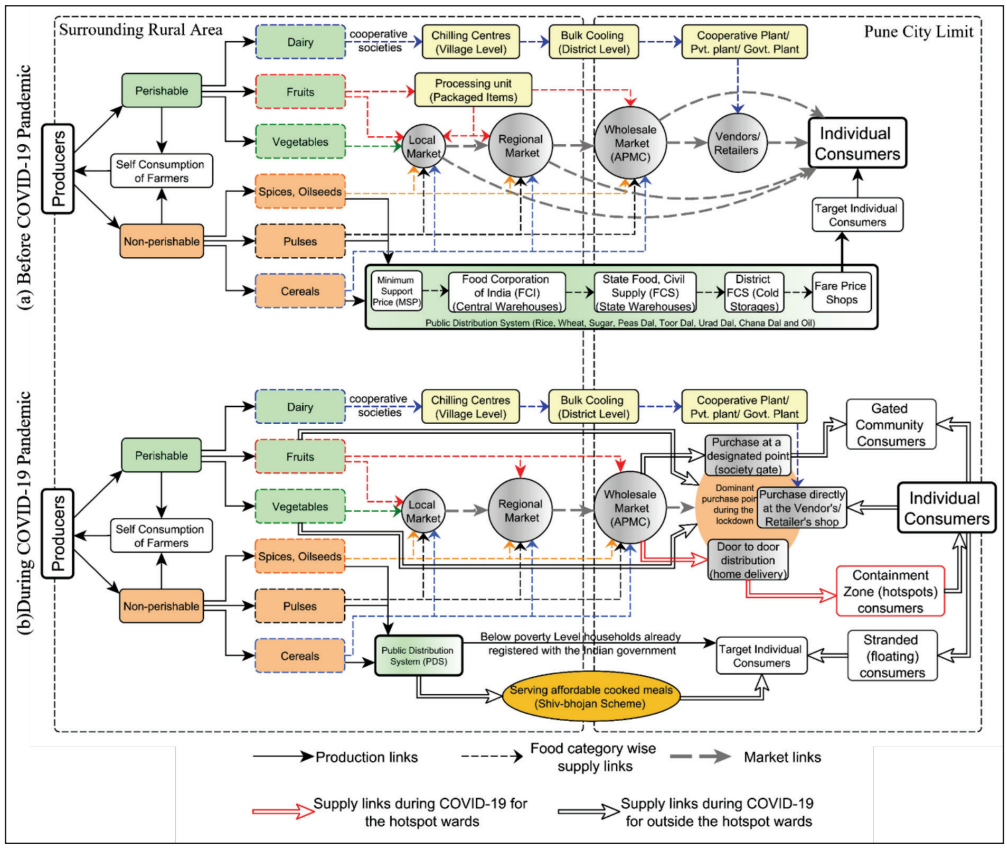


Figure 4: Food group-wise food supply chain for the Pune Metropolitan Region before and during the COVID-19 lockdown

Source: Pune- Agriculture Produce Market Committee and (Garud & Rao, 2018b)

This resulted in the prices of the items shooting up as there was no monitoring from the government with providers claiming increased costs of transportation and limited supply for the price escalation. The adapted food supply chain has been mapped in Figure 4(b), which shows a supply links during COVID-19 for the hotspot wards, and

for non-hotspot wards in the city. On comparing the before and during COVID-19 supply chains, it is seen that the consumers during the COVID-19 were divided into four major categories namely, consumers from the gated communities, consumers from the hotspot areas (containment zones), consumers stranded due to mobility restrictions, and target consumers identified under the PDS. This categorization of the consumers led to the inception of parallel contingent supply links during the COVID-19 lockdown. Otherwise, the two categories dominant in the region before COVID-19 lockdown were individual consumers and target consumers identified under the PDS. In the non-perishable items, such as cereals, pulses, and oilseeds, the central government agencies usually play an essential role with the minimum support price driving the supply chain. The large farmers directly approach the local and regional markets to fetch a higher price, while the small and marginal farmers prefer the minimum support price to shield from market vulnerabilities and cover their initial investments with a marginal profit which becomes a part of the Public Distribution System (PDS) and is distributed under two flagship schemes, namely Antodaya Anna Yojana (AAY) and Priority Households (PHH).

During the COVID-19 national lockdown, the two important interventions introduced were firstly, for the lockdown period the central government announced an additional support of 2 kilograms foodgrains per person for 3 months starting from 26th March 2020 for India, and secondly the Maharashtra government channelized the 'Shiv-Bhojan' flagship scheme through which instead of distributing raw food grains, a basic Indian meal was served twice a day. As per the AePDS[5] -Maharashtra data, the maximum number of plates served for Pune city were 4500 per day[6]. As the scope of the research was to study produce and not cooked meals, the data for actual daily plates served was not studied. Also, the scheme seems to cater to daily emergencies hungry rather than household's food security; hence, to what extent the problem of food security during the lockdown period was catered through the Shiv-Bhojan scheme is not discussed further.

[5] Aadhaar enabled Public Distribution System - AePDS portal for Maharashtra is available on http://mahaepos.gov.in/index.jsp On this portal stock receipts and details of the fair price shops are maintained.

[6] The Shiv-Bhojan plates allotted for the Pune city i.e. Pune FDO were 4500 plates per day, and for rural Pune district i.e. Pune DSO were 7150 plates per day.

C) Impact on the daily food inflows

The food inflow data for the studied eight categories have been plotted in Figure 5 where months and years are on the x-axis, a total summation of the daily inflows for a particular month are along the primary y-axis and average per day maximum and minimum price fetched, per respective unit of the inflow, are along the secondary y-axis. The during-COVID-19-lockdown time frame has been marked on every graph so that the visual comparison of the three scenarios, namely, pre-COVID-19, during-COVID-19-lockdown, and during-COVID-19-unlock, is easy.

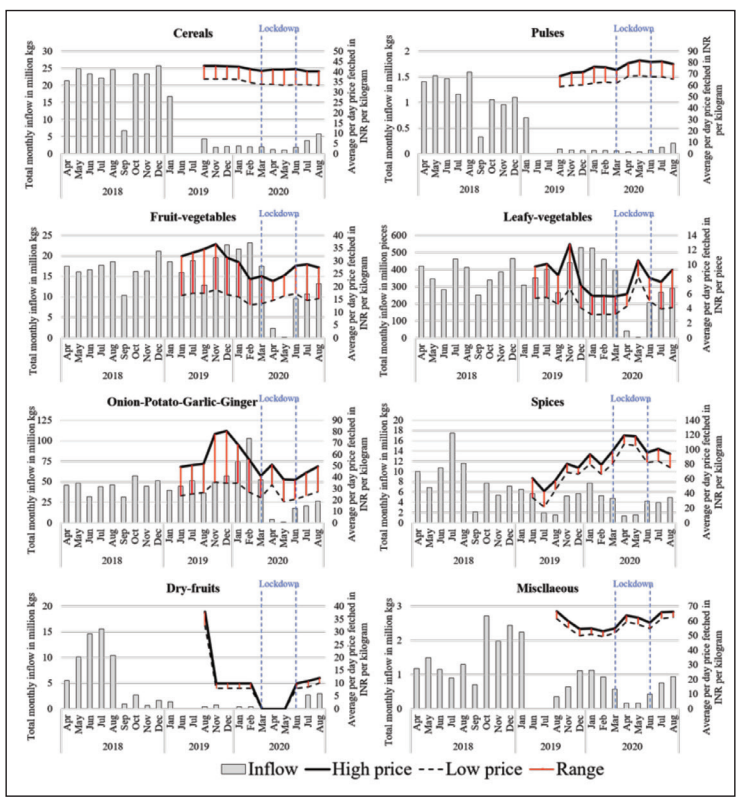


Figure 5: Food category type-wise graphs showing monthly inflow on the primary Y-axis and on along the secondary Y-axis, high and low prices fetched per kilogram for all the food categories except for vegetables which are per piece, received and auctioned at the APMC

Source: Data accessed from the Pune-Agriculture Produce Market Committee.

It was observed that prior to the COVID-19 lockdown, cereals and pulses had a seasonal inflow depending upon the harvesting cycles and onion-potato-garlic-ginger, fruit-vegetables, and leafy-vegetables showed continued monthly inflow. Also, on the prices front, the per-unit prices fetched by all the food categories have recorded a decrease in overall prices (from pre-COVID-19 to during-COVID-19-unlock), except for pulses and miscellaneous items, because of their longer shelf life. As the COVID-19 national lockdown was announced in the end of March 2019, there was a considerable sudden decline in the prices for cereals, pulses, onion-potato-garlic-ginger, and leafy-vegetables food groups which can be linked to the confounded market conditions amidst the first phase of the lockdown. Further, food group wise implications on the inflow and prices have been discussed below, and a comparative summary for the three scenarios has been represented in Table 2.

Impact on inflows of Cereals and Pulses

For the considered time frame in the research, the cereals and pulses inflows in 2018 are much higher than the average monthly inflows during the 2019 and 2020. The decline in the inflows can be linked to the heavy rains in August-September 2019 and the COVID-19 outbreak in 2020. The average monthly inflow in the pre-COVID-19 scenario (period from April 2018 to 23rd March 2020) for cereals and pulses was around 13.28 and 0.69 million kilograms, respectively. During the lockdown (period from 23rd March 2020 to May 2020), the average monthly inflow for cereals and pulses went down to 1.50 and 0.04 million kilograms amounting to a deficit of approximately 88.69% and 93.66% in the inflow, respectively. The recorded deficit was the second-highest deficit among the food categories (dry fruits being the first-highest deficit recorded) considered in this section. On the other hand, in the during-COVID19-unlock scenario, amidst the partial lockdown (June 2020 to August 2020), when the market started opening slowly, there was a steady increase of 2.44 million kilograms in the inflow of the cereals, and interestingly, pulses recorded a decrease of 0.09 million kilograms. In the during-COVID19-lockdown scenario, cereals have recorded a decrease of ₹1.59/kilogram and pulses an increase of ₹5.61/kilogram in the high average price per kilogram, which was due to the supply shortages. The shortage in supply may have happened because of the travel restrictions and unavailability of the daily labour due to the strict nation-wide lockdown, which also happened to be the harvest season for pulses.

Impact on onion-potato-garlic-ginger

The onion-potato-garlic-ginger category is an essential category for a typical household's daily food consumption preference in India as well as study area. These are usually bought in bulk as their shelf life is more than a week at a normal temperature, and consumed more frequently after cereals and pulses than other food items. The onion-potato-garlic-ginger category's average monthly inflow in 2018 and 2019 i.e. pre-COVID-19 scenario, ranged between 32 to 57 million kilograms. However, in 2020, the inflow for the month of January and February was much higher amounting to 75 and 103 million kilograms for onion-potato-garlic-ginger category. This unexpected rise in the local market inflow in February was because India halted its onion export since the last quarter of 2019 which in turn was due to a severe supply shortage in the domestic market following the heavy flooding in western Maharashtra. The average monthly inflow in the pre-COVID-19 scenario for onion-potato-garlic-ginger was around 50 million kilograms, and during-COVID19-lockdown scenario, the average monthly inflow went down to approximately 19 million kilograms which is a deficit of approximately 62%. The onion-potato-garlic-ginger food group witnessed a substantial dip in the inflow quantities to the APMC as many providers preferred to sell their produce directly to the consumers with a shorter and adapted supply chain that incorporated the lockdown conditions. In the during-COVID19-unlock scenario, there was a slight increase of average 2.6 million kilograms per month in the inflow. The average inflow in the unlock scenario for July and August 2020 was 21.6 million kilograms. The average daily price fetched per kilogram for onion-potato-garlic-ginger, in the pre-COVID-19 scenario, ranges between ₹29.75 to ₹62.11, which was reduced to ₹24.77 to ₹43.33 in the during-COVID19-lockdown scenario. The price drop might have happened because of the alternate parallel food supply chain amidst the lockdown; hence consumers were served directly by the providers avoiding the APMC channel.

Impact on fruit-vegetables

The inflow of the fruit-vegetables in the pre-COVID-19 scenario was 17.85 million kilograms, which went down to 6.64 million kilograms in the during-COVID19-lockdown scenario and again revived to 11.15 million kilograms during-COVID19-unlock scenario. The fruit-vegetables have comparatively a longer shelf life than leafy-vegetables, thus, in the during-COVID19-unlock scenario, they seem to have a fair number of inflows in the APMC market. The month of May 2020 has recorded an increase in the prices

for fruit-vegetables and leafy-vegetables as the supply was not able to meet the demand. The per kilogram prices for fruit-vegetables in the pre-COVID-19 was ranging between ₹16.59 to ₹31.45, which was reduced to ₹14.79 to ₹23.51 in the during-COVID19-lockdown scenario and improved in the during-COVID19-unlock scenario to ₹15.71 to ₹28.11 as the inflow of the fruit vegetables in the APMC market increased by 67.94%.

Table 2: Food group-wise comparative summary of the inflows and prices calculations for pre-COVID-19 and during-COVID-19-lockdown and during-COVID-19-unlock scenarios

Note: Column heads I: Monthly inflow in a million kilograms/number*; H: Average high price fetched by the produce in INR per kilogram/piece; L: Average low price fetched by the produce in INR per kilogram/piece;									
(a) Comparison of the food inflows and prices as per the record for the three scenarios									
Food Categories	**Pre-COVID-19**			**During-COVID-19-lockdown**			**COVID-19-unlock**		
	(Apr 2018 to Feb 2020)			**(March 2020 to May 2020)**			**(June 2020 to Aug 2020)**		
	I	**H**	**L**	**I**	**H**	**L**	**I**	**H**	**L**
Column Reference	***a***	***b***	***c***	***D***	***e***	***f***	***g***	***h***	***i***
Cereals	13.28	₹ 42.53	₹ 36.19	1.50	₹ 40.94	₹ 33.82	3.94	₹ 40.64	₹ 33.72
Pulses	0.69	₹ 72.71	₹ 61.02	0.04	₹ 78.32	₹ 66.11	0.14	₹ 80.10	₹ 66.97
Onion-otato-Garlic-Ginger	50.43	₹ 62.11	₹ 29.75	19.00	₹ 43.33	₹ 24.77	21.62	₹ 43.53	₹ 23.97
Fruit Vegetables	17.85	₹ 31.45	₹ 16.59	6.64	₹ 23.51	₹ 14.79	11.15	₹ 28.11	₹ 15.71
Spices	6.99	₹ 70.23	₹ 54.87	2.55	₹ 111.96	₹ 97.92	4.39	₹ 97.21	₹ 80.83
Dry Fruits	3.87	₹ 15.57	₹ 12.91	0.00#	₹ 0.00#	₹ 0.00#	1.89	₹ 11.01	₹ 8.89
Miscellaneous	1.20	₹ 57.75	₹ 53.45	0.30	₹ 60.38	₹ 56.29	0.71	₹ 63.72	₹ 59.77
Leafy Vegetables (no)*	3.90*	₹ 8.55	₹ 4.67	1.46	₹ 7.42	₹ 5.32	2.54	₹ 8.38	₹ 4.38

(b) Differences calculated for food inflows and prices between the three scenarios									
Food Categories	**Difference between During-COVID-19-lock-down and Pre-COV-ID-19**			**Difference between COVID-19-unlock and During-COV-ID-19-lockdown**			**Difference between COVID-19-unlock and Pre-COVID-19**		
	I	**H**	**L**	**I**	**H**	**L**	**I**	**H**	**L**
Column Reference	***j = (d)-(a)***	***k = (e)-(b)***	***L= (f)-(c)***	***m= (g)-(d)***	***n= (h)-(e)***	***o= (i)-(f)***	***p= (g)-(a)***	***q= (h)-(b)***	***r= (i)-(c)***
Cereals	-11.78	-₹ 1.59	-₹ 2.37	2.44	-₹ 0.30	-₹ 0.10	-9.34	-₹ 1.89	-₹ 2.47
Pulses	-0.64	₹ 5.61	₹ 5.09	0.09	₹ 1.78	₹ 0.87	-0.55	₹ 7.39	₹ 5.95
Onion-Potato-Garlic-Ginger	-31.43	-₹ 18.78	-₹ 4.99	2.62	₹ 0.20	-₹ 0.80	-28.81	-₹ 18.59	-₹ 5.79
Fruit vegetables	-11.21	-₹ 7.94	-₹ 1.80	4.51	₹ 4.60	₹ 0.92	-6.70	-₹ 3.34	-₹ 0.89
Spices	-4.44	₹ 41.73	₹ 43.05	1.84	-₹ 14.75	-₹ 17.08	-2.60	₹ 26.98	₹ 25.96
Dry fruits	-3.87	-₹ 15.57	-₹ 12.91	1.89	₹ 11.01	₹ 8.89	-1.98	-₹ 4.56	-₹ 4.02
Miscellaneous	-0.89	₹ 2.63	₹ 2.84	0.41	₹ 3.34	₹ 3.47	-0.48	₹ 5.97	₹ 6.31
Leafy vegetables (no)*	-2.45	-₹ 1.12	₹ 0.65	1.09	₹ 0.96	-₹ 0.93	-1.36	-₹ 0.17	-₹ 0.29

(c) Percentage fluctuation in food inflows and prices for the three scenarios									
Food Categories	**Percentage fluctuation between During-COVID-19 lockdown over Pre-COVID-19**			**Percentage fluctuation between During-COVID-19 unlock over Pre-COVID-19**			**Percentage fluctuation between During-COVID-19 unlock over During-COVID-19 lockdown**		
	I	**H**	**L**	**I**	**H**	**L**	**I**	**H**	**L**
Column Reference	***s= (j/a)%***	***t= (k/b)%***	***u= (L/c)%***	***v= (p/a)%***	***w= (q/b)%***	***x= (r/c)%***	***y***	***z***	***aa***
Cereals	-88.69%	-3.73%	-6.54%	-70.30%	-4.44%	-6.82%	162.56%	-0.74%	-0.31%

Pulses	-93.66%	7.71%	8.34%	-80.15%	10.17%	9.76%	213.03%	2.28%	1.31%
Onion-Potato-Garlic-Ginger	-62.32%	-30.24%	-16.76%	-57.13%	-29.92%	-19.44%	13.77%	0.45%	-3.23%
Fruit vegetables	-62.79%	-25.24%	-10.87%	-37.52%	-10.62%	-5.34%	67.94%	19.55%	6.21%
Spices	-63.53%	59.41%	78.45%	-37.23%	38.41%	47.32%	72.11%	-13.17%	-17.45%
Dry fruits	-100.00%	-100.00%	-100.00%	-51.10%	-29.30%	-31.14%	100.00%#	100.00%#	100.00%#
Miscellaneous	-74.48%	4.56%	5.31%	-40.30%	10.34%	11.81%	133.94%	5.54%	6.17%
Leafy vegetables (no)*	-62.66%	-13.16%	13.80%	-34.85%	-1.96%	-6.19%	74.50%	12.90%	-17.57%

*Units for leafy vegetable is in number (no.) The color coding used is - Red: Deficit; Green: Surplus; Yellow: Moderate # if a or d or g=0, then s,v,y=100% in other words, if the inflow is 0 for any scenario, then the percentage fluctuation for the next consecutive scenario will be 100%.

Note: The colour coding used is - Red: Deficit; Green: Surplus; Yellow: Moderate; # if a or d or g=0, then s,v,y= 100%, in other words, if the inflow was 0 for any scenario, then the percentage fluctuation for the next consecutive scenario will be 100%.

Impact on spices

Spices are a food category, though in smaller quantity are consumed daily in the Indian diet, irrespective of the season. The demand for spices often increases prior to the festival seasons, when varieties of dishes prepared and consumed are comparatively higher. It was evident that, in the year 2018, there was a spike in inflows of the spices for July, October, December, and January, as these months are known for the most celebrated festivals in the locality, namely, Ganpati, Dussehra, Diwali and Christmas holidays respectively. The average monthly inflow of the spices pre-COVID-19 was around 6.9 million kilograms, and during-COVID-19-lockdown, it reduced to 2.55 million kilograms, a reduction by 63.5% which increased in the during-COVID-19-unlock scenario by 72.1% to 4.39 million kilograms. The per kilogram average price for spices, in the pre-COVID-19 period, was ranging between ₹54.87 to ₹70.23, in the during-COVID-19-lockdown period between ₹97.92 to ₹ 111.96. This increase in the price was limited to the lockdown period as there was a supply shortage. However, as

the markets started to open in the during-COVID-19-unlock phase, the average per kilogram prices are ranging between ₹80.83 to ₹97.21. The highest price increase during the lockdown period was for the spices category amongst all other categories.

Impact on inflows of Dry-fruits

The dry-fruit items are majorly imported which depend mostly on the buyer's preferences and well-known varieties from specific location plays an important role, for example, dates from the Middle East, cashews from the Konkan area, walnuts from Northern States. The average monthly inflow of dry-fruits in the pre-COVID-19 scenario was around 3.87 million kilograms, during-COVID-19-lockdown it was null, and in the during-COVID-19-unlock phase, it was 1.89 million kilograms. The average prices for dry-fruits in the pre-COVID-19 scenario was ₹12.91 to ₹15.57, and in the during-COVID-19-unlock phase, ₹8.89 to ₹11.01. The reason for the inflow of dry-fruits during the lockdown period being null might be due to the ban on international and national imports.

Impact on leafy-vegetables

The average monthly inflow for leafy-vegetables in the pre-COVID-19 scenario was 3.90 million, which declined to 1.46 million in the during-COVID19-lockdown scenario. The unlock phase did better in terms of the inflows, with an increase of 74.05% within just two months. The per piece higher and lower prices for leafy-vegetables in the pre-COVID-19 was ranging between ₹4.67 to ₹8.55, which fell down to ₹5.32 to ₹7.42 in the during-COVID19-lockdown scenario and improved to ₹4.38 to ₹8.38 in the during-COVID19-unlock scenario, which are closer to the pre-COVID-19 prices. The short-term increase in the prices in the during-COVID19-lockdown scenario was due to the supply shortage of 62.66%.

Impact on miscellaneous food items

The miscellaneous category included varieties of peanuts and jaggery, which are essential in cooking a typical local meal for the Pune district and usually bought in bulk for a month's consumption. The average monthly inflow for the miscellaneous items was 1.20 million kilo-grams, 0.30 million kilograms, and 0.71 million kilograms for the pre-COVID-19, during-COVID-19-lockdown, and during-COVID-19-unlock period, respectively. The average monthly prices for the miscellaneous items were around

₹53.45 to ₹57.75 during the pre-COVID-19 scenario and increased to ₹56.29 to ₹60.38 in the during-COVID-19-lockdown scenario, which further continued to increase to ₹59.77 to ₹63.72 in the during-COVID-19-unlock scenario, as the inflow in the market saw an increase of 133.94% as the festive seasons for the region were approaching.

4. Conclusion and Recommendations

Overall, this research focusing on the sudden in-accessibility of food due to the COVID-19 pandemic quantitatively established the deficit in the daily food inflows and decline in the prices in Pune's APMC market. For this decrease in the inflows, two evident reasons were first, the 2019 heavy monsoon and flooding as the majority of the agricultural field and produce were ruined and the supply chains during this period were badly affected which followed by the COVID-19-lockdown resulting in sudden mobility restrictions. The inter-state restrictions in the first phase of the lockdown and uncertainty of the lockdown situation impacted the food inflow from other states resulting in short term food insecurity from March 2020 onward and this constraint on the supply side led to a short-term escalation in the prices. However, it is still unclear if this price escalation was a result of supply shortage because of the sealed city limits or because of the limited daily time-frame granted for consumers for purchasing as per the issued lockdown guidelines or due to the increased demand because of the citizen's food hoarding panic behaviour. It was also evident how the local markets become redundant when such a pandemic hit, as the producers (food providers) preferred direct interaction with the consumers. The food supply chains of the perishable items were quick in adapting themselves to a shorter supply chain compared to the non-perishable items. However, the logistics constraints for establishing a quick short supply chain may not be viable and feasible for small farmers; hence, they may have failed to gain any additional profit which large farmers gained during the lockdown condition. The way food supply chains of the perishable items adapted themselves to a shorter supply chain shows a high potential of the region to become locally self-reliant and avoid unnecessary mediators in the supply chain. This pandemic has surely put forth the high dependency of the city on the food imports for catering its food demands with even a brief shutdown of the local market impacting severely on the city's food security. However, the potential of local farmers and mediators in responding quickly

to mitigate the implications of the market shutdown gives an opportunity for planning local strategies for food self-sufficiency achieving food miles.

Table 3: Stage wise Recommendations to mitigate food in-accessibility disaster due to mobility restriction

Disaster: Food in-accessibility due to mobility restrictions				
		Policy Makers	**Regional Planners**	**Business Opportunities**
DISASTER MANAGEMENT CYCLE	PREVENTION	Policies concerning emergency rationing system allowing equitable access to food for all Setting up Food Miles benchmark for emergency situation	Mobilize Local Food Production and encourage Urban Farming, community Gardens, Targeted planning efforts on Food Self-sufficient community	Digital Smart Inventory Management Tool for real-time monitoring of food availability and supply chains
	MITIGATION	Policies streamlining emergency food supply chain bare minimum bureaucratic control	Identification of Food clusters based on populations' food demand and agriculture resource scenario,	Investing in Cluster wise Contract Farming
	PREPAREDNESS	Multi-Stakeholder Task force ensuring representation from Citizens. Policy Makers, Producers and Distributors	Establishing Network between local food cooperatives for quick 1st line response	Human Centric Application development to quickly collect demographic data in the cluster
	RESPONSE	Food vouchers in case of loss of livelihood, Extending Public Distribution System benefits		Digital Delivery Systems ensuring continuous Food Accessibility
	RECOVERY	Post-Disaster Needs Assessment study and indicators for resilient recovery of local food security		Cluster wise Partnership with private grocery stores, wholesalers, and food distributors to rebuild supply chain

In conclusion, when the five stages of the Disaster Management Cycle (Ngcamu, 2023) are evaluated against the Food in-accessibility disaster caused due to mobility restrictions during COVID-19 Lockdown, more focus has to be given to the Mitigation, Preparedness, Response and Recovery. Recommendations for policy makers, regional planners and entrepreneurs based on the insights drawn from the research have been given in Table 3. Outlining policies for Prevention would be very difficult as the mobility restriction disaster would happen because of some other major disastrous event. As a Mitigation strategy, regional clusters for food self-sufficiency to be identified under the District Disaster Management Plan keeping the regions' bare minimum food demand in focus and a committee consisting of representatives from Citizens, local government, regional food producers and distributors to be formed for to monitor distribution and prices for that cluster. Necessary provisions for cluster identification and management should be made under the District Disaster Management Plan. As a Response strategy, the at the doorstep delivery model seem to have worked very well. Thus, developing a digital tool for lodging the demand and identifying which cluster consumer belong to would add certainty to the consumers. Additionally, the presented research could be extended to develop a framework for assessing post-disaster impact and indicators for resilient recovery of local food security is the future.

5. Acknowledgement

This research did not receive any specific grant from funding agencies in the public, commercial, or not-for-profit sectors. We acknowledge the use of daily published inflow and price data from the Pune APMC website (http://www.puneapmc.org/).

6. Conflict of Interest

The authors declare that they have no actual or potential conflict of interest in relation to this article.

References

1. APMC. (n.d.). A*gricultural Produce Market Committee*. Retrieved September 1, 2020, from http://www.puneapmc.org/rates.aspx
2. Dev, B. Y. S. M. (2020). *Addressing COVID-19 impacts on agriculture , food security , and livelihoods in India*. https://www.ifpri.org/blog/addressing-covid-19-impacts-agriculture-food-security-and-livelihoods-india
3. Elsahoryi, N., Al-Sayyed, H., Odeh, M., McGrattan, A., & Hammad, F. (2020). Effect of Covid-19 on food security: A

cross-sectional survey. *Clinical Nutrition ESPEN, 40,* 171–178. https://doi.org/10.1016/j.clnesp.2020.09.026
4. Fan, S., Si, W., & Zhang, Y. (2020). How to prevent a global food and nutrition security crisis under COVID-19? *China Agricultural Economic Review*. https://doi.org/10.1108/CAER-04-2020-0065
5. Food Security Information Network. (2020). Global report on food crises 2020. In Fao.Org. https://www.wfp.org/publications/2020-global-report-food-crises
6. Garud, A., & Rao, B. (2018a). Urbanizing India and the Need for Natural Resources Planning. In U. P. Singh, B. R. Chahar, H. R. P. Yadav, & S. K. Vij (Eds.), *Urbanization Challenges in Emerging Economies* (p. 558). American Society of Civil Engineers. https://doi.org/10.1061/9780784482025.057
7. Garud, A., & Rao, B. (2018b). Urbanizing India and the Need for Natural Resources Planning. In U. P. Singh, B. R. Chahar, H. R. P. Yadav, & S. K. Vij (Eds.), *Urbanization Challenges in Emerging Economies* (p. 558). American Society of Civil Engineers. https://doi.org/10.1061/9780784482025.057
8. Gray, R. S. (2020). Agriculture, transportation, and the COVID-19 crisis. *Canadian Journal of Agricultural Economics*, 68(2), 239–243. https://doi.org/10.1111/cjag.12235
9. Madzorera, I., Ismail, A., Hemler, E. C., Korte, M. L., Olufemi, A. A., Wang, D., Assefa, N., Workneh, F., Lankoande, B., Chukwu, A., Ourohire, M., Mattei, J., Soura, A., Berhane, Y., Sie, A., Oduola, A., & Fawzi, W. W. (2021). Impact of COVID-19 on nutrition, food security, and dietary diversity and quality in Burkina Faso, Ethiopia and Nigeria. *American Journal of Tropical Medicine and Hygiene*, 105(2), 295–309. https://doi.org/10.4269/ajtmh.20-1617
10. Ministry of Home Affairs, G. of I. (2020). *CIRCULARS FOR COVID-19*. https://www.mha.gov.in/notifications/circulars-covid-19
11. Mohamed Shaluf, I. (2007). Disaster types. *Disaster Prevention and Management: An International Journal*, 16(5), 704–717. https://doi.org/10.1108/09653560710837019
12. Ngcamu, B. S. (2023). Application of the disaster management cycle and climate change: Studying flood disasters in South Africa. *Social Sciences and Humanities Open*, 8(1), 100657. https://doi.org/10.1016/j.ssaho.2023.100657
13. Nundy, S., Ghosh, A., Mesloub, A., Albaqawy, G. A., & Alnaim, M. M. (2021). Impact of COVID-19 pandemic on socio-economic, energy-environment and transport sector globally and sustainable development goal (SDG). *Journal of Cleaner Production, 312*(September 2020), 127705. https://doi.org/10.1016/j.jclepro.2021.127705
14. PIB. (2021). *Effective Response in the face of a Pandemic: Measures Adopted by the Government of India to Combat COVID-19*. Press Information Bureau. https://static.pib.gov.in/WriteReadData/specificdocs/documents/2021/dec/doc2021122421.pdf
15. Ranjbari, M., Shams Esfandabadi, Z., Zanetti, M. C., Scagnelli, S. D., Siebers, P. O., Aghbashlo, M., Peng, W., Quatraro, F., & Tabatabaei, M. (2021). Three pillars of sustainability in the wake of COVID-19: A systematic review and future research agenda for sustainable development. *Journal of Cleaner Production*, 297, 126660. https://doi.org/10.1016/j.jclepro.2021.126660
16. Reardon, T., Mishra, A., Nuthalapati, C. S. R., Bellemare, M. F., & Zilberman, D. (2020). COVID-19's Disruption of India's Transformed Food Supply Chains. *Economic and Political Weekly, 18*.
17. Siche, R. (2020). What is the impact of COVID-19 disease on agriculture? *Scientia Agropecuaria*, 11(1), 3–9. https://doi.org/10.17268/sci.agropecu.2020.01.00
18. Tirivangasi, H. M. (2018). Regional disaster risk management strategies for food security: Probing Southern African Development Community channels for influencing national policy. *Jamba: Journal of Disaster Risk Studies, 10*(1), 1–7. https://doi.org/10.4102/jamba.v10i1.468
19. UN. (2020). The sustainable development goals report 2020. In *United Nations*. https://doi.org/10.29171/azu_acku_pamphlet_k3240_s878_2016
20. WHO. (2024). *Statistical release Daily COVID-19 cases and deaths by date reported to WHO*. WHO. https://data.who.int/dashboards/covid19/data?m49=356&n=o

Multi-Hazard Susceptibility Assessment in the Mountainous Regions Using Machine Learning Techniques: A Review

Hemwati Nandan Bahuguna[1], Sushma Bahuguna[2]
Syed Hameedur Rahman Zaini[3], Sudipta Sen Gupta[4]

Abstract

Mountainous regions of the world are sites of multiple and overlapping natural hazards that often lead to loss of life, property, and environment. An accurate and timely prediction and assessment of hazardous events can save lives and reduce economic losses in these regions. Multi-hazard susceptibility assessment of mountainous regions may provide holistic valuable insights for effective risk mitigation strategies for future disasters. Currently, Machine learning modeling techniques have enabled novel advances for multi-hazard susceptibility evaluation of natural hazards owing to the availability of the various types of data pertaining to earth observation from multiple sources. Though machine learning modeling techniques have been applied by researchers to provide multi-hazard susceptibility maps for the mountainous regions, building generalized learning techniques of susceptibility and risk evaluation is still a challenge due to the high level of complexity of hazards in these regions. This article contributes a systematic review of machine learning techniques applied by the researchers, especially in the past 10 years for multi-hazard susceptibility assessment in the mountainous regions with adequate contextual information.

Keywords: *Multi-hazard, Machine Learning, Susceptibility, Mountainous Regions, Disaster Management*

[1] Hemwati Nandan Bahuguna, Doctoral Scholar, School of Management, GD Goenka University, Gurgaon, India
[2] Sushma Bahuguna, Professor, Tecnia Institute of Advanced Studies, affiliated to Guru Govind Singh Indraprastha University, Delhi
[3] Syed Hameedur Rahman Zaini, Asst. Professor, School of Management, GD Goenka University, Gurgaon, India
[4] Sudipta Sen Gupta. Associate Professor, School of Management, GD Goenka University, Gurgaon, India

1. Introduction

Climate change is upon the world and continued unsustainable practices by humans are paving the way to many imbalances. There is an increase in the frequency of natural extreme events worldwide causing great human and environmental losses (Barthel and Neumayer, 2012; Zschau, 2017; GAR, 2022). Over the last 20 years, medium to higher disasters have increased five times higher than disasters reported in the previous three decades and this rapid rise in the frequency of disasters can be attributed to climate change and inadequate risk management (GAR, 2022). Mountainous regions are highly hazardous and natural hazards strike the regions independently, simultaneously, or in a series of cascading events causing huge losses of life (Khatakho et al., 2021; Rusk et al., 2022). UNISDR (2015) report states that between 2005 and 2014, over 70% of the more than seven lac disaster-related deaths occurred in mountainous countries (Rusk et al., 2022). Further, the IPCC report's sixth assessment prediction proclaims multiple changes in many regions due to the changing climate and the incidence of compound hazards may increase multi-hazard risk in mountainous environments (IPCC, 2021).

Since it is difficult to predict coexisting multiple natural hazards, most of the previous studies have focused on assessing individual hazards (Pourghasemi et al., 2017; Javidan et al., 2021). These studies have also neglected the human impacts and the exposure component of natural hazards (Kalantari et al., 2019). Exposure pertains to the situation of people, housing, infrastructure, production capacities, and other tangible human assets located in hazard-prone areas (GAR, 2022). The exposure of communities to hazards can be reduced through an accurate predictive model based on expert analysis, a thorough understanding of influencing factors, and the implementation of mitigation and preparedness measures (Yousefi et al., 2020). Additionally, the effects of hazards can be minimized by adopting new approaches and providing data-driven support for decision-making processes (Michielsen et al., 2016). A wide range of methods namely Opinion driven models, physical-based models, statistical models, and ML models have been applied for hazard susceptibility mapping with advantages and limitations of each of these methods over the other methods (He Qian et al., 2021). Susceptibility is related to spatial aspects of hazard and refers probability of hazard incidences within a selected type during a given location (Azemeraw, 2021). Although single hazard assessments yield insights, they can also lead to ambiguous interactions

between hazards (Kappes et al., 2010; Cutter, 2018). The mitigation strategy of a single hazard in a region may not be definite as one hazard may exacerbate the intensity, frequency duration, and density of another hazard (Kappes et al., 2012; Pouyan et al., 2021). Therefore, it is necessary to integrate studies of the collective likelihood of hazardous events to describe a holistic scenario of hazards in the region (Kappes et al., 2012; Gruber and Mergili, 2013; Karlsson et al., 2017).

The concept of multi-hazard was first introduced by the United Nations in the context of sustainable development and Agenda 21 (UNEP, 1992), with a focus on risk reduction and disaster management as essential components of the planet's sustainable management. Furthermore, it defines the vulnerable areas for multiple hazards with their levels and recognizes priority zones for sustainable development (UN Johannesburg Plan, 2002). Since multiple hazards of a region usually interact with each other and contribute to an overall threat in a complex way (Rocchi et al., 2022), the development of a multi-hazard risk assessment approach is necessary (Schmidt et al., 2011) and is receiving increasing attention (Gruber and Mergili, 2013). Bell and Glade (2004) adopted a general method for multi-hazard analysis of debris flow, rock-fall, and snow avalanches in Iceland. An adaptable software was created by Schmidt et al. (2011) in which researcher was allowed to analyze the natural processes of their concern. Multi-hazard assessment was conducted by Gruber and Mergili (2013) to generate a comprehensive regional scale map for rock slides, ice avalanches, periglacial debris flow, and Lake Outburst flood. Researchers are enhancing natural hazard assessments through the use of Remote Sensing (RS) and Geographic Information System (GIS) technologies (Van Westen, 2013). These tools efficiently identify hazard-prone areas by enabling the collection, storage, combination, manipulation, retrieval, analysis, and visualization of data (Samanta et al., 2018). Recently, Multi-Criteria Decision Making (MCDM) and Machine Learning (ML) methods have gained popularity for multi-hazard analysis and mapping (Bordbar et al., 2022; Cao et al., 2020). Machine Learning, due to its excellent generalization of data and interpretation capacity is more suitable than statistical and MCDM techniques for hazard assessment (Huang et al., 2020).

The machine learning approach plays a significant role in disaster risk reduction by forecasting extreme events, situational awareness, susceptibility and hazard exposure mapping of the events in real-time, and decision support (Kuglitsch et

al., 2022). There is growing recognition of the importance of Machine Learning for effective and informed disaster management that is necessary to address the scale and impact of disaster (Linardos et al., 2022). The ML approach: (i) enables the machine to learn and improve by themselves from experiences of historical events (Barthel and Neumayer, 2012), (ii) can identify patterns and trends in big and complex datasets, and is capable of handling multi-dimensional and multi-variety data from many sources (Pourghasemi et al., 2017; Sarkar, 2021) and (iii) can analyze and map relationship between spatial pattern of historical events and their predisposing factors (Rahmati et. al., 2019). Researchers have applied the ML approach for multi-hazard susceptibility assessment in mountainous regions that include ensemble ML algorithms and combining multiple classifiers to have improved results. This article reviews machine learning approaches applied by researchers in the last 10 years for mountainous regions of the world to evaluate models as useful, universal, and accurate multi-hazard mapping products that can be applied by managers and planners.

2. Methodology

For this review document, a search was conducted on Google Scholar, Web of Science, and relevant journal databases using the terms "multi-hazard", "machine learning" "natural disaster", "disaster management," "mountainous region" and "case studies" as keywords (Table1), aiming articles published in the period from 2012 to 2022. The search yielded 48 relevant articles excluding review articles. After a manual search based on journal ranking, citation of the articles, and excluding studies outside the scope of the present review, sixteen papers were included in the present review study. The search revealed that an increasing trend of the ML approach about multi-hazard susceptibility in mountainous regions has been initiated by the researcher in recent years.

Table 1: Keyword combinations used to search the papers included in the review

Combination No.	Keywords
1	Multi-hazard, machine learning, exposure assessment
2	Multi-hazard, susceptibility evaluation, machine learning
3	Disaster management case studies, machine learning
4	Natural disaster, mountainous region, machine learning
5	Multi-hazard, mountainous region, machine learning

3. Literature Review

Multi-hazard susceptibility assessment (MSE) is an initial step of comprehensive risk assessment that can help planners and disaster managers with effective mitigation management (Pourghasemi et al., 2019, 2020). It might be a significant key tool in enhancing resilience and can play an important role in ensuring the long-term sustainability of local ecosystems and communities (Van Westen, 2017). In MSE, data are analyzed to predict the class or category of data points and upcoming events or escalation of an event. Although the methodology and configuration of ML techniques affect the result and performance of the models, different modeling approaches provide valuable information to policymakers and managers to understand the phenomena of the region for effective management of measures (Hill and Minsker, 2010). ML-based multi-hazard susceptibility assessment by the researchers in the mountainous regions of Hindu Kush Himalaya, Iran, Saudi Arabia, Austria, Southeast Asia, Nepal, Italy, and China is summarized in Table 2.

Table 2: Summary of ML-based multi-hazard susceptibility assessment in the mountainous regions

S. No.		Dataset	**Conditioning Factors	Performance
1	**Author:** Rusk J.et al., (2022). **Phenomena:** Floods, Landslides and Wildfires **Area of study:** Hindu Kush Himalaya ***Technique:** *Maxent*	Hazard catalog (flood, landslide), VIIRS fire archive, DEM from STRM, CHELSA, FAO-UNESCO, Global Surface Water Explorer, Land Scan data	**DEM-derived:** El, S, A, and flow accumulation **Meteorological:** AMT, AMR **Surface characteristics:** LC and soil suborder **Hydrological:** Distance to permanent water and SM	Area under the receiver operating characteristic curve **(AUC) for** (Maxent Model) Floods : 0.93 Landslides : 0.91 Wildfires : 0.86

S. No.		Dataset	**Conditioning Factors	Performance
2	**Author:** Javidan N. et al., (2021) **Phenomena** Floods, Landslides, and Gullies **Area of study:** Gorgan-rood Watershed, Gole-stan province, Iran ***Technique:** *Maxent*	Google Earth images, field investigation, water resource organization (national and regional documents), and the Department of Natural Resource Management of Golestan.	**Floods:** El, Sa, Sp, LU, PC, PrC, TWI, Lth, DD, Stx, DtS, AMR, RSP, TRI, SPI **Landslides and Gullies:** El, Sa, Sp, LU, PC, PrC, TWI, Lth, DD, Stx, DtS, AMR, RSP, TRI, SPI, DtF, LS factor, DtR	**Average AUC for three sample data sets** (Maxent Model) Floods : 0.93 Landslides : 0.87 Gully erosion : 0.92
3	**Author:** Youssef A.M. et al., (2022) **Phenomena:** Floods, Landslides and Gully erosion **Area of study:** Hasher-Fayfa Basin, South-western Saudi Arabia ***Techniques:** **Floods:** *RF, MDA, and FDA* **Landslides and**	Google Earth images, field investigation applying GPS, national and regional data: civil defense, Jazan region authority, Ministry of Transportation, Saudi Geological Survey, review of technical reports and scientific	**Floods:** Topography (El, S, TWI PC, A) Climatology (R), Hydrology (DtW, SD), Land cover (LULC NDVI), Geology (Lth), Anthropogenic (DtRd) **Landslides:** Topography (El, S, TWI PC, A), Hydrology (DtW), Land cover (LULC NDVI), Geology	**AUC for Floods** RF Model : 0.97 MDA Model : 0.93 FDA Model : 0.94 **Landslides** RF Model : 0.91 BRT Model : 0.90 GLM Model : 0.92 MDA Model : 0.92 FDA Model : 0.92 **Gully erosion** RF Model : 0.83 BRT Model : 0.82

S. No.		Dataset	**Conditioning Factors	Performance
	Gully erosion: *RF, BRT, GLM, MDA and FDA*	publications.	(Lth, DtF), Anthropogenic (DtRd) **Gully erosion:** Topography (El, S, TWI PC, A, TRI, PrC,VD), Climatology(R), Hydrology (SD), Land cover (LULC NDVI), Geo (Lth)	GLM Model : 0.77 MDA Model : 0.73 FDA Model : 0.79
4	**Author:** Yousefi, S. et al., (2020) **Phenomena:** Floods, Landslides, Land subsidence, Snow avalanches and Wildfires **Area of study:** Chaharmahal and Bakhtiari Province of Southwestern Iran ***Techniques:** *SVM, FDA and GLM*	Field work, scientific reports, topographic maps, geologic maps, meteorological stations, digital stream layer and piezometric wells	**Floods:** R, DEM, LU, Lth, S, DtR, NDVI, DtRd, TWI, PC, A, DD **Landslides:** DEM, LU, Lth, DtF, S, DtR, DtRd, TWI, PC, A, DD, CI **Land subsidence:** DEM, LU, Lth, DtF, S, DtR, GwL, NDVI, DtR, TWI, PC, A **Snow avalanches:** DEM, LU, S, PC, A, WEI, TRI, SnD	**AUC for Floods** SVM Model : 0.97 FDA Model : 0.96 GLM Model : 0.96 **Landslides** SVM Model : 0.84 FDA Model : 0.77 GLM Model :0.77 **Land subsidence** SVM Model : 0.94 FDA Model : 0.92 GLM Model : 0.92 **Snow avalanches** SVM Model : 0.89 FDA Model : 0.91 GLM model : 0.90

S. No.		Dataset	**Conditioning Factors	Performance
			Wildfires: R, DEM, S, DtR, NDVI, DtRd, TWI, A, T (min), T (max), DtU, WEI	**Wildfires** SVM Model : 0.83 FDA Model : 0.82 GLM Model : 0.83
5	**Author:** Nachappa T. G. et al., (2020) **Phenomena:** Floods and Landslides **Area of study:** Federal State of Salzburg, Austria *** Techniques:** *SVM and RF*	Geological Survey of Austria, incidence of historic flooding, DEM	**Floods:** EL, S, A, LC, R, Geo, DtRd, DtD, NDVI, TWI, SPI **Landslides:** EL, S, A, LC R, Geo, DtRd, DtD, Lit, DtF	**AUC for Floods** SVM Model : 0.87 RF Model : 0.87 **Landslides** SVM Model : 0.89 RF Model : 0.90
6	**Author: Pouyan,** S. et al., (2021) **Phenomena:** Flooding, Gully erosion, Forest fires and Earthquakes **Area of study:** Kohgiluyeh and Boyer-Ahamad Province, Iran	Google Earth images and field survey supported by GPS, Sentinel Satellite imagery, Google Earth engine	**Floods:** El, AMR, DtRd, S, LU, TWI, NDVI, DD, PC DtR,Lth, A **Gully erosion;** AMR,El, Lth, Stx (sand, silt, clay), DD, DtRd, NDVI, TWI, LU, S, DtR. PC, PrC **Forest fires:** AMT, AMR,El,	**AUC for Floods** SVM Model : 0.94 RF Model : 0.98 BRT Model : 0.88 **Gully erosion** SVM Model : 0.95 RF Model : 0.99 BRT Model : 0.93 **Forest fires** SVM Model : 0.72 RF Model : 0.88 BRT Model : 0.68

S. No.		Dataset	**Conditioning Factors	Performance
	***Techniques:** *SVM, RF, BRT and PSHA (for earthquakes)* ***Techniques:** *SVM, RF, BRT and PSHA (for earthquakes)*		DtRd,DtV,NDVI, S,WEI, DtR and TWI, A **Earthquakes:** PGA	
7	**Author:** Rahmati O. et al., (2019) **Phenomena:** Floods Rock falls, and Avalanches **Area of study:** Asara watershed, Alborz Mountains, Iran ***Techniques:** *SVM, GAM and BRT*	Field survey, documents from road organization of Iran and regional water company	**Floods:** El, TPI, TRI, TWI, Sd, DtS, PrC, Lth and LU **Rockfalls:** El, TPI, TRI, LS, RSP, VRM, A, Sd, PrC, Lth and LU **Snow avalanches:** El, TPI, TRI, LS, RSP, VRM, WEI, A, Sd, PrC, Lth and LU	**AUC for Floods** SVM Model : 0.89 GAM Model : 0.86 BRT Model : 0.94 **Rock Falls** SVM Model : 0.93 GAM Model : 0.90 BRT Model : 0.88 **Avalanches** SVM Model : 0.92 GAM Model : 0.83 BRT Model : 0.89
8	**Author: He** Qian et al., (2021) **Phenomena:** Landslides and Wildfires **Area of study:** South-east Asia	MODIS, fire archive, global landslide catalog (GLC) SRTM data (DEM), terra climate(climate) OSM, global lithological map	**Landslides:** El, S, A, PC, PrC, DtR, DtRd, DtF, NDVI, P, SM, Lth, LU, TWI, SPI **Wildfires:** El,S, DtU, DtR,	**AUC for Landslides** RF Model : 0.89 GBDT Model : 0.87 AdaBoost : 0.86 **Wildfires** RF Model : 0.91 GBDT Model : 0.88 AdaBoost : 0.81

S. No.		Dataset	**Conditioning Factors	Performance
	***Techniques:** *RF, GBDT and AdaBoost*		DtRd, NDVI, P, T, TWI and wind speed	
9	**Author:** Pourghasemi H.R.,Gayen, A. et al., (2020) **Phenomena:** Floods Landslides and Forest fires **Area of study:** Fars Province, Southern Iran ***Techniques:** *SVM and MARS*	ASTER-GDEM, DEM, Geological Survey of Iran, weather stations	**Floods:** Sa, Al, A, PC, TWI, Geo, LULC, DtR, DtRd, AMR, DD and soil features **Landslides:** Sa, Al, A, PC, PrC, Geo, LULC DtR, DtF, DtRd **Forest Fires:** Sa, Al, A, TWI, LULC, DtR, DtRd AMT and distance to residential areas.	**AUC for Floods** SVM model : 0.75 MARS model : 0.76 **Landslides** SVM model : 0. 89 MARS model : 0.91 **Forest fires** SVM model : 0. 91 MARS model : 0.90
10	**Author:** Pourghasemi H.R., Kariminejad, N. et al., (2020) **Phenomena:** Floods, Landslides, and Forest fires **Area of study:** Fars Province, Shiraz city, Iran ***Technique:** *RF*	Terrain mapping through field work using GPS, DEM (ASTER-GDEM), river, Google Earth Images, road and urban maps, maps of the Geological Survey of Iran and natural resources,	**Floods:** Al, Sa, A PC, TWI, DtR, DtRd, DD, Lth,R, LU and soil features. **Landslides:** Al, Sa, Sd, PC, PrC, DtR, DtRd, DtF, Lith and LU **Forest fires:** Al, Sa, Sd, TWI. DtR, DtRd, DD, DtU, R, AMT	**AUC for RF Model** Floods : 0.83 Landslides : 0.93 Forest fires : 0.94

S. No.		Dataset	**Conditioning Factors	Performance
11	**Author:** Khatakho, R. et al., (2021) **Phenomena:** Floods, Landslides, Urban fires and Earthquakes **Area of study:** Kathmandu Valley ***Techniques:** *AHP in integration with the GIS*	Arial photo interpretation, Google Earth engine, survey, historical data, literature review and pilot field observations	**Floods :** S, DtS, LULC, Lth , P, El **Landslides:** DtF, S, A, PrC, DtS, LULC, Lth, DtR, NDVI, P, El **Fires :** LULC, DtR, PD, Distance to (fire brigades, gas station, transmission line, electric substation, main settlement, and old settlement) **Earthquakes:** DtF, S, LULC, Lth, PD, Distance to (old settlement, soil liquefaction, seismic intensity, dominancy building type)	**For Floods, , landslides and urban fires** Validation by superimposition of historical hazard events; **AUC for Earthquake:** 0.63, moderate performance 4calculated for the damage due to the 2015 Gorkha earthquake. **Damage density** 0.33 to 0.06
12	**Author:** Rocchi, A. et al., (2022)	Italian National Institute of Statistics (ISTAT) database	**Building sharing features:** building material, period	**Silhouette coefficient:** Good Silhouette

S. No.		Dataset	**Conditioning Factors	Performance
	Phenomena: Floods and Earthquakes **Area of study:** Emilia Romagna Region, Italy ***Techniques:** *PCA and K-means*		of construction, state of conversion, superficial extension, number of inhabitants, population density, peak acceleration etc. **Variables have been grouped into three categories:** vulnerability instances, exposure instances and hazard instances	values relative to cauterization. Overall risk label assigned to each cluster confirmed previous risk classification study
13	**Author:** Bordbar M. et al., (2022) **Phenomena:** Floods, Landslides and Earthquakes **Area of study:** Kermanshah Province in Western Iran	**Floods:** Google Earth engine and sentinel - 3 images **Landslides:** historical data and field investigation applying GPS	**Floods:** Al, Sa, Sd, PC, DtR, Lth, R, LU **Landslides:** Al, Sa, Sd, PC, DtR, DtF, dtRd, Lth, LU **Earthquakes:** PGA map	**AUC for** SWARA-ANFIS-PSO ensemble model Floods : 0.93 Landslides :0.89

S. No.		Dataset	**Conditioning Factors	Performance
	***Techniques:** *Ensemble SWARA-ANFIS-PSO and SWARA-ANFIS-GWO models.*	**Earthquake inventory map:** International Institute of Earthquake Engineering and Seismology		
14	**Author:** Pourghasemi H.R. et al., (2019) **Phenomena:** Floods, Landslides and Earthquakes **Area of study:** Lorestan Province in Iran **Techniques:** *Ensemble SWARA-ANFIS-GWO models.*	Historical information, field surveys; ASTER-GDEM, Landsat (OLI). Geological Survey of Iran, topographical map, weather stations, agriculture organization	**Floods and Landslides:** Al, Sa, Sd, PC, SD, PrC, DtR, DtF, Lth, R and LU **Earthquakes:** PSHA	**AUC for** SWARA-ANFIS-GWO ensemble model Flood : 0.84 Landslides : 0.80
15	**Author:** Cao,J. et al., (2020) **Phenomena:** Landslides Rock fall and Debris flow **Area of study:** Jiuzhaigou region of China	Bureau of land and resources of Sichuan (BLRS), Satellite interpretation in Google Earth	**Landslides Rock fall and Debris flow** Al, A, S, LU, FD, DtR, DtRd, NDVI, AMR, DtF, DtE, and Lth	**AUC for Landslides** SVM Model : 0.88 **Rock Falls** XGBoost : 0.97 **Debris Flow** XGBoost : 0.97

	***Techniques:** *SVM, RF and XGBoost.*			
16	**Author:** Zhao, Z.et al., (2022) **Phenomena:** Landslides and Rock falls **Area of study:** Hengduan Mountains Region, China ***Techniques:** *SVM, RF and BP NN*	On spot visits, natural resources bureaus ASTER GDEM, national Qinghai-Tebet plateau Science data center, open street map	**Landslides and Rock falls** El, S, A, PC, Lth, DtF, P, NDVI, DtR, and DtRd	**AUC for Landslides** RF Model : 0.83 **Rock falls** RF Model : 0.88

Abbreviation Used

***Techniques:** AdaBoost; Adaptive Boosting (Freund and Schapire, 1997), AHP; Analytical Hierarchy Process (Saaty, 1988), ANFIS; Adaptive Neuro - Fuzzy Inference System (Jang, 1993) , BPNN; Back Propagation Neural Network (Rumelhart et al., 1986) BRT; Boosted Regression Tree (Friedman, 2001); FDA; Functional Discriminant Analysis (Ramsay and Dalzell, 1991), GBDT; Gradient-Boosted Decision Tree (Friedman, 2002), GAM; Generalized Additive Model (Hastie and Tibshirani, 1986), GLM; Generalized Linear Model (Nelder and Wedderburn, 1972), GWO; Grey Wolf Optimization (Mirjalili et al., 2014), K-Means; K-mean clustering Algorithm (Lloyd, 1982), MARS; Multivariate Adaptive Regression Splines (Friedman, 1991), Maxent; Maximum Entropy (Phillips et al., 2021), MDA; Multivariate Discriminant Analysis (Duda et al., 2001), PCA; Principal Component Analysis (Hotelling, 1933), PSO; Particle Swarm Optimization (Kennedy and Eberhart, 1995), RF; Random Forest (Breiman and cutler, 1993), SVM; Support Vector Machine (Cortes and Vladimir, 1995), SWARA; Stepwise Weight Assessment Ratio Analysis (Kersuliene and Turskis, 2011), XGBoost ; Extreme Gradient Boosting (Chen and Guestrin, 2016).

Conditioning Factors: A; Aspect, Al; Altitude, AMR; Annual Mean Rainfall, AMT; Annual Mean Temperature, CI; Convergence Index, DD; Drainage Density, DEM; Digital Elevation Model, DtD; Distance to Drainage, DtE; Distance to Epicenter, DtF; Distance to Faults, DtR; Distance to Rivers, DtRd: Distance to Roads, DtS ; Distance to Stream, DtU; Distance to Urban, DtV; Distance to Villages, DtW; Distance to Wadis, El; Elevation, FD; Fault Density, Geo; Geology, GwL; Ground Water Level, H; Humidity, Lth; Lithology, LC; Land Cover LU; Land Use, LULC; Land Use and Land Cover, LS; Length Slope, NDVI; Normalized Difference Vegetation Index, P; Precipitation, PC; Plan Curvature, PD; Population Density, PrC; Profile Curvature, PGA ; Peak Ground Acceleration, PSHA; Probabilistic Seismic Hazard Analysis, R; Rainfall, RSP; Relative Slope Position, S; Slope, Sa; Slope aspect, Sd; Slope degree, SD; Stream Density, SG; Slope Gradient, SM; Soil Moisture, SnD; Snow Depth Sp; Slope percent, SPI; Stream Power Index Stx; Soil texture, ST; Soil Types, T; Temperature, TPI; Topographic Position Index, TRI; Terrain Ruggedness Index, TWI; Topographic Wetness Index, VD; Valley Depth, VRM; Vector Ruggedness Measures, WEI; Wind Exposition Index, WS; Wind Speed.

3.1 Machine Learning Techniques

Machine learning techniques comprise a group of computational algorithms that learn from historical data, build predictions and classification models, and predict the output whenever it receives new data. ML Algorithms can be broadly classified into three groups namely Supervised ML, Unsupervised ML, and Reinforcement learning. Supervised ML models are trained with labeled data sets, which allow the models to learn and grow more accurately over time. In Unsupervised, ML algorithms learn from the unlabeled data and find the hidden patterns in the data. Reinforcement machine learning trains machines through trial and error to take the best action by establishing a reward system. In hazard susceptibility assessment, the ML approach learns and analyses the relationship between the spatial pattern of historical events and the spatial pattern of the conditioning factors influencing their likelihood (Pourghasemi et. al., 2019). An overview of ML workflow for hazard susceptibility is depicted in Figure 1. The performance of the machine learning approach for an

assigned task is established based on the availability of sufficient quality data and the selection of the right model architecture. **Different ML modeling techniques applied by the researchers for MSE in mountainous regions are mentioned in Table 2.**

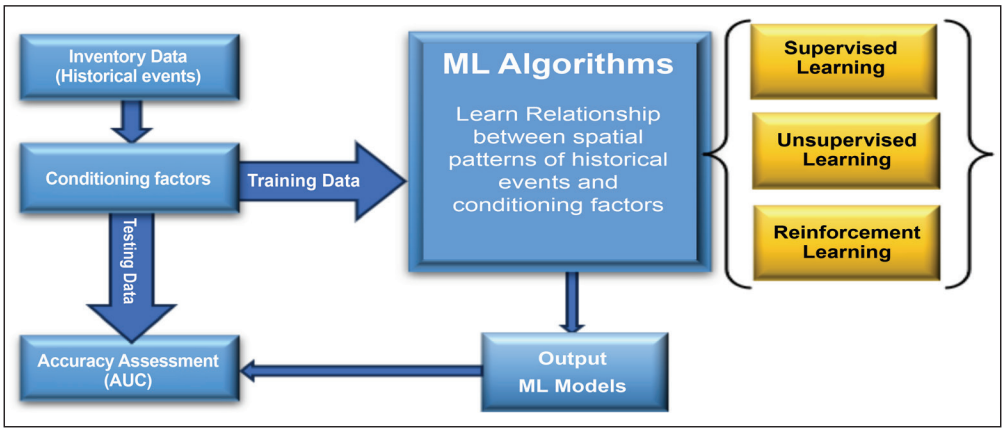


Figure 1: Overview of machine learning workflow for hazard susceptibility

3.2 Hazard Inventory

Preparation of Hazard Inventory of landforms by recording the location of disaster occurrences is a key step for susceptibility mapping (Javidan et al., 2021). ML is a data-driven technology and the accuracy of predicted output depends on the quality and amount of data. Therefore, it is imperative to have a good set of inventories for improved modeling and mapping. Data generation of events primarily depends on the scale of study, purpose of the study, and accessibility to the study area. Earth observation data provides critical input for machine learning models that improve hazard prediction, detection, and management, ultimately mitigating the impacts of natural disasters. Earth observation data sources can be categorized based on the platform, sensor type, temporal frequency, and spatial resolution. Satellite-based remote sensing provides various data types, such as optical, radar, thermal, and multispectral imagery. These data sources provide geospatial, environmental, climatic, and socio-economic data, which are essential to develop accurate hazard models. Key satellites include Landsat for long-term land monitoring, Copernicus Sentinel satellites for high-resolution optical and radar data, World View Satellites for damage analysis

and land cover change, and Terra SAR-X for terrain monitoring. Airborne sensors like drones can capture detailed local-level data for rapid hazard response. The advantages of ground-based sensors include real-time observation capability, but are localized by space. Earth observation data spans a range of spatial and temporal resolutions, from meters to kilometers and daily to annual intervals.

The data sources used by the researchers for multi-hazard susceptibility mapping include hazard catalog, Visible Infrared Imaging Radiometer Suite (VIIRS) fire archive, Shuttle Radar Topography Mission (SRTM), CHELSA (Climatologist at High Resolution for the Earth's Land Surface Areas, Food and Agriculture Organization (FAO) and United Nations Educational, Scientific and Cultural Organization (UNESCO), Google Earth, Sentinel-2, Moderate Resolution Imaging Spectroradiometer (MODIS), Advanced Spaceborne Thermal Emission and Reflection Radiometer (ASTER) Global Digital Elevation Model (GDEM), Operational Land Imager (OLI), United States Geological Survey (USGS), Global surface water explorer, Geological maps, topographical maps, open street map, weather station, seismic stations, and meteorological stations.

3.3 Conditioning Factors

Conditioning factors are essential for hazard susceptibility mapping and modeling (He Qian et al., 2021). Integration of hazard inventory data and the development of a dataset of conditioning factors is a crucial part of multi-hazard susceptibility assessment. Since each mountainous region has a unique geotectonic and hydrologic setting, there is no uniform list of conditioning factors of each hazard (Rahmati et al., 2019). Therefore, researchers have selected conditioning factors based on literature review, expertise towards phenomena, topographical, geological, hydrological, climatological, anthropogenic characteristics of the study area, and scale of analysis. Ideally, the selected conditioning factors should be operative, quantifiable, and non-uniform (Nacchapa et al. 2020). Some of the studies have used variance Inflation Factors (VIF) and tolerance (TOL) for multicollinearity tests and Random Forest (RF), Mean Decrease Gini (MDG), and Buruta algorithm for priority of effective conditioning factors. Jackknife test is also used to assess the relative strength of each predictor variable in some studies. Conditioning factors of each hazard applied for multi-hazard modeling by the researcher have been listed in Table 2.

3.4 Accuracy Assessment

The area under the receiver operating characteristic curve (AUC) is the most commonly used threshold-independent method for analyzing the performance of the ML models (Marzban, 2004). The goodness-of-fit and predictive performance of ML models are evaluated by using the training group and validation group of data respectively. The receiver operating characteristic (ROC) curve is a plot of sensitivity vs. "1 - specificity" of an investigative test.

$$\textbf{Sensitivity} = TP \div TP + FN$$

$$\textbf{Specificity} = TN \div FP + TN$$

Where True positive (TP), True negative (TN), False positive (FP), and False negative (FN) are the fundamental elements of the confusion matrix.

Sensitivity and specificity represent the probability of correct predictions of the positives and negatives as observed in reality (Pourghasemi et al., 2020). AUC values vary between 0 to 1, where 0 implies a completely inaccurate test and 1 infers a perfect accuracy of the test. While classifying model accuracy, an AUC value under 0.7 is unacceptable, 0.7 to 0.8 is considered good, 0.8 to 0.9 is measured as very good, and more than 0.9 is excellent (Swets, 1988; Tien et al., 2017).

Other accuracy measures applied by researchers to evaluate the performance of the multi-hazard models are as follows:

(i) **Overall accuracy (ACC) = TP + TN ÷ TP + TN + FP + FN**
(Measures the percentage of correctly classified samples)

(ii) **True skill statistics (TSS) = sensitivity + specificity – 1**
(Measures the ability of a predicted value to discriminate between the events and nonevents using all the elements in the confusion matrix)

(iii) **Precision = TP ÷ TP + FP**
(Measures of exactness indicating the percentage of samples predicted as positive are exactly positive)

(iv) **Corrected classified instances (CCI) = (TN + TP ÷ (TN + TP + FP+ FN) * 100**
(Considers TN and FN for true and false negative predictive events, and TP and FP for true and false positive, respectively)

(v) **Gini coefficient = 2 * AUC – 1**
(Measures the inequality among values of variable and evaluates the performance of binary classifier models)

(vi) **Silhouette coefficient:** Silhouette score is a measure of accuracy for classified observation and represents object similarity to its cluster compared to other clusters. Its value ranges from -1 to +1, where a high value shows that the object is well-matched to its cluster and poorly matched to neighboring clusters. Euclidean distance and Manhattan distance metrics can be used to calculate silhouette. The disadvantage of the reliability of the approach in the silhouette method is the dependency on the existence of valid quantitative initial data of the region (Rocchi et al., 2022).

3.5 Multi-Hazard Susceptibility Modeling

To explore population exposure to multi-hazard risks (landslides, floods, and wildfires) across the Hindu Kush Himalaya, the maximum entropy ML technique was applied by Rusk et al. (2022). A set of 10 environmental covariates was employed to build Maxent models for each hazard. The covariates included meteorological (annual temperature and annual precipitation), surface characteristics (land cover and soil suborder), hydrological (soil moisture and distance to permanent water), and DEM-derived factors (elevation, slope, aspect, and accumulation). Variance inflation factors (VIF) were used to perform a test of multicollinearity and Pearson's correlation coefficient was applied to determine the nature of the correlation. AUC reported single hazard model performance of test data as 0.93 for floods, 0.91 for landslides, and 0.86 for wildfires. Exposure was determined by a multi-hazard susceptibility map integrated from three hazard maps and population distribution data. Javidan et al. (2021) also presented the Maxent ML technique to generate susceptibility maps for landslides, floods, and gullies in the Gorganrood watershed of Iran. Seventeen Geo- geo-environmental factors were selected as predictors for flood, landslides, and Gully erosion. VIF and Tolerance (TOL) were applied for the multi-collinearity test and sensitivity analysis was implemented to examine the relative strength of predictor variables using the Jackknife test. The most influencing predictors for each hazard were considered as; (i) river density, distance from stream, and elevation for floods; (ii) elevation, lithology, and annual mean rainfall for landslides and (iii) annual

mean rainfall, elevation, and lithology for gully erosion. The accuracies gained by the validation model based on AUC values for floods and landslides are comparable to the results of the Maxent model of Rusk et al. (2022).

Yousefi et al. (2020) proposed SVM, GLM, and FDA methods to address the probabilities of landslides, land subsidence, floods, snow avalanches, and wildfire hazards for the mountainous region in southwestern Iran. For this purpose, effective factors were classified into five categories namely topography, geology, hydrology and climatology, social, and vegetation/land cover. Models of each hazard with high accuracies were integrated using Boolean algorithms based on low, moderate, high, and very high classes of each hazard. SVM provided the best accuracy for the prediction of landslides, floods, and land subsidence. GLM predicted the best accuracy for wildfire and FDA generated the best results for snow avalanche risks. Youssef et al. (2022) worked to map the probabilities of landslides, floods, and gully erosion hazards using GLM, FDA, MDA, RF, and BRT models in the Hasher-Fayfa Basin of southwestern Saudi Arabia. Five ML models (GLM, FDA, MDA, RF, and BRT) for landslide and gully erosion and three models (FDA, MDA, and RF) for floods were developed to evaluate hazard occurrences. Based on the literature review topographical, geological, meteorological, hydrological, and anthropogenic factors were incorporated to develop a multi-hazard risk model. Sixteen factors (11 factors for landslides, 12 factors for floods, and 13 factors for gully erosion) were selected to generate hazard susceptibility maps. VF and TOL were used for multicollinearity whereas the RF algorithm was implemented to measure the importance of independent indicators for their contribution to each hazard modeling. FDA model produced the best results for predicting landslides and the RF model provided the best results for predicting floods and Gully erosion. FDA model reported better predictive ability for landslide prediction and lesser predictive ability for flood prediction as compared to the FDA model of Yousefi et al. (2020).

Random Forest model yielded high predictive accuracies for multi-hazard modeling by Nachappa et al. (2020) and Pouyan et al. (2021). Nachappa et al. (2020) produced a multi-hazard exposure map using SVM and RF for landslides and flooding in the Federal State of Salzburg, Austria. Multi- hazard exposures were recognized using a total 13 influencing factors (10 factors for landslides and 11 factors for floods). A quartile

classification approach was applied to categorize the exposure map into five classes of exposure levels. The approach allocated all the values into clusters that contain an equal number of values for better classification compared to the natural break classification approach. The accuracy assessment of the exposure maps was derived through ROC and R-Index (relative density). RF model yielded better performance for both landslides and floods. Pouyan et al. (2021) developed SVM, RF, and BRT models to produce a multi-hazard map for flood, gully erosion, forest fire, and earthquake in Kohgiluyeh and Boyer-Ahmad Province, Iran. The earthquake hazard map was generated from a probabilistic seismic hazard analysis and PGA values were divided into low moderate and high classes. The mean decrease Gini (MDG) method was applied to examine the relative importance of effective factors of each hazard. Elevation was measured most important factor for flooding, whereas annual temperature and mean annual rainfall were measured as the most important factor for forest fire and gully erosion respectively. Aspect was ascertained least important factor for all three hazards. The RF model outperformed other classifiers with AUC Values of 0.99, 0.99, and 0.88 for gully erosion, flooding, and forest fires respectively. The SVM model provided better accuracies for flood predictions than the SVM models of Nachappa et al. (2020) and Rahmati et al. (2019).

Rahmati et al. (2019) proposed SVM, BRT, and GAM for rock fall, avalanche, and flood hazards in the mountainous area of the Asara watershed, Iran. Fourteen predictive factors (topo-hydrological, geo-environmental, and morphometric) were selected for hazard susceptibility mapping based on a literature review. The hazard susceptibility map of each disaster was integrated using the weight linear combination (ELC) technique to produce a multi-hazard map. TSS and AUC were used to evaluate the model performance of each hazard. The SVM model achieved the highest accuracy for snow avalanches and rock falls while the BRT model established the highest accuracy for flood hazards. Proximity to residential areas, road networks, and power transmission lines was defined as a vulnerable component for exposure mapping. AHP was used to determine the weight of each factor and five classes of exposure from very low to very high exposure were assigned. Exposure and multi-hazard maps were assigned risk equation (Risk = Hazard * Exposure) to produce a multi-hazard exposure map of the region.

He Qian et al. (2021) studied the intersection of landslides and wildfires using RF, AdaBoost, and GBDT ensemble ML algorithms in Southeast Asia. Fifteen factors for landslides, ten factors for wildfires, and a total of eighteen conditioning factors were chosen for the hazard susceptibility assessment based on information collected from the literature. VIF and TOL were used to detect the quantity of multicollinearity and the mean decrease Gini Index of RF was applied to determine the relative importance of the variables. For landslides, distance to road and distance to faults were considered the most important factors whereas distance to urban areas followed by distance to roads and slopes were considered the most important factors for wildfires. The model performance was evaluated using (ACC), Precision, AUC, and confusion matrix values. RF model outperformed other classifiers for both landslide and wildfire prediction. The authors also computed the coefficient of variation (CV) for the reliability test by intersecting the susceptibility map with uncertainty.

Pourghasemi, Gayen et al. (2020) developed individual and collective multi-hazard risk maps for floods, landslides, and forest fires using the SVM and MARS, models in Fars province, Southern Iran. The sixteen conditioning factors identified by the literature review were considered to model the risk distribution for floods, landslides, and forest fires. The performance of the models for each hazard was evaluated by AUC, TSS, and correlation and deviance values from each model for each hazard. The AUC values of the MARS model were slightly better than the SVM model for floods and landslides whereas the SVM model performed slightly better than MARS for forest fires. The TSS values depict better landslide prediction by the MARS model but were less able to predict flood and forest fire risk patterns.

Pourghasemi, Kariminejad et al. (2020) conducted a multi-hazard probability assessment using RF classifier for landslides, floods, and forest fires hazards in Fars Province, Iran. The influencing factors were divided into biophysical and human categories. The biophysical category was divided into atmospheric (humidity, rainfall, and temperature) and topographic factors (altitude, slope aspect, and slope degree). The human factors included land use, access to the forest, and fuel management processes. To evaluate the importance of effective factors controlling hazard locations, 12 factors for floods and 10 factors each for landslides and forest fires were selected. Boruta algorithm was applied to prioritize the impact of each respective factor on

the occurrence of each hazard. Susceptibility maps of each hazard were integrated to produce a multi-hazard probability map. The AUC values for validation were reported as 0.83, 0.93, and 0.94 for flood, landslide, and forest fire prediction respectively. Other accuracy measures i.e. sensitivity, specificity, CCI, TSS, and Gini coefficient also approved the AUC results.

Khatakho et al. (2021) developed AHP in integration with GIS to assess multi-hazard risk in Kathmandu Valley for floods, landslides, earthquakes, and urban fire hazards. Multi-hazard risk assessment was performed by pair-wise comparison of floods, landslides, earthquakes, and urban fire hazards. Twenty-one influencing factors were selected based on available information and a suitable class of influencing factors and corresponding rating factors were assigned. Individual maps were generated by selected influencing factors and thereafter four maps were superimposed based on their weights to generate multi- hazard risk map. AUC and hazard density were used to validate the earthquake hazard map based on damage data from the 2015 Gorkha earthquake. While an AUC value of 0.68 reported moderate performance, hazard density analysis illustrated a good correlation between classified hazard zones and past earthquake incidences. Validation for floods, landslides, and urban fire hazards was carried out by superimposing historical hazard events.

Rocchi et al. (2022) presented qualitative multi-hazard risk analysis methodology with large and heterogeneous input data sets to assess overall combined seismic and hydraulic risk for different municipalities of the Emilia Romagna region of Italy. The input dataset of the Italian National Institute of Statistics (ISTAT) was organized as a matrix with rows of municipalities and columns corresponding to quantitative variables associated with different characteristics of flood and seismic risk. PCA method was used to quantify the relative importance between variables and the relation among them. The different municipalities of the region were grouped into homogeneous clusters through the K-mean clustering algorithm and the Silhouette coefficient was used to validate the clustarization.

Pourghasemi et al. (2019) proposed a SWARA-ANFIS-GWO ensemble model in the Lorestan province of Iran for a multi-hazard probability map of landslide, flood, and earthquake. Eleven influencing factors related to terrain and land use were adopted to generate susceptibility maps of landslides and flood. Probabilistic seismic hazard

analysis (PSHA) was employed to generate an earthquake map with 5 different classes from very high to very low based on magnitude. SWARA approach was applied for weighing contributing factors whereas the ANFIS method was implemented to acquire weighs on each value while using the GWO algorithm. The AUC indicated accuracies of 84% and 80% for floods and landslides respectively. Multi-hazard probability map was produced by combining landslide, flood, and earthquake maps. Bordbar et al. (2022) also worked on ensemble SWARA - ANFIS - GWO and SWARA - ANFIS - PSO models to provide a multi-hazard map for floods, landslides, and earthquakes in Kermanshah province of western Iran. Influencing factors were selected based on previous research. Altitude, lithology, slope degree, distance to river, plan curvature, and aspect were considered common factors for flood and landslide mapping. Rainfall and land cover for floods and distance to road, distance to fault, and land use were considered as specific influencing factors for landslides. VIF and TOL were used to examine multicollinearity. The SWARA method was applied to weigh the subclass of the influencing factors for landslides and floods. ANFIS, ML algorithm was used in combination with PSO and GWO meta-heuristic algorithms to train the data. A PGA map was generated to study earthquakes in the region. The hazard accuracy of the models was validated using ROC, root mean square Error (RMSE), and mean square error (MSE) methods. SWARA-ANFIS-PSO ensemble models performed best for flood susceptibility maps and provided excellent results for landslide maps. The model reported better accuracies than the SWAEA – ANFIS - GWO ensemble model of Pourghasemi et al. (2019) for predicting floods and landslides.

Zhao et al. (2022) developed and compared six models using three ML methods namely SVM, RF with different nuclear functions, and BPNN model for landslide and Rockfall hazard susceptibility in the Handgun mountains region of China. They adopted 10 factors in susceptibility assessment based on mean decrease Gini and mean decrease indicators by the RF model. RF model provided the highest accuracy compared to other models considered in the study. Cao et al. (2020) implemented SVM, RF, and XGBoost techniques to generate a multi-hazard susceptibility map for landslide, rock fall, and debris flow in the Jiuzhaigou region of China. For this purpose, multi-hazard inventory from 2000 to 2015 was used along with 12 factors associated with trigging mechanisms as conditioning factors. XGBoost performed best for rock fall and

debris flow whereas SVM provided the best prediction for landslides. XG Boost model also reported better accuracy than the RF model of Zhao et al. (2022) for rock fall prediction.

4. Discussion

Multi-hazard susceptibility modeling worked out by researchers in different mountainous regions of the world reveals that models differ in their accuracy of prediction for different hazards and the type of hazard can affect the ranking of the model. In most of the studies individual hazard susceptibility models were created using different ML algorithms including ensemble methods, and multi-hazard susceptibility maps were assembled from the most accurate individual model for each hazard. Figure 2 depicts the performance of individual ML Models based on AUC Values (Table 2) calculated by researchers for different hazards in the mountainous regions. The Random Forest model (AUC= 0.97, 0.87, 0.98) performs excellently in some tests but exhibits variability in others when predicting floods. The SVM model also exhibits greater variability, with one notably low result of AUC (0.75) for flood prediction. The FDA demonstrates strong overall performance, though it can struggle with certain data, achieving an AUC of 0.77 for landslide prediction. The SVM is highly variable, with AUC ranging from 0.91 to 0.72, suggesting that the performance of this model might depend on the particular subset of data or class distribution for wildfire prediction. The BRT model is highly variable, with an excellent AUC of 0.93 and a poor AUC of 0.63, which may suggest that it will not be good at some subsets of the data for gully erosion prediction.

Mapping processes have the significant disadvantage of being sensitive to changes in input variable weighting and the researcher's judgment on the assessment scale (Chang et al., 2008). All the methodologies have their advantages and limitations, and each model's performance depends on the input data, structure, and accuracy of the model. There is neither a standard for a specific model to be used for a specific situation, hazard, or study area nor universal guidelines on choosing influential factors for each natural hazard (Khosravi et al. 2018).

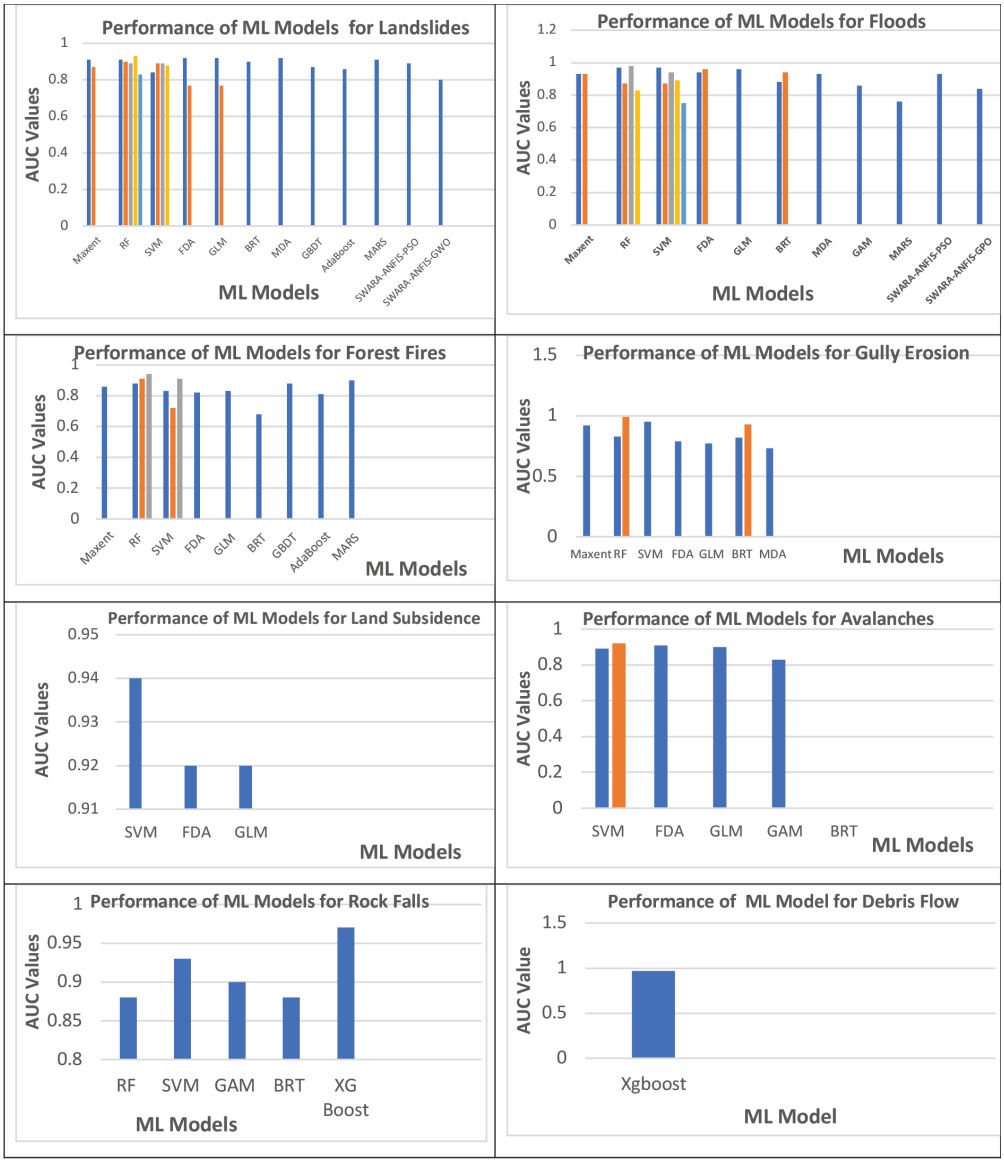


Figure 2: Bar Plots showing the performance of individual ML Models for different hazards

Natural hazards are complex phenomena and have a strong relationship with the characteristics of the landscape (Geotectonic, hydrologic, climatic etc.) and anthropogenic activities of the region. An accurate knowledge of factors affecting these hazards may be incomplete and some of unknown factors may still be present. To assess the performance of various models, relative and proportional research is necessary for similar conditions and influencing factors to make comparisons and rational conclusions on the appropriate model for a specific hazard at a certain region (Goetz et al., 2015). The performance of the models is determined by data sets of historical environmental processes but the reshaping of the environment due to anthropogenic, climate change and urbanization may reshape the distribution of future hazards (IHCAP, 2017; Mukherji et al., 2018; Sharma et al., 2019).

Natural hazards do not operate in isolation and hazard interactions and interaction network modeling are necessary as the occurrence of primary hazard can significantly modify the probability of secondary hazard (Gill and Malamud, 2016). Machine learning models are not definite about the mechanisms giving rise to multi-hazard. Single-hazard and multi-hazard environments differ by mechanistic connection between hazards and one hazard may compound the effects of another hazard (Cutter, 2018). Although a hazard interaction matrix has been given by Kappes et al. (2010) to identify the influence of one hazard on another, but compound effect is somewhat more complex due to various geological, geographical, hydrological, seismic, and anthropogenic processes of the region. Gill and Malamud (2016) suggested that management priorities could be distorted if interactions between important environmental and anthropogenic processes are ignored and considering interactions helps us for better prioritization of resources for disaster risk reduction. Integration of hazard interaction aspects in the multi-hazard modeling approach can contribute to a better holistic assessment of the hazard risk of the region.

Mountain regions are habitat to 17% of the world's population, most of which are poor and marginalized (UNISDR, 2010). Assessment of exposure needs to be interpreted into risk assessment with the help of additional data on social vulnerability within the population (Rigg et al., 2016). The adaptive capacity of different social groups may make substantial differences in vulnerability to hazards among different population sections. For instance, poverty may be the reason for settlement in high-risk areas (Tuladhar et al., 2015) causing increased vulnerability to multiple hazards.

Each disaster type is unique, and each mountainous region has diverse vulnerabilities and resiliency levels. Multi-hazard susceptibility and exposure analysis approach is a cost-effective engineering that can assist the population in adapting to hazardous events. Integrated multiple hazard interaction data capture techniques are necessary in the domain of multi-hazard susceptibility and exposure assessment to develop clean and big structured data that can support the ML approach for improved results. With hazard interactions and networks being integrated with vulnerability and exposure factors along with other important features like the effects of climate change on multi-hazards, remote sensing and earth observation data, socio-economic and infrastructure vulnerabilities, resilience and adaptive strategies, real-time data assimilation, public awareness and an interdisciplinary approach, a treasure trove of valuable insights can be gained. These knowledge inputs can improve disaster preparedness and mitigation measures in the mountainous regions through better hazard prediction, optimizing resource allocation, promoting sustainable land use, and strengthening community resilience.

Challenges

One of the major challenges for multi-hazard susceptibility assessment is that of building generalized learning techniques by understanding and applying integrated interaction matrices between multiple hazards in learning algorithms. Besides, the availability and collection of data on hazard interactions and interaction networks with correct sampling and sufficient representation of each pattern of hazards is a challenge. ML algorithms require correctly sampled training data having sufficient representation of patterns for the statement of the problem to be merged in the data server. The ML approaches are processed as an integrated approach and may also face challenges related to personal privacy risk and country-specific data leading to limitation of data availability (Kuglitsch et al., 2022). Another data-related challenge relates to ethical concerns. Socio-economic biases in the data sets could not be disseminated through the models developed by the system. Possible harms associated with ML, such as underrepresentation due to human or technical bias should be mitigated and the assistance of ML can be recognized for all, particularly those who are more vulnerable to the impacts of hazards (Kuglitsch et al., 2022). Ensuring unbiased and ethical machine learning tools applied to the ML approach for disaster risk management is one of the

important traits (Rocchi et al., 2022). Mellowed machine learning tools should not be used in safety-critical situations for which they are not prepared (Gevaert et al., 2021). We obtain huge amounts of data from different sources for research applicability and ethics should be carefully considered and misuse should be avoided (Gevaert et al., 2021; Wagenaar et al., 2020; Stahl, 2021). The ethical issues include malicious use, loss of human decision-making, prioritization in risk management, and prioritization of the wrong problems concerning the expectations of stakeholders (Rocchi et al., 2022). The clusterization labeling should be essentially filled with the intention of the end user (Stahl, 2021).

While publicizing results, sensitive aspects should be kept in mind from the privacy point of view (GFDRR, 2018). The results must be humanly explicable and acceptable but this can be challenging as there is no general out-of-the-box human-machine interface that delivers evidence about how and why certain decisions are made by the ML model. Ultimately, faith in timely and fully transparent communication tools is the major challenge to be overcome. This requires effective collaboration among skillful disaster responders, ML developers, geoscientists, regulators, and government agencies, to meet the necessities of all stakeholders. Expertise in communicating results, uncertainties of machine learning, and identification of sensitive groups for overcoming bias are other significant aspects. So, before being applied it is essential to confirm promising results and assessment proneness of tools (Rocchi et al., 2022; Gevaert et al., 2021).

5. Conclusion

Mountainous regions are highly prone to a variety of nature-triggered disasters affecting the lives of millions of people worldwide each year. There is a great need to assess hazards holistically which may be helpful to manage the potential threats of these regions. The multi-hazard approach supports the holistic susceptibility assessment of the hazard potential of a particular region that can assist disaster management operations to prepare collectively for the greater risk from multiple hazards. In this article, a review study has been carried out to explore the machine learning models applied by researchers for multi-hazard susceptibility assessment in different mountainous regions of the world.

The performance evaluation of the models reveals that RF, FDA, GLM, Maxent, and MDA consistently deliver the highest AUC values for flood and landslide prediction. Random Forest stands out as the most reliable and effective model for wildfire prediction,

with SVM and Maxent also demonstrating strong potential. For gully erosion prediction, Maxent and Random Forest are the most effective models. In terms of land subsidence prediction, both SVM and GLM are excellent options, with SVM slightly outperforming GLM. For snow avalanche prediction, GLM and BRT yield good results while XGBoost achieves exceptional accuracy for rockfall and debris flow prediction. The machine learning methods achieved acceptable accuracy in predicting the different hazard types and multi-hazard susceptibility maps are generated by the researchers to provide useful information for proactive management and hazard mitigation.

Future research on the integration of hazard interaction aspects and interdisciplinary approach combining data science, engineering, environmental science, social science, and policy studies into multi-hazard modeling can contribute to an enhanced framework for disaster risk reduction. Further, the exploration of strategies for building generalized learning models and methods for improved accuracy can expand disaster management procedures in mountainous regions.

References

1. Azemeraw, W.A. (2021). Landslide Inventory, Susceptibility, Hazard and Risk Mapping. In book: *Landslide*, Zhang, Y., & Cheng, Q. (Eds.) pp. 1-31.10.5772/intechopen.100504
2. Barthel, F. & Neumayer, E. (2012). A trend analysis of normalized insured damage from natural disasters, *Climatic Change* 113(2), 215–237. https://ssrn.com/abstract=1831633
3. Bell, R. & Glade, T. (2004). Multi-hazard analysis in natural risk assessment. *WIT Trans on state–of–the–art in science and engineering*, 53. https://api.semanticscholar.org/CorpusID:55274221
4. Bordbar, M., Aghamohammadi, H., Pourghasemi, H.R. & Azizi, Z. (2022). Multi-hazard spatial modeling via ensembles of machine learning and meta-heuristic techniques. *Scientific reports*, 12, 145. Doi: 10.1038/s41598-022-05364-y
5. Breiman, L. & Cutler, A. (1993). A deterministic algorithm for global optimization. *Mathematical Programming*, 58 (1-3), 179-199. https://doi.org/10.1007/BF01581266
6. Cao, J., Zhang, Z., Du, J., Zhang, L., Song, Y., & Sun, G. (2020). Multi- geohazards susceptibility mapping based on machine learning - A case study in Jiuzhaigou, China. *Natural hazards*, 102 (3), 851-871.doi: 10.1007/s11069-020-03927-8
7. Chang, N.B., Parvathinathan, G. & Breeden, J.B. (2008). Combining GIS with fuzzy multi-criteria decision making for landfill siting in a fast-growing urban region. *J Environ Manage*, 87 (1), 138-153. doi: 10.1016/j.jenvman.2007.01.011
8. Chen, T. & Guestrin, C. (2016). XGBoost: A scalable tree boosting system. In *Proceedings of the 22nd ACM SIGKDD International Conference on Knowledge Discovery and Data Mining*, pp. 785-794 https://doi.org/10.1145/2939672.2939785
9. Cortes, C. & Vladimir, V. (1995). Support-vector networks, *Machine learning*, 20, 273-297. https://doi.org/10.1007/BF00994018
10. Cutter, S.L. (2018). Compound, cascading, or complex disasters: what's in a name? *Environ Sci Policy Sustain Dev*, 60 (6), 16-25. https://doi.org/10.1080/00139157.2018.1517518
11. Duda, R.O., Hart, P.E. & Stork, D.G. (2001). *Pattern Classification*, second edition, Wiley- Interscience, United States. P688 ISBN: 978-0-471-05669-0

12. Freund, Y. & Schapire, R.E. (1997). A Decision-Theoretic Generalization of On-Line Learning and an Application to Boosting. *J. Comput. Syst. Sci, 55(1)*, 119–139. https://doi.org/10.1006/jcss.1997.1504
13. Friedman, J.H. (1991). Multivariate adaptive regression splines. *The Annals of statistics, 19* (1), 1-67 http://www.stat.yale.edu/~lc436/08Spring665/Mars_Friedman_91.pdf
14. Friedman, J.H. (2001). Greedy function approximation: a gradient boosting machine. *Annals of Statistics, 29*(5), 1189-1232. doi: 10.1214/aos/1013203451
15. Friedman, J.H. (2002). Stochastic gradient boosting. *Computational statistics & data analysis, 38* (4), 367-378. doi: 10.1016/S0167-9473(01)00065-2
16. GAR (2022). Global assessment report on disaster risk reduction. Our world at risk: Transforming governance for a resilient future, United Nations office for disaster risk reduction. https://www.undrr.org/gar/gar2022-our-world-risk-gar
17. Gevaert, C.M., Carman, M., Rosman, B., Georgiadou, Y. & Soden, R. (2021). Fairness and accountability of AI in disaster risk management: Opportunities and challenges. *Patterns, 2* (11):100363. https://doi.org/10.1016/j.patter.2021.100363
18. GFDRR (2018) Machine Learning for Disaster Risk Management. Washington, DC: GFDRR. A guidance note on how machine learning can be used for disaster risk management, including key definitions, case studies, and practical considerations for implementation. https://www.gfdrr.org/sites/default/files/publication/181222_WorldBank_DisasterRiskManagement_Ebook_D6.pdf
19. Gill, J.C. & Malamud, B.D. (2016). Hazard interactions and interaction network (cascades) within multi-hazard methodologies. *Earth Syst. Dynam*. 7, 659-679. Doi:10.5194/esd-7-659-2016
20. Goetz, J., Brenning, A.H. & Petschko, P.L. (2015). Evaluating machine learning and statistical prediction techniques for landslide susceptibility modeling. *Comput Geosci, 81*(C), 1-11. doi: 10.1016/j.cageo.2015.04.007
21. Gruber, F.E. & Mergili, M. (2013). Regional-scale analysis of high-mountain multi-hazard and risk indicators in the Pamir (Tajikistan) with GRASS GIS. *Nat. Hazards Earth Syst Sci, 13* (10), 2779–2796. https://doi.org/10.5194/nhess-13-2779-2013
22. Hastie, T. & Tibshirani, R. (1986). Generalized additive Models. *Statistical Science, 1*(3), 297-310. http://www.jstor.org/stable/2245459
23. He, Q., Jiang, Z., Wang, M. & Liu, K. (2021). Landslide and wildfire susceptibility assessment in Southeast Asia using ensemble machine learning methods. Remote Sens, 13, 1572. https://doi.org/10.3390/rs13081572
24. Hill, D.J. & Minsker, B.S. (2010). Anomaly detection in streaming environmental sensor data: A data-driven modeling approach. *Environ. Model. & Softw., 25*(9), 1014-1022. doi: 10.1016/j.envsoft.2009.08.010
25. Hotelling, H. (1933). Analysis of a complex of statistical variables into principal components. *Journal of Educational Psychology, 24* (6), 417. https://doi.org/10.1037/h0071325
26. Huang, X., Li, Z., Wang, C. & Ning, H. (2020). Identifying disaster-related social media for rapid response: A visual-textual fused CNN architecture. *Int J Digit Earth, 13* (9), 1017-1039. doi: 10.1080/17538947.2019.1633425
27. IHCAP (2017). Urbanization Challenges in the Himalayan Region in the context of climate change adaptation and disaster risk mitigation; Indian Himalayan Climate Change Program, New Delhi.
28. IPCC (2021). *Summary for Policy Makers, Climate Change 2021: The Physical Science Basis.* Contribution of Working Group I to the Sixth Assessment Report of the Intergovernmental Panel on Climate Change, Masson - Delmotte, V. P., Zhai, A. et al. https://www.ipcc.ch/report/ar6/wg1/chapter/summary-for-policymakers/
29. Jang, J.S. (1993). ANFIS: Adaptive-network-based fuzzy inference system. *IEEE Trans. Syst. Man Cybern,* 23 (3), 665–685. doi: 10.1109/21.256541
30. Javidan, N., Kavian, A., Pourghasemi, H.R., Conoscenti, C., Jafarian, Z. & Rodrigo-Comino, Z.J. (2021). Evaluation of multi-hazard map produced using MaxEnt machine learning technique, *Sci Rep, 11*, 6496. https://doi.org/10.1038/s41598-021-85862-7
31. Kalantari. Z., Ferreira, C.S.S., Koutsouris, A.J., Ahmer, A.K., Cerdà, A. & Destouni, G. (2019). Assessing flood probability for transportation infrastructure based on catchment characteristics, sediment connectivity, and remotely sensed soil moisture. *Sci Total Environ, 661*,393–406. doi: 10.1016/j.scitotenv.2019.01.009
32. Kappes, M.S., Keiler, M. & Glade, T. (2010). From single to multi-hazard risk analysis; a concept addressing emerging challenges. In: Malet, J.P., Glade, T., Casagli, N. (ed) *Mountain Risks; Bringing Science to Society* (International conference), CERG edition, Strassbourg, France http://cerg.eu ISBN 2-95183317-1-5
33. Kappes, M.S., Keiler, M., Von Elverfeldt K. & Glade, T. (2012). Challenges of analyzing multi-hazard risk: A review, *Nat Hazards, 64*, 1925-1958. https://doi.org/10.1007/s11069-012-0294-2
34. Karlsson, C.S.J., Kalantari. Z., Mörtberg, U., Olofsson, B. & Lyon, S.W. (2017). Natural hazard susceptibility assessment for road planning using spatial multi-criteria analysis. *Environ Manag, 60*, 823–851. https://doi.org/10.1007/s00267-017-0912-6
35. Kennedy, J., Eberhart, R.C. (1995). Particle swarm optimization. *Proceedings of ICNN'95 - International Conference on Neural Networks*, Perth, WA, Australia, 1995, pp 1942-1948 vol 4. doi: 10.1109/ICNN.1995.488968

36. Keršulien. V. & Turskis, Z. (2011). Integrated fuzzy multiple criteria decision-making model for architect selection. *Technol. Econ. Dev. Econ.,* 17 (4), 645–666. doi:10.3846/20294913.2011.635718
37. Khatakho, R., Gautam, D., Aryal, K.R., Pandey, V.P., Rupakhety, R., Lamichhane, S., Yi- Chung Liu et al. (2021). Multi-hazard risk assessment of Kathmandu Valley, Nepal. *Sustainability,* 13(10), 5369. https://doi.org/10.3390/su13105369
38. Khosravi, K., Panahi, M., Bui, D.T. (2018). Spatial prediction of groundwater spring potential mapping based on an adaptive neuro-fuzzy inference system and metaheuristic optimization. *Hydrol Earth Syst Sci, 22* (9), 4771- 4792. doi: 10.5194/hess-22-4771-2018
39. Kuglitsch, M., Arif, A., Aquino, R. et al. (2022). Artificial intelligence for disaster risk reduction: opportunities, challenges, and prospects. *World Meteorological Organization Bulletin, 71* (1). https://public.wmo.int/en/resources/bulletin/artificial-intelligence-disaster-risk-reduction-opportunities-challenges-and
40. Linardos, V., Drakaki, M., Tzionas, P. & Karnavas, Y.L. (2022). Machine learning in disaster management: Recent developments in methods and applications. *Machine learning knowledge extraction, 4* (2), 446-473. https://doi.org/10.3390/make4020020
41. Lloyd, S.P. (1982). Least squares quantization in PCM, *IEEE Transactions on Information Theory, 28*(2), 129–137
42. Marzban, C. (2004). The ROC curve and the area under it as performance measures, *Weather Forecast, 19* (6), 1106-1114. doi: https://doi.org/10.1175/825.1
43. Michielsen, A., Kalantari, Z., Lyon, S.W. & Liljegren, E. (2016). Predicting and communicating flood risk of transport infrastructure based on watershed characteristics. *J Environ Manag. 182*, 505–518. https://doi.org/10.1016/j.jenvman.2016.07.051
44. Mirjalili, S. Mirjalili, S.M. & Lewis, A. (2014). Gray Wolf optimizer. *Adv. Eng. Softw. 69*, 46–61. https://doi.org/10.1016/j.advengsoft.2013.12.007
45. Mukherji, A., Scott, C., Molden, D. & Maharjan, A. (2018). Megatrends in Hindu Kush Himalaya: climate change, urbanization and migration and their implications for water, energy and food. In: Biswas, A.K., Tortajada, C., Rohner, P. (ed) *Assessing Global Water Megatrends*, *Water Resources Development and Management*, Springer, Singapore pp 125–146. https://doi.org/10.1007/978-981-10-6695-5_8
46. Nachappa, T.G., Ghorbanzadeh, O., Gholamnia, K. & Blaschke, T. (2020). Multi-hazard exposure mapping using machine learning for the stare of Salzburg., Austria. *Remot Sens*, 12, 2757. https://doi.org/10.3390/rs12172757
47. Nelder, J.A. & Wedderburn, R.W.M. (1972). Generalized Linear Models. *Journal of the Royal Statistical Society, Series A (General), 135* (2), 370–384 https://doi.org/10.2307/2344614
48. Phillips, S.J., Dudík, M. & Schapire, R.E. (2021). Maxent software for modeling species niches and distributions. http://biodiversityinformatics.amnh.org/open_source/maxent/
49. Pourghasemi, H.R., Gayen, A., Edalat, M., Zarafshar, M. & Tiefenbacher, J.P. (2020). Is multi-hazard mapping effective in assessing natural hazards and integrated watershed management? *Geosci Front, 11*(4), 1203-1217. https://doi.org/10.1016/j.gsf.2019.10.008
50. Pourghasemi, H.R., Gayen, A., Panahi, M., Rezaie, F. & Blaschke, T. (2019). Multi-hazard probability assessment and mapping in Iran. *Sci Total Environ, 692*, 556–571. doi: 10.1016/j.scitotenv.2019.07.203
51. Pourghasemi, H.R., Kariminejad, N., Amiri, M. et al. (2020). Assessing and mapping multi-hazard risk susceptibility using machine learning technique. *Scientific reports, 10*, 3203. https://doi.org/10.1038/s41598-020-60191-3
52. Pourghasemi, H.R., Yousefi, S., Kornejady, A. & Cerdà, A. (2017). Performance assessment of individual and ensemble data-mining techniques for gully erosion modeling. *Sci Total Environ, 609*, 764–775. doi: https://doi.org/10.1016/j.scitotenv.2017.07.198
53. Pouyan, S., Pourghasemi, H.R., Bordbar, M., Rehmanian, S. & Clague, J.J. (2021). A multi-hazard map based flooding, gully erosion, forest fires and earthquakes in Iran. *Scientific Reports, 11* (1), 4889. doi: 10.1038/s41598-021-94266-6
54. Rahmati, O., Yousefi, S., Kalantari, Z. et al. (2019). Multi-Hazard exposure mapping using machine learning techniques: A case study from Iran, *Remote Sens, 11*(16), 1943. https://doi.org/10.3390/rs11161943
55. Ramsay, J.O. & Dalzell, C.J. (1991). Some Tools for Functional Data Analysis. *Journal of the Royal Statistical Society. Series B (Methodological), 53* (3), 539–572. http://www.jstor.org/stable/2345586
56. Rigg, J., Oven, K.J., Basyal, G.K., Lamichhane, R. (2016). Between a rock and a hard place: vulnerability and precarity in rural Nepal. *Geoforum, 76*, 63–74. https://doi.org/10.1016/j.geoforum.2016.08.014
57. Rocchi, A., Chiozzi, A., Nale, M. et al. (2022). Machine learning framework for multi-hazard risk assessment at the regional scale in earthquake and flood prone areas. *Appl sci, 12*, 583. https://doi.org/10.3390/app12020583
58. Rumelhart, D., Hinton, G. & Williams, R. (1986). Learning representations by back-propagating errors. *Nature* 323, 533–536. https://doi.org/10.1038/323533a0
59. Rusk, J., Maharjan, A., Tiwari, P., Chen, T.K.C., Shneiderman, S., Turin, M. & Seto, K.C. (2022). Multi-hazard susceptibility and exposure assessment of the Hindu Kush Himalaya. *Sci Total Environ, 15*,804: 150039. doi: https://doi.org/10.1016/j.scitotenv.2021.150039

60. Saaty, T.L. (1988). What is the Analytic Hierarchy Process? In: Mitra, G., Greenberg, H.J., Lootsma, F.A., Rijkaert, M. J. Zimmermann, H.J. (eds) *Mathematical Models for Decision Support. NATO ASI Series, 48*, Springer, Berlin, Heidelberg. https://doi.org/10.1007/978-3-642-83555-1_5
61. Samanta, S., Pal, D.K. & Palsamanta, B. (2018). Flood susceptibility analysis through remote sensing, GIS and frequency ratio model. *Appl Water Sci, 8* (66), 1-14. https://doi.org/10.1007/s13201-018-0710-1
62. Sarker, I.H. (2021). Machine Learning: Algorithms, Real-World Applications and Research Directions. *SN Comp sci*, 2,160. https://doi.org/10.1007/s42979-021-00592-x
63. Schmidt, J., Matcham, I., Reese, S. et al. (2011). Quantitative multi-risk analysis for natural hazards: a framework for multi-risk modelling. *Nat Hazards, 58* (3), 1169–1192. https://doi.org/10.1007/s11069-011-9721-z
64. Sharma, E. et al. (2019) Introduction to the Hindu Kush Himalaya Assessment. In Wester. P., Mishra, A., Mukherji, A. & Shrestha, A.B. (2019). (ed) *The Hindu Kush Himalaya Assessment*. Springer, Cham. https://doi.org/10.1007/978-3-319-92288-1_1
65. Stahl, B.C. (2021). Ethical Issues of AI. In Artificial Intelligence for a better future. Springer Briefs in Research and Innovation Governance. Springer, Cham. https://doi.org/10.1007/978-3-030-69978-9_4
66. Swets, J.A. (1988). Measuring the accuracy of diagnostic systems. *Science, 3*, (240): 1285–1293. doi: 10.1126/science.3287615
67. Tien Bui, D., Tuan, T.A., Hoang, N.D. et al. (2017). Spatial prediction of rainfall induced landslides for the Lao Cai area (Vietnam) using a novel hybrid intelligent approach of least squares support vector machines inference model and artificial Bee colony optimization. *Landslides, 14*, 447-458. doi: 10.1007/s10346-016-0711-9
68. Tuladhar, G., Yatabe, R., Dahal, R.K. & Bhandary, N.P. (2015) Disaster risk reduction knowledge of local people in Nepal. *Geoenviron Disasters*, 2 (5). https://doi.org/10.1186/s40677-014-0011-4
69. UN Johannesburg Plan (2002). Report of the World Summit on Sustainable Development Johannesburg, South Africa, 26 August 4 September 2002. file:///F:/Downloads/A_CONF.199_20-EN%20(2).pdf
70. UNEP, (1992). Technical report, United Nations Environment Programme. http://www.un.org/esa/dsd/agenda21/res_agenda21_07.shtml
71. UNISDR (2010). A View from the top: Vulnerability in Mountain Systems, Social Development Notes; social dimension of climate change. https://www.unisdr.org/files/15567_vulnerabilitymountainsystemsjune201.pdf
72. UNISDR (2015). HFA Decade - The Economic and Human Impact of Disasters in the Last 10 Years. https://www.unisdr.org/files/42862_economichumanimpact20052014unisdr.pdf
73. Van Westen C.J. (2013). Remote sensing and GIS for natural hazards assessment and disaster risk management. In: Schroder, J.F. & Bishop, M.P. (Eds.), *Treatise on Geomorphology, 3*, pp 259-298. https://doi.org/10.1016/B978-0-12-374739-6.00051-8
74. Van Westen C.J. & Greiving, S. (2017). Multi-hazard risk assessment and decision making, In: *Environmental Hazards Methodologies for Risk Assessment and Management*, IWA publishing, London, UK, pp 31–94 doi: 10.2166/9781780407135_0031
75. Wagenaar, D., Curran, A., Balbi, M. et al. (2020) Invited perspectives: how machine learning will change flood risk and impact assessment. *Natural Hazards and Earth System Sciences, 20* (4), 1149 1161. https://doi.org/10.5194/nhess-20-1149-2020
76. Yousefi, S., Pourghasemi, H.R., Emami, S.N., Pouyan, S., Eskandari, S. & Tiefenbacher, J.P. (2020). A Machine learning framework for multi-hazards modeling and mapping in mountainous area. *Scientific reports*, 10 (1), 12144 doi: 10.1038/s41598-020-69233-2.
77. Youssef, A.M., Mahdi, A.M., Al-Katheri, M.M., Pouyan, S. & Pourghasemi, H.R. (2022). Multi-hazards modeling using machine learning algorithms in southwestern Saudi Arabia. *Research Square*, pp 1-33. doi: https://doi.org/10.21203/rs.3.rs-1554302/v1
78. Zhao, J., Zhang, Q., Wang, D. et al. (2022). Machine learning-based evaluation of susceptibility to geological hazards in the Hengduan mountains region, China. *Int J Disaster Risk Sci*, *13*(1), 305-316.https://doi.org/10.1007/s13753-022-00401-w
79. Zschau. J. (2017). Where are we with multi-hazards, multi-risks assessment capacities? In: *Understanding disaster risk: Risk assessment methodologies and examples*. https://drmkc.jrc.ec.europa.eu/portals/0/Knowledge/ScienceforDRM/ch02/ch02_subch0205.pdf

Soil Erosion Assessment Using the RUSLE Model and Geospatial Analysis: A Case Study of Majuli Island of Assam, India

Pragyashree Mahanta[1], Nitashree Mili[1]

Abstract

Soil erosion is a major environmental issue that affects the sustainability of agricultural lands and ecosystems. The condition is more severe in the riverine areas. The RUSLE (Revised Universal Soil Loss Equation) model is a widely used tool for assessing soil erosion risk. This study aims to evaluate the soil erosion in Majuli Island, India which is situated in the mid-stream the Brahmaputra River. In this study, RUSLE Model has been paired up with Geospatial Techniques to evaluate the annual soil loss of the island. The parameters used for the assessment are the Rainfall Erosivity (R), Soil Erodibility (K), Slope Length and Steepness (LS), Crop and Management (C) and Conservation Practice (P). The results categorized the island into five classes from very high to very low. The high-class area needs immediate attentions. The results show that the highest soil loss occurs in the riverbank areas whereas it is low to very low in the central part. It indicates that bank erosion by the Brahmaputra is a major cause of soil loss in Majuli .The results of this study can help in the development of soil conservation strategies and management practices to mitigate soil erosion in Majuli Island.

Keywords: *Brahmaputra River, Erosion, Geospatial Techniques, Majuli Island, RUSLE, Soil Loss.*

1. Introduction

Soil erosion is a critical environmental issue with far-reaching consequences, impacting agricultural productivity, water quality, and ecosystem health. The process of soil erosion is when the top fertile and productive soil layer is washed away or detached

[1] Department of Geography, Cotton University, Guwahati, Assam, India

from its original surface and is gradually deposited at a further location, resulting in the exposure of the sub-surface soil (Jain et.al. 2001). The rapid increase in the rate of soil loss poses adverse effects on the economy and environment, especially is the economy is primarily dominated by agriculture (Lal, 1998). With thorough observation, it can be noticed that the direct threat of the soil erosion is held over the developing nations as they have to feed their ever-growing population but the agricultural land gets limited (Erenstein, 1999). The problem of soil erosion is not an issue of present origin but a phenomenon persisting on the earth for a long time, but the impact is greater in the recent era due to the increased man-environment relationship and the pressure exerted by man to modify the environment (Rasool et.al. 2014). The root cause of the issue concerning the soil erosion is a combined action of change in land-use of a region and large-scale deforestation (Karamage et al. 2016; Lee et al. 2017).

Assessing soil erosion accurately is essential for effective land management and conservation efforts. The Revised Universal Soil Loss Equation (RUSLE) model, coupled with geospatial analysis, provides a powerful tool for quantifying soil erosion rates and identifying vulnerable areas. This case study focuses on Majuli Island in Assam, India, a region prone to significant soil erosion due to its unique geographical characteristics and land use practices. By applying the RUSLE model and geospatial analysis techniques to Majuli Island, the aim is to evaluate the extent of soil erosion and identify key factors contributing to erosion.

1.1. Study Area

Majuli is considered to be the largest river island situated in the course of the mighty Brahmaputra. It is the center of neo-vaishnavite culture. Majuli island extends from 93º30' E to 94º35' E longitude and 26º50' N to 27º10' N latitudes. It is the one and only island district of India surrounded by three major rivers viz. Subansiri and Kherkutia Suti to the north and the mighty Brahmaputra to the south cutting off its land routes. The elevation of this island varies from about 60 m to 85 m above the sea level (Bhaskar and Sarkar, 2013). Majuli is severely affected by bank erosion and frequent floods caused by the Brahmaputra on the southern bank of Majuli and Subansiri on the northern of the island. These hazards were not displayed with the present intensity before the great earthquake of 1950. The area of the island was recorded to be about 1249 sq.km in the year 1915 and gradually reduced to 645.49 sq.km in the year 1995 (Sarma, 2005 and

Kotoky et.al, 2005). At present the area of Majuli island measures upto only about 474.39 sq.km (LANDSAT 2023). Due to high deposition rate, the river Brahmaputra have taken the form of braided channel and anabranches and as Majuli is constituted of silty and sandy clay loam soil structures the intensity of soil erosion has also increased (Dutta et.al.,2010) and its topsoil is highly susceptible to erosion as it is composed of sandy silt mixed with clay (Sarma, 2013).

Majuli island enjoys a sub-tropical climatic condition, with average summer temperature of about 34ºC and winter temperature ranging from 7ºC to 18ºC with average annual rainfall accounting for about 215 mm. Keeping into account all the parameters, RUSLE model have been applied with an aim to assess the soil erosion and its rate on Majuli island as it is being eroded very rapidly.

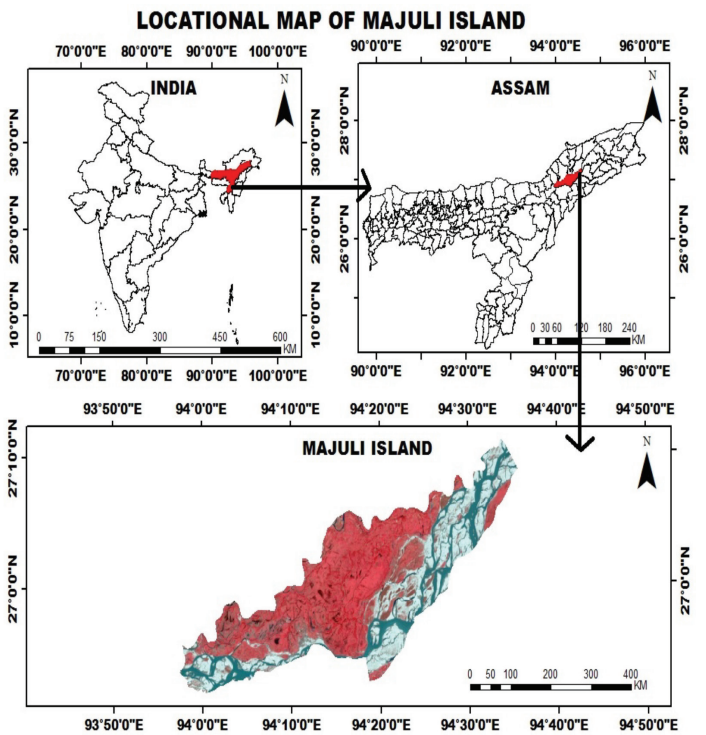


Figure 1: Location Map of Majuli Island

1.2. RUSLE Model

The working principle of RUSLE Model uses five parameters, it is a physical based empirical model that analyses the soil erosion of a region or basin. This model mainly uses the climatic data and topographic characteristics to run the analysis over a region or basin (Pathan and Sil, 2020). The input parameters of the model are Rainfall Erosivity (R) Factor, Soil Erodibility (K) Factor, Slope Length and Steepness (LS), Cover Management (C) and Support Practice (P) Factor and these factors are independent for calculating RUSLE Model. Thus the equation used for RUSLE Model is given below (Wischmeier and Smith, 1978):

A = R x K x LS x C x P (Renard et.al., 1997)

Where,

A is the Average Annual Soil Loss, usually on yearly basis (ton ha^{-1} yr^{-1})

R is the Rainfall Run-off Erosivity Factor (MJ mm ha^{-1} hr^{-1} $year^{-1}$)

K is the Soil Erodibility Factor (ton ha hr MJ^{-1} mm^{-1})

LS is Slope Length and Steepness (Dimensionless)

C is the Cover Management Factor (Dimensionless), and

P is the Support Practices Factor (Dimensionless).

With the help of GIS, these factors used in RUSLE Model can be overlapped and multiplied to acquire the result i.e., the soil loss value.

2. Methodology

This study is done for the year 2022 and for the input materials to carry out this assessment, the date required were: Cartosat DEM of 30m resolution downloaded from BHUVAN. Majuli have an elevation ranging from 60m to 85m the land-use and land-cover map have been downloaded from Sentinel Copernicus for the year 2022. The soil map is taken from FAO DSMW and extracted as per the study area shapefile. Majuli was constituted by only one soil type, Sandy Clay Loam. The shapefile of the study area has been digitized from LANDSAT-8 OLI with a 30m resolution. The rainfall data was downloaded from CRU- Climate Research Unit for the year 2022. The map projection system used for all input layers is WGS 1984 UTM Zone 46N.

Table 1: Input Data Used for RUSLE Model

DATA	RESOLUTION	SOURCE	YEAR
Cartosat DEM	30 m	BHUVAN	2022
LULC	10 m	Sentinel Copernicus	2022
Soil Data	5*5 arc minutes	FAO/UNESCO (DSMW)	
Rainfall Data	0.5*0.5º (grids)	Climate Research Unit	2022
Study Area Shapefile	30 m	LANDSAT-8 OLI	2022

The methodology that has been used in carrying out this study are as follows:

- ***Rainfall Erosivity Factor (R)***

  The R-factor is determined on the basis of mean annual rainfall. Rainfall is considered to be significant in terms of soil loss rate and surface run-off rate (Wischmeier and Smith, 1978). R-factor is dependent upon the intensity and calculate the R-factor, the rainfall data of 2022 is considered. The equation used in this paper is Lambordi Method given as R = 1.03 x P (where, P = Mean Annual Rainfall). Using this equation in ArcGIS software by raster calculator the R-factor can be received. And the R-factor is expressed as MJ mm $ha^{-}1$ $hr^{-}1$ $year^{-}1$.

- ***Soil Erodibility Factor (K)***

  Determination of the soil type is very essential for the construction of K-factor. It is one of the factors responsible for the soil loss. The soil type that constitutes the riverine island is sandy clay loam (as per DSMW). The K-factor for RUSLE model can be calculated from the equation given as

  K-factor =fsand* fclay* forgc* fsilt*0.1317

  $$\text{fsand} = \left(0.2 + 0.3 * \exp - \left[-0.256 * m_{sand} * \left(1 - \frac{m_{silt}}{100}\right)\right]\right)$$

  $$\text{fclay} = \left(\frac{m_{silt}}{m_{clay} + m_{silt}}\right)^{0.3}$$

$$\text{forgC} = \left(1 - \frac{0.0256 * OrgC}{OrgC + exp[3.72 - 2.95 * OrgC]}\right)$$

$$\text{fsilt} = \left(1 - \frac{0.7\left(1 - \frac{m_{sand}}{100}\right)}{\left(1 - \frac{m_{sand}}{100} + exp\left[-5.51 + 22.9 * \left(1 - \frac{m_{sand}}{100}\right)\right]\right)}\right)$$

given by Wischmeier and Smith, 1978

where, m_sandis the proportion (%) of sand content,

m_siltis the proportion (%) of silt content,

m_(clay)is the proportion (%) of clay content,

OrgC is the amount (%) of the organic carbon content of the layer (%)

In ArcGIS software, using field calculator to find out the values of fsand, fclay, forgc and fsilt. After obtaining the required values respectively, the K- factor is calculated again using the field calculator tool by placing equation

K-factor =fsand* fclay* forgc* fsilt*0.1317

- **Slope Length and Steepness (LS)**

  This is the most influential factor while calculating RUSLE as it determines total sediment load and soil erosion. For the computation if slope length, the DEM is required from where fill sink, flow direction and flow accumulation can be calculated with the help of ArcGIS tool (Pathan and Sil, 2020). The USPED (Unit Stream Power Erosion and Deposition) method is used to compute the LS, which used the flow accumulation and slope. The equation for slope length is

$$L = (m+1)\left(\frac{\lambda_A}{22.1}\right)^m$$

Where, L is the slope length, λ_A is the area of upland flow, m is an adjustable value depending on the soil's susceptibility to erosion, 22.1 is the unit of plot length.

Again, the equation used for calculating slope is,

$$S = \left(\frac{\sin(0.01745 * \theta_{deg})}{0.09}\right)^{n}$$

Where, θ is the slope in degree, 0.09 is the slope gradient constant and n is an adjustable value depending on the soil's susceptibility to erosion.

Therefore, the equation used for calculation of the LS factor using ArcGIS raster calculator tool is given below

Power("flow accumulation"*[cell resolution]/22.1,0.4)* Power(Sin("slope degree"*0.01745)/0.09,1.4)*1.4

- **Support Practice (P)**

  After preparation of the LS factor, as the P factor is based on slope. The P factor is generated with the help of slope of the study area. It is mainly dependent on the agriculture type and slope of Majuli (study area). After confirming the cultivation type the values of the slope length is paired with the values of cultivation type. For calculation of the P-factor the values are taken from Korean Institute of Construction Technology, 1992, which is tabulated as

Table 2: P factor depending on cultivation types and slope

SLOPE	CULTIVATION TYPE VALUE
0.0-7	0.55
7-11.3	0.60
11.3-17.6	0.80
17.6-26.8	0.90
26.8 >	1

- **Cover and Management factor (C)**

  The C factor is obtained from the land-use pattern which was downloaded from the Sentinel Copernicus for the year 2022. Here, using the ArcGIS software the C values are determined depending on the land-use and land-cover classes. The C values obtained for LULC if Majuli island are tabulated below:

Table 3: Cover Management (C) factor values for the study area

FEATURES	C-FACTOR	AREA IN HA.
BUILT-UP	0.004	63.46
CROP	0.15	341.32
TREES	0.01	28.09
WATER	0	14.46
BAREGROUND	1	2.07
RANGE LAND	0.05	24.61
FLOODED VEGETATION	0.35	0.35

The C-Factor represents the effects of soil cover, productive level of crop sequence and soil-disturbing activities on soil erosion (Pathan and Sil, 2020). The C-Factors used in this paper is derived from Tiruneh, G., & Ayalew, M. (2015) and Gelagay, H. S., & Minale, A. S. (2016).

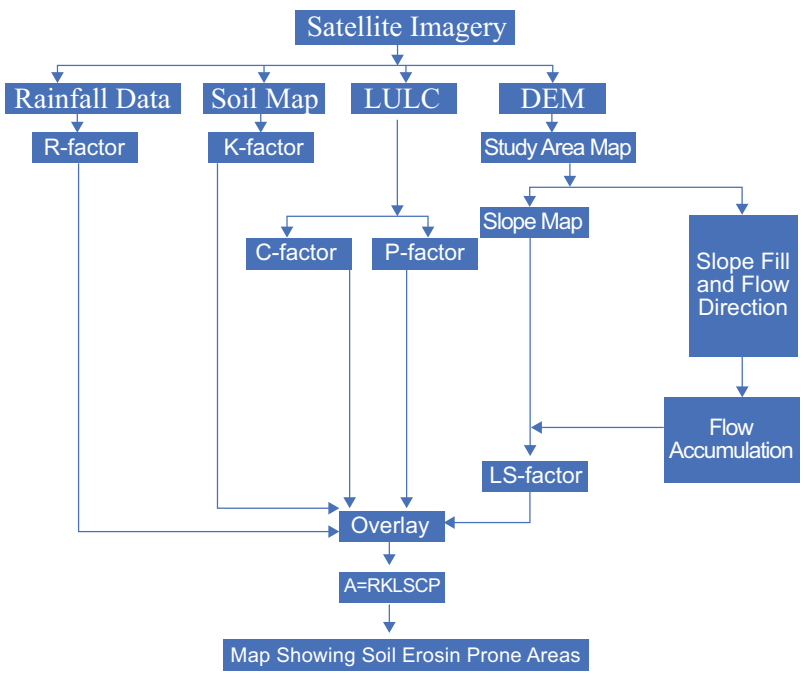


Figure 2: Methodological Framework of RUSLE Model

3. Results and Discussion:

3.1 Change in Area

As Majuli island is prone to severe flood and devastating act bank erosion, the area of the island is gradually shirking over the years. The area of Majuli island was estimated to be about 425.03 km^2. in the year 2000. But it can be seen to have certain changes like erosion in major parts along the bank as well as some sediment deposition as well. With all these changes, the area of Majuli island has been reduced to around 380 km^2 by the year 2023-24.

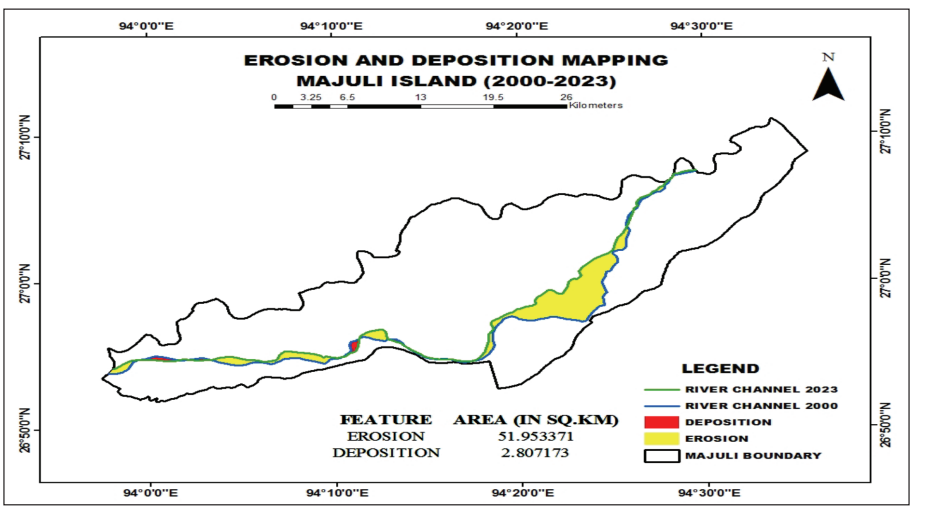


Figure 3: Pattern of Bankline Shifting (2013-2024)

3.2 Land use and Land Cover

The term "land use" and "land cover" (LULC) is used to depict the maps that describe about the types of landforms found on the surface of the earth (land cover) and the anthropogenic activity that is associated with them (land use). Land cover is an important parameter for a number of models associated with agriculture, hydrology and ecology which constitutes necessary tools for development, planning and management of natural resources in the region.

The GIS and Remote Sensing technology combined makes the perfect tool to identify and locate various types of land features. LANDSAT imagery year of 2000 and 2023 were used for preparation and interpretation of land use/land cover. The study area has been classified into five major categories to determine LULC. The areas identified and mapped as settlement in the year 2000 has been noticed to have gradually increased by the year 2023. This provides information the intense anthropogenic activities taking place within the island have changed the surface features. Agricultural land has been converted into built-up area. On the contrary, the continuous effect of flood and severe erosion have been cutting the land area by actions of lateral erosion. Thus with the shrinking land area and increasing population and settlement size, there is a drastic change that is noteworthy in case of the river island, Majuli.

Table 4: LULC changes from 2000 to 2023

YEARS	2000	2023
FEATURES	AREA (IN SQ.KM)	AREA (IN SQ.KM)
RIVER	92.24	69.44
SANDBAR	175.98	143.56
VEGETATION	410.43	317.16
OPEN AREA	67.68	122.15
WATER BODIES	9.74	16.92
SETTLEMENT	30.43	117.35

Source: Calculated by author

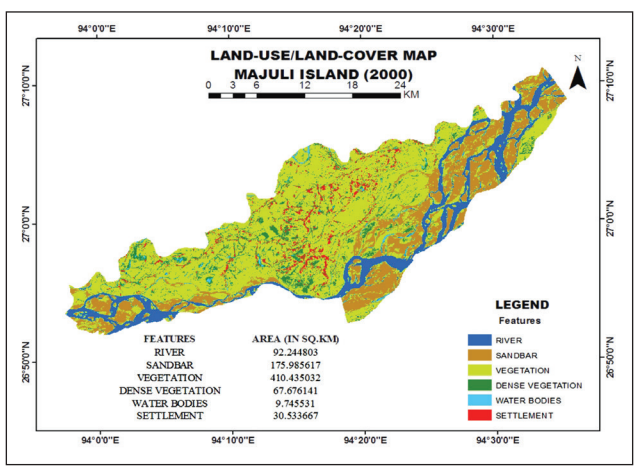


Figure 4: LULC of Majuli Island, 2016

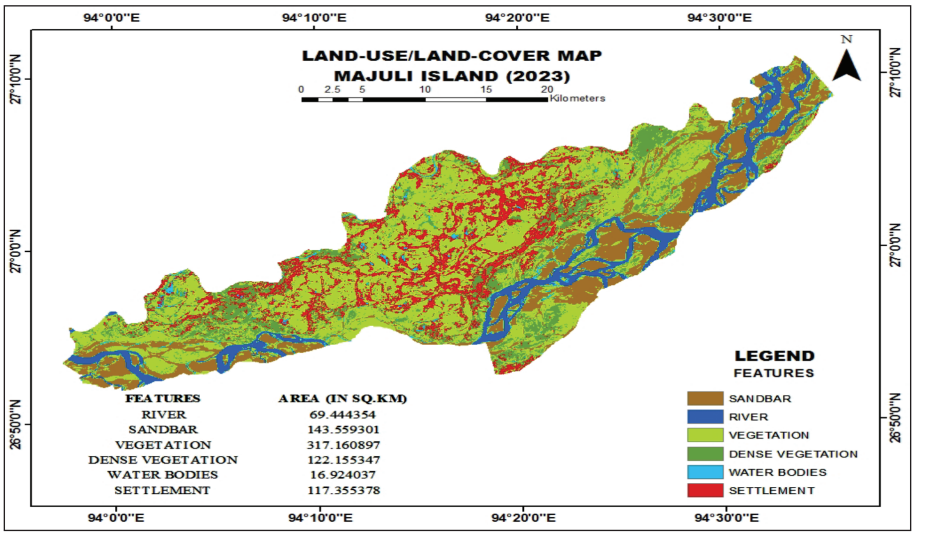


Figure 5: LULC of Majuli island, 2023

3.2 Analysis of Factors of RUSLE Model

After computation of all the required factors individually, multiplication is done to obtain the final soil loss map using ArcGIS software. The equation is calculated using the Map Algebra -Raster Calculator tool. The equation is: A = R x K x LS x C x P

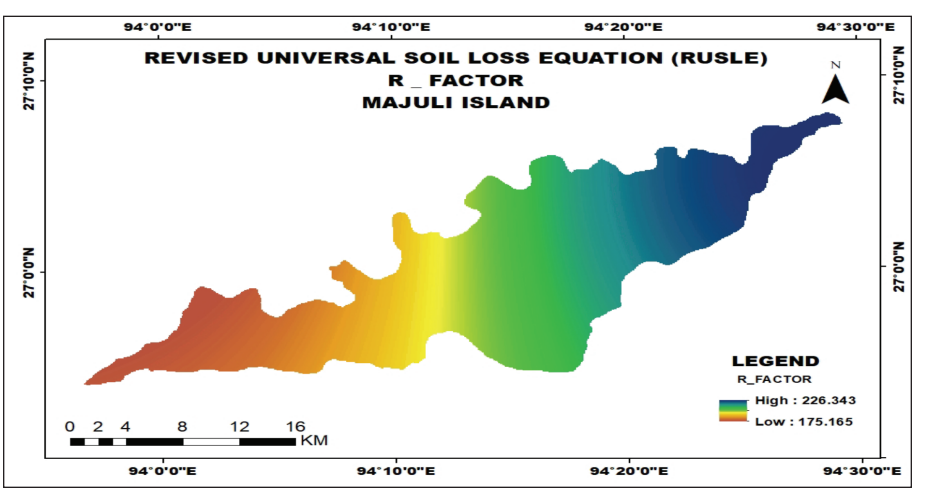


Figure 6: R- Factor obtained from the rainfall date using IDW

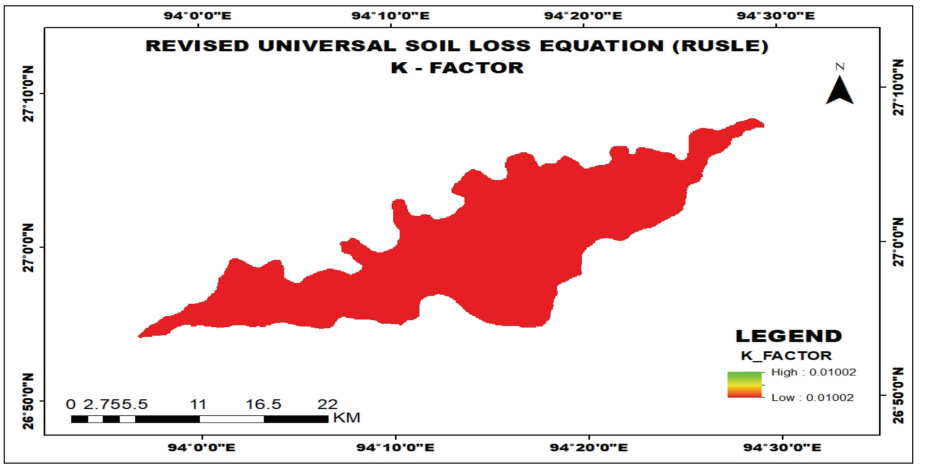


Figure 7: K- Factor obtained from soil data downloaded from FAO

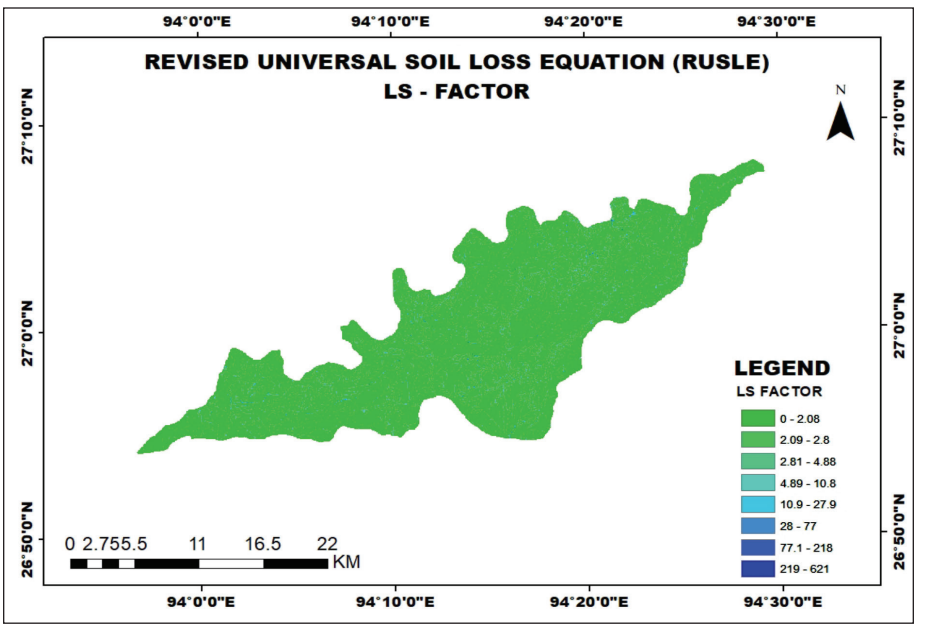


Figure 8: LS -Factor obtained from the DEM representing slope and flow accumulation

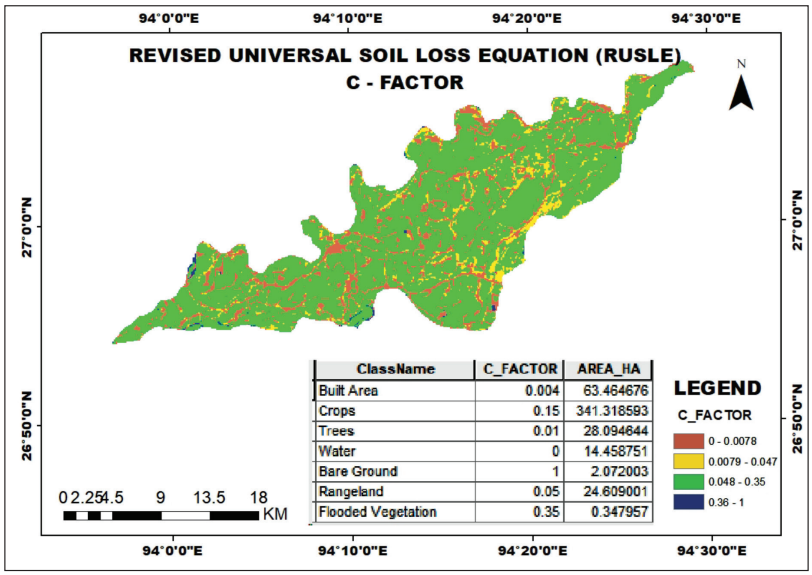


Figure 9: C–Factor is calculated on the basis of given values for each land-use class

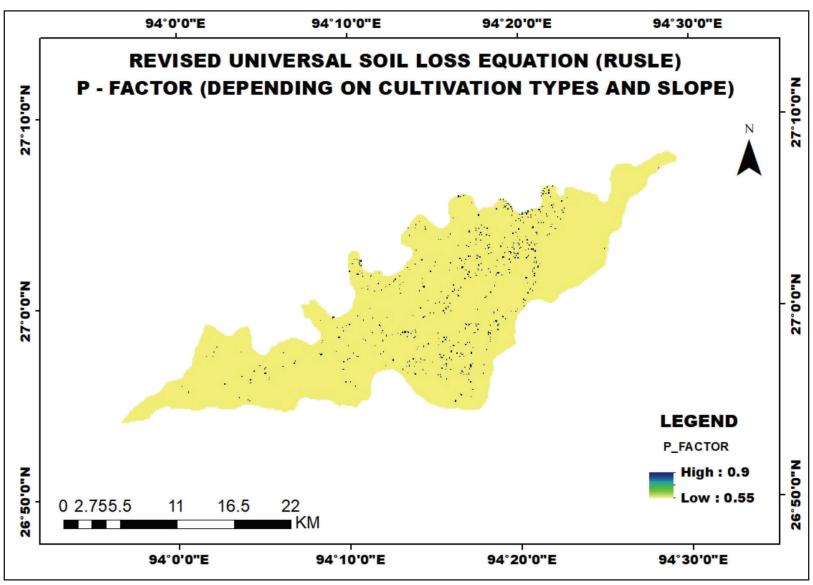


Figure 10: P-Factor is calculated on the basis of slope and cultivation type of an area.

The rainfall erosivity factor is determined by MJ mm/ha/hr/yr. Here, the R-Factor is calculated for Majuli island. The value of R-Factor is obtained to be 175.165 to 226.343 MJ mm/ha/hr/yr for the year 2022. The areas receiving relatively higher rainfall have high R-value than the areas receiving less amount of rainfall.The soil erodibility factor that is determined as K-factor. Majuli island is composed of a single soil type viz., sandy clay loam. That is why, the value of the K-Factor is not in range but a singular value 0.01002.The LS-Factor ranges from 0 to 621. The C-Factor is obtained from the LULC map from Sentinel Copernicus, where the value of C is given depending on the land-use class such as, for Built-up area the value of C is 0.004, for crops it is 0.15, for trees it is 0.01, for water it is 0, for bare-ground it is 1, for rangeland it is 0.05 and for flooded vegetation it is found to be 0.35. The P-Factor is described by the slope and type of cultivation done on the study area. The value of P usually ranges from 0 to 1, but as per calculation, here the P-Factor ranges from 0.55 to 0.90. When the value of P is closer to 1, it denoted healthy vegetation and when the value reaches close to 0, it denoted soil cover.

The output map of the above-mentioned values shows that the soil loss of Majuli island is 53.2148 ton/ha/yr for the year 2022. When the intensity of rainfall increases the soil loss also increases and with the decrease of rainfall intensity, the amount of soil loss also decreases. The value of soil loss is also influenced by the soil type. As the soil of Majuli island is sandy, it is loss in structure and is prone to be washed away by rain or river flow. Thus, these factors actively influence the outcome of soil loss.

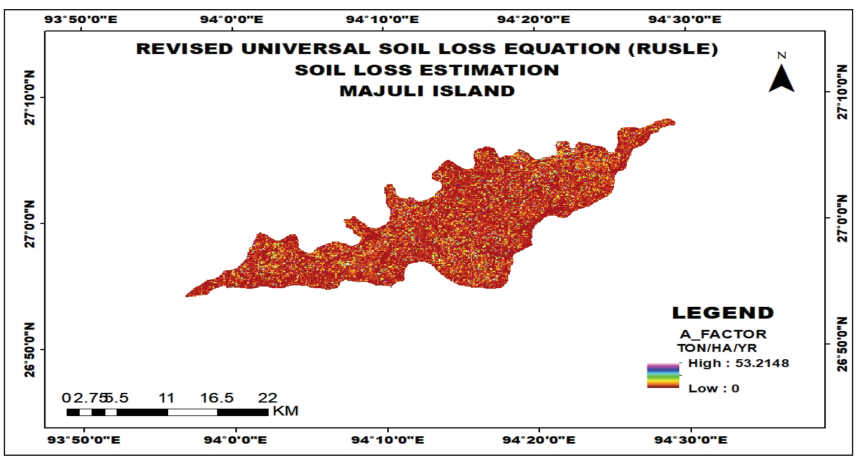


Figure 11: Soil Loss Map of Majuli Island (2022)

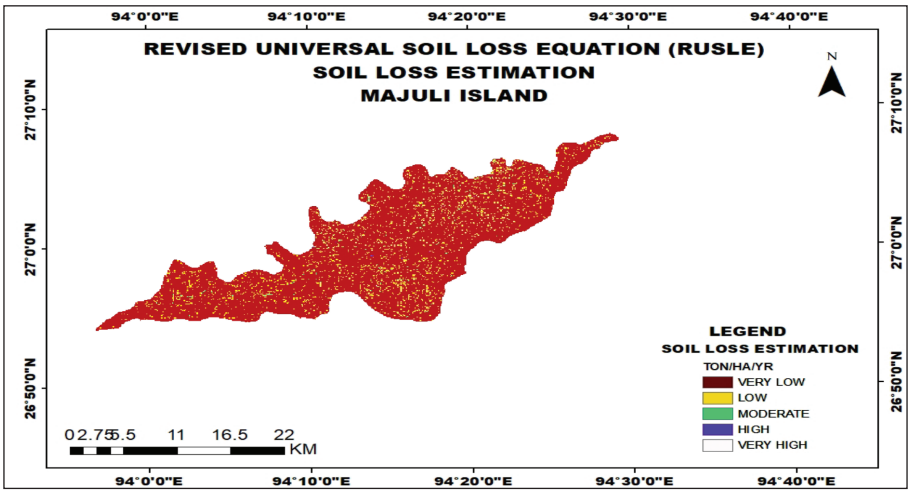


Figure 12: Soil Loss Estimation Map of Majuli Island

Table 5: Showing Soil Erosion in different classes with Area and Percentage

SOIL EROSION CLASS	RANGE (ton/ha/yr)	AREA (in SQ.KM)	PERCENTAGE (%)	PRIORITY CLASS
VERY LOW	0-0.417	444.277939	95.38412	V
LOW	0.418-2.92	19.396025	4.164224	IV
MODERATE	2.93-9.39	1.809983	0.388594	III
HIGH	9.40-20.9	0.241398	0.051827	II
VERY HIGH	21-53.2	0.052333	0.011236	I

4. Conclusion

The application of the Revised Universal Soil Loss Equation (RUSLE) model, coupled with geospatial analysis, is instrumental in estimating annual soil loss and prioritizing erosion-prone areas in the region. The study emphasizes the significance of GIS-based RUSLE models in assessing soil erosion dynamics, particularly in Majuli Island, which

are susceptible to significant erosion due to various factors especially geographical characteristics. Soil erosion is the prevailing hazard in the periphery regions of Majuli island as the soil structure is very loose and does not have a thick vegetation cover along its bank. Rainfall is another significant factor. In Majuli island the higher range of soil loss occurs along the bank and places with high elevation. Majuli island accounts to a total of 53.2148 ton/ha/yr of soil loss in the year 2022. Thus, the preventive measures are needed to be adopted along the bank of Brahmaputra primarily and also along river Subansiri and Kherkutia-Lohit suti.

4.1 Preventive Measures

There must be certain activities that are to be taken into account for implementing preventive measures from soil loss. Some cautions have been mentioned below:

a) Identification of the most vulnerable areas is the first essential step to prevent soil loss and soil erosion.

b) As the island is mostly constituted with sandy soil, the washing out of the top soil with heavy rainfall or frequent flood inundation is very common. Thus, plantation of vegetations with deep roots should be helpful in minimizing the soil loss in runoff.

c) Concrete blocks and pillars must be laid out near the bank to control the bank erosion as well to hold the loose soil from slipping away.

Thus, there are some preventive measures that can be looked upon for minimizing the impact on soil loss and soil erosion.

References

1. Bhaskar, B. P., & Sarkar, D. (2013). Capability and quality assessment of rice growing hydric soils in Majuli river Island, Assam, India. *Journal of Agriculture and Environment for International Development, 107* (1): 13 – 32
2. Dutta MK, Barman S, Aggarwal SP. 2010. A study of erosion-deposition processes around Majuli Island, Assam. *Earth Science India.* 3(4):206–216
3. Erenstein, O. C. (1999). The economics of soil conservation in developing countries: the case of crop residue mulching. *Wageningen University and Research*.
4. Gashaw, T., Tulu, T., & Argaw, M. (2017). Erosion risk assessment for prioritization of conservation measures in Geleda watershed, Blue Nile basin, Ethiopia. Environmental. *Systems Research, 6*, 1–14.
5. Gelagay, H. S., & Minale, A. S. (2016). *International Soil and Water Conservation Research*.
6. Jain, S. K., Kumar, S., & Varghese, J. (2001). Estimation of soil erosion for a Himalayan watershed using GIS technique. *Water Resource Management*, 15, 41–54.

7. Karamage, F., Zhang, C., Ndayisaba, F., Shao, H., Kayiranga, A., Fang, X., Nahayo, L., Muhire Nyesheja, E., & Tian, G. (2016). Extent of cropland and related soil erosion risk in Rwanda. *Sustainability, 8*, 609.
8. Lee, E., Ahn, S., & Im, S. (2017). Estimation of soil erosion rate in the Democratic People's Republic of Korea using the RUSLE model. *Forest Science and Technology, 13*(3), 100– 108.
9. Pathan, S. A., & Sil, B. S. (2022). Prioritization of soil erosion prone areas in upper Brahmaputra River Basin up to Majuli River Island. *Geocarto International, 37(*7), 1999-2017.
10. R. Lal. (1998). Soil erosion impact on agronomic productivity and environment quality. *Critical Reviews in Plant Sciences*, 17, 319-464.
11. Rasool, S. N., Gaikwad, S. W., & Saptarshi, P. G. (2014). Soil erosion assessment in Sallar Wullarhama watershed in the Lidder catchment of Jammu and Kashmir using, USLE, GIS and remote sensing. International Journal of *Advanced Engineering Research and Studies*, 3(2), 46–54.
12. Renard. K.G., Foster. G.R., Weesies. G.A., McCool. D.K. and Yoder. D.C. Predicting Soil Erosion by Water: A Guide to Conservation Planning with the Revised Soil Loss Equation (RUSLE). *U.S. Dept. of Agriculture, Agricultural Research Service*.
13. Sarma D. 2013. Rural risk assessment due to flooding and riverbank erosion in Majuli, Assam, India. *University of Twente Faculty of Geo-Information and Earth Observation* (ITC).
14. Singh, Amarinder & Singh, Bikramjit & Singh, Sarabjit & Singh, Rajanbir. (2022). Assessment of Rainfall Erosivity Index Using Lombardi Method for Amritsar, Punjab. *Ecology, Environment and Conservation*. 28. DOI:10.53550/EEC.2022.v28i06s.063
15. Tiruneh, G., & Ayalew, M. (2015). Soil loss estimation using geographic information system in enfraz watershed for soil conservation planning in highlands of Ethiopia. *International Journal of Agricultural Research, Innovation and Technology (IJARIT), 5*(2355-2020-1587), 21-30.
16. Wischmeier WH, Smith DD. 1978. Predicting rainfall erosion losses: a guide to conservation planning (No. 537). *Department of Agriculture, Science and Education Administration*, USDA-ARS, USA.

Identification of Flood-Vulnerable Village Clusters in the Southwestern Fringe of Guwahati City Using GIS-Based Spatial Autocorrelation Technique and Real-Time SAR Imagery

Rakesh Kumar Sarmah[1], Santanu Sarma[2]

Abstract

This study employs a multifaceted approach, combining remote sensing, GIS-based spatial autocorrelation techniques, and Sentinel-1 Synthetic Aperture Radar (SAR) imagery to comprehensively evaluate flood-affected areas in the southwestern fringe of Guwahati city. The unplanned urban expansion within the adjacent main city is causing issues like flooding and waterlogging, impacting the city's residents. Critical assessment is needed in the fringe areas to avoid similar consequences. The historical Annual Flood Inundation Layers available in the ISRO-BHUVAN portal are analyzed in a GIS environment village-wise considering 10 maps spanning from 2001 to 2010 to identify the vulnerable villages. The National Remote Sensing Centre (NRSC) generates these layers by integrating different flood waves in a calendar year considering the maximum flood extent. The village-wise inundation statistics are analyzed using the Global Moran's I to understand whether the inundation is clustered, dispersed, or random during this timeframe. The results show very high z-score and very low p-values indicating the presence of statistically significant spatial clusters. The historical data are further analyzed using Local Moran's I and Getis-Ord Gi statistics and vulnerable village clusters are delineated towards the study area's north, west, and central portion during these 10 years. The clusters show temporal dynamism and interconnection in major flood years. To assess these areas in real-time after a decade, the Sentinel-1 Synthetic Aperture Radar (SAR) imagery was used during a major flood event in 2020. The village-wise inundation is determined by extracting the flood signatures through the intensity*

[1] Research Scholar, Department of Geology, Cotton University, Panbazar, Guwahati – 781001, Assam, India
[2] Professor, Department of Geology, Cotton University, Panbazar, Guwahati – 781001, Assam, India

thresholding method. The method segregates land pixels against water pixels based on the backscattered value range of the Radar signal. The SAR data analysis is compared with the 2010 results due to their similar areal extent. The Area Under the Receiver Operating Characteristic (ROC) Curve is 70.38%, indicating that the analysis demonstrates good prediction accuracy. The study provides a roadmap for urban planning, disaster management, water resource management, and related disciplines.

Keywords: *Urban Expansion, Fringe Area Development, Flood-prone Villages, Spatial Autocorrelation, Synthetic Aperture Radar*

1. Introduction

It is crucial to address the issue of flooding in the peri-urban or fringe areas of developing cities, especially in the face of climate change. These areas are at risk due to the prevalence of informal settlements in low-lying agricultural lands, floodplains, protected areas such as Ramsar sites, and areas with high biodiversity (Winter & Karvonen, 2022). The dynamism in these areas with a gradual transition of green spaces into impervious surfaces with the blocking of natural waterways makes them more vulnerable to flood disasters in comparison to rural areas (Wang et al., 2023). Due to lower property and service tax compared to the city, peri-urban areas attract industries, commercial establishments, etc. amplifying the urbanization process (Nallathiga, 2015). Urbanization indicates economic growth but at the same time, it has negative impacts in terms of the physical environment such as loss of agricultural land, surface, and groundwater depletion, changes in geomorphic features, flooding, and landslides (Mahapatra et al., 2014). Proper planning is required to make these areas resilient and sustainable to ensure supporting quality standards of life as they are carriers of urban expansion and act as a distribution centre of goods and energy between the city and external regions (Dong et al 2022; Mahanta and Borgohain; 2022).

Guwahati, the gateway to northeast India, is continuously expanding in terms of population and urbanization. The city's growth is due to the development of infrastructure to support the ever-increasing population. However, this growth has caused encroachment in hills, wetlands, and government lands. Flash floods and waterlogging occur annually in Guwahati city during monsoon season due to

overflowing feeder drains (ASDMA, 2014). Urban flooding causes socio-economic impacts such as education, health, transportation, drinking water, sanitation, and livelihood insecurity (Kashyap & Mahanta, 2020). Anthropogenic activities magnify the inundation (Rashiq & Prakash, 2023), and poor urban planning makes the city vulnerable to natural disasters. Spatial planning with proper land use allocation is crucial in minimizing exposure to natural hazards (Abdrabo et al., 2021). Remote sensing and GIS technology are extensively used in site suitability analysis for urban expansion (Saleh & Rawashdeh, 2007, Huang et al., 2010, Sun et al., 2020, Sahin et al., 2024). Flood vulnerability assessment regarding people and places is essential for emergency management (Chen et al 2021). The city's Southwest direction is a potential site for a sustainable satellite township. The study aims to identify spatially significant clusters of flood-vulnerable villages, by adopting spatial autocorrelation techniques by analyzing past data and real-time SAR imagery in a GIS environment. The concept of spatial autocorrelation is based on Waldo Tobler's first law of geography, which emphasizes that "near things are more related than distant things" (Manning et al., 2023). This spatial autocorrelation technique is commonly used in various fields to understand spatial clustering of variables, for example in health sciences (Shariati et al., 2020, Vilinová & Petrikovičová., 2023, Yin et al., 2024), traffic analysis (Le et al., 2022), rainfall pattern analysis (Rousta et al., 2017), pollution concentration (Liu et al., 2013), waste management (Tsui et al., 2022), and natural hazards (Lin et al., 2017). To confirm these vulnerable villages in real-time, Sentinel 1 Synthetic Aperture Radar (SAR) imagery of a particular flood date, after a decade is used. Having up-to-date information on flooding is important for emergency response and reducing the risk of flood damage. SAR is particularly useful as it can penetrate through clouds and provide day and night images making it an effective remote sensing method for mapping real-time flood events (Garg et al. 2024). The village-wise real-time inundation statistics obtained from SAR are compared with the vulnerable villages demarcated for multiple major flood years to ensure the clustered pattern.

1.1 Study Area:

The study area encompasses the administrative blocks of Rani and Chayani Barduar in Kamrup – Metro and Rural districts of Assam, spanning a total of 423.03 km^2 with a total population of 184411 in 129 villages. The southwestern region of the city is

primarily utilized for agriculture, while the southern area is a narrow valley encircled by hills and the picturesque Chandubi Lake. The Guwahati Metropolitan Development Authority (GMDA) Master Plan aims to build a new town featuring an Information Technology hub and Special Economic Zone. The study area is bordered by the Brahmaputra River in the north, the Kulshi River in the west, Meghalaya plateau hills in the south and southeast, and Guwahati city in the northeast (Figure 1). The major geological formations within the study area are alluviums of the Brahmaputra River and its tributaries and Precambrian rocks of the Meghalaya plateau. The distinguishable geomorphic features within the study area are floodplains, alluvial plains, piedmont zones, and denudational hills. The Kulsi river system is also present in the area, with all streams flowing towards the north to merge with the Brahmaputra River. The region is prone to annual flooding due to heavy rainfall. As per the Indian Meteorological Department report (IMD), the average annual rainfall in the study area betwee 2018-2022 is 1583.07 mm. The region experiences a tropical monsoon climate with rainfall from June to September. The average temperature varies from 9°C in winter to 35°C in summer.

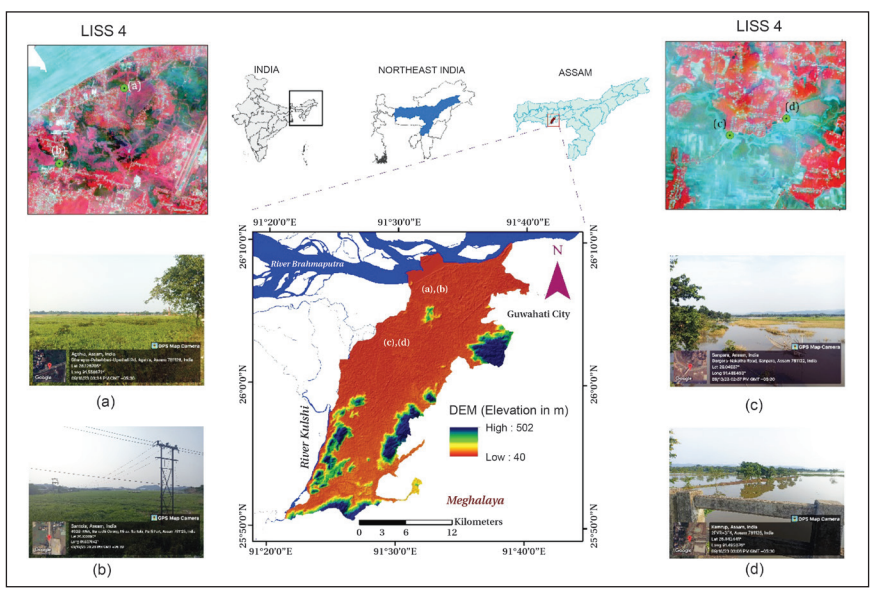


Figure 1: Study area map with recent field photographs of flood-vulnerable sites

2. Materials and Methods:

2.1 Flood History

The Decision Support Centre (DSC) under the National Remote Sensing Centre (NRSC) in Hyderabad, India is responsible for incorporating space technology into the Disaster Management Support (DMS) program by the Indian Space Research Organization (ISRO). The DSC has released an annual flood inundation atlas (1998-2010) for Assam and Bihar using optical and microwave remote sensing techniques to analyze different flood waves throughout the year with an accuracy of up to a scale of 1:250000. This archive is freely available in ISRO-BHUVAN portal. Hailin et al. (2009) have used the same scale to assess flood risk in Hubei Province. Out of 13 available maps, the inundation history of the study area has been analyzed for 10 years (2001-2010). The available maps are georeferenced using Arc GIS 10.8 in WGS 84 UTM 46 N projections, the raster maps are converted to vector polygons, and year-wise flood inundation is calculated. The village layer of the study area is collected from Assam Remote Sensing Application Centre, Govt of Assam, India, and the population data are collected from the District Census Handbook (DCHB) published by Census of India (2011). The village layer is superimposed in the GIS environment, and the village-wise inundation area is calculated for the specific period.

2.2 Flood Clusters Using a Spatial Autocorrelation Technique

Spatial autocorrelation is a type of correlation that measures the degree of alignment between two attributes based on their relative magnitudes (Griffith & Chun, 2018) or their similar patterns within a geographic area (Lo et al., 2022). Positive spatial autocorrelation occurs when closer geographic locations have similar attributes (Griffith & Lea, 2005), whereas negative spatial autocorrelation is observed when distant values are more similar than nearby values, contradicting Tobler's law (Fischer & Wang, 2011).

Spatial correlation can be global or local, with global Moran's I being a common measure for evaluating whether the pattern expressed is clustered, dispersed, or random for a given set of features and associated attributes in a study area (Fasona et al., 2011, Prasannakumar et al., 2011). The village-wise inundation statistics in terms

of percentage of inundation are considered as the numerical field used in assessing spatial autocorrelation. A small village with a large inundation area is considered more vulnerable than a large village with a relatively small inundation.

The global Moran's I can be calculated for n observations on a variable x at locations (i,j)

$$I = \frac{n}{S_0} \frac{\sum_i^n \sum_j^n w_{ij} \quad (x_i - \bar{x}) \quad \left(x_j - \bar{x}\right)}{\sum_i^n (x_i - \bar{x})^2}$$

Where,

$\bar{x}$ = the mean of the variablex, x_i = the value of the variable x at location i, x_j = the value of the variable x at location j, w_{ij} = the elements of the weight matrix, n = number of observations, S_0 = Sum of the elements of the weight matrix = $\sum_i^n \sum_j^n w_{ij}$

The Global Moran's I value ranges from -1 to +1. A value of '-1' indicates perfect clustering of dissimilar values or perfect dispersion. A value of 0 indicates no autocorrelation or perfect randomness. A value of +1 indicates perfect clustering of similar values. The Global Moran's I use inferential statistics, meaning the results of the analysis are interpreted within the context of its null hypothesis, considering a random distribution of the attributes under scrutiny. A significant p-value, coupled with a positive Moran's I, suggests that the high and/or low values in the dataset are more spatially clustered than would be expected under such a random distribution, leading to the rejection of the null hypothesis. Conversely, a significant negative Moran's I indicate that the spatial distribution of high and low values is more dispersed than expected (Raza et al., 2020). For spatial relationships, the 'contiguity edges only' option in ArcGIS is used where only neighboring polygon features that share a boundary, or overlap will influence the computations of the target polygon.

Global Moran's I measures the clustering strength of a map as a whole, whereas local Moran's I identifies the location of clusters on the map. The formula for local Moran's I is similar to its global counterpart, with the only difference being that it only iterates through the neighbors of one polygon instead of all pairs of polygons (Tsui et al. 2022).

$$I_i = \frac{x_i - \bar{x}}{S_i^2} \sum_{j=1}^{n} w_{ij} (x_j - \bar{x})$$

Where, $S_i^2 = \frac{\sum_{j=1}^{n}(x_j - \bar{x})^2}{n-1} - \bar{x}^2$

$$E(I) = \frac{-1}{n-1}$$

Moran's I value greater than E(I) implies positive autocorrelation and smaller implies negative spatial autocorrelation. The clusters can be either high-high (meaning high values in a high-value neighborhood) or low-low (meaning low values in a low-value neighborhood), a high-low (meaning a high value in a low-value neighborhood), or a low-high (meaning a low value in a high-value neighborhood) outlier (Fu et al., 2014).

Another reliable geostatistical technique for mapping clusters and determining statistically significant hot or cold spots is the Gi* statistic, also known as the Getis-Ord Gi. It assesses the Gi* for each feature in a dataset and identifies where features with high or low z-scores and p-values are spatially clustered. A positive z-score indicates a higher clustering of high values, while a negative z-score indicates a higher clustering of low values (Hazaymeh et al., 2022).

$$Gi^* = \frac{\sum_{j=1}^{n} w_{i,j} x_j - \bar{X} \sum_{j=1}^{n} w_{i,j}}{s\sqrt{\frac{n \sum_{j=1}^{n} w_{i,j}^2 - (\sum_{j=1}^{n} w_{i,j})^2}{n-1}}}$$

$$\bar{X} = \frac{\sum_{j=1}^{n} x_j}{n}$$

$$S = \sqrt{\frac{\sum_{j=1}^{n} x_j^2}{n} - \bar{X}^2}$$

Where x_j is the attribute value for the feature j, $w_{i,j}$ is the weight between features *i* and *j* and n is equal to the total number of features. The*Gi** statistics is the z score.

The vulnerable village clusters are finally delineated year-wise integrating Asselin's Local Moran's I and the Getis-Ord Gi statistics.

2.3 Real-time validation using SAR after 10 years on a significant flood date

To identify the real-time extent of flood inundation within the study area a decade later, a significant flood date, July 16, 2020, was selected based on heavy rainfall in Kamrup Rural and Metro districts of Assam and the adjacent RiBhoi district of Meghalaya, as per INSAT-3D images provided by the India Meteorological Department (IMD). The state's leading newspaper, The Assam Tribune, published a report on the same date detailing the severity of the flood conditions in Kamrup Rural and Kamrup Metro, where the study area is an integral part (Figure 6).

2.3.1 SAR Data

The Sentinel 1 mission involves two operational satellites called Sentinel 1A and Sentinel 1B that were launched by the European Space Agency in April 2014 and April 2016, respectively. These satellites carry a C Band Synthetic Aperture Radar (C-SAR) payload and follow a sun-synchronous orbit with a repeat cycle of 12 days (Raspini et al., 2018; Potin et al., 2016). The data they collect is available for free on the Copernicus Open Access Hub platform of the European Space Agency (ESA) and is used extensively in critical decision-making during emergencies such as natural disasters or humanitarian crises (Skoda & Adam, 2020). These RADAR datasets can be analyzed using the Sentinel Application Platform (SNAP), an open-source architecture developed by the European Space Agency. To download the necessary product, users only need to create a login ID. To determine the exact extent of flooding on a specific date, it is crucial to have data on permanent bodies of water and their extent before the flood season. Therefore, two images depicting pre-flood and during-flood conditions are required. The pre-flood image is a Sentinel 1A Ground Range Detected (GRD) product from February 15th, 2020, while the during-flood image is a Sentinel 1B GRD product captured on July 16th, 2020.

Table 1: Details of Sentinel 1 products considered for the study

Satellite	Product Name	Date and Time	Product Type	Acquisition Mode	Spatial Resolution
Sentinel 1A	S1A_IW_GRDH_1SDV_20200215T115719_031263_031263_03988A_A076	15 Feb 2020, 14:31:22	Level-1 GRD	IW	10×10 m
Sentinel 1B	S1B_IW_GRDH_1SDV_20200716T234628_20200716T234657_022503_02AB64_13F1	16 Jul 2020, 17:40:35	Level-1 GRD	IW	10×10 m

2.3.2 Processing of the data

To process the downloaded data, SNAP open-source software is used. The image needs to be pre-processed to remove any distortion and enhance its quality. The pre-processing involves several steps that are performed sequentially. The raw data, which comes in a zip format from Copernicus Open Access Hub, is directly processed using the SNAP software step by step. To ensure the accuracy of the orbital data, improve geocoding, and the subsequent processing steps, the orbit file is applied (Hong et al., 2017). To convert the pixel intensity or radar reflectivity (DN number) to radar cross-section (RCS), or scattering cross-section, the radiometric calibration technique is used (Schmidt et al., 2020; WeiB, 2018). The RCS is the measure of the reflective strength of the radar target, and it is indicated by the symbol 'sigma'. The value of 'sigma' depends upon the shape, dielectric properties, orientation, roughness, etc. of the target, which also varies for different observation angles, frequencies, and polarizations. Since the radar return signifies the proportion of energy scattered by the distributed area corresponding to the size of the image pixel, a normalized measure is required to relate the inferred target area, derived from the scattering cross-section, to the actual geometrical area on the ground surface. This unit-less normalized measure is defined as 'backscatter coefficient', 'differential radar cross-section,' or 'normalized radar cross-section,' denoted by 'sigma nought' (Woodhouse 2006; Sentinel user guide). Due to the low backscattering

response, flooded areas appear dark, and strong backscattering from rough soil surfaces and vegetation causes land surfaces to appear bright (Manjusree et al., 2012). 'Speckles' are random, high-frequency noises present in SAR images, causing a granular, salt, and peppery pattern with degradation of image quality, as well as loss of information (Choi & Jeong 2019; White et al., 2015). To enhance the image quality, the 'speckle filtering' technique is applied. Different speckle filters are available in SNAP, such as Gamma Map, Lee, Refined Lee, and Lee Sigma, with different window sizes. Comparing different filters, the Lee (5*5) window size is found to be suitable for the study. The side-looking geometry of RADAR and topographic relief causes several geometric distortions, such as foreshortening, layover, and shadow (Chen et al., 2018; Esmaeilzade et al., 2015). The geometric distortion caused by topography is corrected using the Range Doppler terrain correction, which uses a digital elevation model to rectify the location of each pixel. The process utilizes available orbital information in the metadata, radar timing annotations, and slant-to-ground range conversion parameters with the reference DEM (Filipponi, 2019). For this study, the SRTM DEM with 3 arcsec and bilinear interpolation resampling technique has been used for geometrical correction. The final product is converted to decibel (dB) units using logarithmic transformation. Conversion of linear amplitude to decibels (dB) improves the image display by compressing a wide range of values and reducing the impact of multiplicative noise (Filipponi, 2019).

3. Results

3.1 Historical Flood Vulnerable Villages (2001-10)

Based on the area of inundation, the villages are classified into five categories: Very High (above 75%), High (75-50%), Moderate (50-25%), Low (25-10%), and Very Low (below 10%). The year-wise frequency distribution for different categories is determined for 10 years. Figure 2 shows the significant distribution of flood events in all five categories. During peak flooding years, such as 2002 and 2004, six to eight villages fall under the 'high' category, while twelve to sixteen villages fall under the 'moderate' category, indicating the severity of flood hazards in the study area.

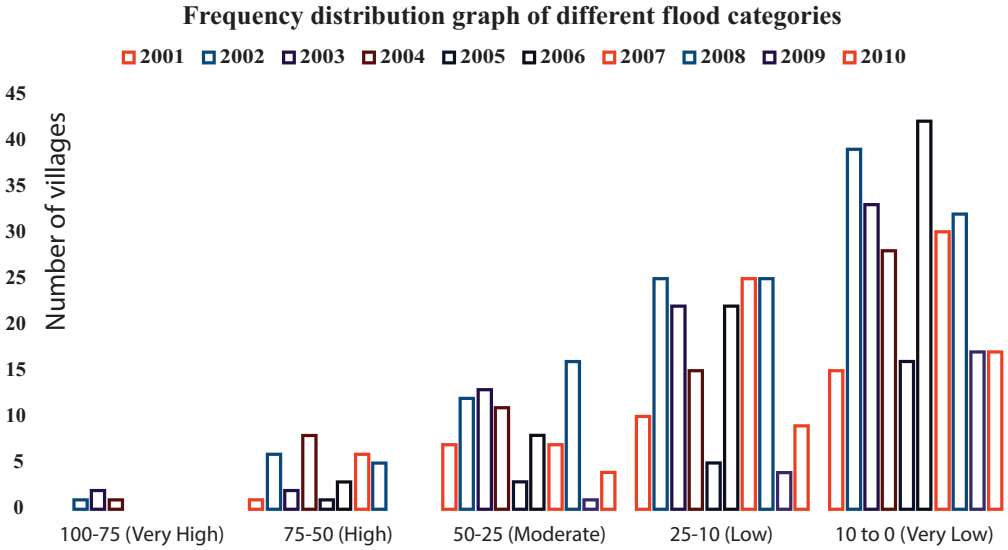


Figure 2: Frequency distribution graph of different flood categories

Out of 10 years of analysis, the highest flood inundation is observed for the year 2003 followed by 2007, 2002, and 2004. The area undergoing inundation is 67.23, 64.33, 61.35, and 58.49 km2 respectively. The lowest inundation observed within this timeframe was in 2009 with only 4.75 km2 area undergoing inundation. Table 2 depicts the number of villages and populations affected during each flood event. The figures show that more than 1 lakh people are vulnerable during major flood years.

Table 2: The vulnerability of villages and population during the study period, and z-score, p-values of the spatial autocorrelation analysis.

Year	Total Area under flood (km²)	Total Village	Total population	Global Moran's I			Getis–Ord Gi*			Type of distribution
				Moran's I	z-score	p-value	General G	z-score	p-value	
2001	15.94	26	69688	0.31	8.23	0	0.019599	7.83	0	Clustered
2002	61.35	97	166139	0.34	8.87	0	0.010899	8.88	0	Clustered
2003	67.23	87	158527	0.32	8.34	0	0.010530	8.81	0	Clustered
2005	10.16	29	78721	0.11	3.49	0.00049	0.015892	3.36	0.000793	Clustered

Year	Total Area under flood (km²)	Total Village	Total population	Global Moran's I			Getis–Ord Gi*			Type of distribution
				Moran's I	z-score	p-value	General G	z-score	p-value	
2008	33.07	76	135240	0.24	6.24	0	0.011231	7.24	0	Clustered
2009	4.75	25	70693	0.11	3.26	0.00109	0.014244	3.04	0	Clustered
2010	10.96	33	64261	0.16	4.55	0.000005	0.013685	3.81	0	Clustered
2020 SAR	13.39	50	83359	0.16	4.71	0.000002	0.010994	4.62	0.000004	Clustered

3.2 Spatial Autocorrelation Results

Based on the positive z-score and significant p-value of Global Moran's I, it seems likely that the null hypothesis can be rejected. This means that the distribution of high and/or low values in the dataset is more spatially clustered than expected by chance, with less than a 1% likelihood that the pattern is random. To identify flood vulnerable clusters, we need to examine the local level of clustering and identify villages where the percentage of inundation is particularly high. Figure 3 displays the results of Anselin's Local Moran'I statistics during major flood years. High-High clusters are concentrated in the north, west, and central parts of the study area, while low-low clusters are mainly found in the east and south. Spatial outliers, such as low-high clusters, are prominent near-high clusters, as these are locations with low values and high-value neighbors.

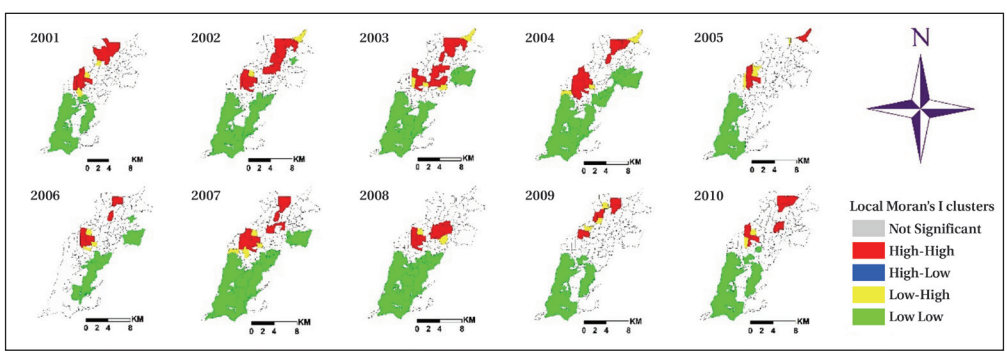


Figure 3: Local Moran's I cluster analysis of the study area between 2001 and 2010

According to the analysis using the Getis-Ord Gi* statistics, there are both flood hot spots and cold spots. These spots have confidence levels of 90%, 95%, and 99%. The hot spots indicate an intense clustering of high positive z values, while the cold spots show an intense clustering of low negative z values (Figure 4). These spots are located spatially in accordance with the clusters identified by the local Moran's I.

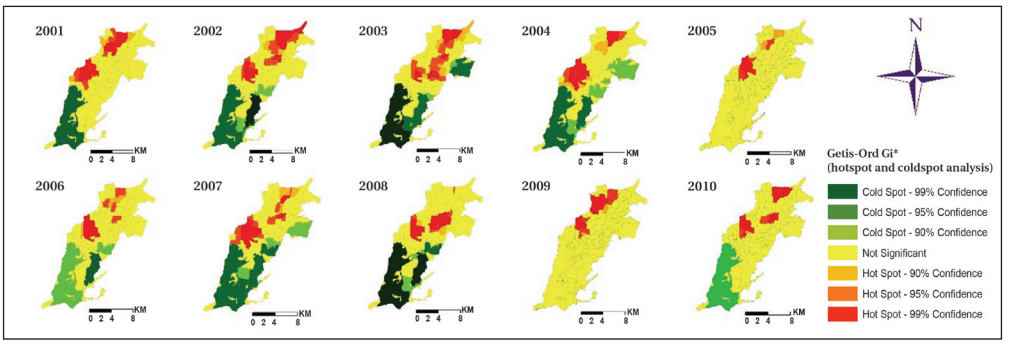


Figure 4: Getis-Ord Gi* hot spot and cold spot analysis of the study area between 2001 and 2010

The flood-vulnerable clusters are finally delineated by integrating the Local Moran's I High-High clusters and hotspots from Getis-Ord Gi* analysis (Figure 5)

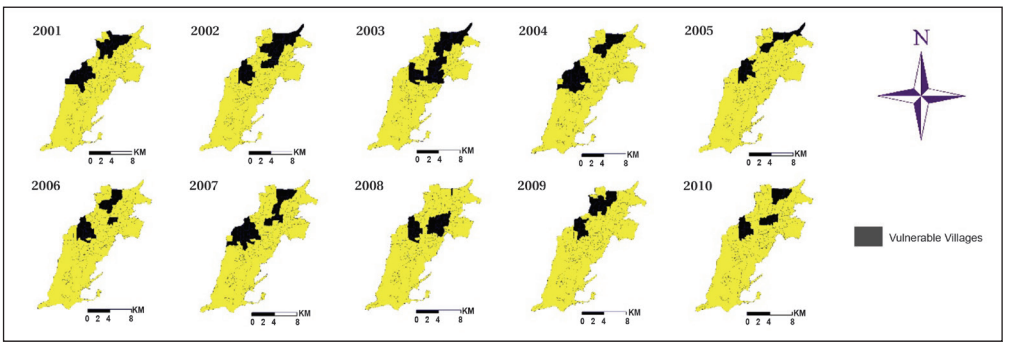


Figure 5: Vulnerable village clusters during 2001 and 2010

3.3 Results of SAR data analysis

The pre-flood image analysis provides information about permanent water bodies so that there won't be any overestimation of flooded areas during the flood. Permanent

water bodies contain smooth open surfaces acting as specular reflectors, scattering the radar energy away from the sensor. Thus relatively dark pixels appear in the image in comparison to non-water areas (Martinis and Rieke, 2015). The pre-flood imagery of 15th February 2020 is processed following the steps as mentioned earlier and the final terrain corrected product in dB for both VV and VH polarization is obtained. VH polarization generates correctly defined surfaces and is found more suitable for demarcating flooded areas in comparison to VV polarization (Conde & Munoz, 2019). The most widely accepted technique in differentiating land pixels vs. water is the intensity thresholding method (López-Caloca et al., 2018). The backscattered value range can provide significant discrimination between water and non-water regions. Careful observation of the histogram provides a threshold value to separate water bodies from other features (Conde and Munoz 2019; Zhang et al. 2020). By using a suitable band maths expression (Sigma0_VH_db < -21.22), the water pixels can be extracted. The permanent water bodies within the study area are mainly stretches of river Brahmaputra, river Kulshi, Deepor Beel Lake, Chandubi Lake, and some ponds. The total area of permanent water bodies is found to be 14.03 km^2. Flood extent delineation is done using Sentinel 1B GRD product captured on 16th July 2020. The image is pre-processed to the final terrain-corrected dB product of both VV and VH polarization. The histogram has been analyzed and a threshold backscatter value (dB = -24.26) has been identified to separate water and non-water pixels from the image. The total area undergoing inundation is calculated in the GIS environment and found 27.42 km^2. This also includes the area of permanent water bodies, misclassified pixels, and topographic shadows. Misclassified pixels mainly occur in and around airport premises, flat surfaces such as airport runways, parking, and new construction sites. These areas are showing low backscattering which is not related to flooding. In many works of literature, misclassified pixels in airport runways and other flat-constructed surfaces are mentioned and validated using suitable techniques. Topographic shadow also shows dark tone not necessarily water pixels and are mainly found in forest areas at higher elevation. Validation is done using LISS-4 imagery and Google Earth. Nearly 0.107 km^2 areas are found under misclassified pixels due to airport runways and other flat construction sites and 0.023 km^2 due to topographic shadow. Excluding these areas, the total inundation on 16th July 2020 was found to be 13.39 km^2.

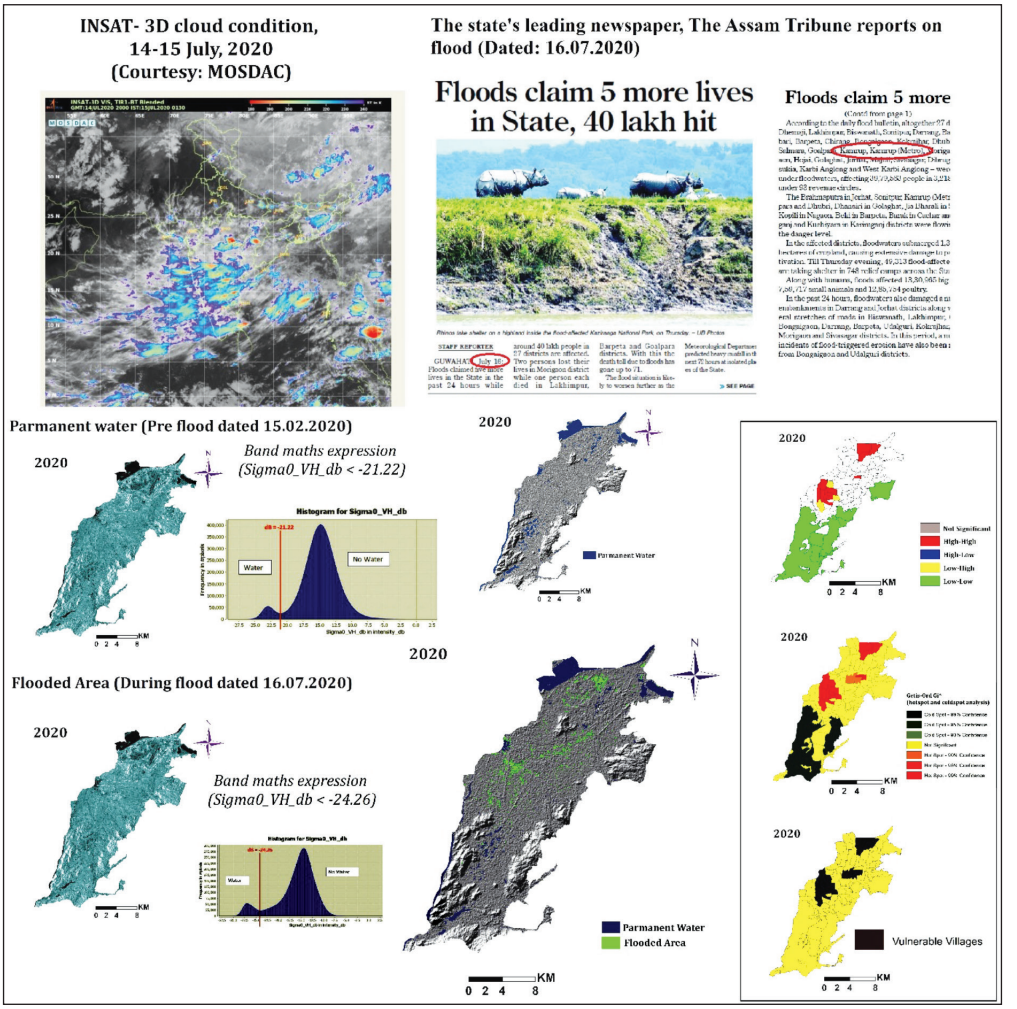


Figure 6: Sentinel-1 SAR-derived flood area estimation during a major flood date (evident from the cloud condition by INSAT-3D and news report) using histogram-based intensity thresholding method, cluster analysis using Local Moran's I and Getis Ord G* statistics

3.4 Validation

The Receiver Operating Characteristic (ROC) curve is a proven technique to ensure the classifier's efficiency and sensitivity of the method (Avand et al. 2021). Due to their

similar area coverage, the village-wise inundation statistics obtained from SAR data analysis are compared with the 2001 results. In Figure 7, the Area under the ROC curve (AUC) shows 70.38% indicating good predictive ability (Tao et al. 2021).

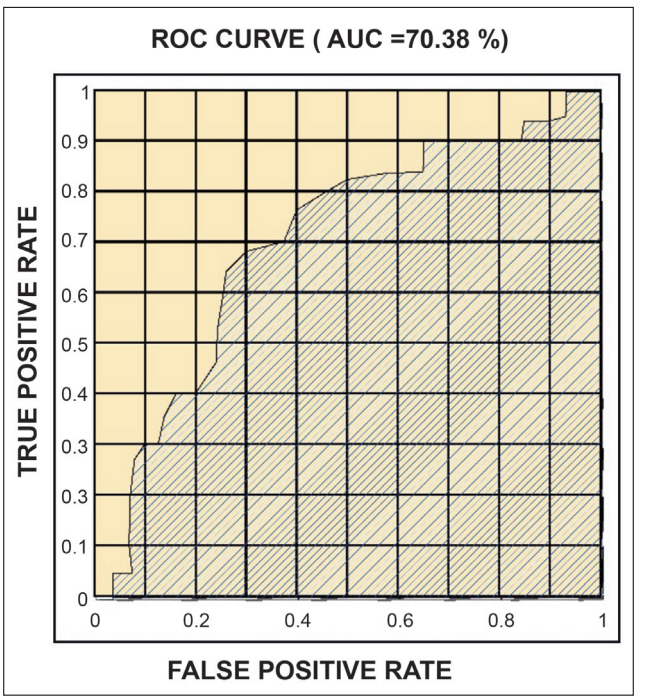


Figure 7: ROC analysis between 2001 historical data and 2020 SAR data

4. Discussion

The Local Moran's I and Getis-Ord Gi* analysis results reveal prominent flood clusters in the study area's north, west, and central parts. A similar trend of clustering is also evident from the SAR analysis. Figure 5 shows the dynamics of these vulnerable village clusters during the study period. The north and west clusters are seen throughout the analysis period and there is a chance of flood accumulation initiation. The central cluster is prominent in 2003, 2008 and 2010. During major flood events, the clusters tend to get interconnected. Though the vulnerable villages show interconnectivity, for the administrative and socio-economic point of view, the villages are classified

into three major clusters: the clusters in the west consisting of 19 villages with an area coverage of 49.06 km^2 with total population of 26578; the clusters in the north consisting of 18 villages covering 61.03 km^2 with a total population of 74442; and the clusters in the central portion consisting of 17 villages with 37.29 km^2 coverage with a total population of 16915.

Figure 8 shows the location of the clusters considering land use land cover, existing stream network, and a digital elevation model in the background. The analysis of the cluster in the west shows a complex network of interconnecting streams and wetlands making this area flood-prone. The Kulshi and Batha Rivers from the south, and 'Rani Nadi' from the east interconnect here. In Figure 1 (c) and (d), a recent field photograph within this cluster, taken in October 2023, shows the receding floodwaters, providing evidence of the devastating floods during the monsoon season. The prominent hill ranges visible in the photograph are part of the elevated Meghalaya plateau upstream of this catchment, known for receiving the world's heaviest rainfall.

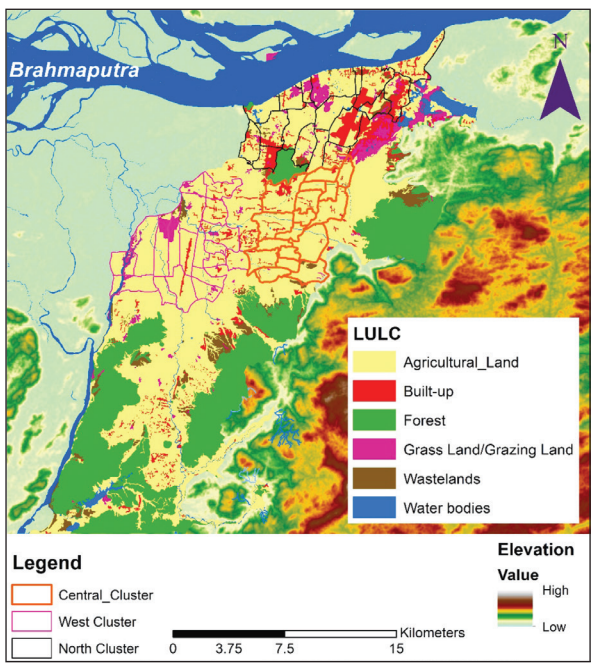


Figure 8: Cluster location considering land use land cover, stream network, and DEM

Similar flood concentrations are observed in the northern part of the study area. This region is gradually urbanizing with the establishment of industrial facilities and apartment complexes near the Guwahati Lokpriya Gopinath Bordoloi International Airport. Field photographs in Figure 1 (a) and (b) show the presence of water hyacinth and wetland-like features, which get inundated during the rainy seasons. These natural features are crucial for floodwater mitigation. It is essential to regulate concrete construction in these eco-sensitive areas to ensure future sustainability. The cluster in the central portion of the study area is mainly agricultural lands. The location of the study area is a narrow valley adjacent to the Shillong plateau and River Brahmaputra with a complex fluvial-morphological scenario, based on the intensity of rainfall in the upper catchments of River Brahmaputra as well as in the Meghalaya, the flood situations vary, and the dynamism may be witnessed in vulnerable clusters.

5. Conclusion

The primary objective of this study is to identify areas in the southwest vicinity of Guwahati city that are susceptible to flooding and natural waterlogging, with a focus on future urbanization. Identifying flood-vulnerable clusters through historical data and real-time imagery is crucial for urban planning. The fringe or peri-urban landscape is vulnerable in terms of rapid urbanization due to the rural-urban policy dichotomy. Towards west and north, the clusters are seen in interconnected networks of natural drains, wetlands, and swampy-marshy features adjoining the Brahmaputra floodplain, these features are important for flood mitigation, acting as storage for major flood events, filtering sediments, and recharging aquifers. A proper hydro-ecological assessment is needed before any urban intervention. The landscape of Guwahati city was like its fringe areas before urbanization with an abundance of wetlands, swamps, and marshes. The unplanned urbanization has led to the encroachment in wetlands, blockage of feeder drains intensifying waterlogging, and flash floods. The clusters identified in the central portion of the area are mainly vast agricultural lands. Due to the proximity of the city and relatively cheap land prices, these parcels are easy targets for investors for future ventures. The government should keep a critical eye on the infrastructure projects and strong policy decisions to ensure future sustainability to avoid water-related hazards. The study will provide a holistic overview of integrating

remote sensing and GIS addressing flood vulnerability mapping in the context of urban developments.

6. Acknowledgement

The authors would like to thank different government and non-government organizations for providing valuable data.

References

1. Abdrabo, K. I., Kantosh, S. A., Saber, M., Sumi, T., Elleithy, D., Habiba, O.M., & Alboshy, B. (2022). The role of urban planning and landscape tools concerning flash flood risk reduction within arid and semiarid regions. In Sumi, T., Kantoush, S.A., Saber, M. (Eds.), *Natural Disaster Science and Mitigation Engineering:* DPRI Reports. Wadi Flash Floods Challenges and Advanced Approaches for Disaster Risk Reduction (pp. 283-316). *Springer: Singapore*.
2. Annual Flood Inundation- Assam and Bihar. NRSC/ISRO. (2012). Retrieved from https://bhuvan-app1.nrsc.gov.in/2dresources/documents/al.pdf
3. Assam State Disaster Management Authority. (2014). Review of Studies on urban floods in Guwahati from flood knowledge to urban action. Retrieved from https://asdma.assam.gov.in/sites/default/files/Guwahati%20floods.pdf
4. Avand M., Moradi H.R., Lasboyee M.R.: Spatial Prediction of Future Flood Risk: An Approach to the Effects of Climate Change. *Geosciences*, vol. 11, 2021, 25. https://doi.org/10.3390/geosciences11010025
5. Bharali, K.K., & Sarma, S. (2012). Bank erosion of the Brahmaputra River in the downstream of Palasbari and Soalkuchi, Kamrup district, Assam. *Journal of Indian Geomorphology*, 1(2012):103-106.
6. Carreno Conde, F., De Mata Munoz, M. (2019). Flood monitoring based on the study of Sentinel-1 SAR images: the Ebro River case study. *Water*, 11(12) :2454.
7. Chen, X., Sun, Q., & Hu, J. (2018). Generation of Complete SAR Geometric Distortion Maps Based on DEM and Neighbor Gradient Algorithm. *Applied Sciences*, 8(11):2206.
8. Chen, Y., Ye, Z., Liu, H., Chen, R., Liu, Z., & Liu, H. (2021). A GIS-based approach for flood risk zoning by combining social vulnerability and flood susceptibility: a case study of Nanjing, China. *International Journal of Environmental Research and Public Health*, 18(21): 11597.
9. Choi, H., & Jeong, J. (2019). Speckle noise reduction technique for SAR images using statistical characteristics of speckle noise and discrete wavelet transform. *Remote Sensing*, 11(10):1184.
10. District Census Handbook published by Census of India. Retrieved from https://censusindia.gov.in/census.website/data/handbooks
11. Dong, Q., Qu, S., Qin, J., Yi, D., Liu, Y., & Zhang J. (2022). A method to identify urban fringe area based on the industry density of POI. *International Journal of Geo-Information*, 11(2):128.
12. Esmaeilzade, M., Amini, J., & Zakeri, S. (2015). Georeferencing on synthetic aperture RADAR imagery. *The International Archives of the Photogrammetry, Remote Sensing and Spatial Information Sciences*, XL-1/W5:179-184.
13. Fasona, M., Omojola, A., Soneye, A. (2011). A study of land degradation pattern in the Mahin mud-beach coast of southwest Nigeria with spatial-statistical modelling geostatistics. *Journal of Geography and Geology*, 3(1): 141-159.
14. Fischer, M.M., & Wang, J. (2011). Spatial data analysis: models, methods and techniques. *Springer*, Heidelberg.
15. Filipponi, F. (2019). Sentinel-1 GRD preprocessing workflow. *Proceedings*, 18(1):11.
16. Fu, W.J., Jiang, P.K., Zhou, G.M., & Zhao, K.L. (2014). Using Moran's I and GIS to study the spatial pattern of forest litter carbon density in a subtropical region of southeastern China. *Biogeosciences*, 11(8), 2401–2409.
17. Garg, S., Dasgupta, A., Motagh, M., Martinis, S., & Selvakumaran, S. (2024). Unlocking the full potential of Sentinel-1 for flood detection in arid regions. *Remote Sensing of Environment*, 315: 114417.
18. Griffith, D.A., & Lea A.C. (2005). Locational Decision Making. In K. Kempf-Leonard (Ed.), *Encyclopedia of Social Measurement* (pp. 559-575). University of California: Elsevier Science.
19. Griffith, R.B., & Chun, Y. (2018). GIS and Spatial Statistics/Econometrics: An Overview. In B. Huang (Ed.), *Comprehensive Geographic Information Systems* (pp. 1-26). *Elsevier*, Netherlands.
20. Hailin, Z., Yi, J., Xuesong, Z., Gaoliao, J., Yi, Y., & Baoyin, H. 2009. GIS-Based Risk Assessment for Regional Flood Disaster. *International Conference on Environmental Science and Information Application Technology*, 2009: 564-567.

21. Hazaymeh, K., Almagbile, A., & Alomari, A.H. (2022). Spatiotemporal analysis of traffic accidents hotspots based on geospatial techniques. *International Journal on Geo-information*, 11(4):260.
22. Hong, S., Choi, Y., Park, I., & Sohn H.G. (2017). Comparison of orbit-based and time-offset-based geometric correction models for SAR satellite imagery based on error simulation. *Sensors*, 17(1): 170.
23. Huang, B., Zhang, L., & Wu, B. (2010). Spatiotemporal analysis of rural–urban land conversion. *International Journal of Geographical Information Science*, 23(3): 379-398.
24. Kashyap, S., & Mahanta, R. (2021). Socioeconomic vulnerability to urban floods in Guwahati, northeast India: an indicator-based approach. In T. Chaiechi (Ed.), *Economic Effects of Natural Disasters* (pp. 457-475). United Kingdom: Academic Press.
25. Le, K. G., Liu, P., & Lin, L. (2020). Traffic accident hotspot identification by integrating kernel density estimation and spatial autocorrelation analysis: a case study. *International Journal of Crashworthiness*, 27(2): 543-553.
26. Lin, S.C., Ke, M.C., & Lo, C.M. (2017). Evolution of landslide hotspots in Taiwan. *Landslides*, 14:1491-1501.
27. Liu, G., Bi, Rutian., Wang, S., Li F., & Guo, G. (2013). The use of spatial autocorrelation analysis to identify PAHs pollution hotspots at an industrially contaminated site. *Environmental Monitoring and Assessment*, 185(11): 9549–9558.
28. Lo, D., Chau, K.W., Wong, S.K., McCord, M., & Haran, M. (2022). Factors affecting spatial autocorrelation in residential property prices. *Land*, 11(6):931.
29. López-Caloca, A.A., Tapia-Silva, F. O., Rivera, G. 2018. Sentinel-1 satellite data as a tool for monitoring inundation areas near urban areas in the Mexican tropical wet. In M. Glavan (Ed.), *Water Challenges of an Urbanizing World* (pp. 127-144). Croatia: Intech.
30. Mahanta, A., & Borgohain, P. (2022). Urban livability and contextual uncertainties: an assessment of livability through the lens of urban dwellers in Guwahati, India. *Journal of Infrastructure, Policy and Development*, 6(1): 1395.
31. Manjusree, P., Kumar, L.P., Bhatt, C.M., Rao, G.S., & Bhanumurthy, V. (2012). Optimization of threshold ranges for rapid flood inundation mapping by evaluating backscatter profiles of high incidence angle SAR images. *International Journal of Disaster Risk Science*, 3: 113-122.
32. Manning, N., Li Y., & Liu, J. 2023. Broader applicability of the metacoupling framework than Tobler's first law of geography for global sustainability: A systematic review. *Geography and Sustainability*, 4(1): 6-18.
33. Martinis, S., & Rieke, C. (2015). Backscatter analysis using multi-temporal and multi-frequency SAR data in the context of flood mapping at River Saale, Germany. *Remote Sensing*, 7(6):7732-7752.
34. Mahapatra, S.N., Pani, P., & Sharma, M. (2014). Rapid Urban Expansion and Its Implications on Geomorphology: A Remote Sensing and GIS Based Study, *Geography Journal*, 2014: 361459.
35. Nallathiga, R., Taneja, S., Gupta, A., & Gangal B. (2018). Sustainability of Urban Fringe Development and Management in NCT-Delhi: A Case Study. In: J. Mukherjee (Ed.), Sustainable Urbanization in India: Challenges and Opportunities Exploring Urban Change in South Asia (pp. 109-133). *Springer* : Singapore.
36. Potin, P., Rosich, B., Miranda, N., & Grimont, P. (2016). Sentinel-1 Mission Status. *Procedia Computer Science*, 100: 1297-1304.
37. Prasannakumar, V., Vijith, R., Charutha, N., Geetha, N. (2011). Spatio-temporal clustering of road accidents: GIS based analysis and assessment. *Procedia- Social and Behavioral Sciences*. 21: 317-325.
38. Rashiq, A., & Prakash, O. (2023). Assessment of spatio-temporal variability of climate in the lower Gangetic alluvial plain. *Environmental Monitoring and Assessment*, 195: 945.
39. Raspini, F., Bianchini, S., Ciampalini, A., Soldato, M.D., Solari, L., Novali, F., Conte, S.D., Rucci, A., Ferretti, A., & Casagli, N. (2018). Continuous, semi-automatic monitoring of ground deformation using Sentinel-1 satellites. *Scientific Reports*, 8: 7253.
40. Raza, O., Mansournia, M.A., Foroushani, A.R., & Holakouie-Naieni, K. (2020). Exploring spatial dependencies in the prevalence of childhood diarrhea in Mozambique using global and local measures of spatial autocorrelation. *Medical Journal of the Islamic Republic of Iran*, 34: 59.
41. Rousta, I., Doostkamian, M., Haghighi, E., Malamiri, H. R. G., & Yarahmadi, P. (2017). Analysis of spatial autocorrelation patterns of heavy and super-heavy rainfall in Iran. *Advances in Atmospheric Sciences*, 34: 1069-1081.
42. Sahin, E., Iban, M. C., & Bilgilioglu, S. S. (2024). Remote Sensing-Enabled Urban Growth Simulation Overlaid with AHP-GIS-Based Urban Land Suitability for Potential Development in Mersin Metropolitan Area, Türkiye. *Applied Sciences*, 14(8): 3484.
43. Saleh, B., & Rawashdeh, S. A. (2007). Study of urban expansion in Jordanian cities using GIS and remote sensing. *International Journal of Applied Science and Engineering*, 5(1):41-52.
44. Schmidt, K., Schwerdt, M., Miranda, N., & Reimann, J. (2020). Radiometric Comparison within the Sentinel-1 SAR constellation over a wide backscatter range. *Remote Sensing*, 12(5):854.
45. Sentinel User Guide. Retrieved from https://sentinel.esa.int/web/sentinel/user-guides/sentinel-1-sar/definitions
46. Shariati, M., Mesgari, T., Kasraee, M., & Jahangiri-rad, M. (2020). Spatiotemporal analysis and hotspots detection of

COVID-19 using geographic information system (March and April, 2020). *Journal of Environmental Health Science and Engineering*, 18(2):1499-1507.
47. Skoda, P., & Adam, F. (2020). Knowledge Discovery in Big Data from Astronomy and Earth Observation Astrogeoinformatics. USA: *Elsevier Science*.
48. Sun, W., Shan, J., Wang, Z., Wang, L., Lu, D., Jin, Z., & Yu K. (2020). Geospatial analysis of urban expansion using remote sensing methods and data: a case study of Yangtze River delta, China. *Complexity*, 2020: 3239471.
49. Tao S., Zhang T., Wang K., Xie F., Ni L., Mei Z., Song S. (2021): Identification of the risk factors in perioperative respiratory adverse events in children under general anesthesia and the development of a predictive model. *Translational Pediatrics*, vol. 10(7), 2021, pp. 1877-1882. doi: 10.21037/tp-21-257
50. Tsui, T., Derumigny, A., Peck, D., Timmeren, A. V., & Wandl, A. (2022). Spatial clustering of waste reuse in a circular economy: A spatial autocorrelation analysis on locations of waste reuse in the Netherlands using global and local Moran's I. *Frontiers in Built Environment*, 8: 954642.
51. Vilinová, K., & Petrikovicová, L. (2023). Spatial autocorrelation of COVID-19 in Slovakia. *Tropical Medicine and Infectious Disease*, 8(6): 298.
52. Wang, M., Fu, X., Zhang, D., Chen, F., Su, J., Zhou, S., Li, J., Zhong, Y., & Tan S.K. (2023). Urban flooding risk assessment in the rural-urban fringe based on a bayesian classifier. *Sustainability*, 15:5740.
53. Weiβ, T. (2018). SAR pre-processing documentation. Retrieved from https://buildmedia.readthedocs.org/media/pdf/multiply-sar-pre-processing/get_to_version_0.4/multiply-sar-pre-processing.pdf
54. White, L., Brisco, B., Dabboor, M., Schmitt, A., & Pratt, A. (2015). A collection of SAR methodologies for monitoring wetlands. *Remote Sensing*, 7(6):7615-7645.
55. Winter, A.K., & Karvonen, A. (2022). Climate governance at the fringes: Peri-urban flooding drivers and responses. Land Use Policy, 117: 106124.
56. Woodhouse, I.H. (2006). Introduction to Microwave Remote Sensing. *CRC Press*:Florida.
57. Yin, Z., Dong, Y., Wang, Q., Ma, Y., Gao, Z., Ling, Z., Aihaiti, X., Abudusaimaiti, X., Qiu, R., Chen, Z., & Wushouer, F. (2024). Spatial-temporal evolution patterns of influenza incidence in Xinjiang Prefecture from 2014 to 2023 based on GIS. *Scientific Reports*, 14(1):21496.
58. Zhang, W., & Hu B. Brown G.S. (2020). Automatic surface water mapping using polarimetric SAR data for long-term change detection. *Water*, 12(3):872.

Manuscript Submission Guidelines: Notes for Authors

1. Manuscript may be submitted in English only. Contributions are considered for publication only on the understanding that they are not published already elsewhere, that they are the original work of the authors(s), and that the authors assign copyright to the National Institute of Disaster Management, Delhi.

2. Papers should normally be submitted as e-mail attachments to the Editor with copy to editor (journal.nidm@nidm.gov.in). The subject of the e-mail should be typed CONTRIBUTION FOR DISASTER AND DEVELOPMENT.

3. Papers can also be sent in hard copies by registered post but these must always be accompanied by a CD with manuscript in MS Word format. CD should be labeled with the name of the article and the author.

4. Title of the paper in bold, 14 point size (Times New Roman). Title of the paper should be followed by the name(s) of Authors, Affiliation(s), abstract, introduction, methodology, analysis, results, discussion, conclusion, acknowledgments and references.

5. Length of the paper should be maximum of 8000 words or 16, A4 pages including tables and illustrations (1.5 spaced with 1 inch margins and justified).

6. An abstract of upto 200 words with 4-5 key words, 12 point size italics. Figures, maps and diagrams should be of good resolution (150 dpi or more), numbered consecutively

7. Referencing and index citations should be as per American Psychological Association (APA) guidelines.
   a. Journal Articles: Scruton, R. (1996). The eclipse of listening. The New Criterion, 15(30), 5-13.
   b. Article in a Magazine: Henry, W.A., III. (1990, April 9). Making the grade in today's schools. Time, 135, 28-31.
   c. Book (Single and multiple Author(s))
      i. McKibben, B. (1992). The age of missing information. New York: Random House.
      ii. Larson, G. W., Ellis, D. C., & Rivers, P. C. (1984). Essentials of chemical dependency counseling. New York: Columbia University Press.
   d. Article or Chapter in an Edited Book
      Barlow, D. H., Chorpita, B. F., & Turovsky, J. (1996). Fear, panic, anxiety, and disorders of Emotion. In R.Dienstbier (Ed.), Nebraska Symposium on Motivation: Vol. 43. Perspectives on anxiety, panic, and fear (pp. 251-328). Lincoln: University of Nebraska Press.
   e. Conference Proceedings
      Schnase, J. L., & Cunnius, E. L. (Eds.). (1995). Proceedings from CSCL '95: The First International Conference on Computer Support for Collaborative Learning. Mahwah, NJ: Erlbaum.
   f. Individual document/report/web page authored by an organization and available on organization Web site, no publication date:

   Accreditation Commission for Programs in Hospitality Administration. (n.d.). Handbook of accreditation. Retrieved from http://www.acpha cahm.org/forms/acpha/acphahandbook04.pdf

8. Authors receive proofs of their articles, soft copy of the published version and a soft copy of the journal.

9. Authors are responsible for obtaining copyright permission for reproducing any illustrations, tables, figures or lengthy quotations published elsewhere.

Design & Print : kam@kamstudio.net

Resilient India - Disaster free India

National Institute of Disaster Management (NIDM)
(Ministry of Home Affairs, Government of India)

Plot No. 15, Block B, Pocket 3, Sector 29, Rohini, Delhi 110042
Website : https://nidm.gov.in